Reconstruction of thermal history of the Ahnet and Mouydir basins (southern Algeria)

PhD thesis presented by Mateusz Zieliński

Institute of Geology, Faculty of Geographical and Geological Sciences,
Adam Mickiewicz University, Poznan (2011)

Acknowledgements:

First, I would like to thank Prof. Zdzislaw Belka (Poznan) who supervised this thesis. I received a lot of guidance and kind attitude during work on this project from him. I am also indebted to him for opportunity to learn geochemical preparatory and measurements procedure.

The thesis would not have been prepared without extensive field work initiated and leaded by Prof. Jobst Wendt (Tübingen). Utilized conodont material has been gathered by his team as a part of projects financially supported by Deutsche Forschungsgemeinschaft (DFG), grants number We 239/11; 239/15.1-4; Ko 1829/3-1.

I wish to thank dr Jolanta Dopieralska (Poznan) who introduced me into the separation procedure of strontium isotopy and into the operation of the mass spectrometer. Performance of isotopic measurements is also appreciated.

Dr hab. Jacek Michniewicz, dr Malgorzata Mrozek-Wysocka, dr Danuta Nawrocka and dr Monika Lutynska (all Poznan) offered their time and performed chemical analysis of mineralization. Additionally, dr hab. Jacek Michniewicz took photographs of mineralized conodonts under ultraviolet light what is also appreciated.

I thank dr Bernadeta Dobosz, prof. Ryszard Krzyminiewski and dr Zdzislaw Kruczynski (all Poznan) for performance of electron spin resonance measurements and help in their interpretation.

Michal Jankowiak (Poznan) is acknowledged for preparation of thin plates. Dr Agata Duczmal-Czernikiewicz (Poznan) is acknowledged for help in identification of mineral components in thin plates.

I thank dr Edward Chwieduk (Poznan) for permission to use graphic designed by him.

Financial support for study was provided by Polish Ministry of Science and Higher Education, project number N N307 029337.

Table of contents:

STRESZCZENIE

Wstęp

Określenie dojrzałości termicznej osadów, rozpoznanie procesów odpowiedzialnych za wzrost temperatury w ich obrębie oraz ramy czasowe zdarzeń termicznych (modelowanie historii termicznej) jest jednym z podstawowych zadań w procesie określania potencjału naftowego basenów sedymentacyjnych. Dane te są powszechnie wykorzystywane w obliczeniach dotyczących czasu formowania się węglowodorów. Stopień dojrzałości termicznej skał osadowych wyznacza się za pomocą tzw. geotermometrów (e.g., Tissot et al., 1987). Najczęściej, jako geotermometry wykorzystuje się fizyczne i chemiczne właściwości minerałów lub komponentów organicznych (przegląd w Héroux et al., 1979). Jednym z najczęściej stosowanych geotermometrów są konodonty (e.g., Epstein et al., 1977; Wardlaw i Harris, 1984; Helsen i Königshof, 1994; Narkiewicz et al., 1998). Konodonty są małymi (przeważnie 0,2-2 mm) elementami szkieletowymi o zróżnicowanej morfologii (elementy platformowe, gałązkowe, ostrzowe) zbudowanymi z fluoroapatytu i rozproszonej w jego obrębie materii organicznej (Belka, 1993). Tworzyły one aparat gębowy wymarłych morskich strunowców, które powszechnie występowały w morzach paleozoiku i triasu (patrz Sweet, 1988). U podstaw zastosowania konodontów jako geotermometru leży zjawisko stopniowej, postępującej i nieodwracalnej zmiany ich barwy od koloru jasnożółtego (konodonty niezmienione) do czarnego, w związku z przemianami chemicznymi materii organicznej w odpowiedzi na wzrost temperatury w czasie geologicznym. Aby uczynić tą sekwencję bardziej użyteczną została ona podzielona na zakresy którym przypisano wartości liczbowe od 1 do 5 (Epstein et al., 1977). Pełen zestaw zakresów barw elementów konodontowych został nazwany konodontowymi wskaźnikami przeobrażeń termicznych (conodont colour alteration index-CAI). Eksperymentalnie wyznaczona zależność pomiędzy wartością CAI, temperaturą oraz czasem pogrążenia sukcesji osadowych została ekstrapolowana na czas geologiczny. Do oszacowania palaeotemperatur służy diagram opracowany przez Epstein et al. (1977). Ponadto dane CAI można wykorzystać także przy szacowaniu gradientu geotermalnego w trakcie pogrzebania rozpatrywanej sekwencji osadowej. Oryginalna skala CAI (Esptein et al., 1977) została rozszerzona do wartości indeksu 8 przez Rejebian et al. (1987). W rezultacie przeprowadzonych przez tych autorów eksperymentów okazało się, że dane CAI mogą znaleźć zastosowanie w rozpoznawaniu metamorfizmu regionalnego i

kontaktowego oraz aktywności hydrotermalnej w obrębie skał. Ten ostatni proces jest często odpowiedzialny za powstawanie złóż mineralnych.

Celem prezentowanej rozprawy doktorskiej jest opracowanie modelu historii termicznej dla utworów środkowego i górnego dewonu oraz karbonu występujących w basenach sedymentacyjnych Ahnet i Mouydir. Oba baseny są rozległymi (razem pokrywają obszar o powierzchni ok. 10 000 km^2) paleozoicznymi obniżeniami położonymi przy NW krawędzi masywu Hoggar w południowej Algierii. Baseny Ahnet i Mouydir wypełnione są miąższą do ok. 7000 m sekwencją obejmującą morskie oraz rzeczne piaskowce i mułowce przewarstwione stosunkowo cienkimi poziomami wapieni. Wiek tej sekwencji siega od środkowego kambru do karbonu (Fabre et al., 2005; Vecoli et al., 2008). Skały paleozoiku są podścielone zmetamorfizowanymi skałami orogenu pan-afrykańskiego, którego charakterystyczną cechą jest system południkowych uskoków, które odgrywały zasadniczą rolę w rozwoju strukturalnym badanego obszaru. Po raz pierwszy w basenach Ahnet i Mouydir dojrzałość termiczna skał została określona za pomocą konodontowych wskaźników CAI. Ponadto obserwacje ujawniły obecność stosunkowo powszechnej mineralizacji na konodontach. Została ona wykorzystana do wyznaczenia dróg migracji fluidów odpowiedzialnych za jej powstanie. W badaniach wykorzystano 384 środkowo i późno-dewońskie oraz karbońskie próby konodontowe pobrane z 69 powierzchniowych odsłonięć. W przygotowaniu modelu historii termicznej dane CAI zostały uzupełnione o badania defektów sieci krystalicznej konodontów za pomocą elektronowego rezonansu paramagmetycznego (EPR), które dostarczają przydatnych informacji o ostatnim podgrzaniu elementów konodontowych (Belka et al., 1987). Fazy mineralne porastające konodonty były analizowane przy pomocy detektora EDS. Ponadto wykonano pomiary stosunków izotopów strontu ($^{87}Sr/^{86}Sr$) w konodontach i ich skałach macierzystych.

Dojrzałość termiczna osadów

Skały środkowego i górnego dewonu w basenie Ahnet wykazują wysoką jednorodność poziomu dojrzałości termicznej na obszarze całego basenu. W zdecydowanej większości odsłonięć skał eiflu, żywetu, oraz franu i famenu konodonty pokazują wartości CAI 2. Tylko lokalnie konodonty pokazują nieznacznie niższe (CAI 1,5-2) lub wyższe (CAI 3) wartości. Ponadto w obrębie skał żywetu występuje 9 prób, które zawierają konodonty z anomalnymi wartościami CAI (w jednej próbie występują elementy konodontowe o dwóch różnych wartościach CAI oraz elementy odbarwione). Istotna zmiana w stopniu dojrzałości utworów dewonu następuje dalej na wschód w sąsiednim

basenie Mouydir. Tutaj skały wykazują dojrzałość termiczną na poziomie od CAI 2 do 3,5. Należy zwrócić uwagę na niższą jednorodność stopnia dojrzałości termicznej na obszarze tego basenu. W utworach środkowego dewonu dominują skały z CAI 3, podczas gdy w utworach górnego dewonu dominują skały z CAI 2. Dane dla skał karbonu są znacznie bardziej skąpe niż dla dewonu i pozwalają one na prześledzenie trendu tylko na obszarze basenu Ahnet. Stopień dojrzałości termicznej utworów karbonu zmienia się od umiarkowanego (CAI 3,5) w skałach turneju, przy czym na większości obszaru pokazują one CAI 1,5-2 i 2, do bardzo niskiego (CAI 1 i 1,5) w skałach baszkiru. W basenie Mouydir występują tylko utwory turneju i pokazują one umiarkowany stopień dojrzałości termicznej wyrażony wartością indeksu CAI 3.

Zgromadzone dane wskazują, że w obu basenach wyznaczona dojrzałość termiczna skał zarówno dewonu jak i dolnego karbonu została osiągnięta głównie w wyniku regionalnego pogrążenia. Późny karbon koresponduje z okresem maksymalnego pogrążenia sukcesji osadowej. Oprócz regionalnego pogrążenia skały na badanym obszarze były wystawione na oddziaływanie roztworów hydrotermalnych. Świadczy o tym lokalne występowanie anomalii CAI. Dodatkowo lokalnie podwyższone, w porównaniu do prób tego samego wieku w innych rejonach, wartości CAI skał turneju (CAI 3.5) i baszkiru (2) w NW części basenu Ahnet wskazują na ich powstanie w wyniku podgrzania przez ciała magmowe. Argumentami za tym są znacznie niższe wartości pozostałych prób tego wieku w danym profilu oraz fakt, że jest to jedyny rejon badanego obszaru na którym występują skały magmowe. Skały środkowego dewonu w basenie Ahnet były podgrzewane w temperaturach ok. 50-120°C. Należy podkreślić jednak, że w związku z dominacją skał wykazujących dojrzałość termiczną na poziomie CAI 2 podgrzewane one były głównie w temperaturze około 50°C. Wyższa temperatura występowała tylko lokalnie i była spowodowana najprawdopodobniej wzrostem strumienia cieplnego wzdłuż uskoków. Skały górnego dewonu doświadczyły 40 do 50°C, jednakże podgrzewane były głównie w temperaturze ok. 50°C. Zbliżony zakres temperatur został oszacowany również dla skał dolnego karbonu (turneju i dolnego wizenu). Skały dolnego karbonu są pokryte przez utwory baszkiru. bardzo niski stopień dojrzałości termicznej (CAI 1 i 1,5) skał w spągu wskazuje że skały baszkiru nigdy nie były podgrzane powyżej 40°C. Zakładając niski gradient geotermiczny 10°C/km oraz średnią temperaturę powierzchni 10°C temperatura 40°C byłaby osiągnięta przy nadkładzie ok. 4200 m. Ponieważ na badanym obszarze nie są obecne skały mezozoiku i prawdopodobnie nigdy nie były tam zdeponowane pozwala to na stwierdzenie że pokrywa post-wczesnobaszkirska była

złożona wyłacznie ze skał najwyższego karbonu. W rezultacie całkowita miąższość sekwencji karbońskiej mogła wynosić do 6400 m. Biorąc pod uwagę szacowaną miąższość późnego karbonu, średnia miąższość skał karbonu wynosi 5500m. Jest to miąższość wystarczająca by pogrążyć utwory środkowego i górnego dewonu na głębokości na których panują temperatury zgodne z tymi oszacowanymi z danych CAI dla poszczególnych jednostek.

W sąsiednim basenie Mouydir skały środkowego dewonu były podgrzewane w zakresie temperatur od 50 do 150°C. Dominacja skał wykazujących CAI 3 wskazuje, że na większość skał dewonu oddziaływały temperatury ok. 120°C. Utwory górnego dewonu z kolei były wystawione na oddziaływanie temperatur od 50 do 120°C. Ponieważ wśród górnego dewonu dominują skały o CAI 2, więc na większość tych skał działała temperatura ok. 50°C. W basenie zachowane jest tylko 550 m skał karbonu. Jednakże można wykorzystać dane z basenu Ahnet do modelowania. Zakładając maksymalną miąższość utworów na 6400 m oszacowane palaeotemperatury mogły zostać osiągnięte przy gradiencie geotermicznym ok. 35°C/km.

W obrębie skał paleozoiku występują dwa główne poziomy skał macierzystych dla węglowodorów (e.g., Macgregor, 1996). Są to bogate w materię organiczną dolnosylurskie łupki oraz środkowo do późno dewońskie łupki, włączając dolnofrański poziom łuków bogatych w materię organiczną. Dodatkowo w basenie Ahnet jest obecny kolejny poziom o mniejszym znaczeniu. Są to łupki turneju (Lounissi et al., 2007). Obecne są także poziomy skał zbiornikowych (e.g., Klett, 2000). Do głównych należą piaskowce ordowiku, dewonu oraz turneju (nie obecne w basenie Mouydir). W basenie Ahnet wszystkie wymienione skały zbiornikowe zawierają komercyjne nagromadzenia gazu (e.g., Lounissi et al., 2007). Oszacowane temperatury pogrążenia dla skał środkowego dewonu w basenie Ahnet są zgodne z zakresem temperatur dla tzw. „okna ropy naftowej". Wyznacza ono główny zakres temperatur w których formują się węglowodory (60-135°C). Temperatury dla utworów górnego dewonu i dolnego karbonu plasują skały tego wieku w strefie początkowego stadium formowania się ropy i gazu. Dlatego też pomimo dobrych parametrów górnodewońskich osadów (wartości parametru tzw. zawartości całkowitego organicznego węgla do 14%) ich zdolnosc do formowania węglowodorów wydaje się ograniczona. Dojrzałość termiczna łupków syluru odpowiada strefie formowania suchego gazu i kondensatu (Askri et al., 1995). Ponieważ skały syluru podścielają bezpośrednio utwory dewonu wydaje się że dolnodewońskie skały zbiornikowe są zasilane głównie przez węglowodory wytworzone w skałach syluru. Łupki franu i famenu są przykryte

poziomami piaskowców. Stąd wędlowodory obecne w tych skałach najprawdopodobniej migrowały z leżących niżej łupków. Nad łupkami turneju występują piaskowce zawierające węglowodory. Dlatego też jest raczej pewne że zawarte w nich węglowodory pochodzą z niżej leżących łupków. W przeciwieństwie do basenu Ahnet, w basenie Mouydir występowanie węglowodrów jest bardzo słabo rozpoznane (Klett, 2000). Jednakże zakresy temperatur dla skał środkowego i górnego dewonu wskazują że znajdują się one głównie w tzw. oknie ropy naftowej. Dodatkowo temperatura 150°C dla środkowego dewonu rozszerza zakres formowanych węglowdorów do suchego gazu i kondensatu. Ponadto dojrzałość termiczna sylurskich łupków odpowiada strefie formowania się gazu (Askri et al., 1995). W rezultacie obecność gazu uforowanego w łupkach syluru jest spodziewana w piaskowcach kambro-ordowiku. Z koleii węglowodory wygenerowane w łupkach dewonu mogą być magazynowane w piaskowcach środkowego i późnego dewonu.

Widma EPR

Zarejestrowane dla dewońskich konodontów widma EPR mają podobną strukturę przejawiającą się obecnością sygnałów B, C i D, z wyjątkiem jednej próby, w której sygnał C jest nieobecny. Sygnał A występuje tylko w widmach dwóch prób. Ponadto występuje związek pomiędzy intensywnością sygnałów w widmach i ich pozycją na badanym obszarze. Na przykład intensywność sygnału C maleje stopniowo z zachodu ku wschodowi. Przeciwny trend wykazuje intensywność sygnału D, która wzrasta ku wschodowi.

Bełka et al. (1987) przypisują emisję sygnału A atomom fluoru znajdującym się w substancji mineralnej konodontów. Sygnał B wydaje się być generowany przez jony SO_3^-, podczas gdy za źródło sygnału D są uważane niesparowane elektrony powiązane z materią organiczną. W przeciwieństwie do wyżej podanych, źródło sygnału C nie zostało wcześniej rozpoznane. Nowe dane uzyskane z pomiarów algierskiego materiału sugerują, że najprawdopodobniej źródłem sygnału C są centra fosforanowe, które powstały przez podstawienie w sieci krystalicznej konodontów jonów wapnia przez jony uranu i toru. Uzyskane dane potwierdzają także, że za sygnał D odpowiedzialne są niesparowane elektrony powiązane z materią organiczną rozproszoną w obrębie fluoroapatytu.

Według Bełki et al. (1987) sygnał A dostarcza ważnych informacji o ostatnim podgrzaniu elementów konodontowych. Autorzy ci stwierdzili, że centra paramagnetyczne odpowiedzialne za emisję sygnału A powstają w wyniku promieniowania oddziałującego

na konodonty dłużej niż 225 mln lat. W rezultacie obecność w widmach paleozoicznych konodontów tego sygnału wskazuje na to, że były one podgrzane w paleozoiku, podczas gdy brak sygnału A świadczy o jego zresetowaniu w wyniku kolejnego podgrzania, które mogło mieć miejsce w mezozoiku lub kenozoiku.

Obecność sygnału A w widmach dwóch prób wskazuje na podgrzanie w trakcie paleozoiku. Koreluje się ono bardzo dobrze z karbońskim pogrążeniem rozpoznanym na podstawie danych CAI. Jednakże brak sygnału A w widmach pozostałych 3 prób stanowi argument za ponownym podgrzaniem skał w basenach Ahnet i Mouydir. Wzrost intensywności sygnału D koreluje się dobrze ze wzrostem stopnia dojrzałości termicznej konodontów. W widmach konodontów z CAI 3 jego intensywność jest dwa razy większa niż w widmach konodontów z CAI 2. Sygnały B i C są nieistotne dla rozpoznania historii termalnej (Bełka et al., 1987). Struktura sygnału B w algierskim materiale koreluje się dobrze ze strukturą sygnałów otrzymanych przez Belkę et al. (1987) dla konodontów z CAI 2 i 3. Stopniowy spadek intensywności sygnału C jest najprawdopodobniej związany ze zniszczeniem sieci krystalicznej konodontów wykazujących stosunkowo wyższy stopień dojrzałości termicznej.

Mineralizacja i korozja konodontów

Elementy konodontowe w basenach Ahnet i Mouydir są pokryte kryształami apatytu, barytu, hematytu, framboidalnego pirytu oraz szelitu. Apatyt jest najpowszechniejszym minerałem (obecny na ok. 24 % wszystkich prób). Występuje on głównie w postaci małych (0,1-0,2 mm) bezbarwnych automorficznych kryształów o pokroju tabliczkowym i słupkowym. We wszystkich zaobserwowanych przypadkach kryształy występują bezpośrednio na powierzchni konodontów. Niezwykła jest zależność pokroju kryształów od miejsca ich występowania. Kryształy porastające wyrostki mają wyłącznie słupkowy pokrój i ich wzrost odbywał się zgodnie z ułożeniem krystalitów wewnątrz wyrostków. Wytrącanie się kryształów było ułatwione przez obecność licznych i dużych porów w tkance konodonta. Kryształy apatytu występujące wokół jamy bazalnej i wzdłuż kili mają wyłącznie pokrój tabliczkowy. Pierwsze kryształy wytrącały się na przeciętych powierzchniach 001 krystalitów w warstwach fluoroapatytu tworzących kile. Kolejne kryształy krystalizowały wzdłuż powierzchni 001 kryształów zgodnie z przebiegiem krystalitów w obrębie tkanki mineralnej platformy konodonta. Z występowaniem apatytu ściśle powiązana jest obecność framboidalnego pirytu i hematytu. Rozmiar framboidów zawiera się w przedziale od 2 do 5 μm. Są one obecne pomiędzy

kryształami apatytu oraz na ich powierzchni. Często piryt jest zastąpiony przez tlenki żelaza (pseudomorfozy). Hematyt tworzy srebrzystoszare małe (do 50 μm) automorficzne rombohedralne kryształy. Najczęściej występują one na powierzchni kryształów apatytu, aczkolwiek obecne są także bezpośrednio na powierzchni elementów konodontowych. Szelit został znaleziony na ok. 5 % analizowanych prób. Występuje on w postaci białawych, małych (do 10 μm) automorficznych kryształów o pokroju cienkich tabliczek. W świetle ultrafioletowym kryształy szelitu wykazują jasnoniebieską fluorescencję. Szelit występuje bezpośrednio na powierzchni konodontów (porasta je dookoła), jak i został znaleziony na kryształach apatytu i pirytu. Baryt jest najrzadszym minerałem. Został znaleziony tylko na ok. 1% badanych prób. Tworzy masywne skupiska występujące na powierzchni kryształów apatytu i hematytu. Został znaleziony także bezpośrednio na powierzchni konodontów.

Zebrane dane wskazują, że wszystkie minerały wykrystalizowały z roztworów hydrotermalnych. Wzajemne relacje pomiędzy minerałami oraz paragenezy mineralne z literatury wskazują, że apatyt wykrystalizował jako pierwszy. Następnie powstały piryt i hematyt. Jako ostatnie wykrystalizowały szelit i baryt. Źródłem jonów najprawdopodobniej były skały magmowe podłoża prekambryjskiego.

Elementy konodontowe z ok. 5 % analizowanych prób mają skorodowaną powierzchnię. Wyraźnie zarysowane jest zróżnicowanie w wykształceniu tego zjawiska w zależności od morfologii konodontów. Elementy platformowe są skorodowane głównie na brzegach platform i wokół jamy bazalnej oraz wzdłuż kili. Elementy gałązkowe oraz ostrzowe są skorodowane głównie u podstawy wyrostków oraz wzdłuż gałązki i ostrza. We wszystkich przypadkach skorodowana powierzchnia jest pokryta szarą patyną która jest efektem utlenienia materii organicznej zawartej w konodontach. Analiza powierzchni zmineralizowanych konodontów z wykorzystaniem skaningowego mikroskopu elektronowego pokazała, że w większości przypadków jest ona niezmieniona. W kilku przypadkach elementy pokryte kryształami apatytu wykazują skorodowane powierzchnie. W przeciwieństwie do konodontów same fazy mineralne nie noszą śladów korozji. Zgromadzone dane wskazują, że korozja jest efektem oddziaływania roztworów hydrotermalnych. Przygotowane mapy czasowo-przestrzennego występowania mineralizacji i korozji na badanym obszarze pokazują, że oba zjawiska występują wzdłuż prekambryjskich uskoków. Stanowi to mocny argument za tym, że uskoki te stanowiły drogi migracji dla roztworów hydrotermalnych. Apatyt wraz z pirytem i hematytem są obecne tylko na dewońskich konodontach, podczas gdy szelit i baryt występują na

dewońskich i karbońskich konodontach. Mineralizacja, jak i korozja są najliczniejsze w żywecie i stopniowo wygasają ku górze sekwencji osadowej. Wskazuje to na wznoszący typ cyrkulacji hydrotermalnej. Analiza map wskazuje, że na rozpatrywanym obszarze wystąpiły przynajmniej 4 epizody aktywności hydrotermalnej. Pierwszy epizod, który wystąpił w dolnym żywecie i najprawdopodobniej był związany z formowaniem się kopców mułowych (Bełka, 1994) jest odpowiedzialny za korozję części eifelskich i żyweckich elementów konodontowych oraz powstanie anomalii CAI. Agresywna natura roztworów względem fosforanów przy braku korozji węglanów jest najprawdopodobniej spowodowana alkalicznym pH roztworów. Temperatura roztworów mogła maksymalnie wynosić 300°C. Drugi epizod miał miejsce w późnym franie i spowodował korozję frańskich konodontów oraz przypuszczalnie części starszych konodontów. Wypływ roztworów był przypuszczalnie związany ze zwiększoną przepuszczalnością wzdłuż uskoków spowodowaną tensyjną tektoniką w trakcie późnego dewonu. Zapisem trzeciej fazy aktywności gorących roztworów jest mineralizacja apatytowa wraz z pirytem i hematytem. Temperatura fluidów zawierała się w przedziale 50-350°C. W tym przypadku wypływ był najprawdopodobniej spowodowany wyniesieniem bloków skorupy ziemskiej i zwiększeniem przepuszczalności wzdłuż nieciągłości tektonicznych. Ostatni, czwarty, epizod hydrotermalny skutkował krystalizacją szelitu i barytu. W tym przypadku maksymalna temperatura roztworów oscylowała w okolicach 200°C. Podobnie jak w przypadku poprzedniej fazy, wypływ roztworów hydrotermalnych wydaje się być związany z wyniesieniem badanego obszaru. Występowanie dwóch przeciwstawnych zjawisk jakimi są korozja i mineralizacja wskazują na obecność dwóch różnych typów roztworów hydrotermalnych. Jeden typ fluidów był agresywny i spowodował korozję konodontów. Brak jest bezpośrednich danych wskazujących na źródło wody dla tych roztworów. Jednak ponieważ w czasie wypływów hydrotermalnych wiązanych z korozją konodontów baseny Ahnet i Mouydir były stale pokryte epikontynentalnym morzem wydaje się, że najbardziej prawdopodobnym źródłem była woda morska. W przypadku roztworów odpowiedzialnych za mineralizację fluidy pochodziły najprawdopodobniej z solanek formacyjnych uwięzionych w skałach klastycznych kambro-ordowiku, które były okresowo uwalniane w trakcie epizodów wyniesienia i migrowały w górę sekwencji skalnej.

Analiza izotopów strontu

Wartości stosunku izotopów strontu $^{87}Sr/^{86}Sr$ pomierzone dla dewońskich konodontów zawierają się w przedziale od 0,7080 do 0,7085. Wartości stosunku dla węglanów są bardziej radiogeniczne i zawierają się w przedziale pomiędzy 0,7082 i 0,7092. Skład izotopowy zarówno konodontów, jak i węglanów jest przesunięty w kierunku wyższych wartości względem składu izotopowego wody morskiej w trakcie dewonu. Wskazuje to na przyswojenie przez oba komponenty bardziej radiogenicznego strontu z zewnętrznego źródła. Najbardziej prawdopodobnym źródłem strontu są sylurskie mułowce podścielające bezpośrednio skały dewonu. Bardziej radiogeniczne wartości węglanów w porównaniu do wartości stosunku pomierzonych dla konodontów są z pewnością spowodowane niższą temperaturą otwierania systemu izotopowego węglanów niż w przypadku fosforanów. Stąd węglany mogły przyswoić więcej bardziej radiogenicznego strontu. W przypadku węglanów prawdopodobne jest także dodatkowe przyswojenie strontu z kenozoicznych wód meteorycznych.

Historia termiczna basenów Ahnet i Mouydir

W oparciu o informacje o ogólnej geologii badanego obszaru, CAI, EPR oraz analizę mineralizacji i korozji zaproponowano historię termiczną basenów Ahnet i Mouydir obejmującą przedział czasu od dewonu do końca karbonu. Z powodu różnic w rozwoju basenów zaproponowano osobne scenariusze dla każdego z nich. Zaprezentowane modele zostały stworzone dla NW części basenu Ahnet i W części basenu Mouydir.

Basen Ahnet. Środkowodewońskie osady (miąższość skompaktowanej sekwencji wynosi 40 m) deponowana była ze średnim tempem ok. 3 m/mln lat. Osady reprezentują pełnomorskie środowisko, którego głębokość nie przekraczała 200 m (Wendt et al., 1997, 2006). Stanowi to przesłankę ku raczej stałemu tempu subsydencji. We wczesnym żywecie wystąpił epizod hydrotermalny, który spowodował korozję konodontów oraz powstanie anomalii CAI. Pomimo potencjalnie wysokiej temperatury maksymalnej (do 300°C) wpływ roztworów na dojrzałość termiczną skał był nieistotny. Wynika to zapewne z bardzo krótkiego czasu aktywności roztworów. W trakcie późnego dewonu zdeponowane zostało ok. 1200 m osadów w średnim tempie ok. 46 m/mln lat. Tempo sedymentacji musiało przewyższać tempo subsydencji ponieważ cała sekwencja jest zapisem wypłycania się zbiornika morskiego (patrz Wendt et al., 2006). W trakcie późnego dewonu utwory środkowego dewonu doświadczyły niskich temperatur i pozostały niedojrzałe termicznie.

Potencjalnie wyższe temperatury mogły oddziaływać na skały dewonu w związku z wypływem roztworów hydrotermalnych w późnym franie. Jednakże, nie ma zauważalnych efektów termicznych ich oddziaływania. W najwcześniejszym karbonie pogrążanie skał dewonu zostało przerwane przez krótkotrwałe wyniesienie. Wydaje się, że wysoka temperatura roztworów hydrotermalnych które były aktywne w tym czasie spowodowały zresetowanie sygnału A w widmach EPR konodontów, lecz nie wpłynęła ona w widoczny sposób na wzrost stopnia dojrzałości termicznej skał. Głębokość pogrążenia skał dewonu wzrosła pod koniec wczesnego wizenu po zdeponowaniu ok. 600 m osadów w średnim tempie ok. 54 m/mln lat. Jednakże nie miało to znacznego wpływu na wzrost temperatury i skały pozostały nadal niedojrzałe. Dodatkowo przypuszczalnie ok. 300 m osadów których wiek zawierał się w przedziale środkowy wizen do sierpuchow włącznie zostało zdeponowane, lecz także bez istotnego wpływu na dojrzałość skał dewonu. Termiczny wpływ roztworów hydrotermalnych przemieszczających się przez skały dewonu pod koniec wczesnego karbonu był także bez znaczenia. Znaczne zmiany w stopniu dojrzałości termicznej skał dewonu i wczesnego karbonu nastąpiły w późnym karbonie, na skutek depozycji znacznych ilości osadów (średnio przypuszczalnie 4500 m w tempie, które mogło przekraczać 200 m/mln lat). W tym czasie skały środkowego dewonu osiągnęły okno ropy naftowej oraz maksymalną głębokość pogrążenia. Rozpoczęło się formowanie węglowodorów ze skał macierzystych. Utwory górnego dewonu i dolnego karbonu także osiągnęły maksymalną głębokość pogrążenia, jednakże pozostały termicznie niedojrzałe. Na przełomie karbon/perm nastąpiło wyniesienie basenu, które zapoczątkowało spadek temperatury w rozpatrywanych utworach.

Basen Mouydir. Osady środkowego dewonu (miąższość ok. 200 m) były deponowane w średnim tempie ok. 17 m/mln lat. Podobnie jak w basenie Ahnet reprezentują one środowisko otwartego morza (Wendt et al., 1997, 2006). Sugeruje to raczej stałe tempo subsydencji. W trakcie wczesnego żywetu osady były wystawione na oddziaływanie roztworów hydrotermalnych, lecz nie ma dowodów wpływu roztworów na ich dojrzałość termiczną. W trakcie późnego dewonu tempo akumulacji wzrosło do ok. 42 m/mln lat. Wypłycanie się zbiornika morskiego zapisane w osadach górnego dewonu (Wendt et al., 2006) wskazuje na stopniowy zwrost tempa depozycji i spadek tempa subsydencji. Miąższość zdeponowanych osadów była jednak zbyt mała by mieć istotny wpływ na dojrzałość termiczna niżej leżących utworów. W rezultacie osady środkowego dewonu były w tym czasie niedojrzałe. Najważniejszy okres w historii termicznej basenu przypada

na karbon. Jest to związane z depozycją znacznych ilości osadów (średnio prawdopodobnie 3200 m) w tempie przekraczającym 50 m/mln lat. Jednakże, przed osadzeniem i w trakcie depozycji utworów karbonu skały dewonu zostały wystawione na oddziaływanie ciepła przenoszonego przez roztwory hydrotermalne. Lecz jego wpływ na stopień dojrzałości termicznej skał jest niezauważalny. W najwcześniejszym późnym karbonie skały środkowego i górnego dewonu zostały wepchnięte w okno ropy naftowej i pozostały tam do końca karbonu. W tym czasie rozpoczęło się formowanie węglowodorów ze skał macierzystych. W najpóźniejszym karbonie obie sekwencje osiągnęły maksymalną głębokość pogrążenia. Na przełomie karbon/perm doszło do wyniesienia basenu, na skutek czego rozpoczęło się wychładzanie rozpatrywanych sekwencji skalnych.

1. INTRODUCTION

Geological exploration of Algerian territory during second part of the XXth century revealed the existence of hydrocarbon resources in the eastern and southern regions of the country. This was an impulse to intensive geological work during next years which resulted in discoveries of commercial quantities of hydrocarbons in the Palaeozoic basins (Ahnet, Berkine/Ghadames, Illizi, Oued Mya, Sbaa) including enormous oil and gas fields, Hassi Messaoud and Hassi R`mel respectively (see Boote et al., 1998; Traut et al., 1998 for summary). Every commercial occurrence requires detail investigation of the petroleum system consisting of source rocks, migration pathways, reservoir rocks and seal rocks. Another very important issue is the recognition of thermal events that affected sedimentary basin, which have a crucial significance and thus devote many attention of petroleum geologists. This particular element is a subject of modeling of the thermal history, including a recognition of thermal treatment and the timing of its occurrence within sedimentary basin. Hydrocarbons are formed in a specific range of temperatures (roughly 60-150°C). The estimated palaeotemperatures along with the time framework of their influence on the sedimentary successions can be use in calculations of timing of hydrocarbon formation.

The principle of the method for interpretation of past thermal events is realization in geosciences that hydrocarbons are product of thermal transformation of organic matter. With progress in the knowledge on the origin of hydrocarbons, indicators of thermal maturation (the so-called geothermometers) have been developed. These made possible evaluation of thermal maturity of rocks and express it in a useful way (Tissot et al., 1987). Most frequently, physical properties of mineral phases or organic compounds are used as geothermometers (see Héroux et al., 1979 for review). Among these conodont elements are widely used (e.g., Epstein et al., 1977; Wardlaw & Harris, 1984; Sarmiento et al., 1999). Epstein et al. (1977) utilized these microfossils as geothermometer for the first time and expressed changes in thermal maturity of rocks in a sequence of conodont`s colour termed the conodont colour alteration index (CAI). There have been also attempts of evaluation and quantification of thermal maturity of conodonts with the usage of electron spin resonance spectroscopy (Belka et al., 1987), fluorescence spectrometry (Barrick et al., 1990; Mastalerz et al., 1992), infrared spectrometry (Nöth & Richter, 1992), colour image analysis (Helsen et al., 1995), spectral reflectance (Deaton et al., 1996); X-ray photoelectron spectroscopy (Lee et al., 1998), pyrolysis gas chromatography mass spectrometry and Fourier transform infrared emission spectroscopy (Marshall et al., 1999).

Each of these methods offers a unique approach in evaluation of thermal maturity of conodonts. Their usefulness, however, is different depending on investigated material and the temperature range. Valuable data about the number of thermal events might be obtains from the ESR method. Belka et al. (1987) has established that signals emitting by several molecules possessing unpaired electrons in conodont elements provide useful information about timing of their thermal alteration. This technique is also commonly use in dating of geological materials as stalactites, sediments, teeth and bones (Grün, 1989). Its application in conodont dating was proposed by Morency et al. (1970).

Sedimentary succession can be heated up in a few ways. The most common increase in temperature within rocks is caused by burial into deeper part of the crust or by heat produced by magmatic bodies. Less frequently, hot fluids circulating along discontinuities are responsible for the heat transfer. The action of hydrothermal fluids is commonly reflected in occurrences of mineralization. Hence, it may be use as a tracer of circulation pathways. The each heating mechanism influences sedimentary infill in different way and consequently indicators of thermal maturity record their effect in a different manner. Thus, this phenomenon is very helpful in identification of a particular heat source. During geological history of sedimentary basins temporal occurrence of different heat sources (regional burial, magmatic bodies, hydrothermal fluids) exhibits a specific patterns. These mechanisms might influence rocks simultaneously. They also may follow one after the other or occur several times. In all cases heating effects will be superimposed and unfortunately, they might distort information recorded by geothermometers.

Purpose of the study. The present work focuses on thermal history of sedimentary infill of the Ahnet and Mouydir basins located north-west of the Tuareg Shield in southern Algeria (Figure 1). The thermal maturity level of the Middle to Late Devonian and the Carboniferous deposits was determined by using conodonts. These microfossils are abundant and display an ability to record the thermal information expressed in their colour change. Because rocks might be affected by multiple thermal events the study has been supplemented by electron spin resonance investigation of conodont elements. This method enables detection and dating of the last thermal event. A special attention was paid on mm-size mineral overgrowth present on conodont elements. Relatively large number of samples containing mineralized elements enable to draw temporal-spatial pattern of its occurrence. In addition, an attempt was made to recognize pathways and origin of fluids responsible

for mineral overgrowths. This was performed by the investigation of strontium isotopic composition of conodonts and their host-rocks.

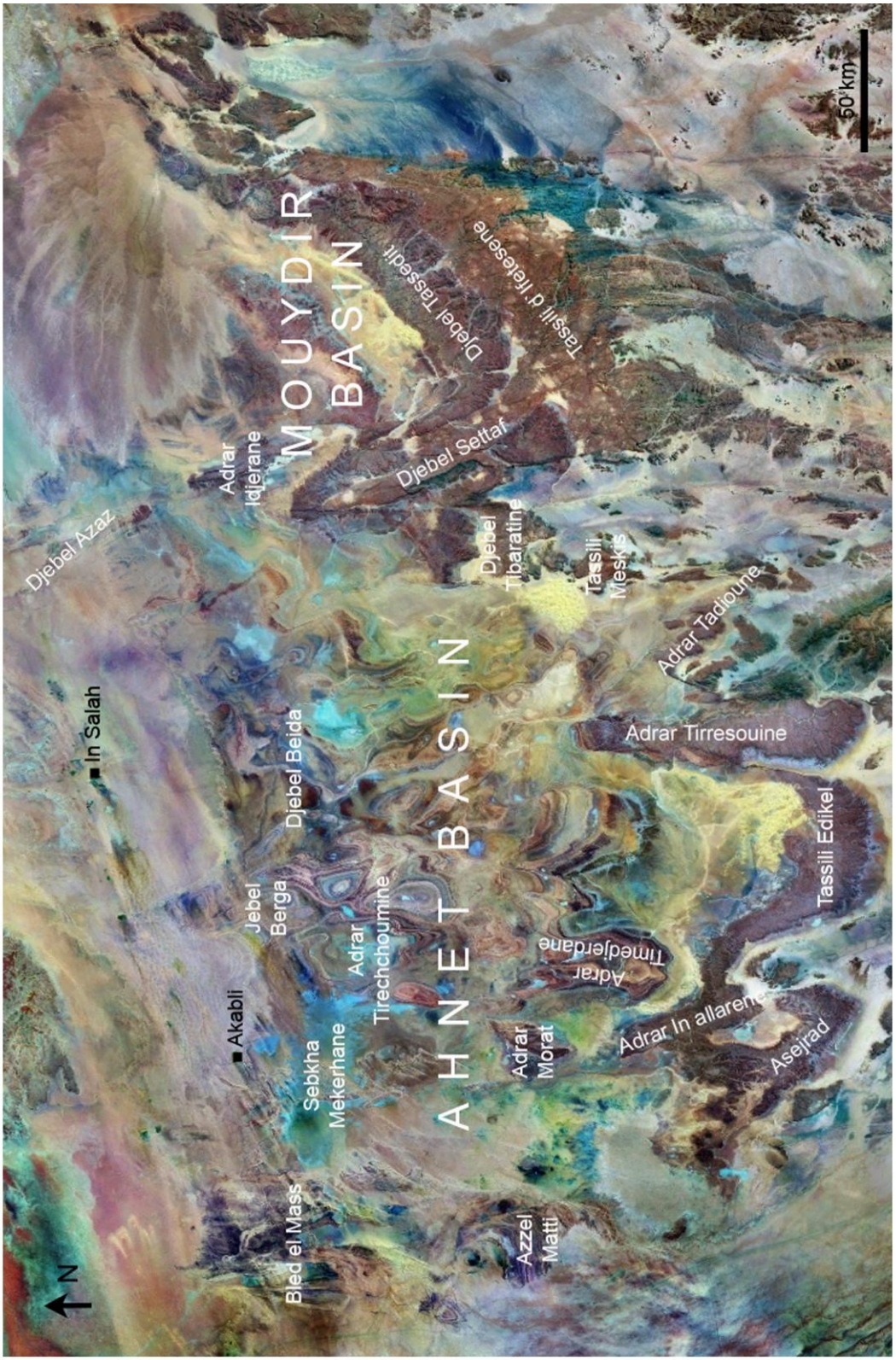

Figure 1. Satelite image of the Ahnet and Mouydir sedimentary basins showing selected geographical areas (geographical names after Follot, 1952 and Moussine-Pouchkine, 1970, unpublished).

2. GEOLOGICAL SETTING

The Saharan Platform originated during the Pan-African orogeny (750-550 Ma) constitutes the main tectonic unit of the Algeria. Younger and older units occur only the northernmost and western parts of the country. The northern part consist of the Alpine orogenic belt (the Atlas Mountains), whereas the western sector is built by the Archaean rocks of the West African Craton (WAC). To the north, the Saharan Platform is delimited by the South Atlas Fault. Its western border forms the Pan-African suture outcropped along the western margin of the Tuareg Shield. To the east, the Saharan Platform is bordered by the Saharan Metacraton (Figure 2). Metamorphosed and folded Precambrian basement of the Saharan Platform (the so-called Trans-Saharan Megabelt, TSM) is covered by a thick succession of clastic, mainly marine Phanaerozoic deposits. During the Palaeozoic this area constituted part of a vast, uniform northern shelf of the Gondwana palaeocontinent subjected to a differentiated subsidence. This led to formation of several sag basins and elevated ridges bordered by reactivated Precambrian lineaments. Among these are the Ahnet and Mouydir basins located the north-west of the Tuareg Shield in the southern Algeria (Figure 3). Both are large (together cover an area of approx. 10 000 km^2), N-S trending depressions filled with a sequence of mainly clastic rocks, up to 7000 m thick, the Middle Cambrian to Carboniferous in age (Figure 4). To the west, the Ahnet Basin is separated by the Azzel Matti Ridge from the Reggane Basin. Its northern limit constitutes the Djoua Saddle separating the basin from a large depression of the Timimoun Basin. To the east, the Ahnet Basin is limited by the Idjerane Mzab Ridge. The neighbouring Mouydir Basin is limited to the north by the large depression of the Oued Mya Basin. To the east, the basin is separated by the Amguid El Biod Ridge from the Illizi Basin. To the south, both the Ahnet and Mouydir basins are delimited by the Tuareg Shield (see Figure 3).

2.1. Precambrian basement

The Precambrian basement of the Saharan Platform is characterized by the N-S running Trans-Saharan Lineaments (TSL), cross-cutting a large region that expands from Algeria and Libya in the north, to Niger in the south. These lineaments constitute one of the three large systems of discontinuities present in North Africa (Guiraud et al., 2000). Arrangement of the TSL is a consequence of a collisional tectonics during the Pan-African orogeny. The lineaments played an important role in development of sedimentary cover and in origin of some geological structures (e.g., mud mounds). A small number of direct

data makes it difficult to recognize details of the structural pattern of the Trans-Saharan Megabelt in areas were the Precambrian rocks are covered by younger deposits. Large uncovered area present in the Tuareg Shield, however, shed light for its structure.

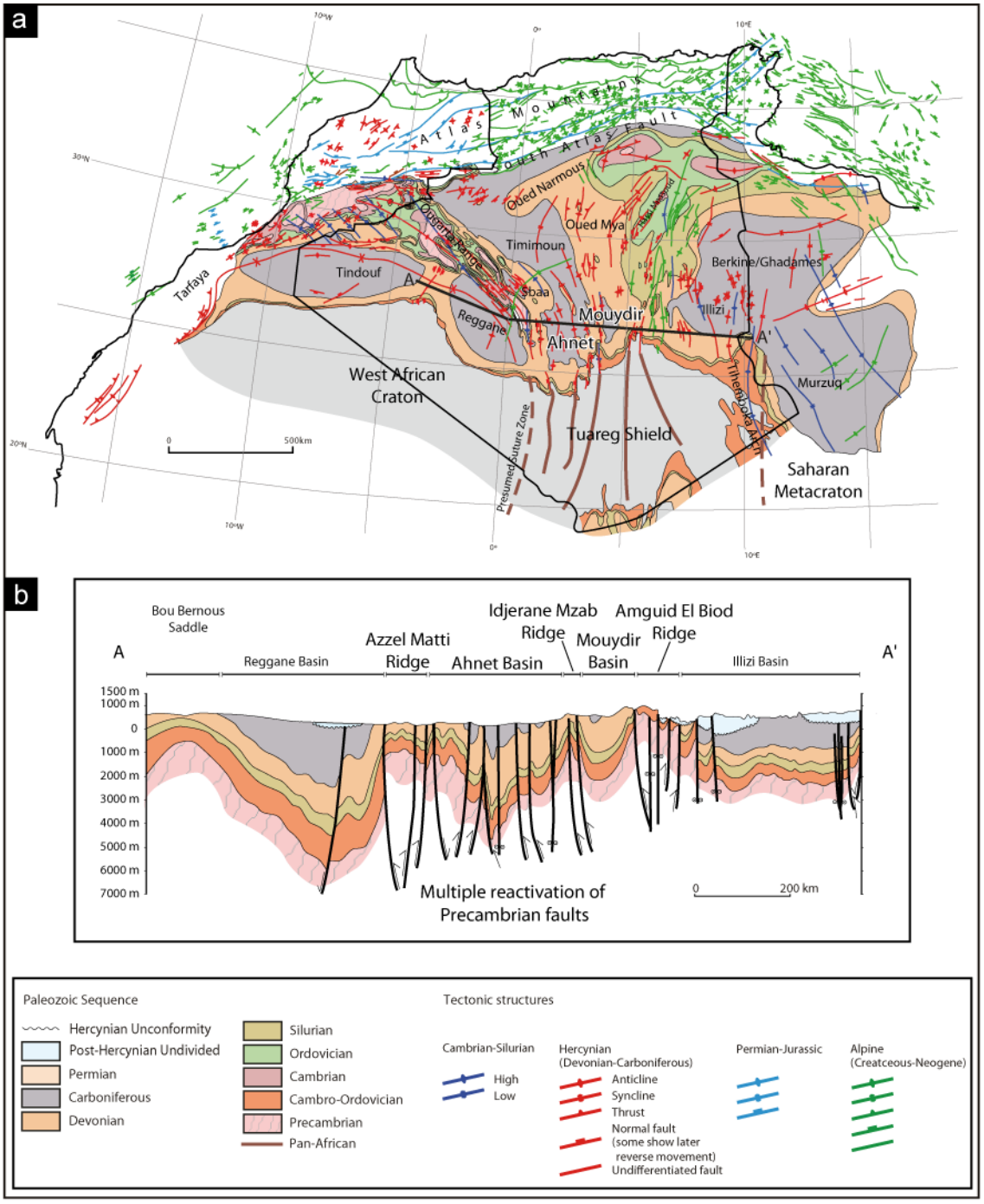

Figure 2. (a) Hercynian subcrop map and age, and nature of the main structural elements across North Africa (adopted from Craig et al., 2006; modified). (b) Regional cross-section along the A-A' line through the Reggane, Ahnet, Mouydir and Illizi basins illustrating their geometry and the distribution of the main structural units (adopted from Craig et al., 2006; modified).

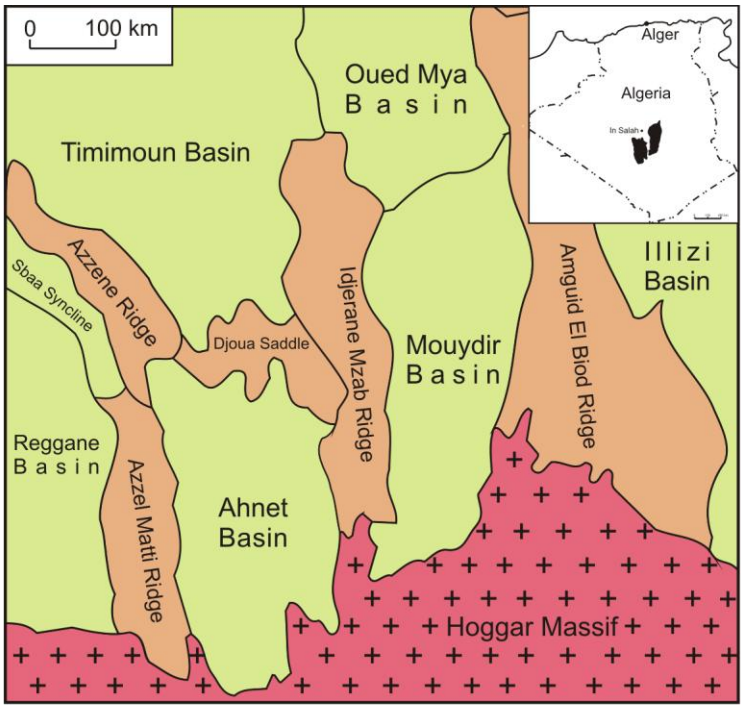

Figure 3. Schematic map showing location of the Ahnet and Mouydir basins, and the surrounding areas (modified after Askri et al., 1995).

The Hoggar Massif in Algeria, the Adrar des Iforas segment in Mali and the Aïr segment in Niger together form approx. 1000 km wide domal structure of the Tuareg Shield. With an average elevation above 900 m it is a predominant element of the south Algerian landscape. It contains several crustal blocks and islands arcs amalgamated during the Pan-African orogenic events along with generally N-S trending subduction zones. Based on age, nature and evolution of the individual parts the Tuareg Shield is interpreted as a blend of displaced terranes separated by suture zones (Black et al., 1994). Subduction zones underwent after collisions transformation into strike-slip ductile shear zones which represent crustal scale terranes boundaries. Because of their precise N-S running their position can be given in longitude units (e.g., 4°50'E shear zone or 8°30'E fault). Major shear zones and faults subdivide the Tuareg Shield into three well individualised domens (Figure 5). From the west to the east, these are:

(1) The Pharusian belt; it consists of two branches (western and eastern) separated by the Archaean In Ouzzal-Adrar des Iforas granulite terrane. The western Pharusian belt consists of various Middle and Upper Proterozoic metasedimentary, igneous and volcanic rocks affected by the Pan-African metamorphism. It represents an active continental margin and contains the main suture zone between the WAC and the Pan-African orogen. The eastern

Pharusian belt is build of Upper Proterozoic clastic deposits intruded by various types of magmatic rocks. The succession is considered as molasse deposits.

(2) The Central Policyclic Hoggar (LATEA Metacraton); the domain comprises terranes located between 4°50'E and 8°30'E faults. It consists of the Archaean and Proterozoic deformed, high-grade metasediments reactivated during the Pan-African orogeny and intruded by large volume of the Upper Proterozoic granites. The LATEA metacraton represent a passive continental margin.

(3) The Eastern Hoggar; terranes within this domain are regarded as the western margin of the Saharan Metacraton delimiting Trans-Saharan Megabelt to the east. They are composed of wide range of gneisses and migmatites intruded by alkaline magmatic bodies.

Some few borehole and geophysical data provide indication that the tectonic pattern of the Tuareg Shield prolongates northwards under the sedimentary cover of the TSM. Hence, it appears that the Ahnet and Mouydir basins are floored by the Pharusian belt (Askri et al., 1995).

2.2. Phanerozoic sedimentary cover

Cambro-Ordovician. The Precambrian basement is unconformably (the "Intratassilienne" unconformity) covered by broadly homogeneous, monotonous succession of continental and shallow marine siliciclastics, dominantly sandstones with a few siltstone and shale intervals (classically called the "Grès Inferiures"). The succession begins with the Ajjers Formation mainly consisting of superimposed channels complexes. The channels are elongated, over several hundreds of meters in length and few meters in width. They are filled with alternating, cross-bedded clastics ranging in grain size from pebbles to silt. Dominant are coarse- to medium-grained sandstones that include arcoses and quartz arenits with intraformational conglomarates of reworked siltstones (Bennacef et al., 1971; Beuf et al., 1971; Selley, 1997). Detailed sedimentological analysis led Beuf et al. (1971) to conclude that the sediments were transported in braided or anastomosed streams. In the middle part of the Ajjers Formation the basal irregularly bedded sandstone bodies progressively pass into parallel layered cross-bedded strata with *Skolithos* and other various trace fossils. Bioturbated sandstones in the upper part of the formation are followed by alternating coarse-grained, cross-bedded sandstones and fine ripple-marked sandstones and well-sorted pure-quartz sandstones (Bennacef et al., 1971). Because of lack of stratigraphic index fossils the age of the Ajjers Formation was a subject of speculation for a

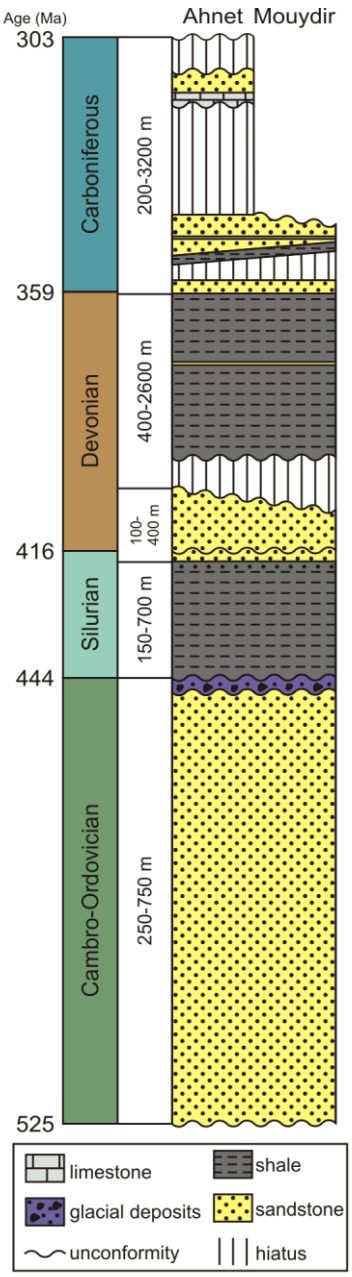

Figure 4. Schematic litostratigraphic column of the Ahnet and Mouydir basins (compiled after Follot, 1952; Beuf et al., 1971; Wendt et al., 2006, 2009 and Vecoli et al., 2008; absolute ages after International Stratigraphic Chart, 2009).

long time. Trace fossils, poor brachiopod fauna in the upper part and the relation to the basement and the overlying strata enabled to attribute this formation to the Late Cambrian-Early Ordovician age (Beuf et al., 1971). Recent palynological investigation, however, indicates that the most of the Ajjers Formation is Middle Cambrian in age (Vecoli et al., 2008). The thickness of the formation changes from 120-150 m in the western Ahnet Basin to 300 m towards the east, and reaches a maximum of 400 m in the western Mouydir Basin (Beuf et al., 1971). The deposition of the Ajjers Formation was followed by the Ordovician transgression resulted in accumulation of well-sorted, medium- and fine-grained, cross-bedded quartzites with *Skolithos* trace fossils, interbedded with argillaceous micaceous siltstones deposited in a shallow marine/deltaic environment. This sequence has been termed the In Tahouite Formation (Bennacef et al., 1971). It attains a thickness of 220-280 m in the western Ahnet Basin, whereas in the eastern part and in the Mouydir Basin it is significantly thinner with only 75 to 100 m.

During the latest Ordovician, due to short-lived (500 Ky to 1 Ma) policyclic glaciations in the western Gondwana, the shallow-marine/fluvial regime underwent a change into the glacio-marine one (Craig et al. 2006). Its record consists of 50-250 m of diamictites, glacio-fluvial sandstones with a wide spectrum of sedimentary structures described as the Tamadjert Formation (Beuf et al., 1971). The ice sheet caused erosion of older deposits, incision of a deep valleys, disturbance of soft sediments and development of a strong glacial relief (Fabre et al., 1976). Recent investigation of Le Heron & Craig (2008) in the Ahnet Basin documented the presence of zones of glacial deposits, 50-100 m wide and 200-300 km long, with a thickness of 60 to 100 m, interpreted as remains of palaeoice-streams.

Silurian. Ice melting and related rapid eustatic sea-level rise generated a transgression in Early Silurian time. The sea entered the glacial palaeorelief and established fully marine regime. Palaeodepressions were filled with 3 to 37 m of dark, organic-rich graptolitic shales (Lüning et al., 2000). This characteristic unit called the "hot-shales", yielding a high organic carbon content up to 17%, is responsible for the origin of 80-90 % of Palaeozoic-sourced hydrocarbons in North Africa and is the most important petroleum source-rock of the entire North African region (Macgregor, 1996; Boote et al., 1998). The "hot shales" are followed by a monotonous succession of black shales with a rather low content of organic matter. The entire shale sequence is described as the Tanezruft Formation and reaches a thickness of 600-700 m in the Ahnet Basin and decreases eastwards attaining max. 150 m in the Mouydir Basin (Follot, 1952). The shales sequentially pass up into clastic unit termed the Acacus Formation (Selley, 1997). It is attributed to the uppermost Silurian and consists of medium- to very fine-grained, well sorted marine sandstones with common trace fossils. Classically, the Acacus Formation is taken as a transition zone to the Lower Devonian sandy deposits and together are distinguished as the "Grès Superieur" (Beuf et al., 1971).

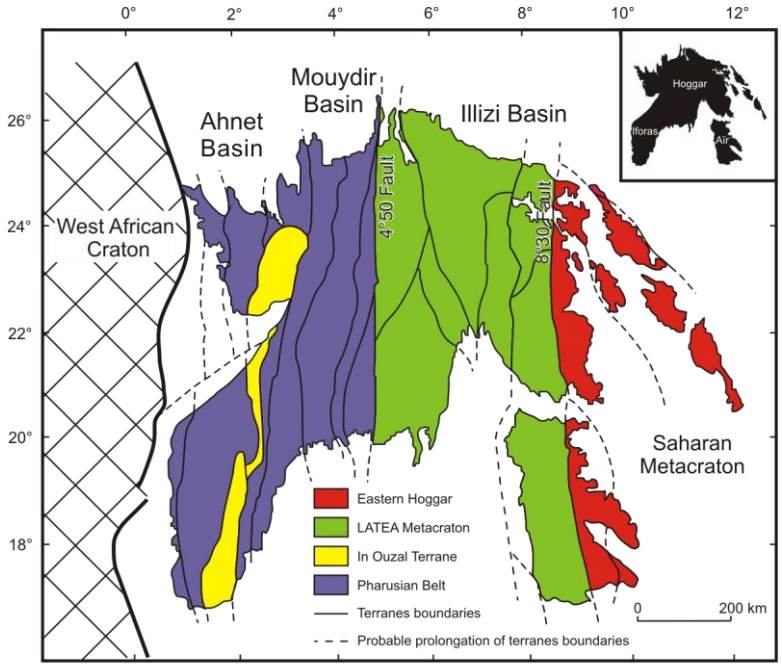

Figure 5. Map of the Tuareg Shield presenting three individualised structural domens (after Black et al., 1994; modified). For location of the Tuareg Shield see Figure 2.

Devonian. Sandy, coarse-grained deposits of the Upper Silurian reflect a regression trend which continued in the Early Devonian. As a result a change of depositional regime from fully marine to shallow marine/continental conditions occurred. Siliciclastic deposition in the Ahnet-Mouydir area was interrupted by erosional events connected probably with the Caledonian orogeny (Follot, 1952; Beuf et al., 1971; Fekirine and Abdallah, 1998). In the south, deposits show continental/fluvial regime, passing into deltaic/shallow-marine towards the north and the northwest (Wendt et al., 2006). The Lower Devonian sequence mainly consists of a cross-bedded sandstones with levels of trace fossils, siltstones, shales, conglomerates and oolitic intercalations. Detailed sedimentological analysis carried out by Beuf et al. (1971) showed that the Lower Devonian strata similar to the Cambro-Ordovician succession was deposited within a SE-NW directed meandric fluvial system that sheded detritus from the area of the Hoggar Massif. The total thickness of the "Grès Superieur" is relatively uniform (100-200 m) in the most of the Ahnet area; only in the north-western Ahnet Basin and central, and eastern Mouydir Basin the unit is 300 to 400 m thick (Beuf et al., 1971).

The Early Devonian continental regime was followed by the Middle Devonian sea-level rise that marks the onset of fully marine conditions. In consequence a transgressive conglomerate, a basal unit of the Argiles de l`Adrar Morat Formation was deposited. The formation consists mostly of silty greenish shales with thin interlayers of fine-grained sandstones and calcareous mudstones. Its thickness varies strongly across the area. Whereas on the ridges highly reduced thickness values from 0 to 15 m are present, basinal parts are characterized by a wide range of thickness from 10 to 140 m. The l`Adrar Morat Formation gradually passes into well-bedded, dark, partly bituminous limestones named the Calcaire de Azzel Matti Formation. It represents a shallow open-marine environment passing laterally into basinal areas with prevailing shale sedimentation. The thickness pattern exhibits similar trends to that of the underlying unit. On the ridges it is highly reduced (2 to 25 m), whereas in the basinal sectors of the Ahnet and Mouydir basins it ranges from 25-50 to 500-1000 m.

The Middle Devonian deposits are covered by the Frasnian Argiles de Mehden Yahia Formation consisting of bituminous limestones with interlayers of black shales and limestone nodules in the lower part. Black shales are characterized by a high content of organic matter (total organic carbon up to 14 %) and considered as an important source rock in North Africa, second next to the Silurian "hot shales" (Macgregor, 1996; Boote et al., 1998). Major part of the unit forms a monotonous sequence of varicoloured clays with

rare calcareous mudstone levels. Clays are followed by the Grès de Mehden Yahia Formation consisting of a thin-bedded, medium-grained sandstones and clays. The thickness of the unit changes from 100-400 m in the western Ahnet Basin to 650-700 m in the eastern Mouydir Basin; it is slightly lower on the ridges in comparison to the adjacent basins. A monotonous clay deposition continued during the Famennian with the Argiles de Temertasset Formation consisting of grey and reddish clays with layers of carbonates and conglomerate, and lenticular intercalations of peebles. Their thickness attains values from 350-600 m to 1100 m in the Ahnet Basin and 450-860 m in the Mouydir Basin. In sum, the total thickness of the Devonian strata reaches 450 m to 2600 m (Beuf et al., 1971; Wendt et al., 2006).

Carboniferous. The Lower Carboniferous deposits are widely present in the study area. In contrast, the Upper Carboniferous strata are only preserved in some isolated occurrences in the northern and western Ahnet Basin. The Carboniferous succession was described in detail by Conrad J. (1984) and recently it was reinvestigated by Wendt et al. (2009). It represents three large (1^{st}, 2^{nd} and 4^{th}) and one minor (3^{rd}) transgression-regression cycles: the first cycle comprises the Upper Tournaisian rocks, the second one encompasses the uppermost Tournaisian and the lowermost Visean. The third cycle comprises the lower Visean and the fourth cycle the Bashkirian-Moscovian rocks. There is no sedimentary record of the latest Carboniferous. In sum, the thickness of the Lower Carboniferous succession in the Ahnet-Mouydir area varies from at least 195 to 2200 m. The Upper Carboniferous deposits attain at least 550-1100 m. Consequently, the total thickness of the Carboniferous reaches at least 745 to 3300 m (Conrad J., 1984; Wendt et al., 2009). The Carboniferous succession in the Ahnet-Mouydir area is interrupted by two prominent stratigraphic gaps (Wendt et al., 2009). The first gap separates the first cycle from the underlying uppermost Famennian and lowermost Tournaisian rocks. The second gap is significantly longer. It includes the middle and late Visean as well as the Serpukhovian time interval. Erosion during this time was probably related to the early and middle Visean regional uplift interpreted as first pulse of the Variscan orogeny (Fabre, 1988).

The Carboniferous begins with clastics of the Grès du Khenig Formation which is late Famennian to early Tournaisian in age. This unit in its lower part consists of alternation of siltstones and fine- to medium-grained, cross-bedded sandstones, with common current and oscillations ripples, ball-and-pillow structures. In contrast, it contains in the upper part several lenticular fossiliferous, calcareous intercalations, the number of

which increases towards the top. Depositional environment is interpreted as a transition from predominantly deltaic in the west and north-east, across open-marine conditions in the centre of the area, to fluvial regime in the south and east (Conrad J., 1984). The thickness of the Grès du Khenig exhibits a minimum 85 m in the western Ahnet Basin and increases towards the east, up to 310 m. In the Mouydir Basin the formation attains a thickness from 75 to 145 m (Conrad J., 1984; Wendt et al., 2009).

The sandstone lithology of the Grès du Khenig is unconformably overlain by predominantly argillaceous sequence of the Tournaisian Argiles de Teguentour Formation which constitutes the basal part of the first cycle. The shaly unit contains rare layers of calcareous nodules in its lower part, and some thin intercalations of fine-grained sandstones higher up in the sequence. Its thickness attains a minimum of 65 m in the western Ahnet Basin and reaches 350 m in the SE part of the basin. In the Mouydir Basin, the formation exhibits a thickness ranging from 100 to 260 m (Conrad J., 1984; Wendt et al., 2009). The Argiles de Teguentour Formation passes continuously into a prominent Tournaisian clastic unit termed the Grés de Tibaradine Formation dominated by cyclic cross-bedded sandstones with thin shales and siltstone intercalations. Frequent ball-and-pillow and dewatering structures attests a very rapid sedimentation. The thickness of the unit changes from 55 m in the western Ahnet to 220 m in the Mouydir Basin (Wendt et al., 2009).

Overlying is the late Tournaisian Formation des Iridet consisting of sequence of several limestone layers (up to 1 m thick) that are separated by dark shales. The unit begins the second transgressive-regressive cycle. Its thickness varies from 1 m in the south-eastern Ahnet Basin to 170 m in the cental part of the basin. In the Mouydir Basin the formation has a thickness of at least 20 m (Wendt et al., 2009). The upper portion of the cycle forms predominantly argillaceous the Argiles de Tirechchoumine Formation encompasses a monotonous clay succession intercalated by numerous thin (10-20 cm) layers of skeletal limestones. Thickness of the unit vary from 40 to 480 m in the Ahnet Basin and attains only 50 m in the Mouydir Basin. Due to minor oscillations of sea level, however, eastwards the clays in the lower part of the unit are replaced laterally by clastics of the Grés de Kreb ed Douro Formation. The unit marks local lowstand conditions and is considered as beginning third, minor cycle within second, longer cycle (Wendt et al., 2009). The unit is composed of cyclic shale-siltstone-sandstone alternations deposited in the prodelta environment. The highest thickness of 220 m was recorded in the central and northern Ahnet, and of 200 m in the Mouydir Basin (Conrad J., 1984; Wendt et al., 2009).

A prominent sandstone unit, the Grès de Garet-Dehb Formation, terminates the second cycle. It deposited under regressive conditions and consists of predominantly thin-bedded, cross-laminated sandstones with shale and siltstone intercalations. Locally, gypsum layers occur recording intemittent sebkha conditions (Wendt et al., 2009). In the western and northern parts of Ahnet fluvial channels originated within deltaic environment are present (Conrad J., 1984). The thickness of the unit is highly variable. Whereas in the north-western Ahnet the unit is completely eroded, further south and east it reaches 450 m in thickness. In the entire Mouydir Basin, the formation has been completely removed by erosion (Wendt et al., 2009).

The sandstones of the Grès de Garet Dehb are unconformably covered by the lower Bashkirian Calcaires du Djebel-Berga Formation consisting of a cyclic alternation of skeletal limestones, shales and cross-bedded sandstones. This lithology is interpreted as reflecting a shallow-marine, neritic environment, mostly above the storm wave base. The thickness of the unit shows fluctuations between 300 and 400 m in the Ahnet (Wendt et al., 2009). The overlying Gypses d`Hassi Taibine Formation was deposited under sebkha conditions. It encompasses sequence of gypsum and salts interrupted by several thin skeletal limestones layers (Wendt et al., 2009). The most complete sequence occurs in the north-westernmost part of the Ahnet Basin, where it reaches thickness of 110 m. Southwards, it decreases to 50 m; in the east only 20 m of the lower part of the formation is preserved (Conrad J., 1984). During the middle Bashkirian the shallow-marine/deltaic environment evolved into the continental one. Rocks deposited during this time (the Formation Rouge) contain three, probably coeval lithostratigraphic units (Conrad J., 1984). In the north-western tip of the Ahnet Basin, the Ain-ech-Chebbi Formation was described. It is composed of red sandy clays passing into fluvial cross-bedded sandstones and microconglomerates with plant remains. Exposed part of the section comprises a 500-550 m thick sequence. In the west-central part of the Ahnet Basin, however, the Azzel-Matti Formation (at least 250 m thick) consisting of lacustrine carbonates with lenses of gypsum and layers of red siliciclastics was distinguished. In the northern part of Ahnet, however, a 230 m thick sequence of the Hassi-Bachir Formation was described. It is composed of red, cross-bedded sandstones with plant debris and clays in the lower part and carbonates with stromatolites in the upper part. The upper boundary of the Formation Rouge is placed into the earliest Moscovian (Conrad J., 1984).

The Carboniferous sedimentary record terminates the Palaeozoic succession in the investigated area. The Permian was period of erosion in southern Algeria (Conrad G., 1969;

Conrad J., 1984). The entire preserved Palaeozoic infill of the Ahnet Basin reaches a thickness from at least 1700 to at least 7100 m. In the Mouydir Basin, however, its thickness is lower and attains from at least 1550 to at least 4800 m (Figure 6).

Mesozoic. In the Ahnet and Mouydir basins the Mesozoic deposits are not present. Data of Conrad G. (1969) and Conrad J. (1984) provide evidence for an extensive erosion during Triassic time. Model calculations suggest that Mesozoic rocks were probably never deposited in the basins itself (Makhous & Galushkin, 2003). But north of the Ahnet Basin Mesozoic continental clays with thin sand intercalations occur. They are approx. 200 m in thickness and probably of Early-Middle Jurassic in age. Overlying are 600-700 m of supposed Lower Cretaceous fluvial sandstones (the "Continental Intercalaire"). These are followed by about 300 m of the Upper Cretaceous mudstones (Logan & Duddy, 1998).

Cenozoic. The sedimentary record of the Cenozoic comprises aeolian and fluvial sandstones with pebbles of the Palaeozoic rocks as well as clays, up to 100 m in thickness. The surfaces of sandstones and clays are covered by crust made up of several generations of recent evaporates and desiccation structures originated under dry climate conditions (Conrad G., 1969).

2.3. Tectonic evolution

The North African continental crust originated as a result of several collisional events between the West African Craton, the Saharan Metacraton, and numerous island arcs and terranes during the Pan-African orogeny (e.g., Black et al., 1994). The amalgamation of these crustal components led to development of two major orogenic belts, the East African Orogen and the Trans-Saharan Megabelt. The latter is forming the basement of the younger successions in the Ahnet-Mouydir area. A prominent feature of the Trans-Saharan Megabelt is N-S running system of strike-slip faults (Precambrian lineaments). The formation of the Pan-African orogenic belts was followed by a period of intracontinental rifting during the Late Neoproterozoic to the Early Cambrian. Extension caused origin of series of tectonic grabens (In Semmen and Ouallen, for instance) which were filled with molasse. Early Cambrian rifting phase was followed by a period of regionally extensive erosion which leveled Precambrian structures into northerly dipping pediplane. During the Early Palaeozoic, up to mid-Silurian time, North African region was in a sagging stage. Some relief on pediplane was possibly already developed at this time.

		name of formation	Ahnet Basin		Mouydir Basin	
			minimum thickness	maximum thickness	minimum thickness	maximum thickness
Carboniferous	Pennsylvanian	Rouge	> 230 m	> 550 m	0 m	0 m
		Gypses d`Hassi Taibine	20 m	110 m	0 m	0 m
		Calcaires du Jebel Berga	300 m	400 m	0 m	0 m
	Mississippian	Grès de Garet Dehb	0 m	400 m	0 m	0 m
		Argiles de Tirechchoumine	40 m	480 m	no data	50 m
		Grès de Kreb ed Douro	a few m	220 m	no data	200 m
		Iridet	1 m	170 m	>20 m	no data
		Grès de Tibaradine	55 m	190 m	no data	220 m
		Argiles de Teguentour	65 m	350 m	100 m	260 m
		Grès du Khenig	85 m	310 m	75 m	145 m
Devonian	Upper	Argiles de Temertasset	350 m	1100 m	450 m	860 m
		Grès de Mehden Yahia	>80 m	750 m	160 m	700 m
		Argiles de Mehden Yahia				
	Middle	Calcaire de Azzel Matti	0 m	300 m	1 m	1060 m
		Argiles de l`Adrar Morat				
	lower	Grès Superieur	100 m	400 m	300 m	365 m
Silurian		Tanezruft	no data	700 m	no data	150 m
Cambro-Ordovician		Tamadjert	50 m	125 m	70 m	250 m
		In Tahouite	75 m	280 m	75 m	100 m
		Ajjers	120 m	300 m	300 m	400 m
		total thickness	at least ~1700 m	at least ~7100 m	at least 1550 m	at least ~4800 m

Figure 6. Thicknesses of the Palaeozoic formations in the Ahnet-Mouydir area (names of the formations after Beuf et al., 1971 and Wendt et al., 2006, 2009; thickness data after Follot, 1952; Beuf et al., 1971; Conrad J., 1984 and Wendt et al., 2006, 2009).

It was associated with increased subsidence within the pre-existing Early Cambrian rifts, leading to setting of sedimentary basins separating by minor structural highs (Craig et al., 2006). Some of Precambrian lineaments may have experienced strike-slip displacement during the Cambro-Ordovician (Coward & Ries, 2003). In the Late Silurian-Early Devonian minor in amplitude but regionally extensive inversion of the basins occurred. It was related probably to the Caledonian orogeny (Follot, 1952; Beuf et al., 1971; Fekirine & Abdallah, 1998). Middle Devonian tectonic movements activated again the Precambrian faults that bordered the basins. In consequence, some blocks were uplifted and this created the characteristic basin-and-ridge topography (Wendt et al., 1997, 2006). During the Middle and Late Devonian, and the Carboniferous the basins were subjected generally to transtensional regime.

The Palaeozoic sedimentation in the Ahnet and Mouydir basins was terminated by an uplift that was followed by faulting in Late Carboniferous/Early Permian time. Deformations were related to far-filed continuous strain of the Variscan compression associated with the collision between Gondwana and Euramerica palaeocontinents (Haddoum et al., 2001; Zazoun, 2001). Although, both basins were distant about 2000 km from the main collision zone, the Palaeozoic underwent erosion, folding and faulting. Folds are NW-SE to longitudinal in running. They originated in result of NE-SW tectonic shortening. Folding affected the entire Palaeozoic succession, but the largest and the most frequent structures can be observed in the Devonian and Carboniferous rocks. Folds are usually asymmetric and sometimes show undulated axes. The Variscan compression leaded also to the origin of numerous mainly N-S trending reverse faults into Palaeozoic rocks. The most dense system of discontinuities occurs within brittle Cambro-Ordovician rocks. It is significantly less frequent in the younger rocks and tend to damp in Upper Devonian shales. Apart folding and faulting the Variscan tectonic forces caused reactivation of the Precambrian lineaments. They exhibit several slickensides, transpression structures and drag folds indicating dextral strike-slip movement.

During the Triassic and the Jurassic, the evolution of North Africa was dominated by strong rifting resulted in opening of the Central Atlantic and Tethys oceans. This event marks the onset of extensional tectonic regime across large region including central and eastern Algeria (Craig et al., 2006). Around the Jurassic/Cretaceous transition some tectonic deformations across North Africa, including investigated area were recorded. These deformations were connected with the approaching of Africa to the European plate and first pulses of the Alpine orogeny (Guiraud et al., 2005).

New palaeomagnetic data of Smith et al. (2006) and Derder et al. (2009) revealed importance of the post-Jurassic tectonics in the Saharan Platform. The Variscan orogeny commonly considered as the main mechanism of deformations within the Palaeozoic rocks (e.g., Fabre et al., 1976, 2005; Haddoum et al., 2001; Zazoun, 2001) seems be responsible only for limited tilt initiating folding. The main phase of deformations was probably related to far-filed stress of the Cimmerian or the Austrian compressional phases (Smith et al., 2006; Derder et al., 2009).

A very important Mesozoic phenomenon was an uplift of the Tuareg Shield. Liégeois et al. (2005) stated that this uplift took place before Cretaceous time and was connected with the Alpine tectonics. It resulted in a partial inversion of the sedimentary basins along the northern margin of the Hoggar Massif and erosion of significant portion of the Palaeozoic sedimentary succession.

In the Cretaceous-Early Cenozoic the sedimentary basins underwent inversion caused by a collision between Europe and Africa. The Alpine compression resulted in reactivation of Precambrian lineaments. Some of them experienced a small displacement (Guiraud, 1998; Guiraud et al., 2005). During middle Cenozoic time North Africa was affected by a continental rifting phase. Its greatest impact can be observed in the eastern part of the region in the origin of the East African Rift system. In the investigated area, however, more important was the Pleistocene tectonics. Wendt et al. (2008) found faults and cracks cross-cutting Pleistocene fluvial terraces as well as older, Silurian and Devonian rocks. They commonly are associated with intense Fe-mineralization and a variety of accompanying, secondary minerals that formed in a subrecent continental regime under pluvial to arid conditions. The Ahnet and Mouydir basins were also affected by recent compressional regime associated with continuous northward drift of Africa. Chorowicz & Fabre (1997) reported minor vertical displacements along Precambrian lineaments and the origin of numerous new relatively small discontiniuties.

2.4. Magmatic activity

In consequence of the opening of the Central Atlantic in large areas around there occur intrusions of magmatic rocks (the Central Atlantic Magmatic Province, CAMP). The biggest concentration of the magmatic bodies in the NW Africa occurs in Mali, Guinea, Liberia and Morocco. The sedimentary cover has been intruded by dykes, sills as well as layered plutons (Wilson & Guiraud, 1998). In Algeria, the occurrence of magmatic rocks is limited only to the western part of the country. Their $^{40}Ar/^{39}Ar$ plateau ages show peak of

the magmatic activity at 192.7 ± 3 Ma and 198.9 ± 1.8 Ma in the Reggane Basin (Chabou et al., 2007). Intrusions related to the CAMP are also present in the northern part of the Azzel Matti Ridge. They are represented by doleritic sills, up to 15-20 m in thickness (Smith et al., 2006).

A strong volcanic activity took place in North Africa during the Cenozoic. It was expressed by the origin of large volcanic fields along the East African Rift system and several relatively smaller fields in the central part of the North Africa. First pulses of the magmatic activity are dated on Late Eocene, whereas its peak fell in Miocene time (Wilson & Guiraud, 1998). Volcanism was also present in the central and eastern Tuareg Shield (Adrar N`Ajjer, Ananet, Atakor, Egéré, In Ezzane, Manzaz, Tahalra, Todra fields). The magmatic activity in the Tuareg Shield is commonly linked with a mantle plume (e.g., Ebinger & Sleep, 1998; Aït-Hamou et al., 2000). But lack of the thermal anomaly associated with these magmatic fields (Lesquer et al., 1988, 1989), led to a proposal of an alternative model. According to Liégeois et al. (2005), mantle material was uplifted by edge-driven convection along the Pan-African lineaments which have been reactivated during the Alpine orogeny.

2.5. Thermal regime of southern Algeria

Measurements of modern heat flow in Algeria revealed the presence of a east-west trending zone with elevated heat values (90-130 mW m^{-2}) across the Saharan basins (Takherist and Lesquer, 1989; Lesquer et al., 1990) (Figure 7). It has been recognized as a part of much larger area with an anomalous hot crust (heat flow > 80 mW m^{-2}) extending from the Canary Islands to Libya. In Algeria, its axis runs across the In Salah and Illizi region. In the northern part of the country there is also differentiation in the heat flow intensity. In contrast to the southern part, the heat flow pattern forms zones which are trending essentially north-south and exhibit heat-flow values below 80 mW m^{-2}. In the south, however, a significantly colder crust was detected in the Tuareg Shield (see Figure 7). Its average heat flow amounts from 40 to 55 mW m^{-2}, which is typical level for the Precambrian belts elsewhere. Even the Cenozoic volcanic fields in the Tuareg Shield are not associated with a positive anomaly in heat flow (Lesquer et al., 1988, 1989). Low values of the heat flow (average 30 ± 10 mW m^{-2}) were measured also in the West African Craton (Lesquer et al., 1989).

The anomalously hot crust detected under the Saharan basins is linked with a metasomatic and rift-like modification of the upper mantle, between the Moho and the

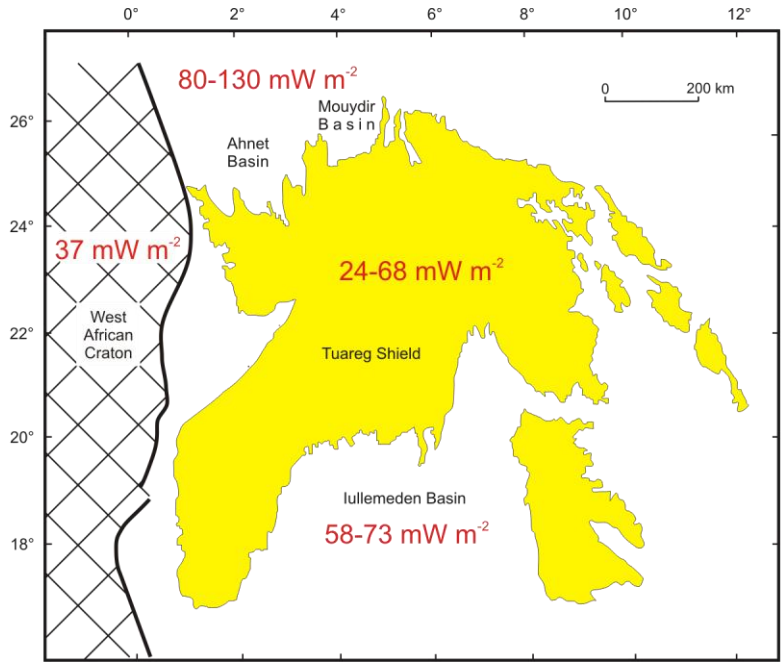

Figure 7. Heat flow values for the Tuareg Shield and surrounding areas (heat flow values after Lesquer et al., 1989, 1990; boundaries of the Tuareg Shield and the West African Craton after Black et al., 1994). For location of the Tuareg Shield see Figure 2.

depth of 160 km. Unfortunately, the time of the origin of this anomaly remains unknown (Lesquer et al., 1990). Moreover, very scarce data from marginal parts of the Hoggar Massif make it very difficult to trace the extension of the anomaly to the south. Recent teleseismic investigation of Ayadi et al. (2000) supports assumption of Lesquer et al. (1990) and points to the existence of anomalous mantle under the Saharan sedimentary basins. These authors placed the southern limit of the anomaly near the latitude 26°N which corresponds with the northern limit of the Tuareg shield.

The present-day high heat flow associated with the Saharan basins produces a geothermal gradient that is significantly higher than those measured in the rest of the NW Africa. According to Logan and Duddy (1998), it ranges from 34°C/km to 45°C/km in the Ahnet Basin. Makhous and Galushkin (2003), however, provided values of 55°C/km for the Ahnet Basin and 30-50°C/km for the Mouydir Basin. In contrast to well-recognized modern heat production in the crust, the past geothermal gradients are poorly known. The most precise data were calculated for Mesozoic time. Logan & Duddy (1998), based on apatite fission track analysis, estimated 60-70°C/km to more the even 100°C/km for the Late Triassic-Early Jurassic interval and linked it to a phase of intensive magmatism. Their estimations for the Palaeozoic are not precise; they only suggested a rather low heat during this time.

3. PREVIOUS WORK

A pioneer reconnaissance in the Ahnet-Mouydir area was carried out by French geologists in the beginning of the XXth century and exploration continued up to the 50`s (summary in Follot, 1952). With the discovery of the hydrocarbon resources geological prospection was intensified in the second part of the XXth century. A first detailed description of the Cenozoic strata was published by Conrad G. (1969). An enormous contribution in the knowledge of Lower Palaeozoic rocks constituted the excellent sedimentological work of Beuf et al. (1971). The next milestone of great importance in documenting the Upper Palaeozoic sediments was the monograph of Conrad J. (1984). In more recent time, extensive work of Wendt and his co-workers significantly improved the Devonian and Carboniferous stratigraphy in both basins and provided a lot of data on their evolution and the depositional environments (Wendt et al., 1993, 1997, 2006, 2009). The Variscan tectonics and deformational structures was described by Haddoum et al. (2001) and Zazoun (2001). New data of Lüning et al. (2004) extended knowledge about anoxic conditions during Devonian time. A very significant reference to importance of Mesozoic tectonic movements in the Saharan Platform was recently provided by Smith et al. (2006) and Derder et al. (2009).

Geological prospection in the Ahnet Basin during the 50`s resulted in discovery of commercial quantities of gaseous hydrocarbon (summarized in Boote et al. 1998; Traut et al. 1998). Unfortunately, the most of information obtained from exploration wells is hidden in internal reports of oil companies operating in this area and it remains inaccessible up to now. Only some selected and rather skimpy information was published in proceedings of trade conferences. Askri et al. (1995), for instance, reported the thermal maturation of Silurian and Frasnian U-rich clays widespread in the entire Saharan Platform. Lounissi et al. (2007), however, provided a simulation for hydrocarbon generation scenario, in which the main stage of generation was postulated during Late Devonian time as a result of regional burial. More detailed data are contained in short abstracts. Cawley et al. (1995) and Takherist et al. (1995) suggested that oil was generated from the Silurian and Devonian source rocks during the Carboniferous burial which was followed by a cooling phase due to the Variscan uplift. The renewed heating should occur during Cretaceous time. Barwise et al. (2003) agreed with this interpretation, but in contrast, they recognized after the maximum burial during the Carboniferous a second heating event in Late Triassic time.

A detailed thermal history of the Ahnet Basin was published by Logan & Duddy (1998) based on apatite fission track analysis. They recognized an early stage of oil and gas

generation as a result of the Carboniferous burial with a “modest” geothermal gradient. This phase was followed by cooling related to the Variscan uplift. In addition, they postulated a second significant thermal activation with temperatures up to 300°C at approx. 200 Ma. This event was regarded as the most significant one which caused cracking of previously originated oil to gas. This Late Triassic treatment was followed by a minor increase of temperature caused by loading of Cretaceous rocks. Logan & Duddy (1998) also estimated the level of thermal maturity of Silurian and Frasnian rocks using the vitrinite reflectance. In contrast, the thermal history of the sedimentary infill in the Mouydir Basin is only poorly recognized.

A general overview of petroleum system in the Ahnet and Mouydir basins was presented by Klett (2000). His compilation comprises short characteristics of source rocks, seal, overburden and trap types as well as an assessment of recognized and potential resources. According to him, hydocarbon formation event took place during the Carboniferous both in the Mouydir and Ahnet basins. In the latter, however, Klett (2000) assumed a second event during Early Mesozoic time.

Another scenario is contained in the study of Makhous & Galushkin (2003). Their model performed by using the GALO software (see Makhous et al., 1997 for description) is based on several types of data from isolated wells. It assumes hydrocarbon generation in the Ahnet and Mouydir basins as a result of the Carboniferous burial, which has been suspended during the phase of Late Palaeozoic uplift and erosion. This model postulates also a significant thermal activation of litosphere related to the Late Jurassic magmatic activity and a heat transfer by magmatic bodies and hydrothermal fluids. This event was followed by a short cooling phase during the Early Cretaceous and renewed heat activation during the Late Cretaceous, which is continuing to the present day.

4. MATERIAL

The present investigation is based on 384 conodont samples recovered from 69 sections exposed in the Ahnet and Mouydir basins (Figure 8a, b, c). Register of samples with their characteristics is given in appendix. Conodonts are small (mainly 0.2-2 mm) mineral remains of primitive extinct marine animals of supposed chordates affinity (Aldridge et al., 1986). Conodont elements of different shape (Figure 9) were positioned in the head part of mainly 50 mm long animal with a slender laterally flat body and at least some of them formed a feeding apparatus. Some elements were too delicate for food fragmenting and probably they supported soft tissue. Mineral component of these microfossils was first recognized as francolite (Pietzner et al., 1969) and later redefined to fluorapatite (Belka, 1993). Conodont elements are composed of two laminated parts: the crown and the basal filling (Figure 9). The crown consists of fluorapatite layers with some addition of organic matter inbetween. It is build of two types of tissue. Hyaline tissue with lamellar structure comprises the major component of the crowns. Length of individual crystallites ranges from 1 to about 30 μm, but usually they have a few μm in length. In simple coniform elements the crystallites are arranged with their longer *c* axes parallel or sub-parallel to the long axis of the element. Thus, the entire crown is composed of single fan-like prism of crystallites. In conodonts with more complex morphology prismatic structure of the element is broken up into a number of individual prisms. Multidenticulate elements are structurally more differentiated than the crown of coniform elements. In consequence, parallel or sub-parallel arrangement of crystallites to the growth lines is not dominant, i.e. crystallites are usually oriented perpendicular to the outer surface. Crystallites adjacent to the basal cavity are inclined upwards and outwards relative to the junction of the crown with the basal filling (Donoghue, 1998). Additionally, surface between crown and basal filling is a surface of weakness along which these two parts readily separate. Consequently, after separation layers and crystallites of fluorapatite of crown are exposed and can easily interact with external factors (Sweet, 1988). Crystals in prisms are generally densely packed, but between their boundaries connected pores are present, up to tens of nanometers in size (Trotter et al., 2007). In contrast, denticles are composed of non-lamellar albid tissue consisting of much larger (hundreds of micrometres) crystallites than those in the hyaline tissue. Within crystals numerous apparently unconnected pores are present, which vary from nano- to microscale in size. The long, *c*-axes of the crystals are parallel or sub-parallel to the growth axes of denticles. Regions intermediate between hyaline and albid domains have a hybrid structure and host numerous

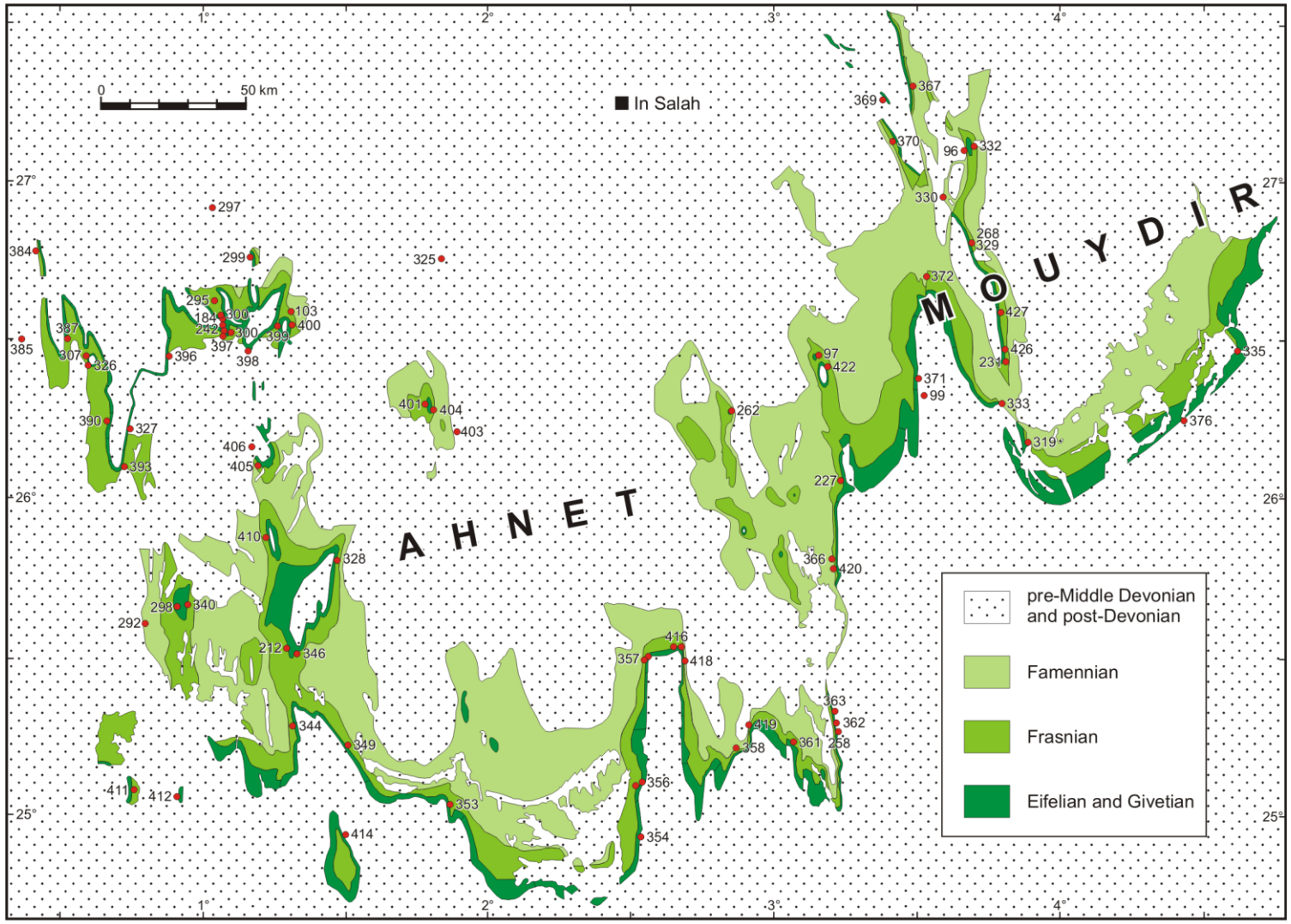

Figure 8a. Simplified geological map of the Ahnet and Mouydir basins showing the extension of Middle and Late Devonian strata, and the locations (numbered small red circles) of the sections and sample localities (after Wendt et al., 2006; modified). For number coding of sections see Figure 8c.

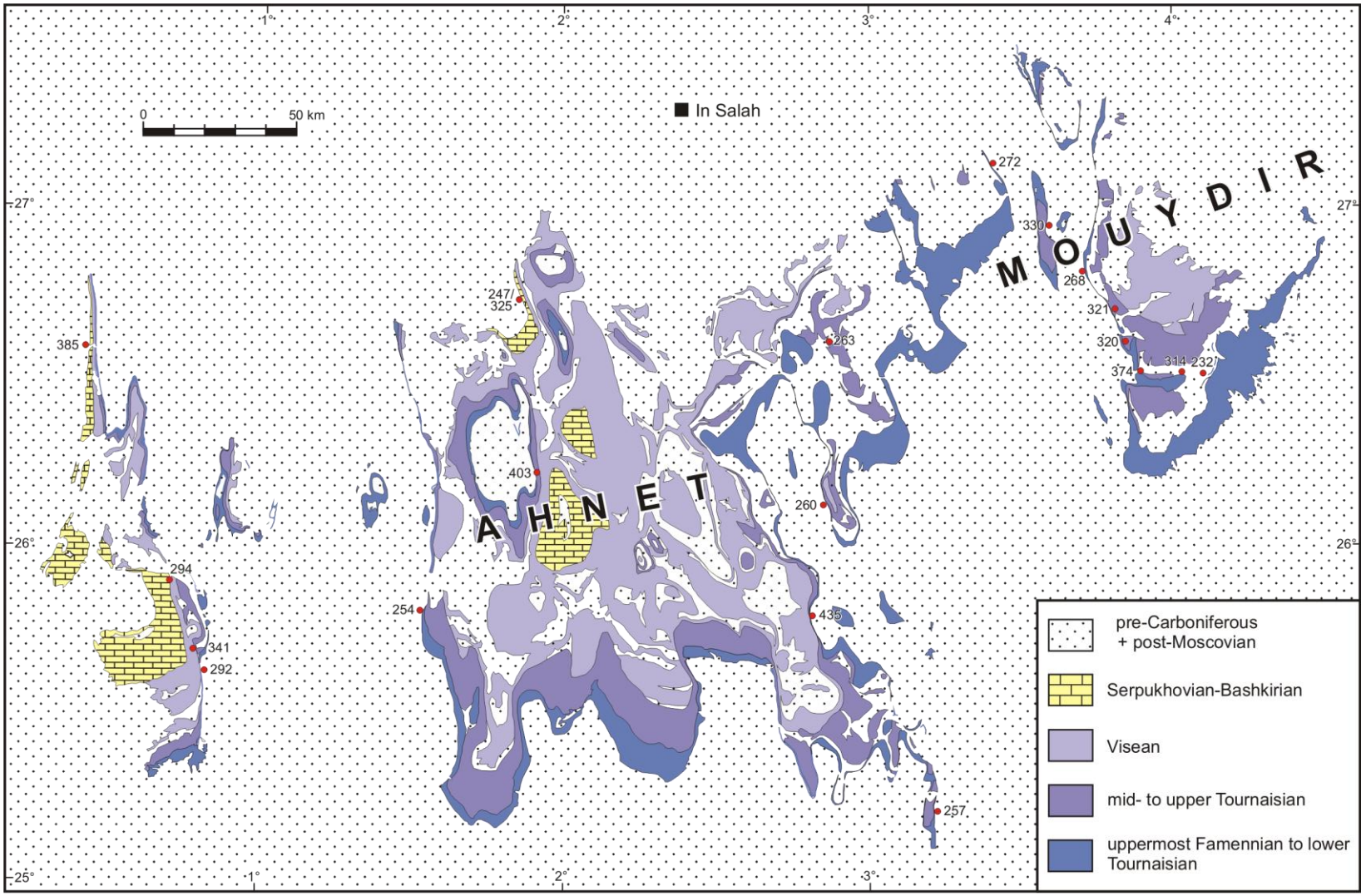

Figure 8b. Simplified geological map of the Ahnet and Mouydir basins showing the extension of Carboniferous strata, and the locations (numbered small red circles) of sections and sample localities (after Wendt et al., 2009; modified). For number coding of sections see Figure 8c.

A 96 Inahas
A 99 Tiguelguemine
A 184 Ouzdaf Atoll SW
A 212 Adrar Morrat SW
A 227 Hassi bel Rezaim
A 231 Ain Redjem
A 242 Ouzdaf Atoll SW
A 258 Tes Ereghet
A 260 SW of Erg Teguentour
A 262 SW of Erg Teguentour
A 268 Ain Behaga
A 292 WSW Gara Azzel Matti
A 295 Oued Ouzdaf N
A 297 Aoulef el Arab
A 299 Illirhene
A 300 Oued Ouzdaf intermound
A 307 Bled el Mas
A 319 Oued in Somar
A 320 Oued Temertasset
A 325 Jebel Berga
A 326 Bled el Mas
A 327 Djebel Tamamat
A 328 Adrar Morat N
A 329 Ain Behaga
A 330 N of Ain Tiouendjiguine
A 332 Ain Inahas
A 333 Ain Bagline
A 335 Rhedir
A 340 Azzel Matti
A 344 Adrar in Allarene W
A 346 Ain Tikkidine
A 349 Erg Tagsist
A 354 Adrar Tiressouine S
A 356 Tiressouine S
A 357 Adrar Tiressouine N
A 358 Adrar Tadioune W
A 361 Bel Khenafis
A 362 Imeddene-n-Azarif S
A 363 Imeddene-n-Azarif N
A 366 Tin Khelifa N
A 367 Ain Kahla
A 369 Jebel Assaz syncline
A 370 Jebel Assaz
A 371 Tiguelguemine
A 372 Ain Tidjoubar
A 376 Erg Teganet
A 385 Hassi Taibine
A 387 Jebel Aberraz
A 390 Jebel Tamamate S
A 393 Jebel Tamamat S
A 396 Gouiret ed Diab
A 397 Oued Ouzdaf
A 398 Sebkha Mekerhane N
A 399 Akabli
A 400 SW Oued in Tarhlift
A 401 Bahar el Hammar W
A 403 Tirechchoumine
A 404 Bahar el Hammar E
A 405 Gouiret Bou el Mout S
A 406 Gouiret Bou el Mout N
A 410 Gouiret es Sud
A 411 Les Haouds W
A 412 Les Haouds E
A 414 Kermaz syncline
A 416 In Heguis N
A 418 In Heguis S
A 419 Adrar Tadioune N
A 420 Tin Khelifa S
A 422 Gour Bou Kreis
A 426 Ain Redjem N
A 427 Ain Tilekchot
A 435 SSE Jebel Mouima

Figure 8c. Codes for sections presented on figures 8a and 8b (after Wendt et al., 2006, 2009).

large (about 0.5-1 μm) elongated intercrystalline pores (Trotter et al., 2007). The basal filling, however, is composed mainly of organic matter which is slightly phosphatized. This is why basal fillings were usually destroyed during diagenesis and thus are rare in the fossil record.

The material used in the study is a part of a large collection (about 600 samples) gathered by prof. Jobst Wendt (Tübingen) and co-workers during several field expeditions. Most of the samples were already used in previous stratigraphic investigations (Belka, 1994; Wendt & Kaufmann, 1998; Wendt et al., 1993, 1997, 2006, 2009; Lüning et al., 2004). The majority of samples (354 samples from 62 sections) contained the Middle and Late Devonian conodonts. The remaining ones (30 samples from 7 sections) were collected from the Carboniferous strata. Devonian fauna encompasses pectiniform as well as

ramiform elements, whereas among Carboniferous conodonts only pectiniform elements are present. Eifelian and Famennian samples exhibit a very low abundance of conodonts. In contrast, Givetian and especially Frasnian conodonts are extremely abundant. The Carboniferous fauna is generally poor with an average number of conodont elements below 5 per kilogram of dissolved rock. All samples were taken from limestones to avoid a potential influence of lithology on the level of thermal maturity of conodonts (for more information see below). Host rocks were investigated in exceptional cases only. This was necessary for recognition and validation of Sr isotope data. In sum, 19 samples of limestones were analysed.

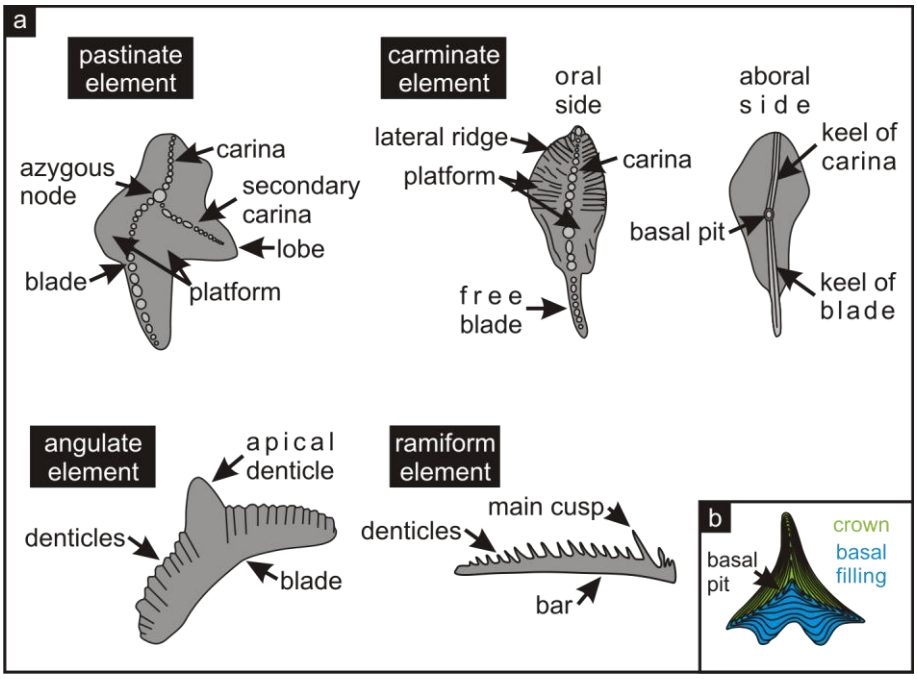

Figure 9. (a) Selected morphological types of conodont elements (after Hass, 1962; modified). (b) Schematic structure of conodont element (after Sweet, 1988; modified).

5. METHODS

A principal parameter used in modelling of thermal history of rock successions is their level of thermal maturity. In the present study the conodont colour alteration index (CAI) was used first of all to reconstruct the thermal history of the Ahnet and Mouydir basins. The CAI method was supplemented by electron spin resonance (ESR) technique in order to date the last thermal treatment of conodonts. Mineralization overgrowing the conodont elements was analysed by EDS detector and evaluated under scanning electron microscope (SEM). In order to recognize the origin of these mineral phases strontium isotope ratio ($^{87}Sr/^{86}Sr$) in conodonts and host rock was measured.

5.1. Conodont colour alteration index (CAI)

5.1.1. Principles

Tooth-like conodont elements are common in Palaeozoic and Triassic marine rocks. They show rapid evolution in geological time and great morphological diversity. Additionally conodonts are very resistant to diagenetic processes and can be easily extracted from rocks. Due to the mentioned features conodonts become an excellent biostratigraphic tool (see for overview Sweet, 1988). Moreover, they offer a geochemical record of past seawater composition and thus are used in palaeoceanographic reconstructions (e.g., McArthur et al., 2001; Dopieralska, 2003; van Geldern et al., 2006). Conodonts when exposed to influence of heat change their colour. The fact that conodont elements vary in colour was observed relatively early in the history of their research. Ellison (1944) was the first who noticed colour variations in conodont collections. Twenty years later, this phenomenon has been correctly attributed by Lindström (1964) to a carbon-fixing process. The first attempt to evaluate systematically these changes has been done by Epstein et al. (1977). They revealed that colour of conodonts and their textural alteration can be used in evaluation of the thermal maturity of sedimentary rocks. Moreover, they discovered that conodont colour data may be useful for assessing hydrocarbon potential and for thickness reconstruction of eroded successions.

Epstein et al. (1977) experimentally heated unaltered conodonts from the Appalachians to induce sequence of colour changes. In series of experiments, conodont elements were subjected to open-air heating in electric furnace for several hours in the temperature range from 300°C to 600°C. This caused a progressive colour change from pale yellow to black. The study has shown that artificially produced colour sequence is the same as that known from the field collections. In order to manage the conodont colour

more univocally Epstein et al. (1977) established five colour intervals and termed them the conodont colour alteration indices (CAI). The conodonts with the CAI value of 1 are assumed to be unaltered, and are generally pale yellow (Figure 10). Colour scale was taken from the Munsell soil colour charts. The heating experiments showed that elements

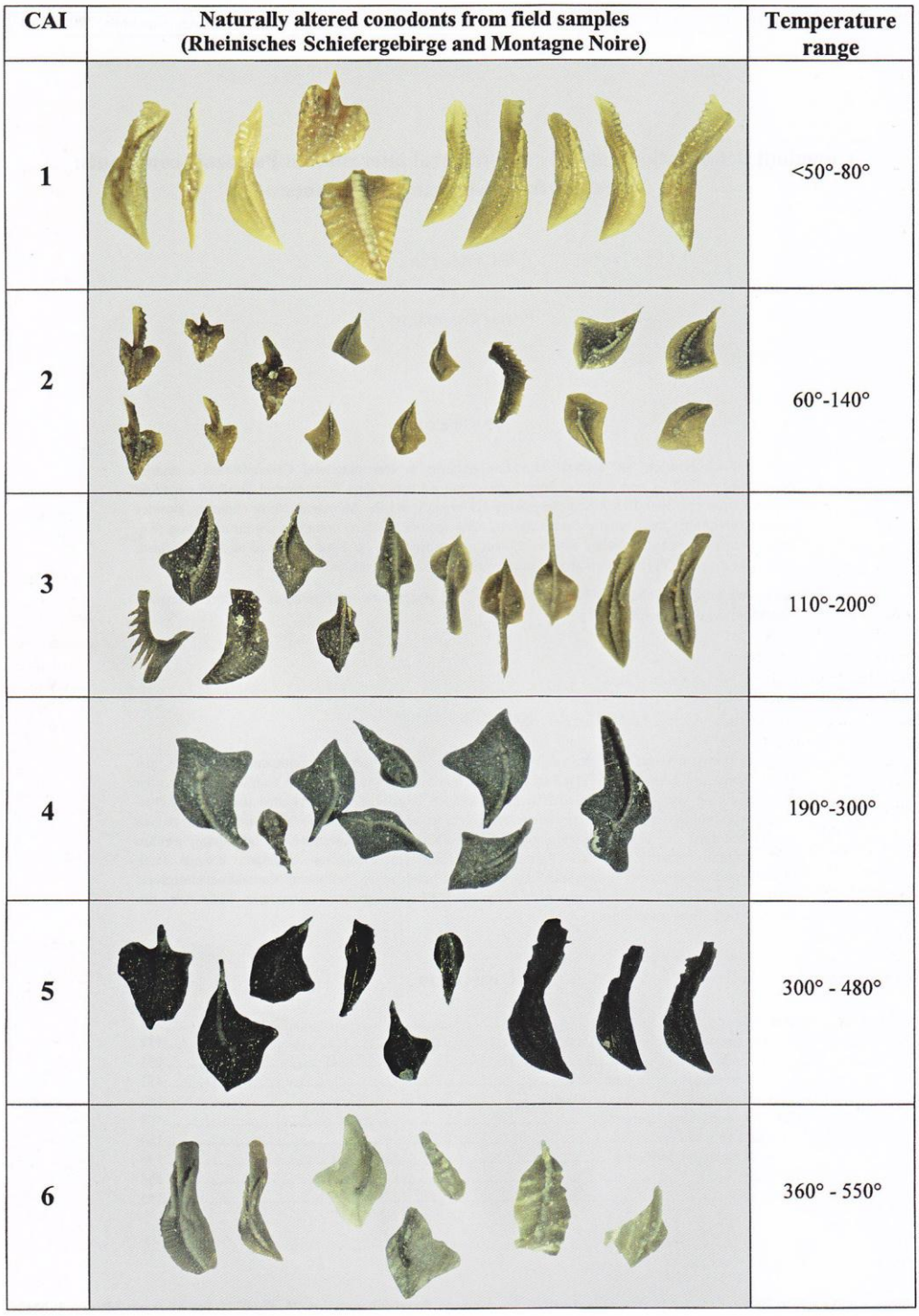

Figure 10. Conodont colour alteration index (CAI) chart (adopted from Konigshof, 2003).

preserve their natural colour in temperatures below 50-80°C. Colour alteration expressed by the colour change to very pale brown (CAI 1.5) begins at temperatures 50-90°C. The CAI value of 2 describes brown to dark brown conodonts and was generated in the temperature range from 60°C to 120°C. The conodont elements attributed to the CAI value of 3 are very dark greyish brown to dark reddish brown. This colour appeared at temperature range from 110°C to 200°C. Black elements corresponding to the CAI value of 4 were obtained after heating at temperatures of 190-300°C. More advanced heating above 300°C provided deep black elements attributed to the CAI value of 5. The partial overlapping of the temperature ranges is because the colour alteration is time and temperature dependant. It means that the same alteration level can be produce either during a short time at high temperature or during a long time at much lower temperature. In addition, Epstein et al. (1977) recognized also that colour alteration is progressive, cumulative and irreversible. Moreover, they observed the temperatures corresponding to the CAI value of 4.5 and higher cause also alteration of the conodont surface from smooth and vitreous to pitted and grainy.

The pioneering work of Epstein et al. (1977) was continued by Rejebian et al. (1987) who expanded the colour alteration scale for temperatures above 300°C. They showed that deep black conodont elements (with CAI 5) while exposed to temperatures above 300°C start to decolourize and becomes dark to light grey (CAI 6) at temperatures 360-550°C (see Figure 10). This change reflects the onset of the organic matter decomposition in crowns. Temperatures above 490°C to 720°C cause the complete decomposition of organic matter and advanced recrystallization of fluorapatite. As a result, conodonts become opaque white (CAI 7). Above the temperature of 600°C conodont elements are colourless or crystal clear (CAI 8) due to advanced or complete recrystallization.

Experiments of Epstein et al. (1977) have revealed that temperature, or more precisely the heat is the main factor influencing the colour and the textural alteration of conodonts. Within sedimentary successions burial is most commonly the reason for temperature increase. Because of predominantly regional scale of subsidence and burial, the CAI pattern displays often a high homogeneity within rocks at the same age across large areas and gradual trends throughout the stratigraphic section. In general, the deeper buried rocks, the higher are the CAI values, and the opposite. However, sedimentary rocks can be also heated by magmatic bodies and/or by circulating hydrothermal fluids. In contrast to magmatic bodies, hot fluids do not generate heat itself, but only transfer it from

other sources. Spatial distribution of the CAI values around magmatic intrusions differs remarkably from that originated due to burial. It is characterized by the presence of a ring (aureole) of very high CAI values (commonly above 5) close to the magmatic body and a rapid drop in CAI outwards in the distance of tens to hundreds of meters. Influence of hydrothermal fluids can be recognized by the occurrence of characteristic textural alteration of conodont elements (see section 5.1.2).

There are several factors that can modify conodont colour alteration process. Epstein et al. (1977) found that in the presence of water-gas mixture this process is retarded. Conodonts heated in the modified experiment, with addition of water-gas component, have had lower CAI values (by 1.5 unit) as those heated under the same time and temperature conditions in an open-air environment. This experiment was repeated by Rejebian et al. (1987) giving again similar results. Moreover, they found new important aspects of water-gas influence on conodont alteration. Above the CAI value of 2 or 3 the colour alteration process changes from predominantly carbonization of the organic matter to its oxidation and volatilization of oxides inside conodont elements. In addition, in the presence of water-gas mixture CAI values of 6 or higher were being produce directly with bypassing values inbetween. Such phenomenon suggests that high CAI values originated under water-gas mixture conditions are not related to the same time-temperature conditions present in an open-air system.

Lee et al. (1998) and Marshall et al. (1999) based on detailed investigation of organic matter structure in conodonts demonstrated that CAI data may be misleading. They showed that the structure of the organic matter in conodonts with relatively high CAI values (they investigated elements with CAI value of 4) is humic-like rather than coal or kerogen type. This appears to reflect oxidative conditions. Hence, due to organic matter oxidation real heating temperatures might be lower than those estimated from CAI values. In addition, investigation of Marshall et al. (2001) provided evidence that migration of nitrogen compounds from deeper parts of the conodont element towards its surface may also be responsible for colour alteration in conodonts.

Some studies showed that host rock can influence the colour alteration of conodonts (e.g., Legall et al., 1981; Belka, 1993). Elements derived from carbonate and clastic rocks which underwent the same thermal history, have different CAI values. Conodonts extracted from terrigenous and marly rocks yield higher CAI values than those extracted from carbonates, but the differences are not higher than the half of the CAI unit. This is why conodonts recovered from the uniform lithology are recommended for palaeothermal

analysis. Investigation of Belka (1993) revealed that high concentration of silica in the host-rock may cause oxidation or removal of organic matter from the conodont elements and consequently, they become fade. This visual effect was also observed in conodont material recovered from rocks affected by hydrothermal fluids (Harris et al., 1990).

Other geological factors, as tectonic stress, for instance, do not influence the colour in conodont elements. Consequently, conodonts from faulted and folded areas show the same colour as elements derived from flat-lying rocks with a comparable overburden (Epstein et al., 1977).

CAI versus other indicators of organic maturity. Optical techniques are widely used for assessing the thermal maturity of organic matter contained in sedimentary successions. They include indices based on optical properties of organic components, such as their reflectance or fluorescence (see for review Héroux et al., 1979). Other methods use sequential colour change in various plant and animal remains. Among these are spores, pollen, acritarchs, dinocysts and graptolites. Colour alteration is related to progressive, cumulative and irreversible chemical alteration of organic matter. All these maturation indices, however, offer an indirect approach to palaeotemperature estimations (Tissot et al., 1987). This fact may cause difficulties to prove significance and validity of particular indices. It influences also on possibilities of precise conversion of one index into another. In practice, application of any thermal maturity indicator exhibits limitations. Vitrinite reflectance, for example, which is considered to be the best method, cannot be used in strata older than the Late Silurian. This is because of lack of land plants in pre-Devonian rocks. Another limitation in application of this method is that "vitrinite" macerals are dependent on the marine or lacustrine origin of organic matter (Durand et al., 1986). In contrast, conodont CAI can be applicable to a wider time span, including Palaeozoic and Triassic. However, the disadvantage of this method is that only thermal maturity of marine sediments can be determined. On the other side, it is compensated due to the abundance of conodonts in a variety of sediments, including those in which vitrinite or graptolites are absent. The procedure is moreover very simple and inexpensive (Epstein et al., 1977). The organic carbon present within conodont elements is certainly less subjected to oxidation due to weathering or diagenesis than is the organic matter dispersed in the host rocks (Belka, 1993). Palynomorphs are good thermal indicators of the low-temperature range of organic metamorphism but they are completely useless in recognition of higher thermal regimes (above 150°C). This is because of their low heat resistance. In addition,

palynomorphs are susceptible to selective loss of organic matter particles during host-rock diagenesis or when oxidative techniques are used for their preparation. As a consequence, the colour change observed does not often correspond to the real maturation level. Another problem is that monitoring of palynomorphs colour is subjective and may cause an inaccurate calibration. Acritarchs may provide a valuable maturation data. The comparative studies showed, however, that the major colour change occurs in acritarchs in temperatures above 100°C. In practice, in order to test the validity of acritarchs colour as a maturation index, a calibration against another known organic indicator is required (Legall et al., 1981) as well as a large set of samples is necessary to eliminate the oxidized material. Otherwise the estimated thermal maturity level is usually too low.

5.1.2. Applications

Geothermal analysis. Experiments of Epstein et al. (1977) provided a basis for application of CAI data in evaluation of palaeotemperatures that affected sedimentary successions. Data of heating time (in hours) and temperatures required to generate the particular CAI indices were plotted on the Arrhenius diagram. Consequently, experimental data provided a graphically expressed relationship between the CAI values, duration of burial and temperature. This relationship was then extrapolated into geological time (Figure 11) and compared with empirical observations inferred from the field samples.

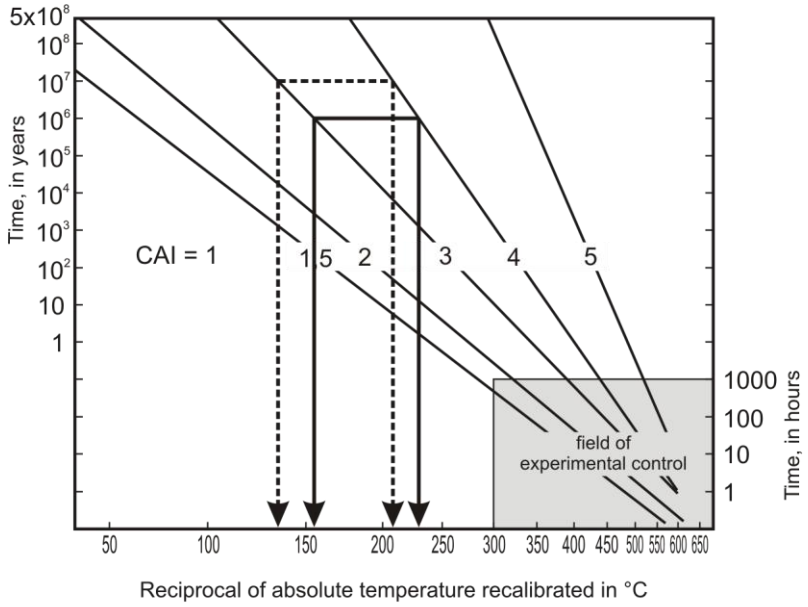

Figure 11. Relationship between CAI, duration of burial and temperature expressed on Arrhenius plot (after Epstein et al., 1977). Projections of burial time (c. 1 m.y. and c. 10 m.y.) for CAI values 3-4 is given as an example.

Now for the assessment of palaeotemperatures from plot of Epstein et al. (1977) information on duration of burial and on level of thermal maturity expressed in the CAI are required. Duration of burial is taken as the difference between the time (in Ma) of supposed initial burial of the succession and the minimum and maximum times for unloading commonly obtained from regional geological data. The CAI value is determined following the procedure described by Epstein et al. (1977). Approximate palaeotemperature is obtained by the projection of the CAI value points at the minimum and maximium burial times on the *x* axis of the Arrhenius plot. Minimum duration of burial gives maximum palaeotemperature estimates, and the opposite (see Figure 11). Because palaeotemperatures are function of the burial depth and heat production in the earth crust the CAI data can be applied for modelling of thickness of eroded successions and for reconstructions of geothermal gradients. Studies of Epstein et al. (1977) and Legall et al. (1981) showed that with rather average geothermal gradient about 30°C/km colour alteration of conodonts begins after burial on depth of about 1200 m. The CAI value of 2 appears from 2400-3600 m of overburden. The CAI value of 3 is generated after burial on depth of 3600 and persisted up to 5500 m of overburden. More advanced thermal maturity in conodonts, expressed by the CAI values of 4 and 5, is a result of burial on depth of at least 5500 m and 8000 m, respectively. Higher geothermal gradient produced the particular CAI values already at shallower burial depths, and the opposite. Various diagrams showing relation between the geothermal gradient and burial enable match the most likely geological conditions for a particular area and dataset (e.g., Legall et al., 1981; Belka, 1990). Since establishing the CAI method, it became widely accepted and commonly applied in palaeothermal analysis (e.g., Legall et al., 1981; Aldridge, 1984; Burnett, 1987; Belka, 1990, 1991, 1993; Gawlick et al., 1994; Helsen & Königshof, 1994; Repetski & Narkiewicz, 1996; Narkiewicz et al., 1998; Sarmiento et al., 1999; García-López et al., 2001; Rasmussen & Smith, 2001; Repetski et al., 2005; Kovács et al., 2006).

Hydrocarbon potential. The compilation of the CAI data for large areas in the eastern USA and Canada (Epstein et al., 1977; Legall et al., 1981) showed a clear relation between hydrocarbon occurrence and the level of thermal maturity expressed by conodont CAI. These observations let Legall et al. (1981) to correlate stages of hydrocarbon formation with the CAI values (Figure 12). They stated that sedimentary rocks with a very low thermal maturity (CAI of 1 and 1.5) define a zone of incipient oil and gas formation. Liquid and gaseous hydrocarbons, however, are generated within rocks which level of

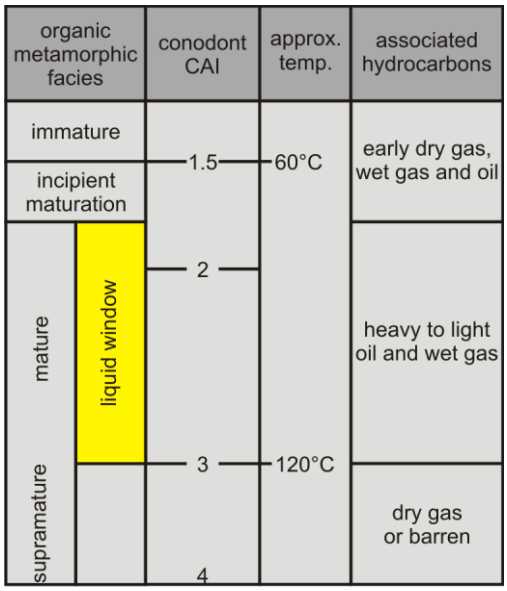

Figure 12. Correlation of conodont CAI with stages of hydrocarbon generation (after Legall et al., 1981; modified).

thermal maturity is expressed by CAI of 2 and 3. Formation of gas is extended to rocks that were even affected by higher thermal treatment (CAI of 4). It should be noticed that hydrocarbons commonly migrate after their formation, thus they are frequent accumulated in reservoir rocks that generally display lower thermal maturity than their original source rock. The relation of the CAI to the stages of the oil and gas formation provides an easy in application and a cheap tool in search for hydrocarbons. The CAI data has been successfully applied in hydrocarbon prospection carried out by oil companies allover the world, but only a limited number of studies was published (e.g., Belka, 1990, 1991, 1993; Jones, 1992; Armstrong et al., 1994; Königshof & Boncheva, 2005; Repetski et al., 2008).

Metamorphism and hydrothermal alteration. Experiments of Rejebian et al. (1987) revealed a potential of the CAI data in recognition of metamorphic regimes that affected sedimentary successions. Conodonts derived from regionally metamorphosed in chlorite-grade facies carbonates and pelitic rocks commonly show corrosion, deformations and are fractured. Their characteristic feature is also the frequent occurrence of the CAI of 5 or 5.5. However, a different characteristics have elements derived from the contact metamorphosed rocks. Such conodonts are generally better preserved and do not show deformations or coarse recrystallization. This seems resulted from a relatively short-term heating. A conspicuous feature of the conodont collections derived from thermal aureoles of magmatic intrusions is the presence of highly elevated CAI values. Consequently, a local occurrence of significantly higher CAI values than in the surrounding area can be used to identify buried intrusions and outline their extent (e.g., Wardlaw & Harris, 1984; Burnett, 1987; Jones, 1992; Belka, 1993; Helsen & Königshof, 1994; Königshof, 2003; Voldman et al., 2008).

Experimental data of Rejebian et al. (1987) provide also a basis for application of the CAI method in recognition of hydrothermal alteration of sedimentary successions. Conodonts derived from hydrothermally altered rocks are corroded (pocked, frosted to pitted) and their surface is commonly covered by grey patina. This patina is most probably

the effect of oxidation of organic matter dispersed within conodonts. Commonly occur also anomalies in the CAI values. They are expressed in the presence of individual conodont elements within the sample with two completely different CAI values (2 and 5, for instance). Sometimes, even one single element displays different CAI in its different fragments. Rocks affected by hydrothermal fluids are commonly associated with ore deposits of commercial value. Characteristic textural alteration of conodonts related to the influence of hot fluids offers a possibility for application of conodont CAI data for searching of mineral deposits (e.g., Wardlaw & Harris, 1984; Nowlan & Barnes, 1987; Jones, 1992; Belka, 1993; Leach et al., 1997).

In the past, attempts were also made to use the CAI data in the recognition of the diagenesis to incipient metamorphism transition (e.g., Kovács & Árkai, 1987; Gawlick et al., 1994; García-López et al., 1997, 2001; Bastida et al., 1999). In different areas, however, boundaries of metamorphic regimes were marked by different CAI values. Additionally, the CAI data required a support of other indicators of thermal maturity (the most commonly illite crystallinity) to obtain reliable results. Thus, the CAI method has a rather limited application in the metamorphic geology.

5.2. Determination of the CAI

Conodont CAI values were determined under binocular, using the standard method described by Epstein et al. (1977). Because colour of conodonts shows slight fluctuations depending on thickness of individual elements, the CAI index was setted, as far as it was possible, by using elements of different size and morphology in each sample. The CAI data presented on temporal-spatial pattern maps have been compiled for four stratigraphic intervals in the Devonian (Eifelian, Givetian, Frasnian and Famennian) and one cumulative map for the Carboniferous. The CAI index values put on the map were selected for all sections following the same generalization procedure. For each stratigraphic interval in the sections the highest CAI index values was taken. The highest values, however, were rejected when they constitute single, isolate anomalous values within a long sequence of uniform values. This procedure was justified because in the Ahnet-Mouydir area the thickness of stage intervals generally does not exceed 100-300 m. The highest values were preferred because of possible local decolourization of the conodonts during diagenetic processes (see section 5.1.1. for more information).

5.3. Optical microscopy

A pilot observation under binocular enabled a general reconnaissance of sample characteristics, i.e. the taxonomic content, number and morphology of conodont elements, as well as their colour and the character of their surface. Ten samples with conodonts yielding mineralization and textural alteration were chosen for conventional photographic documentation. Photographs were taken under *Olympus SZH-10* binocular using a *Olympus c7070* digital camera. One from the samples containing elements mineralized by scheelite was also analysed under *Olympus AX-70 Provis* optical microscope with ultraviolet light. Additionally, 19 host rock samples were analysed in thin sections under *Carl Zeiss Axiolab pol* reflected-light microscope in order to recognize their petrographic composition. Host rocks were selected from those that gave conodonts mineralized by apatite, scheelite and quartz. Six thin sections were chosen for conventional photographic documentation. Photographs were taken by using *Canon PowerShot A640* digital camera.

5.4. The electron spin resonance spectroscopy

The electron spin resonance (ESR) method utilizes the phenomenon of absorption of microwave energy by materials containing paramagnetic molecules, ions or atoms with unpaired electrons, when these materials are subjected to external magnetic field. This technique enables detection and recognition of relative abundance of paramagnetic centres. Every electron has a magnetic moment and a spin quantum number s=1/2. The influence of external magnetic field on electron`s spin causes its align along the direction of this field and rotation around its axis. Increase of magnetic field induces faster rotation of the electrons and causes their division into two groups having specific level of energy. One group contains electrons with magnetic moments aligned parallel to the magnetic field, whereas the second one electrons exhibiting moments aligned antiparallel to the external field. The parallel alignment corresponds with the lower energy stage. Due to the movement of unpaired electrons between two energy levels the electrons emit a signal, which is most commonly visualized as first-derivative absorption spectrum. Peaks observed in the spectra are characterized by several parameters. The most important is g-factor – a dimensionless quantity that characterizes the magnetic moment and gyromagnetic ratio of a particle or nucleus. It enables identification of the paramagnetic centres that are responsible for specific signals. Its value is dependant on microwave energy and range of magnetic field used during measurements. The highest the energy, the highest the value of g-factor. On the other side, the narrower is the magnetic field range,

the most precise is the setting of g-factor. Very common observed are differences in intensity of the same signals measured in different samples. This is because the signal intensity is a function of the abundance of paramagnetic centres. If particular centre is very abundant, the intensity is high, and opposite.

First attempt of usage of the ESR method in evaluation of thermal annealing of conodonts was made by Belka et al. (1987). Their laboratory experiment has established that signals recognized in the spectra of conodonts provide useful information about timing of their thermal alteration. A typical spectrum of Palaeozoic conodonts contains four peaks, labeled as A, B, C and D (Figure 13). These authors concluded that the most useful information provide peaks A and D because their intensity shows a strong correlation with temperature changes. Signal A is generated at temperatures below 100°C and is present only in spectra of conodonts that were not heated during and after Mesozoic time. The intensity of signal D correlates well with the thermal maturity of conodont elements. The higher the thermal maturation of an element, the higher is the intensity of signal D in the spectrum (Belka et al. 1987). Usefulness of the ESR method in the recognition of thermal events within sedimentary successions was demonstrated by Belka (1991, 1993) in his later studies.

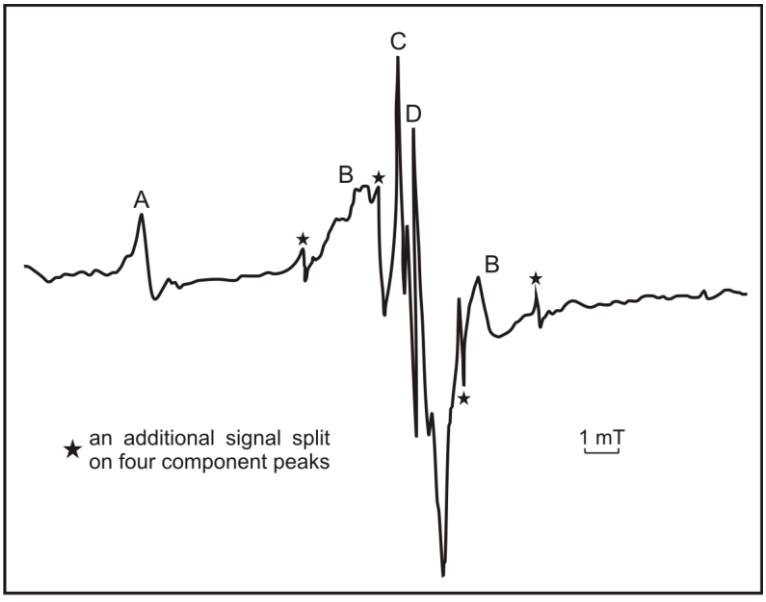

Figure 13. Typical ESR spectrum of Palaeozoic conodonts (after Belka et al., 1987;slightly modified). For description see the text.

Procedure. During the present study the ESR spectra of Givetian and Frasnian conodonts were recorded. Five investigated samples were taken from sections which locations outline the entire study area (Figure 14). Measurements were performed on a *Bruker EMX-10* X-band spectrometer with 100 kHz modulation, in the Medical Physics Division, Faculty of Physics, Adam Mickiewicz University at the Poznan. The samples were measured at ambient temperature using the same microwave energy (20 mW) and a resolution of 1024 points. Spectra were recorded for 100 Gauss range of magnetic field (with 3 Gauss modulation). Cumulative scans with 23 repetitions were performed for each sample.

5.5. Scanning electron microscopy and microanalysis

Textural alteration of conodont elements and mineralization in 54 samples were evaluated under *Hitachi S-3700N* and *Carl Zeiss Evo 40* electron scanning microscopes. Eleven samples were chosen for preparation of microphotographic documentation. The chemical composition of mineralization and host-rock samples in polished thin sections was analysed by *EDS Noran Six* detector attached to the scanning microscope. All samples were coated with graphite for chemical analysis and with gold for microphotographs. Standardless semi-quantitative analysis for the spot were performed in case of mineralization and mapping was carried out for the host-rock samples. The analysis were done in laboratories of scanning microscopy of the Geoscience and Biology Faculties of the Adam Mickiewicz University at Poznan.

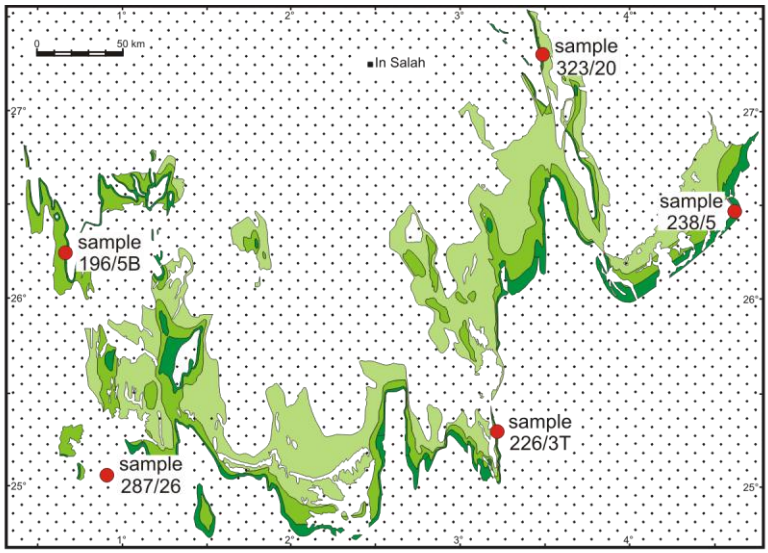

Figure 14. Location of conodont samples used in the ESR investigation (base map after Wendt et al., 2006; modified. For location of samples and legend see Figure 8a. For age of samples see the appendix).

5.6. Strontium isotopic study

The continental crust has higher $^{87}Sr/^{86}Sr$ isotopic ratios values (from 0.704 to 0.750) than oceanic crust (ratios range from 0.700 to about 0.704). There are also differences between the lower and the upper continental crust. The lower part appears to have relatively less radiogenic ratios than upper crustal rocks. It should be noticed however, that there is no clear division in isotopic composition between these parts, and lower crustal rocks may plot anywhere within the crustal field (White, 2007). During the erosion strontium removed from rocks is transported by rivers and introduced into oceanic waters. Geochemical signal of seawater is recorded in sediments and biogenic precipitates, but original signatures are preserved only in phases that precipitated in equilibrium with seawater. Due to significant incorporation of chemical elements, including Sr, and very good diagenetic resistance marine phosphates are commonly used in isotopic studies. In Palaeozoic sediments, conodonts are particularly useful because of their stratigraphic importance, and thermal and chemical stability of fluorapatite. Study of Ebneth et al. (1997) showed that strontium isotopic record is stable in conodonts with the CAI values of lower than 2.5. Since the pioneering work of Peterman et al. (1970) Sr is used as a tracer of evolution of ancient seawater (e.g., Bruckschen et al., 1995; Denison et al., 1997; McArthur et al., 2001; van Geldern et al., 2006). Through Earth history strontium ratios in seawater fluctuated from about 0.7060 to 0.7092 (Figure 15). Due to its uniform value in any given geological time caused by a longer residence time in seawater than the mixing time of the oceanic system, a Sr ratio is a useful tool in correlation of sedimentary successions in regional scale (Veizer et al., 1997). Measurements of Sr isotopic ratios are also commonly used in characterization of hydrothermal systems and recognition of fluids source (e.g., Kesler et al., 1988; Relvas et al., 2001; Bau et al., 2003; Munoz et al., 2005). Water in hydrothermal systems can be derived from several sources (e.g., Pirajno, 2009). It might be magmatic/juvenile or metamorphic in origin. Another common sources of fluids constitute sediment-hosted (connate) waters, meteoric water and/or seawater.

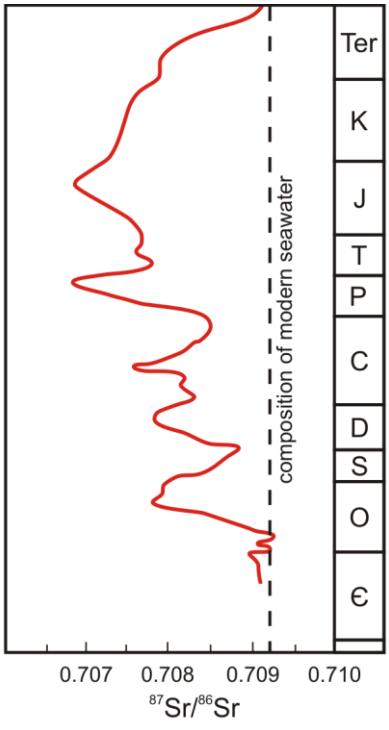

Figure 15. Schematic curve for $^{87}Sr/^{86}Sr$ variations during the Phanerozoic (after White, 2007; modified).

Procedure. The analytical part, including chemical separation of strontium and measurements of its isotopic composition, was carried out in the Isotope Laboratory of the Adam Mickiewicz University at Poznan. Seven conodont samples and corresponding host-rock carbonates were investigated. Samples approx. 1 mg and 100 mg in size, respectively, were dissolved on a hot plate (~100°C, overnight) in closed PFA vials using concentrated nitric acid (~ 14 N) for conodonts and 0.75 N HCL for carbonates. The miniaturized chromatographic techniques described by Pin et. al. (1994) were applied for Sr separation. Some modifications in the column size and concentration of reagents were introduced by Dopieralska (2003). Strontium was loaded with a $TaCl_5$ activator on a single rhenium filament. Sr was analyzed in dynamic collection mode on a *Finnigan MAT 261* mass spectrometer. During the course of this study, the NBS 987 Sr standard gave $^{87}Sr/^{86}Sr$ of 0.710225 ± 10 (2σ mean on twenty-two analyses). The $^{87}Sr/^{86}Sr$ ratios were normalized to $^{86}Sr/^{88}Sr = 0.1194$. Total procedure blanks were less than 80 pg for Sr.

6. CAI TEMPORAL-SPATIAL PATTERNS

6.1. Maturity trends

The analysis of the conodont CAI data obtained from Devonian and Carboniferous rocks in the Ahnet and Mouydir basins provided trends and patterns presented in figures 16-19. The first conspicuous feature, which arises from the data, is a very high regional homogeneity in Devonian CAI values across the entire Ahnet Basin. The majority of conodonts from Eifelian, Givetian, Frasnian and Famennian localities show CAI value of 2. Slightly lower (CAI 1.5-2) or higher (CAI 3) index values show elements from few isolated sections only. Another well-defined characteristics is a sharp change in the thermal maturity east of the Idjerane Mzab Ridge in the Mouydir Basin. Devonian conodont elements there indicate higher thermal maturity of sediments expressed by CAI values from 2 to 3. In the western part of the Mouydir Basin CAI values of 3 are predominant during the Middle Devonian, whereas in the eastern part all conodont samples display this thermal maturity level. Although the Carboniferous dataset was significantly smaller than the Devonian one the CAI values are still relatively uniform regionally within stage intervals and differences do not exceed 1.5 of the CAI unit. In contrast to the Devonian, the CAI values within the Carboniferous decrease upwards in the sequence.

Despite largely uniform regional patterns and gradual changes across stratigraphic sections, conodonts in about 2% of samples show anomalies in the CAI values. They are mainly expressed by the presence of elements displaying two distinctly different index values (2 and 4, for instance) in one sample. There are also two anomalies with a conodont colour resembling that of the CAI value of 6, which occur in areas yielding a generally low thermal maturity.

Eifelian. The CAI data are mainly concentrated in the western (Adrar Morat and Akabli area) and eastern Ahnet Basin (Adrar Tadioune, Djebel Azaz, Djebel Tibaratine area) as well as across the Mouydir Basin (Figure 16). Eifelian CAI datapoints (34 samples from 19 localities) show W-E trend in the level of thermal maturity. The maturity increases from CAI value of 1.5-2 in the NW Ahnet to 3 in the Mouydir Basin. Along western border of the Mouydir Basin conspicuous shift in CAI values, from 2 to 3, occurs within a short distance.

Givetian. Givetian CAI data constitute the most extensive set among the Devonian (176 samples from 48 sections). They are generally regularly distributed across the entire Ahnet-

Mouydir area (Figure 17). Similar to the Eifelian, a W-E trend in CAI can be observed. Thermal maturity changes from the CAI values of 1.5-2 in the NW Ahnet (north of the Sebkha Mekerhane) to CAI values of 3.5 in the eastern Mouydir. Givetian data mark also a rapid change in CAI values from 2 to 3 along western margin of the Mouydir Basin.

Among the whole investigated collection 9 Givetian samples form anomalies in the CAI pattern. Conodonts with the anomalous CAI values are present along major Precambrian lineaments and subordinate smaller faults in the western Ahnet (Azzel Matti and N of Sebkha Mekerhane), eastern Ahnet (Adrar Tiressouine and Djebel Tibaratine) and along western border of Mouydir. Seven anomalies are expressed by the presence of conodonts with CAI values of 2 and 4, of CAI 2 and 3 or of 2 and 4.5 in one sample. Two other samples contained characterized by grey colouration that resembles colour attributed by Rejebian et al. (1987) to CAI value of 6 (pl. 1).

Frasnian-Famennian. Frasnian samples are quite numerous (86 samples from 36 localizations), and they are distributed across the whole investigated area. In contrast, Famennian is represented by only 11 samples derived from 4 locations (Figure 18). Similar to the Middle Devonian patterns, a W-E trend in CAI is also clearly visible in the Frasnian dataset. The lowest values (CAI 1.5-2) are present in the SW Ahnet and increase eastwards up to CAI value of 3 in the Mouydir Basin. In the Ahnet, however, thermal maturity is highly uniform across the entire basin. A change in the pattern occurs in the western Mouydir, where maturity is slightly higher. Famennian data are available only for the NW Ahnet (Bled el Mass area), NE Ahnet (Djebel Azaz) and NW Mouydir (Adrar Idjerane area). They all include conodonts with a low thermal maturity expressed by the CAI value of 2.

Carboniferous. Carboniferous datapoints are scarce (30 samples from 7 sections). This is why a regional trend can be well recognized only within the Tournaisian (Figure 19). It follows the W-E trend that is virtually the same as that recognized within Devonian rocks. The lower thermal maturity characterizes deposits in the western Ahnet (Azzel Matti area) and it gradually increases up to CAI values of 3 in the western Mouydir. The region of NW Ahnet (Bled el Mass area) forms an exception in the trend; Tournaisian deposits have here distinctly higher maturity expressed by the CAI value of 3.5. The Visean CAI data are limited to the Ahnet Basin only. The lowest CAI values occur in the NW Ahnet and increase eastwards up to 2. Within the Bashkirian a trend in CAI is also present, but it has

an opposite direction. The lowest CAI value of 1 is present in the central Ahnet (Adrar Tirechchoumine) and it increases westwards up to CAI 2 in NW Ahnet (Bled el Mass area).

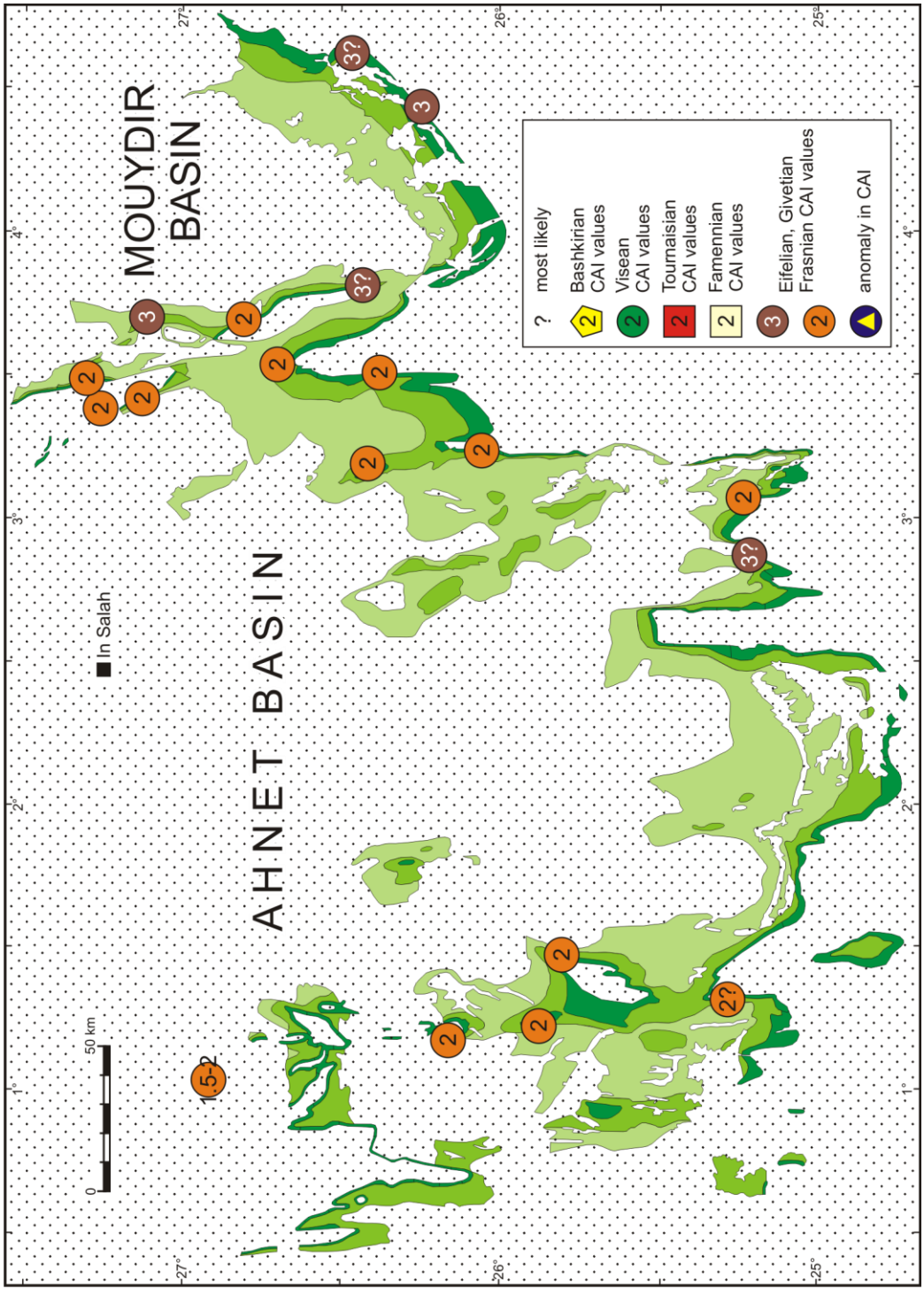

Figure 16. Conodont CAI values in Eifelian rocks of the Ahnet-Mouydir area (base map after Wendt et al., 2006; modified). For legend and location of sections see Figure 8a.

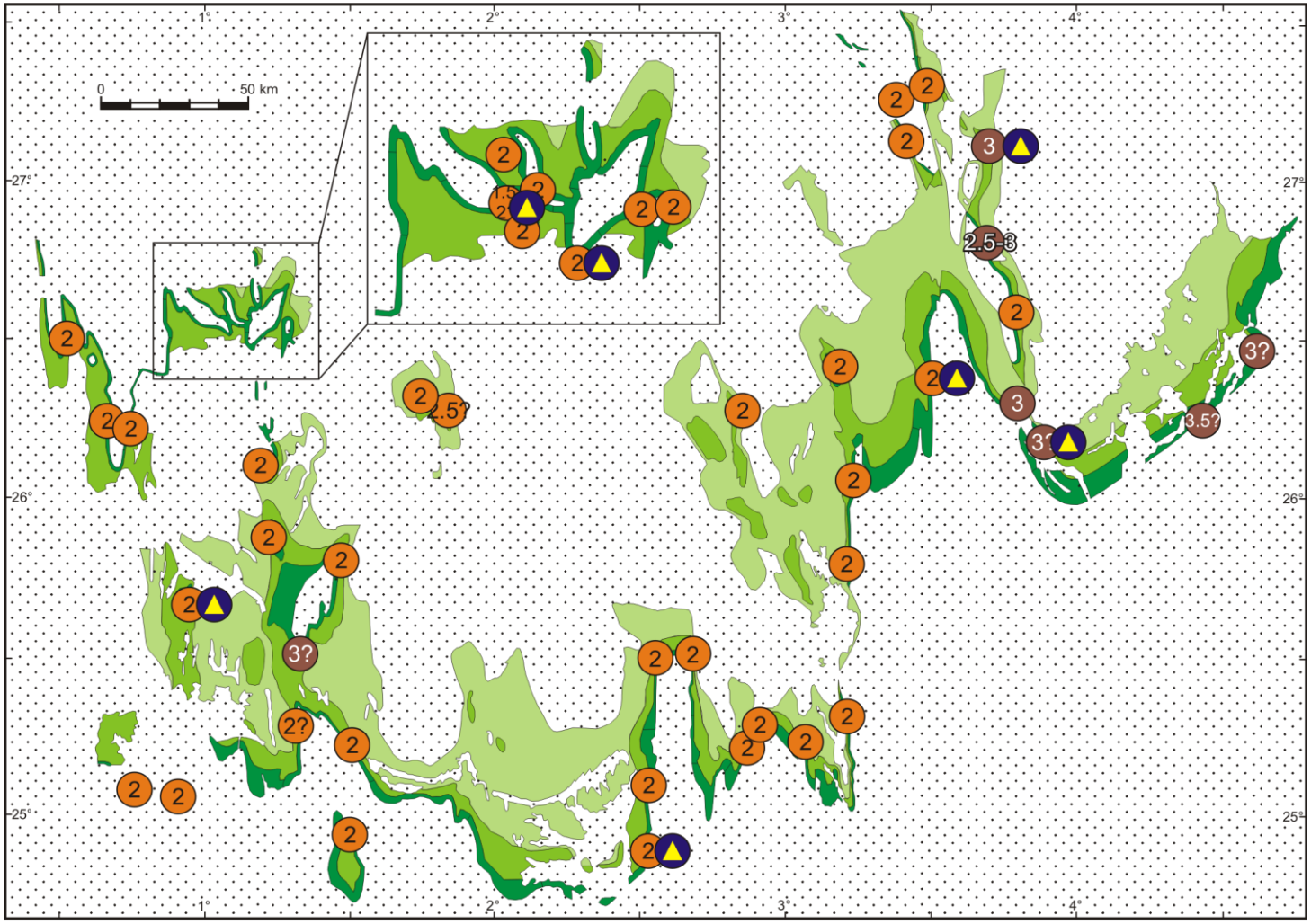

Figure 17. Conodont CAI values in Givetian rocks of the Ahnet-Mouydir area (base map after Wendt et al., 2006; modified). For legend and location of sections see Figures 8a and 16.

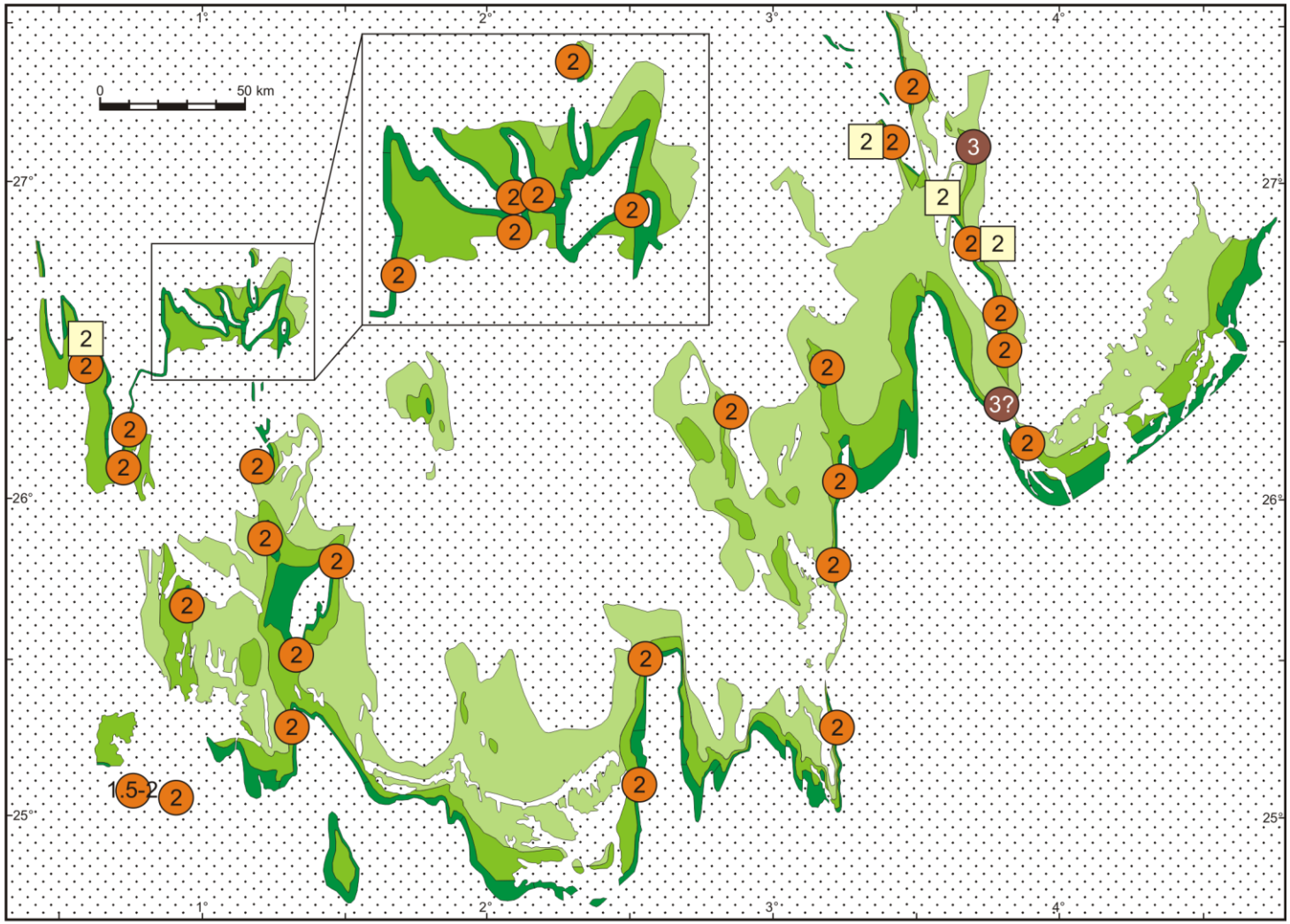

Figure 18. Conodont CAI values in Frasnian and Famennian rocks of the Ahnet-Mouydir area (base map after Wendt et al., 2006; modified). For legend and location of sections see Figures 8a and 16.

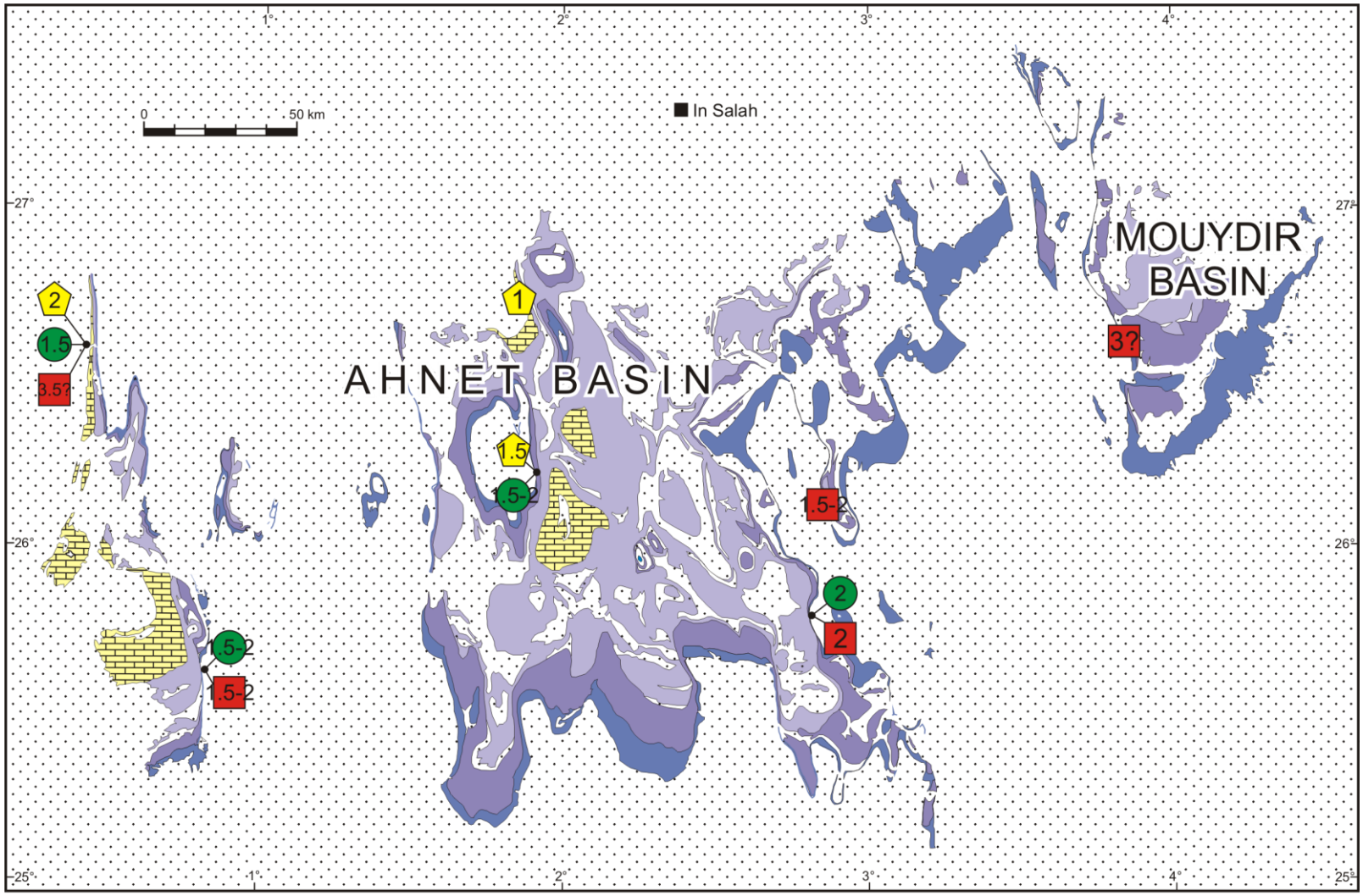

Figure 19. Conodont CAI values in Carboniferous rocks of the Ahnet-Mouydir area (base map after Wendt et al., 2009; modified). For legend and location of sections see Figures 8b and 16.

6.2. Interpretation of maturity trends

The high regional uniformity of the Eifelian, Givetian as well as Frasnian and Famennian CAI patterns across the Ahnet and Mouydir basins indicates that the thermal maturity was achieved most likely as a result of sedimentary burial. A strong argument for a regional burial is the progressive decrease of thermal maturity of the Carboniferous conodonts towards the top of the succession in the Ahnet Basin, from CAI 2 in the Tournaisian to CAI 1 in the early Bashkirian. Decrease of the thermal maturity upward in the sequence is also visible within Devonian rocks in the Mouydir Basin. In addition to heating resulted from the regional burial the Devonian rocks were also subjected to the activity of hydrothermal fluids. This is attested by the occurrence of isolated samples which contain conodonts with two different CAI values and the occurrence of decolourized conodont elements along faults. Moreover, locally elevated CAI values within the Tournaisian (CAI 3.5) and the Bashkirian (CAI 2) rocks in the NW Ahnet suggest an influence of another heat source. Both values seem to be resulted from heating caused by magmatic bodies. The evidence for this is a significantly lower thermal maturity (CAI 1.5) of the overlying Visean samples which are separated by about 500 m of deposits from the Tournaisian sample with elevated CAI value. In the case of the Bashkirian conodonts, another sample in the same section yields a CAI value of 1, only about 300 m below the sample with the value of 2. Relatively thin (up to 20 m) Late Triassic-Early Jurassic doleritic sills are most probably the source of additional heat. This is because the elevated CAI values are present only locally, in the area where the magmatic bodies are known to occur. The Visean rocks, in contrast to Tournaisian and Bashkirian ones, were not re-heated during the Mesozoic because of small dimensions of intrusions and because magma migrated commonly along stratigraphic boundaries (Smith et al., 2006).

In the Ahnet-Mouydir area, the youngest deformed Palaeozoic rocks represent the Bashkirian to early Moscovian Formation Rouge (see chapter 2, section 2.2.). It is covered by thin (up to 100 m) Cenozoic undeformed deposits containing peebles of Palaeozoic rocks. The Permian and Mesozoic rocks are not present in the investigated area and they were probably never deposited here (Logan & Duddy, 1998; Makhous & Galushkin, 2003). But further to the north, in the Timimoun Basin, folded Carboniferous rocks are covered by undeformed Early Jurassic to Cretaceous continental deposits (Logan & Duddy, 1998). In the Oued Mya and Illizi basins, north-east of Ahnet-Mouydir, poorly dated Upper Carboniferous to Lower Permian deformed rocks are present, which are unconformably overlain by undeformed Early Triassic continental series (Lefranc & Guiraud, 1990). These

stratigraphic and tectonic relationships let Haddoum et al. (2001) to conclude that the uplift and first phases of deformation occurred in the Ahnet and Mouydir basins probably around the Carboniferous/Permian transition or during Early Permian time. This is why two scenarios of burial are considered. First, in which burial persisted until c. 300 Ma (Carboniferous/Permian transition) and the second one with burial termination at c. 270 Ma (end of the early Permian). Because both basins, Ahnet and Mouydir, show a very similar development and are located adjacent to each other, identical scenarios of burial have been applied for both basins. Calculations of palaeotemperatures have been performed for the tops of Middle and the Upper Devonian successions as well as for the top of preserved Early Carboniferous (Tournaisian and lower Visean) strata in the Ahnet Basin. Due to generally lack of the Carboniferous rocks in the Mouydir Basin calculations here were performed for the tops of Middle and Upper Devonian successions only.

Assuming an uplift about at 300 Ma, the duration of burial for the Middle Devonian rocks was about 85 m.y. in the Ahnet Basin. Hence, using the Arrhenius plot of Epstein et al. (1977), it seems that the succession was buried in temperatures between about 50 and 120°C (Figure 20a). It should be noted, however, that in most samples across the Ahnet Basin conodonts show CAI 2 values. Hence, the majority of Middle Devonian rocks experienced dominantly relatively lower temperatures closer to 50°C. Higher thermal maturity (CAI 3) is recorded only locally. Because locations with the CAI values 3 do not correspond with the areas with the highest thickness of the Devonian and/or Carboniferous deposits and they occur near the major lineaments, it is very likely that locally elevated heat flow occured along the discontinuities. If the uplift occurred during the Early Permian, burial lasted no longer than 115 m.y. and the temperature ranges would be very similar (see Figure 20a).

The estimations for the Upper Devonian deposits (for both tested time horizons) provide minimum burial temperature below 50°C. Extrapolation of temperature scale on plot of Epstein et al. (1977) below the lower temperature limit presented on the plot suggest minimum temperature near 40°C. Maximum palaeotemperature was estimated on c. 50° (see Figure 20a). Because most locations show CAI 2 values, the Upper Devonian rocks were dominantly exposed to temperatures closer to 50°C rather than to 40°C.

The analogous calculations performed for the Mouydir Basin show that the Middle Devonian rocks were heated to temperatures between 50 and 150°C (Figure 20b). The Middle Devonian rocks, however, show mostly CAI value 3. This suggest that dominant

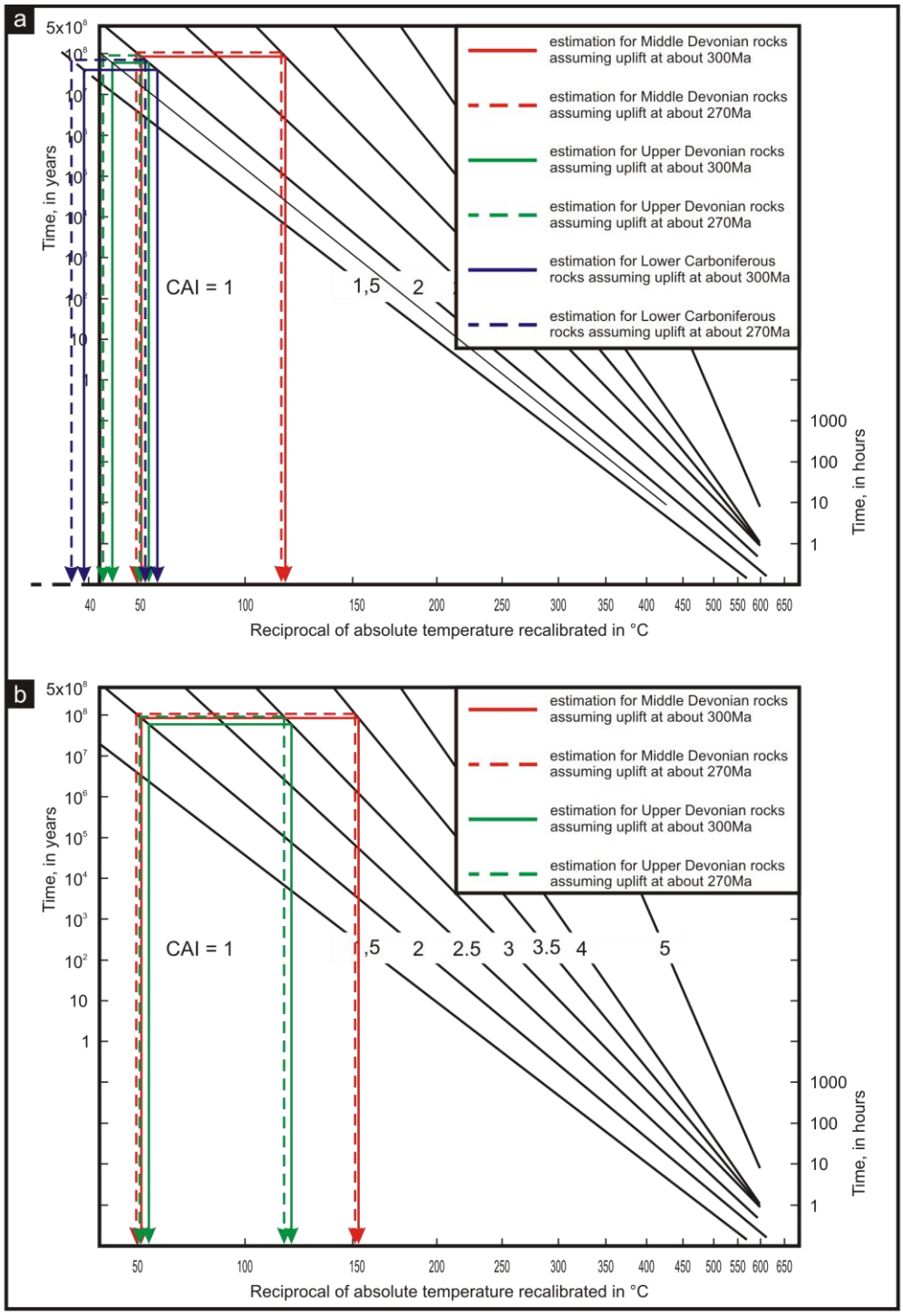

Figure 20. (a) Estimations of palaeotemperatures for Devonian and Carboniferous successions in the Ahnet Basin. (b) Estimations of palaeotemperatures for the Devonian successions in the Mouydir Basin (base diagram after Epstein et al., 1977).

temperature within the succession was near 120°C. In contrast, the Upper Devonian deposits experienced mostly relatively lower temperatures of about 50°C (see Figure 20b).

In the Ahnet Basin, assuming its uplift at c. 300 Ma, the Lower Carboniferous (Tournaisian and lower Visean) strata were subjected to minimum temperatures below

50°C; probably, it was temperature close to 40°C. The maximum palaeotemperatures have been estimated on about 60°C (see Figure 20a). If the uplift occurred at the c. 270 Ma, the minimum temperature was probably between 30-40°C but closer to 40°C, whereas the maximum temperature was about 50°C. The Lower Carboniferous deposits are overlain by the Bashkirian deposits. The very low level of the thermal maturity (CAI 1 and 1.5) of conodonts from the base of the Bashkirian succession indicates that these deposits were never subjected to temperatures of above c. 40°C. The lower Bashkirian deposits are covered by at least 700 m of middle Bashkirian to early Moscovian deposits (thicknesses of Palaeozoic formations are given in Figure 6). Assuming the geothermal gradient of 30°C/km and average surface temperature of 10°C, the temperature of 40°C would be achieved with an overburden of 1500 m would be sufficient. As already mentioned above the Permian and Mesozoic were probably never deposited in the Ahnet and Mouydir basins. This allows to conclude that the post-early Bashkirian cover was exclusively composed of the uppermost Carboniferous deposits. As a result, the total Carboniferous succession must have reached thickness of about 3700 m. But the average thickness of the Carboniferous cover, after took into account inferred above thicknesses, would burial top of the Upper Devonian deposits in depth with temperature of 70°C, whereas estimated from the CAI data maximum palaeotemperature is only 50°C. Hence, this suggests that heat production during the Palaeozoic was below the modern average value. Assuming geothermal gradient of 10°C/km thickness of the post-early Bashkirian cover should amount 4200 m. Consequently, the Carboniferous succession should have thickness up to 6400 m. Taking into account inferred thickness of the Uppermost Carboniferous deposits average thickness of the Carboniferous deposits is 5500 m. Such thick overburden would load the top of the Upper Devonian strata to the depths with a temperature of about 50°C and the top of the Middle Devonian on depths with a temperatures of 65-70°C. These temperatures in general are consistent with estimated heating temperatures from the CAI data.

In the Mouydir Basin there is only 550 m of Tournaisian to lower Visean sediments preserved. But more complete succession in the Ahnet Basin offers data for model study. Assuming geothermal gradient of 30°C/km inferred total thickness of the Carboniferous succession in the Ahnet Basin is c. 3700 m. Assuming lower gradient of 10°C/km thickness have been estimated on 6400 m. Taking into account thickness of 3700 m for the Carboniferous succession in the Mouydir Basin estimated maximum palaeotemperatures for the Devonian strata would be achieved with geothermal gradient of about 35°C/km. But

with thickness of 6400 m maximum heating temperatures could be achieved under geothermal gradient of about 25°C/km.

6.3. Implications for hydrocarbon formation

In the Palaeozoic succession of the Ahnet and Mouydir basins two main units of hydrocarbon source rocks are present (e.g., Macgregor, 1996). These are the Lower Silurian "hot shales" and Middle to Late Devonian shales, including the basal Frasnian organic-rich unit. Additionally, in the Ahnet Basin the Tournaisian shales occur that also are considered as a source rock, but of minor significance (Lounissi et al., 2007). There are several units of potential reservoir rocks (e.g., Klett, 2000; Lounissi et al., 2007). The main are the Ordovician, Lower to Middle Devonian, and Tournaisian (except of Mouydir) sandstones bodies. In the Ahnet Basin, these reservoir units host commercial accumulations of gas (e.g., Lounissi et al., 2007). The Frasnian shales are rich in organic matter with a total organic carbon (TOC) values of up to 14% (Boote et al., 1998). Although very good parameters, the maturation level of the Upper Devonian rocks place them into the zone of incipient hydrocarbon formation. In contrast, the Middle Devonian shales which are poorer in organic matter (TOC value of up to 3%; Makhous et al., 1997) show thermal maturation consistent with the liquid window. The thermal maturity of Silurian shales corresponding with the zone of gas and condensate formation (Askri et al., 1995; Logan & Duddy, 1998). Because Silurian source rocks directly underly the Devonian deposits, it is possible to postulate that the lower Devonian reservoir rocks were supplied by hydrocarbons from the Silurian. The Frasnian shales are covered by sandstones body. Hence, hydrocarbons occurring in the Middle Devonian reservoir most likely migrate from the underlying shales. Similar to the Upper Devonian also the Lower Carboniferous rocks lay in the zone of incipient oil and gas formation. The Tournaisian sandstones which host hydrocarbons are underlain by shales that are considered to have a source rock potential. Consequently, it is rather certainly that these sandstones were fed by hydrocarbons from the Tournaisian shales.

In contrast, in the Mouydir Basin the occurrence of hydrocarbons is poorly recognized (Klett, 2000). However, the estimated palaeotemperatures for the Middle and Upper Devonian deposits are consistent with the temperature range of the liquid window and partly with the zone of dry gas and condensate formation. Additionally, the thermal maturity of the Silurian shales coincide with the zone of dry gas formation (Askri et al., 1995). Consequently, it is highly possible that from both Silurian and Devonian shales

have generated hydrocarbons. Gas from Silurian sources is to be expected in the Lower Devonian sandstones, whereas Middle and Upper Devonian sandstones bodies may hosted hydrocarbons generated from Devonian shales.

7. ESR SPECTRA

Results. ESR spectra are shown in Figure 21. All show a largely similar spectral structure. The similarity of spectra is expressed by the presence of signals B, C and D with exception of one sample (238/5) in which signal C cannot be observed. Signal B displays a similar structure in all samples, but show minor differences in the intensity. Peak A is present only in two spectra (samples 226/3T and 238/5). The signals are characterized by different g-factor values which are as follows: 2.0377 for signal A, 2.0107-2.0109 for signal B, 2.0059 for signal C, and 2.0033 for signal D. It is important to note that there is a remarkable relation between the intensity of signals in the spectra and their position in the Ahnet-Mouydir area. For example, the intensity of peak C decreases progressively towards the east. An opposite trend is shown by signal D, which increases towards the eastern Mouydir. This phenomenon is well expressed in the samples 323/20 and 238/5 in which the intensity of peak D is twice as large as in other spectra.

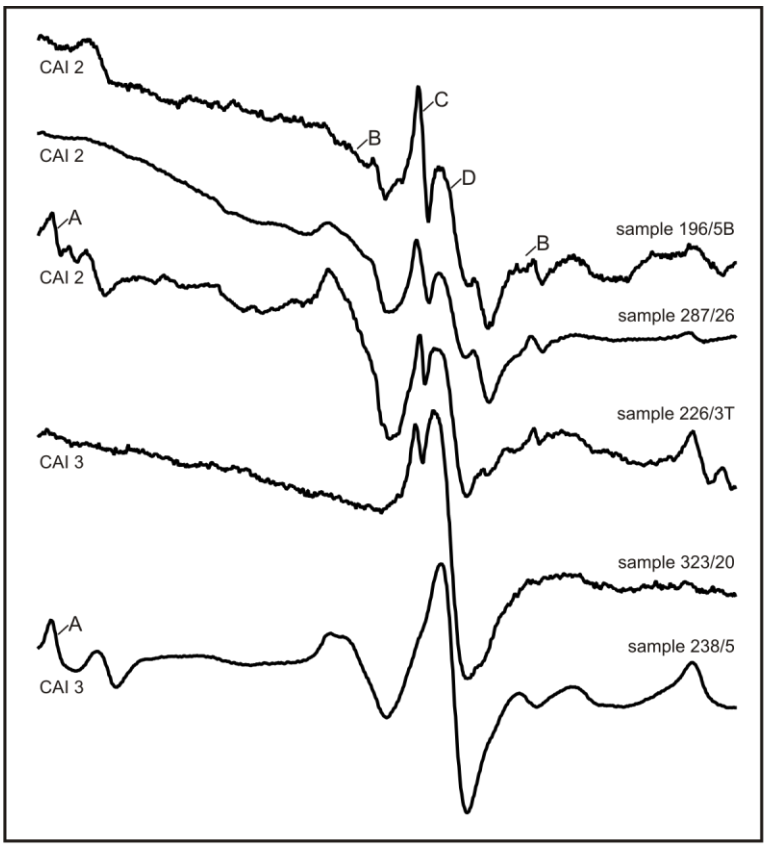

Figure 21. ESR spectra obtained for Devonian conodonts from the Ahnet and Mouydir basins (for location of samples see Figure 14). Note the absence of signal A in the spectra of three samples. Note also decrease in intensity of peak C and increase in intensity of peak D in the spectra of samples yielding higher thermal maturity.

Interpretation - source of signals. Belka et al. (1987) linked emission of signal A to spin of fluorine nucleus present within mineral content of the conodonts. Signal B was attributed to sulphate SO_3^- radicals and signal D was interpreted as generated by unpaired electrons associated to organic matter. In contrast, source of peak C was not recognized by these authors. The g-factor values obtained in the present study differ from those determined by Belka et al. (1987). New data, however, point to similar source for peak D and suggest a possible source for signal C. Unfortunatelly, they do not allow identification of sources which generated signals A and B. Similar spectral structure and g-factor value of the peak D, as recognized in this study, have spectra in natural crystals of apatite presented by Gilinskaya (2005). They attributed peak D to CO^{2-} and CO^{3-} centres. Signals with the same g-factor value as the peak D are also commonly recorded in coal macerals (e.g., Takanohashi & Iino 1990; Doetschman et al., 1994; Bandara et al., 2005). Their apparent relation to carbon compounds seems to confirm the interpretation of signal D by Belka et al. (1987). Similar structure and g-factor values of the peak C obtained during the present study were also noted for signals obtained from apatites by Gilinskaya (1990) and Gilinskaya et al. (1992). They pointed to the PO_3^{2-} centre as a source of these signals. According to Gilinskaya et al. (1992), the formation of the specific PO_3^{2-} centres is related to substitution of Ca^{2+} ions by U and Th ions. Both nuclei are present in the conodont fluorapatite (Trotter & Eggins, 2006). Hence, it is likely that phosphates compounds can be responsible for signal C. The g-factor strongly depends on microwave energy value and a range of magnetic field used during measurements and thus, difference between values obtained now and by Belka et al. (1987) arises most probably from different microwave energy used during the experiments and slightly narrower range of the new spectra. A microwave power of 20 mW and a 100 Gauss range of magnetic field were set during the present study in comparison to approx. 200 Gauss range and unknown microwave power value applied by Belka et al. (1987).

Interpretation - geological significance. According to Belka et al. (1987), the peak A provides information on the last thermal treatment of conodonts. Based on examination of several samples they concluded that the origin of paramagnetic centres responsible for this signal require radiation persisting longer than 225 Ma. Consequently, the presence of this signal in the spectra of Palaeozoic conodonts points to their heating during the Palaeozoic, whereas lack of this signal indicates its reset by another thermal event that must have occurred during or after the Mesozoic time. On the other hand, Belka et al. (1987) noted

that absence of signal A is more function of heating than time. Consequently, signal A may be reset during the Palaeozoic, if conodonts experienced intensive (temperatures above the 100°C) thermal treatment. Samples 226/3T and 238/5, which show a well defined peak A, attest a heating phase during the Palaeozic, consistent with the Carboniferous burial. However, the lack of signal A in spectra of samples 196/5B, 287/26 and 323/20 provide an evidence for another thermal event in the Ahnet and Mouydir basins. Unfortunately, because the absolute concentration of paramagnetic centres in conodonts cannot be estimated, the ESR technique does not allow the determine more precisely the time of this event. But there is indication on cause and timing of the reset of signal A. It is mineralization of conodonts (see chapter 8, section 8.7.). It seems that signal A have been reset by heat transfered by hydrothermal fluids responsible for apatite mineralization. This is because all samples analysed by the ESR method were taken from locations along the major faults and apatite mineralization occurs in all these locations. Additionally, maximium temperature of fluids could reach 350°C. Information related to the thermal maturity of conodonts can be also obtained from the peak D. Belka et al. (1987) noticed that the intensity of this peak is higher in the spectra of conodonts that reveal higher CAI values. Such phenomenon is observed in spectra of two samples (323/20 and 238/5). The intensity of peak D in the spectra of these samples is twice as large as in other spectra. These features correspond well with higher CAI values of samples (CAI=3) in comparison to the CAI values of 2 of the remaining samples.

While peaks A and D provide useful geological information, peaks B and C seem to be irrelevant in the investigation of the thermal history (Belka et al., 1987). Structure of the peak B in Algerian material correlates well with those observed by Belka et al. (1987) in spectra of conodonts with CAI value of 2 and 3. The recognized progressive decrease in intensity of peak C from W to E in the present study can be related to destruction of the crystal structure of fluorapatite in conodonts with relatively high CAI values.

8. MINERALIZATION AND TEXTURAL ALTERATION OF CONODONTS

8.1. Mineralization

Optical and SEM examination of conodont elements revealed the presence of apatite, scheelite, baryte, haematite and framboidal pyrite overgrowing conodonts. Besides these mineral phases conodont elements are also covered by clay minerals, iron oxides, gypsum, quartz and organic matter. Carbonates from which conodonts elements with the mineral overgrowth were recovered were mostly iron-stained bioclastic limestones. Three samples (227/2, 267/20 and 421/3) of sandy limestones and one sample (218/4B) of calcareous sandstone (pl. 2) provided conodonts covered by quartz aggregates. The latter litology contained also reworked clasts of phosphates. Devonian carbonates in the Ahnet and Mouydir area contain commonly numerous framboidal aggregates of pyrite. They are, however, frequently weathered and replaced by iron oxides.

Apatite. Apatite is a common phase overgrowing conodont elements (recognized in 93 samples from 40 sections, i.e. in 24% of all investigated samples). It forms generally 0.1-0.2 mm small, mainly euhedral crystals. They are colourless (with one exception - sample 184/5 contain reddish crystals), hexagonal prismatic and tabular in habit or form massive granular masses which overgrow the surface of conodonts (pl. 3). There is a clear relation between the size and habit of crystals and their location on the conodont element.

The oral sides of carminate and pastinate elements are overgrown by massive granular masses. Sometimes, individual short prismatic crystals that precipitated preferably on carina and blade denticles are present. The orientation of the *c*-axis in prismatic crystals is parallel to the *c*-axis of crystallites within the albid tissue of denticles. In contrast, on the aboral side, apatite crystals are tabular and are relatively larger. Additionally, they are concentrated around the basal pit (form a pile) and/or along the keels. Crystals are attached to the 001 surface of the hyaline tissue crystallites. Their *c*-axes are parallel or sub-parallel to the *c*-axes of crystallites within hyaline tissue of the conodont crown. The growth of subsequent tabular crystals took place along the 001 surface. It is worth to mention that orientation of tabular crystals follows the orientation of the fluorapatite crystallites within prisms building conodont elements (pl. 4). On the angulate and ramiform conodont elements, apatite crystals are generally concentrated around and between denticles. Denticles are overgrown by relatively large hexagonal prismatic crystals. Sometimes, prismatic crystals form a “cap” on the tips of denticles (pl.5). Moreover, all overgrowing apatite crystals are homoaxial (i.e. optically continuous) with the albid tissue of denticles.

Apatite crystals are also frequently present on bars and blades of conodonts. In contrast, they have thick tabular habit. In extreme cases conodont elements are almost completely overgrown by dense crust of apatite crystals (pl. 5).

Scheelite. Whitish scheelite crystals have been identified in 20 samples from 14 sections, i.e. in about 5 % of all investigated samples (pl. 3). They are up to 10 μm large, have thin tabular habit and cover the entire surface of conodont elements (pl. 5). Under ultraviolet light, these crystals display bright blue fluorescence, a typical feature of scheelite (pl. 3). In most cases scheelite crystals grow directly on the conodont surface (pl. 5) or they fill exceptionally fractures within the conodonts tissue. Less frequently, scheelite has also been found overgrowing apatite and pyrite crystals (see appendix).

Baryte. During the EDS analysis of mineralization baryte, massive in habit, was recognized in 5 samples from 5 localizations, i.e. about 1 % of all samples. These aggregates were found on apatite and hematite crystals (pl. 5) or directly on the conodonts surface (see appendix).

Haematite. Silver-grey scalenohedral crystals of haematite, up to 50 μm large, were found mainly on the apatite overgrowth but crystals growing directly on the conodonts surface were also identified (pl. 5). On carminate and pastinate conodont elements haematite is present between apatite crystals, whereas on angulate and ramiform conodonts haematite is concentrated between denticles.

Pyrite. Framboidal (raspberry-like) aggregates of pyrite were identified during the SEM examination of conodonts. They are 2 to 5 μm large and virtually connected with the presence of the apatite mineralization. Pyrite is commonly present between apatite crystals or is distributed on their surface (pl. 5). It should be noted that frequently it is replaced by iron oxides (pseudomorphs).

Clay minerals, iron oxides, gypsum, quartz and organic matter. These mineral and organic phases appear to constitute undisolved remains of the host rocks. Hence they were not analyzed in details and their origin is not discussed in the chapter. Clay minerals form greyish through yellowish to brownish irregular aggregates. They are present in the majority of samples and cover conodont elements as well as crystals of the mineral

overgrowth to various extent. Iron oxides occur most commonly in form of reddish, powdery in habit, accumulations. They are present in the majority of investigated samples. Gypsum forms rosetes of euhedral prismatic crystals. Quartz is present in a few samples only as detrital grains which are bound to form cocoon-like aggregates surrounding angulate and ramiform conodont elements. Another form of quartz grain aggregates are piles located in basal pits of carminate and pastinate conodonts. Organic matter has been recognized in a few, isolated samples only. It builds very characteristic black accumulations covering the entire body of conodonts elements.

8.2. Origin of mineralization.

The phenomenon of mineral overgrowth on conodonts is hitherto poorly known and literature on the subject is very scarce. Schönlaub (1979) and Schönlaub et al. (1980) described quartz and feldspar mineralization on conodont elements originated due to intensive thermal alteration and recrystallization. Nöth (1998) reported dolomite, quartz and feldspar crystals overgrowing conodonts, which attested the influence of hydrothermal fluids related to a magmatic body.

Apatite. Apatite is a very common mineral and occurs in many types of rocks (e.g., Evans, 1993; Klein & Hulburt, 1985; Chang et al., 1996; Wenk & Bulakh, 2004). It is present as accessory mineral in almost all igneous rocks from basic to acid (formation temperature amounts 750-1000°C), fairly common in granitic pegmatites. It can also be formed during contact and regional metamorphism, less frequently during hydrothermal processes (common gangue mineral in meso- and hypothermal ore deposits). As a detrital component, apatite is also present in various sedimentary rocks. Euhedral habit of the apatite crystals overgrowing conodonts in the Ahnet and Mouydir indicates their crystallization from supersaturated hydrothermal fluids. But the conodonts itself did not constitute a source of phosphates. This is indicated by a general lack of any substantial dissolution of conodont elements.

Scheelite. Scheelite is a very rare mineral which originates exclusively during metasomatic processes (e.g., Evans, 1993; Wenk & Bulakh, 2004; Robb, 2005). It is commonly found in skarn ore deposits, in mesothermal (200-400°C) and hypothermal (400-600°C) hydrothermal veins and granitic pegmatites. Accumulations of detrital scheelite are also found in alluvial deposits (see mindat, www.mindat.org). Euhedral habit of scheelite

crystals overgrowing conodonts in the Ahnet-Mouydir area testifies clearly the activity of hydrothermal solutions.

Baryte. Baryte is commonly found as a gangue mineral in epithermal (50-200°C) and mesothermal metallic ore deposits (e.g., Evans, 1993). It may also occur in sedimentary rocks, both of hypogene and supergene origin (e.g., Chang et al., 1996). Baryte co-occurrence with the apatite mineralization and lack of any evidence for detrital character of the observed accumulations suggest a genetic relation to hydrothermal fluids.

Haematite. Haematite is a mineral which occurs in many different geological environments (e.g., Evans, 1993; mindat, www.mindat.org). It is an accessory mineral in felsic igneous rocks and a late-stage sublimate in volcanic rocks. Haematite is also a common mineral in epi- to hypothermal hydrothermal veins as well as can be formed during contact metamorphism. It is abundant on weathered iron-bearing minerals. Large ore bodies of haematite are usually of sedimentary origin. Sunagawa (2005) reported that among few others habits scalenohedral one exhibit haematite crystals in metasomatic deposits. This and co-occurrence of haematite with the apatite mineralization suggest crystallization from hydrothermal fluids. If haematite would be a product of weathering, crystals should occur on majority of conodont elements.

Pyrite. Framboidal aggregates of pyrite are commonly found in recent and ancient sediments originated under anoxic conditions as well as in coals, magmatic and carbonate rocks (e.g., Wilkin & Barnes, 1996; Wilkin et al., 1996). Framboidal pyrite occurs also frequently in various ore deposits, including hydrothermal veins (e.g., Sassano & Schrijver, 1989). Experimental synthesis of framboids showed that they can be formed in ambient temperatute (Wang & Morse, 1996) as well as in higher temperatures, from 150 to 350°C (Graham & Ohmoto, 1994). But large (few to tens of mμ) and well-developed framboids are formed in high temperatures (150-350°C) only (see Ohfuji & Rickard, 2005 for review). The co-occurrence of the framboids overgrowing Algerian conodonts with the apatite mineralization suggests their formation during hydrothermal activity. On the other hand, Lüning et al. (2004) provided evidence for widespread anoxic conditions during the early Frasnian, hence pyrite could potentially originate from seawater under redox conditions. If, it was true, framboids should be present on Frasnian conodonts only. However, they overgrown the Middle and Late Devonian conodont elements. Thus, the

above mentioned arguments strongly support formation of pyrite from hydrothermal fluids. But frequent pseudomorphoses of iron oxides after pyrite point subsequent oxidation. Because the Palaeozoic succession is widely exposed, it is very likely that meteoric waters are responsible for oxidation of pyrite.

8.3. Mineralization sequence

The mutual relationships between minerals allow to define the mineralization sequence. All observations show that apatite crystallized as the first mineral phase. In every case apatite crystallized directly on the surface of conodonts only. It does not overgrow any other mineral phases. Haematite or piryte precipitated during the second phase. Both occur on apatite but never were found together on one conodont element. This is why, their relation to each other is unknown. Scheelite and baryte were formed during the last phases, but their mutual order is also not known. These were not observed to occur together on one conodont element. The recognized mineral association is known to occur in W (tungsten) and W-Sn skarns and metamorphic aureoles of granitic intrusions (e.g., Williams & Kennan, 1983; Singoyi & Zaw, 2001). In such paragenetic sequences haematite and pyrite can be formed simultaneously, whereas scheelite is formed before baryte. Despite a similar mineral association there are, however, differences between the investigated mineralization and those of the ore deposits. In the studied mineralization on conodonts apatite is the most frequent mineral, whereas in the skarns apatite is only an accesoric mineral. Moreover, sulphides and calc-silicates are predominant phases in the skarns (e.g., Houzar et al., 2008; Souza Neto et al., 2008; Chowdhury & Lentz, 2011). The differences are most likely resulted from the mechanism of skarn formation. Skarns are formed in temperatures from 200 to 700°C and at the pressure of 0.3-3 kbar, by contact metasomatic processes related to igneous intrusions. Hence, the ore-forming fluids are reach in various metals and elements (e.g., Evans, 1993, Pirajno, 2009). In contrast, old Precambrian magmatic rocks were most probably a source of ions for the investigated association (see section 8.5.). These rocks were resistant to dissolution and thus the variety of compounds remaind limited. Another difference is that habit of pyrite is cubic in the skarns and/or it occurs as massive aggregates, whereas pyrite overgrowing conodonts forms framboids. During metasomatic processes pyrite crystallizes directly from fluids. On the other hand, not all aspects of framboids formation process has been understood yet but important role in it play mineral precursor which constitute source of iron and enable formation of framboid. Iron sulfides or iron oxides are commonly considered as a

precursor phases (see Ohfuji & Rickard, 2005 for review). Some role in framboids formation, but also not fully recognized, has organic matter (Morse & Wang, 1997). It seems that haematite which co-occur with apatite and organic matter on conodont elements participated in formation of framboidal pyrite on Algerian conodonts.

8.4. Nucleation and relation to conodont tissue

Although conodonts did not constitute source of the mineralization they acted as nucleation centres. Because mineralization has not been found within the host-rocks, the mineral overgrowth on conodont elements is the only one evidence for hydrothermal activity in the Ahnet and Mouydir area. Preferential crystallization of apatite on the denticles, around basal pits and along keels seems to be clearly related to the internal structure of conodont crowns (see chapter 4 for detail description). The porous structure of denticles facilitated infiltration of hydrothermal fluids and promoted precipitation of apatite crystals which grew homoaxial with *c*-axes of internal crystallites of the conodonts tissue. SEM examination revealed that tabular crystals occuring on the aboral side of the conodont elements precipitated on the cutted 001 surface of crystallites in hyaline tissue of keels (see pl. 4). In the next step subsequent crystals grew parallel to the orientation of the *c*-axes of crystallites of the platform, i.e., homoaxial with their long axes. Consequently, they spread on the platform area around keels and basal pits. Similar to the apatite overgrowth on denticles, numerous pores in the albid tissue facilitated penetration of denticles by hot fluids and precipitation of haematite crystals.

8.5. Source of mineral phases

Because the mineralization occurs along faults and damps upwards in the succession, Precambrian rocks of the crystalline basement seem to be the main source of ions contained in the hydrothermal fluids. Apatite is widespread in the magmatic and metamorphic rocks of the Tuareg Shield (e.g., Cottin et al., 1998; Acef et al., 2003; Caby, 2003; Liégeois et al., 2003; Ouzegane et al., 2003). Large tungsten ore accumulations of commercial value were documented in the so-called “Taourirts” granites in the central domain of the Tuareg Shield (Figure 22) and also other parts of the Trans-Saharan Megabelt (Boissonnas, 1974; Benmoussa et al., 1987; Mining potentialities map of Algeria, 2001; Mining potentialities map of Hoggar Massif, undated; Geology map of Africa with major ore deposits, 2004). Various Precambrian magmatic rocks exhibit also widespread baryte mineralization (e.g., Chaouche, 2008).

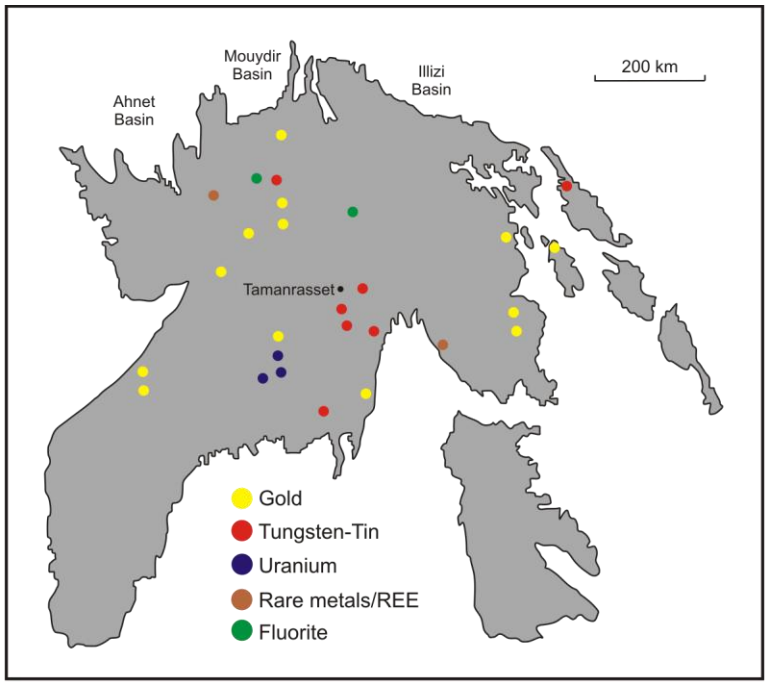

Figure 22. Occurrences of selected ore deposits in the Hoggar Massif (For location of the Tuareg Shield see Figure 2. Boundaries of the Tuareg Shield after Black et al., 1994. Locations of ore deposits after „Mining potentialities map of Algeria", 2001 and „Mining potentialities map of Hoggar Massif", undated).

8.6. Textural alteration

Results. Optical examination of conodonts revealed that about 5% of samples contains elements with a corroded surface. In addition, there is a relation between the development of corrosion and the morphology of conodont elements. Carminate and pastinate elements are corroded mainly at the edges of the platform, around the basal pit and along the keels. Corroded surface is always covered by superficial grey patina. Exceptionally, the entire conodont element is covered by the patina, but corrosion is restricted to local places only. In contrast, on angulate and ramiform conodonts corrosion is developed mainly around the base of denticles; less frequently, it occurs around the basal pits and along the keels (pl. 1 and 6). SEM evaluation showed that in the most cases conodont elements overgrown by apatite crystals have a smooth surface, without any signs of corrosion or recrystallization. Traces of corrosion but without grey patina were observed in a few samples only, and recrystallization of the conodonts`s fluorapatite was identified in one case only. Unaltered surface was identified also in elements overgrown by scheelite and baryte. It is important to note that while corrosion was observed on the surface of conodont elements, crystals of apatite, scheelite, baryte, haematite and pyrite do not exhibit any signs of corrosion.

Interpretation. Experiments of Rejebian et al. (1987) showed that corroded surface covered by surficial grey patina is almost certainly caused by influence of hydrothermal fluids on conodonts. The patina is an effect of oxidation of organic matter dispersed within the conodont crowns. Consequently, the occurrence of conodont elements in the studied material with a corroded surface attests the action of hydrothermal fluids. Because the hyaline tissue is generally less resistant to chemical etching than the albid tissue (e.g., Lindström, 1964; Barnes et al., 1973), and edges are the thinnest and most external parts of the platform, edges first of all subjected to corrosion. Susceptibility of the hyaline tissue on etching along with the high porosity of the hyaline and albit tissue are responsible for preferential corrosion of areas around the base of the denticles. A very common corrosion phenomena occurying around basal pits, keels and adjacent areas are caused by cutting of the layers forming basal pit and keels surface and their stepwise arrangement. This facilitates infiltration of the fluids into the deeper parts of the tissue and its dissolution. The most probable explanation for oxidation of the organic matter on the entire surface of the crown along with a very limited corrosion is the infiltration of oxidative fluids through corroded area and their migration along connected pores in the hyaline tissue.

8.7. Temporal-spatial patterns

Description. The occurrence of mineralization and textural alteration on Devonian and Carboniferous conodonts in the Ahnet-Mouydir area forms patterns presented in Figures 23-26, which were compiled for four stratigraphic intervals in the Devonian (Eifelian, Givetian, Frasnian and Famennian) and for one cumulative Carboniferous map. Data for apatite and scheelite mineralization are based both on the optical and the SEM examination, whereas baryte overgrowth was identified exclusively under the SEM. The phenomenon of corrosion was evaluated both under the binocular and the SEM but textural alteration presented on the maps is based on the binocular examination only. The occurrence of mineralization and textural alteration within particular sections was generalized. If different minerals are indicated at one site (e.g., apatite and scheelite), it does not necessary indicate that these minerals occurred together in one sample. In most cases these phases were identified separately in different samples.

Although mineralization has been recognized both on Devonian and Carboniferous conodonts, this phenomenon is significantly more frequent within the Devonian. Another characteristic feature is the occurrence of mineralization and textural alteration on

conodonts in samples collected along major Precambrian lineaments and subordinate faults.

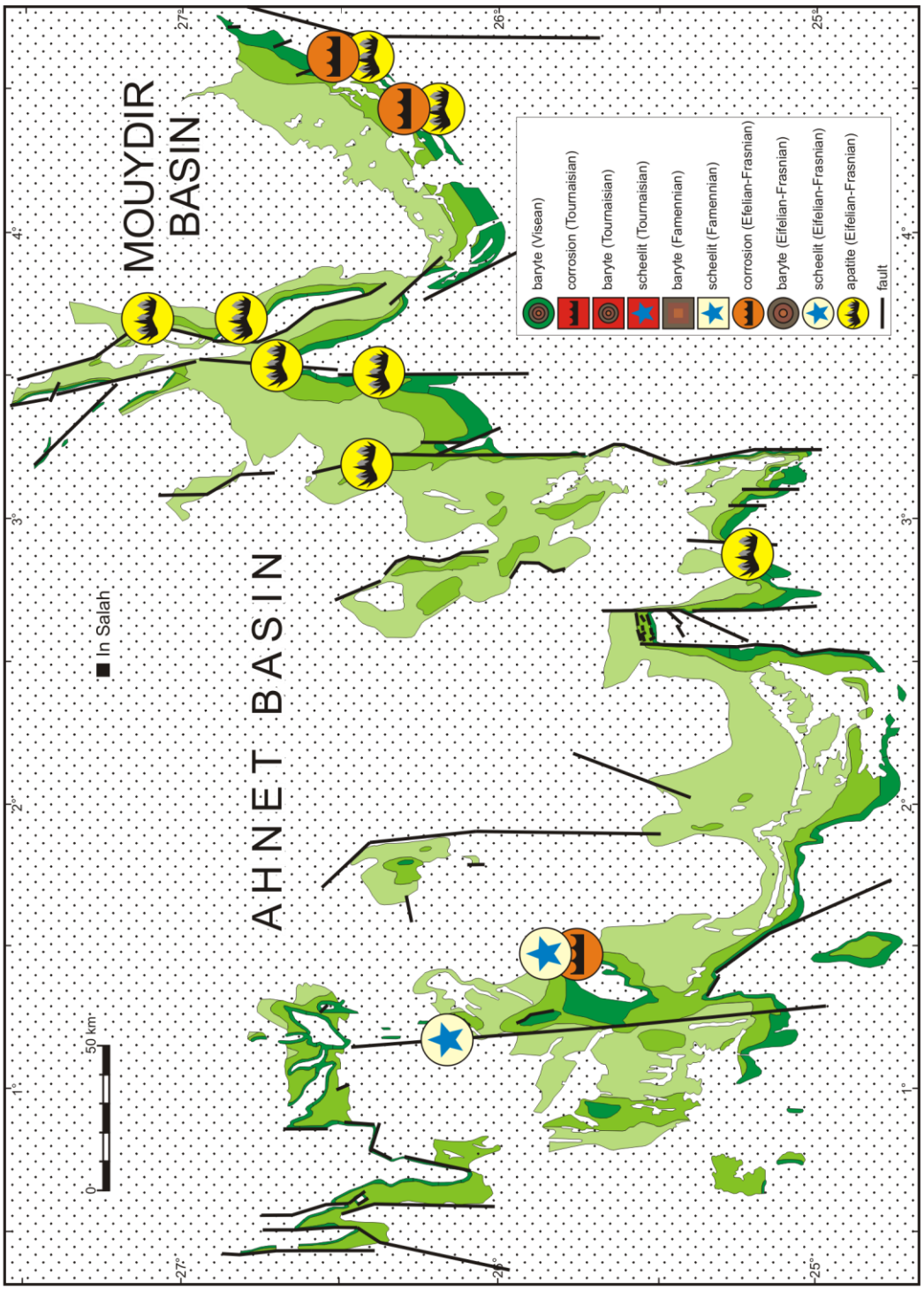

Figure 23. Distribution of mineralization and corrosion in Eifelian rocks of the Ahnet-Mouydir area (base map after Wendt et al., 2006; modified). For legend and location of sections see Figure 8a. Distribution of faults after Moussine-Pouchkine, 1970, unpublished; Conrad, J., 1984; Haddoum et al.,2001; Zazoun, 2001 and Smith et al., 2006.

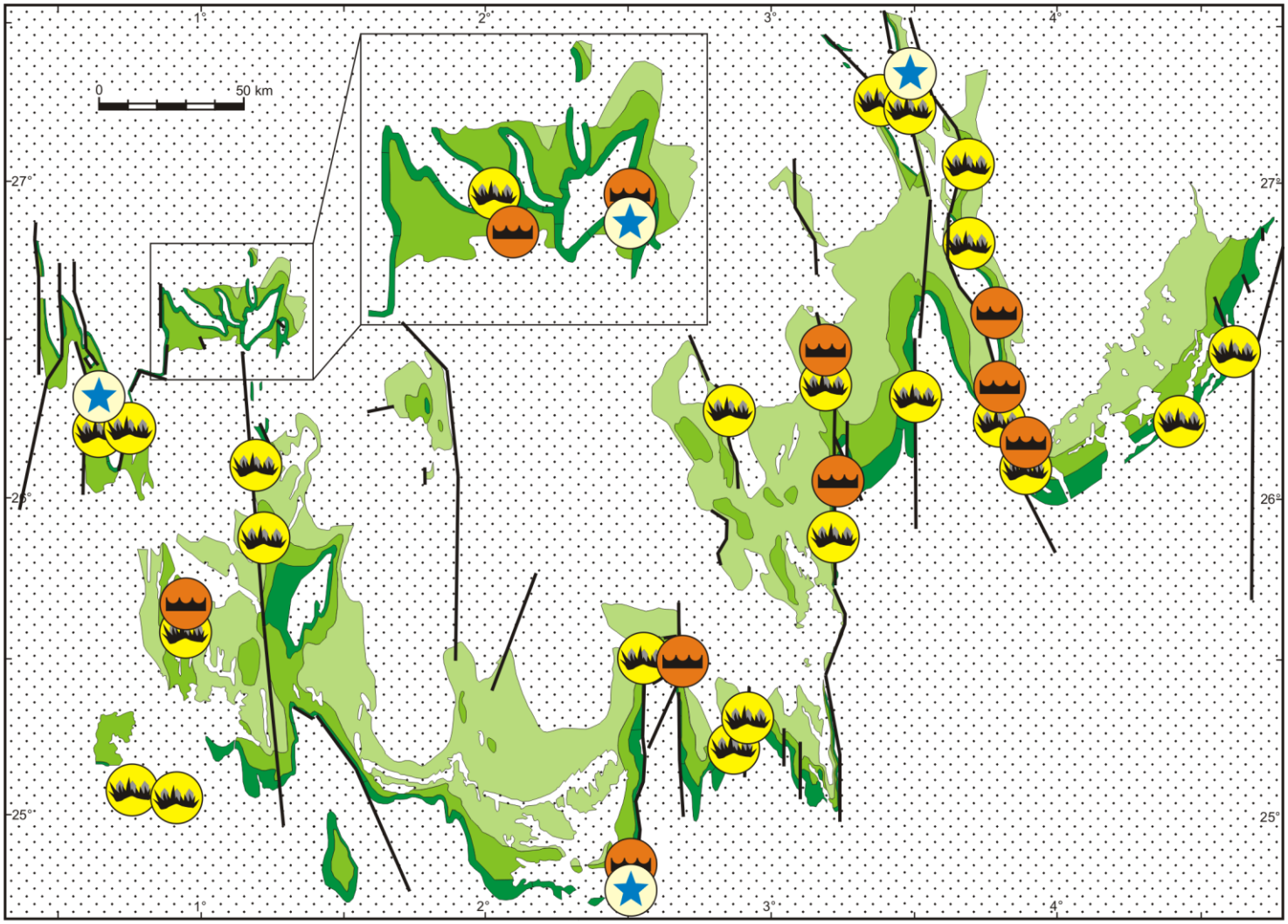

Figure 24. Distribution of mineralization and corrosion in Givetian rocks of the Ahnet-Mouydir area (base map after Wendt et al., 2006; modified). For legend and location of sections see Figures 8a and 23.

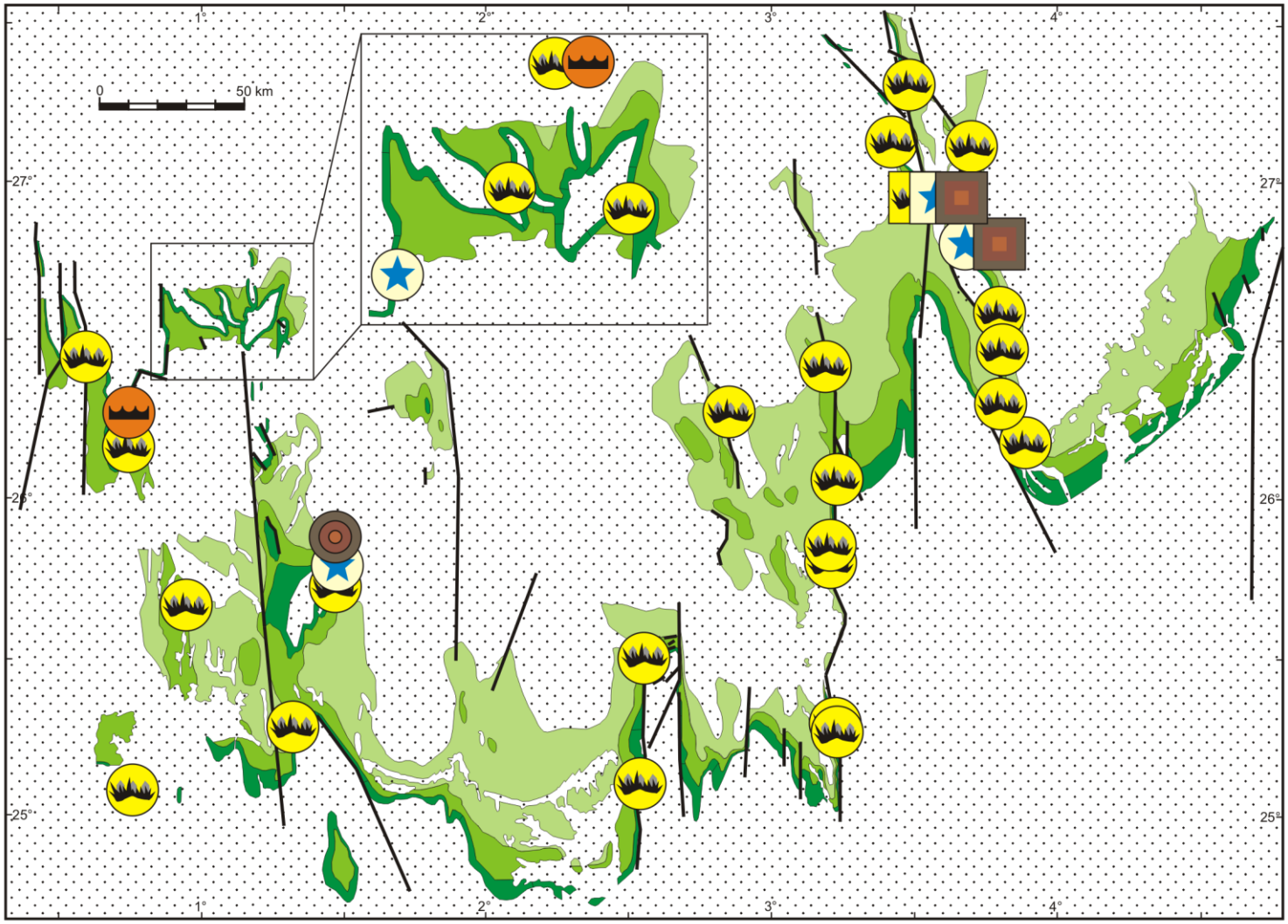

Figure 25. Distribution of mineralization and corrosion in Frasnian and Famennian rocks of the Ahnet-Mouydir area (base map after Wendt et al., 2006; modified). For legend and location of sections see Figures 8a and 23.

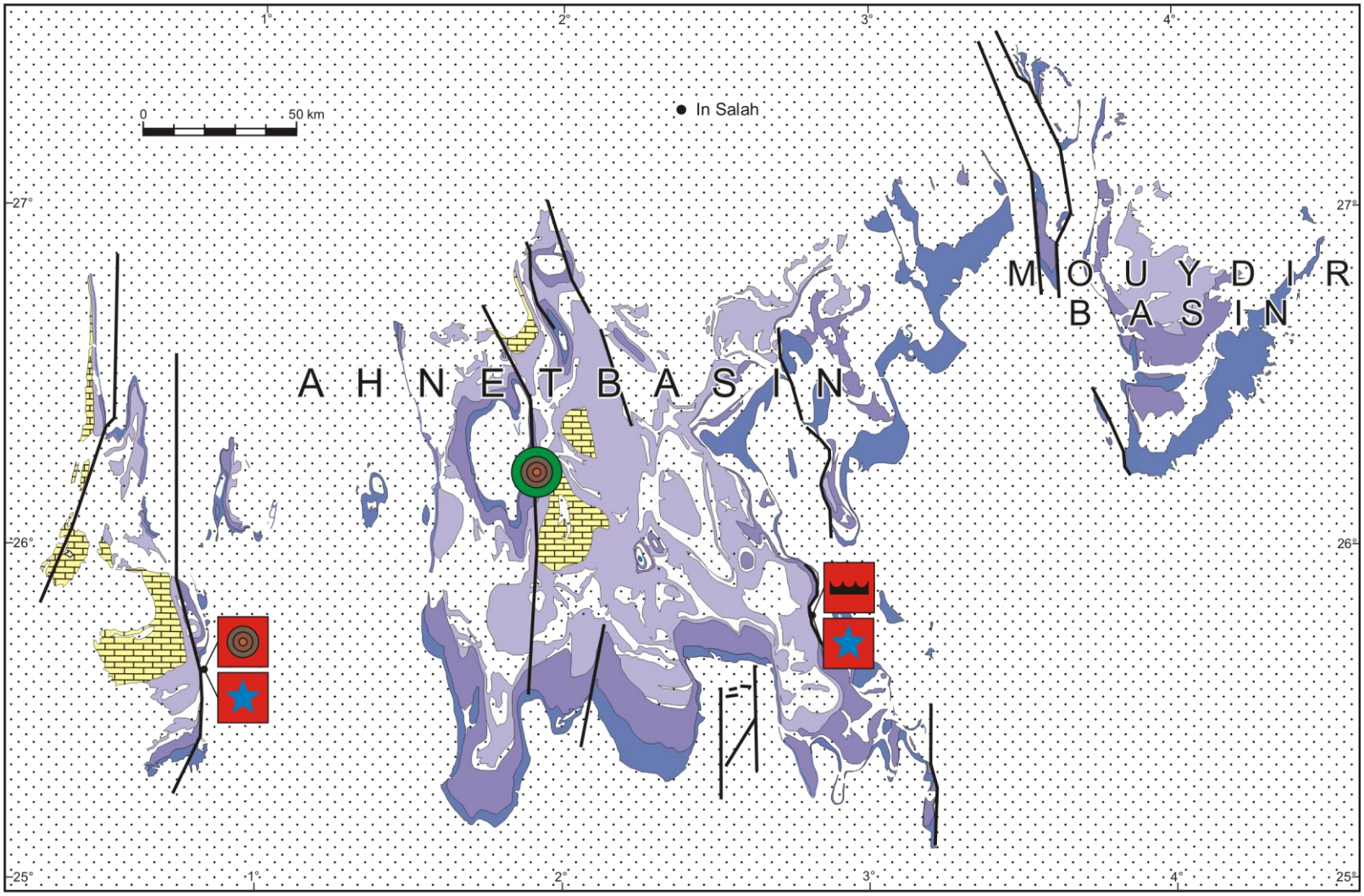

Figure 26. Distribution of mineralization and corrosion in Carboniferous rocks in the Ahnet-Mouydir area (base map after Wendt et al., 2009; modified). For legend and location of sections see Figures 8b and 23.

Moreover, it is remarkable that apatite mineralization is present on the Devonian conodonts only, whereas scheelite and baryte overgrowths occur both on the Devonian and Carboniferous ones. Additionally, a common feature almost as a rule is that, if apatite mineralization occurs in the Eifelian, it occurs also in the Givetian and Frasnian in the same locality. Corrosion occurs across the entire investigated stratigraphic succession but obtained data clearly show that corrosion phenomenon is most frequent in the Givetian and tends to decline in the Upper Devonian and Carboniferous succession. Moreover, the occurrence of textural alteration within Givetian rocks coincides well with the occurrence of the CAI anomalies (compare Figures 17 and 24). At first sight, the patterns reveal a common co-occurrence of the apatite mineralization and corrosion. But a careful analysis shows that scheelite and baryte occur along selected lineaments only, and frequently both minerals co-occur in one site but never in the same samples.

Conodont samples that host mineralization and corrosion are relatively frequent within the investigated collection. Among the Eifelian material, about 35% of samples show these phenomena. Mineralization and corrosion are present in the western Ahnet Basin (Adrar Morat area), along its eastern margin and in the neighbouring Mouydir Basin (Figure 23). In the Givetian, mineralization and corrosion occur in about 24% of samples and they are distributed in the almost entire Ahnet-Mouydir area (Figure 24). Significantly more frequent are these phenomena within the Frasnian samples (in about 50% of samples). Similar to the Givetian, the Frasnian samples yielding mineralization occur across the entire investigated area (Figure 25). Number of samples that host mineralization drops to about 27% in the Famennian and the mineralization has been identified in the western Mouydir (Adrar Idjerane area) only (Figure 25). About 17% of the Carboniferous samples hosts mineralization and corrosion and they occur in the Ahnet Basin only (Figure 26). The presented data show that mineralization tend to decline upward in the investigated succession.

Interpretation. Collected data indicate that rocks in the Ahnet and Mouydir basins experienced four episodes of hydrothermal activity. While the timing of two these events is well documented (1^{st} and 4^{th}), the occurrence of two of them (2^{nd} and 3^{rd}) can only be placed within a wide time range. The occurrence of apatite crystals on corroded surfaces of conodonts attests action of two different types of fluids. One type was undersaturated in relation to phosphate, hence it caused corrosion of conodonts. Second type of fluids was supersaturated, and thus their action is manifested by a frequent mineral overgrowth. The

large number of samples hosting mineralization and corrosion across the entire Ahnet and Mouydir area suggest a high intensity of the hydrothermal processes. Additionally, gradual upward decline of mineralization and corrosion points to ascending character of circulated fluids. The clear relation between the occurrence of mineral overgrowths and corrosion phenomenon, and the location of Precambrian lineaments and faults provides a strong argument that these tectonic discontinuities constituted migration pathways for hydrothermal fluids.

First phase. The first episode of hydrothermal activity in the Ahnet and Mouydir basins is most probably connected with the formation of spectacular early Givetian (*varcus* conodont zone) carbonate mounds (Belka, 1994). However, in the Givetian conodont material samples with corroded conodonts occur, the age of which falls in the stratigraphic interval of mounds formation. Additionally, in the western Ahnet corroded conodonts are present in the same areas as the mounds. Moreover, samples with corroded conodont elements co-occur in most cases in the same localities with the CAI anomalies. The latter have been recognized only among the samples of the v*arcus* zone. Hence, the facts mentioned above strongly suggest that the early Givetian hydrothermal activity resulted partly in corrosion of the Eifelian and Givetian conodont elements. Destructive influence of hydrothermal fluids on conodonts but without any dissolution effect on carbonates seems to be resulted from the pH level of fluids. Nathan & Sass (1981) presented model of chemical stability of apatite and calcium carbonate. It shows that increase in pH from neutral towards alcalic level causes decrease in stability of phosphates and increase in the stability of carbonates. This indicates that corrosive fluids must have been most likely alkalic. Experiments of Rejebian et al. (1987) showed that anomalous CAI values may be used for temperature estimation of hydrothermal fluids. The anomalous CAI values of 4.5 indicate that the temperature of fluids could reach locally even 300°C.

Second phase. The corrosion phenomenon is observed also among the early Frasnian conodonts but its distribution is limited to the NW Ahnet only. Hence, the inference is that their corrosion is probably a result of an another hydrothermal event, which locally could certainly caused a corrosion of older conodonts. This is presumably why corroded conodont elements occur also in the Givetian sediments younger than the v*arcus* zone. During the Frasnian extensional tectonics occurred across North Africa. It resulted in stronger subsidence in the Ougarta Range and formation of pull-apart basins in Morocco

(e.g., Fabre et al., 2005; Michard et al., 2008). Consequently, it is likely that also in the Ahnet-Mouydir area extension could increase permeability along the faults and facilitate migration of fluids.

Third phase. If the widespread apatite and co-occurring haematite and pyrite mineralization originated within one episode of hydrothermal activity only, it must have occur during Early Carboniferous time. This is because the apatite mineralization does not occur on conodonts younger than the uppermost Famennian. The precipitation of apatite took place most likely in the early Tournaisian. This time interval corresponds with the shortlasting (shorter than 10 Ma) emergence event which resulted in formation of a regional stratigraphic gap (Wendt et al., 2009). An uplift of crustal blocks usually opens migration pathways, and thus can facilitate migration of fluids. From the three minerals of this phase, apatite, haematite and pyrite, the pyrite framboids have the lowest maximum formation temperature. This indicates that temperature of fluids responsible for apatite overgrowth was no higher than 350°C (Graham & Ohmoto, 1994). Haematite, however, sets the lower temperature limit of hydrothermal fluids being not lower than 50°C.

It is possible that apatite mineralization was genetically related with scheelite-baryte precipitation (see fourth phase). An argument for that is the paragenetic mineralization sequence. Because Devonian strata was buried deeper than Carboniferous ones the temperature of ascending fluids must have been higher within the Devonian rocks than in the Carboniferous strata. This could explain why apatite overgrowth was only formed within the Devonian. During upwards migration through the Carboniferous succession the temperature of fluids must have decreases and, in consequence, scheelite and baryte precipitated. However, differences in the distribution of apatite (commonly occurs along major lineaments as well as subordinate faults), and scheelite and baryte (present mainly along major lineaments) seems to suggest that scheelite-baryte mineralization represents a separate hydrothermal phase.

There is some indication that during the late Tournaisian a next hydrothermal event occurred at least locally. It is one corroded late Tournaisian sample from the SE Ahnet. Hydrothermal leakage could be related with increased permeability along the faults that is indicated by occurrence of late Tournaisian magmatic intrusions further south in the Tin Serririne Basin (Djellit et al., 2006). But the number of analysed Carboniferous material

was very low (30 samples). Hence, available data are to scarce to set separate hydrothermal event responsible for corrosion of Tournaisian conodonts.

Fourth phase. Scheelite and baryte overgrowth on Devonian and Early Carboniferous (Tournaisian and Visean) conodonts document the last episode of hydrothermal activity. Lack of any signs of mineralization on Bashkirian conodonts indicates that hot fluids were most likely active somewhere in the late Visean-Serpukhovian time interval. It is suggested that this hydrothermal activity was promoted by the regional uplift of the Ahnet-Mouydir area (Fabre, 1988; Logan & Duddy, 1998), which resulted in formation of a regional stratigraphic gap during that time (Wendt et al., 2009). The uplift could certainly facilitate migration of hydrothermal solutions. Because conodonts do not show an increased thermal maturity level along the faults hosting mineralization, the temperature of fluids was rather close to the lower precipitation limits. This is 200°C for scheelite and 50°C for baryte.

Fluids from two different sources participated in the hydrothermal processes. This is indicated by the occurrence of corrosion on the one hand and mineralization on the other hand. There is no direct data indicating sources for hydrothermal fluids in the investigated area. But strontium isotopic data obtained from the Devonian conodont elements point that fluids migrate through the Silurian shales (see chapter 9). This indicate that hot solutions percolate upwards. Enrichment of one type of fluids in phosphorus and tungsten ions from Precambrian magmatic rocks (see section 8.5.) is an additional argument for ascending circulation type. If hydrothermal fluids circulated upwards, there are three potential sources of water: juvenile/magmatic, connate (sediment-hosted) and deeply circulated seawater. Due to lack of any magmatic activity during the Devonian and Carboniferous in the Ahnet-Mouydir area and no Sr isotopic signal indicating magmatic source (see chapter 9) juvenile fluids are rather unlikely. Seawater seems to be the most likely source of fluids responsible for the corrosion of conodont elements and the formation of CAI anomalies. This is because the Ahnet-Mouydir area was continuously covered by the epicontinental sea during Devonian time (e.g., Guiraud et al., 2005; Wendt et al., 2006). Triggered by higher heat flow along the lineaments seawater could infiltrate into deeper parts of the earth crust where the waters were heated, evolved, and subsequently migrated upwards. Because mineralizing hydrothermal events occurred probably at the time of emergence of the investigated area (see above) connate waters hosted by the Cambro-Ordovician clastics are the most probable source for hydrothermal processes resulted widespread

mineralization. Occurrence of salt brines in the Cambro-Ordovician complex in the Saharan Platform have been confirmed (Askri et al., 1995). Sediment-hosted waters could have had interact with the rocks of the Precambrian basement and assimilate various ions. Water trapped in pores are heated during the burial could be periodically released during emergence episodes. Uplift of crustal blocks usually casues increase of permeability along tectonic discontinuities, hence circulation is facilitated. Volume of released waters can be considerable. Pirajno (2009), for example, noted that the average shale can yield 3.5×10^3 litres of water for every 1 m^3 of solid material deposited.

9. STRONTIUM ISOTOPIC COMPOSITION

Results. The measured $^{87}Sr/^{86}Sr$ isotopic ratios in the Middle and Late Devonian conodont samples range from 0.708044 to 0.708583, whereas the Sr composition of their host carbonates is generally more radiogenic and yield ratios from 0.708259 to 0.709298 (Table 1). A conspicuous feature is that isotopic ratios in all conodont and carbonates samples are more radiogenic than those of the Devonian seawater (Figure 27). Moreover, carbonates have generally more radiogenic ratios than conodonts. Differences amount from 0.00008 to 0.00104. In one sample (218/4B), however, ratio in both phases is identical within the measurement error.

Table 1. $^{87}Sr/^{86}Sr$ ratios of conodonts and corresponding host-carbonates in the Ahnet-Mouydir area.

sample no.	age (zone)	conodonts	carbonates
184/5	lower asymmetricus	0.708154 ± 15	0.708295 ± 11
196/5B	middle varcus	0.708250 ± 12	0.709298 ± 9
218/4B	frasnian zone 8-11	0.708583 ± 22	0.708588 ± 14
233/2	costatus	0.708044 ± 22	———
317/2T	middle varcus	0.708158 ± 18	0.709005 ± 13
323/20	frasnian zone 13	0.708161 ± 18	0.708858 ± 12
335/4	ensensis-timorensis	0.708175 ± 12	0.708259 ± 13

Interpretation. More radiogenic $^{87}Sr/^{86}Sr$ ratios recorded in conodonts and carbonates from the Ahnet and Mouydir basins than ratios determined for the Devonian seawater suggest a significant influx of radiogenic strontium from an another, secondary source. In the investigated area there are several potential sources of Sr. A first source might constitute a thick (up to 700 m) succession of Silurian marine shales. Unfortunately, there are no Sr isotopic data for Palaeozoic sediments in the Ahnet-Mouydir area. However, an extensive Sr dataset for clays from elsewhere shows that they are commonly characterized by $^{87}Sr/^{86}Sr$ ratios ranging from 0.71 to 0.74 (e.g., Douglas et al., 1995; Derry & France-Lanord, 1996; Fagel et al., 1997; Winter et al., 1997; Colin et al., 1999; Stancin et al., 2006). Another source of Sr could be various magmatic Precambrian rocks of the Trans-Saharan Megabelt. The acidic rocks commonly show ratios from 0.71 to 0.79 (e.g., Acef et al., 2003; Abdallah et al., 2007; Djouka-Fonkwé et al., 2008). A third potential source of radiogenic Sr could constitute the Cenozoic meteoric waters. During the Pliocene-Pleistocene pluvial periods large amounts of rainwaters percolated the Palaeozoic rocks in the area (Rognon, 1967).

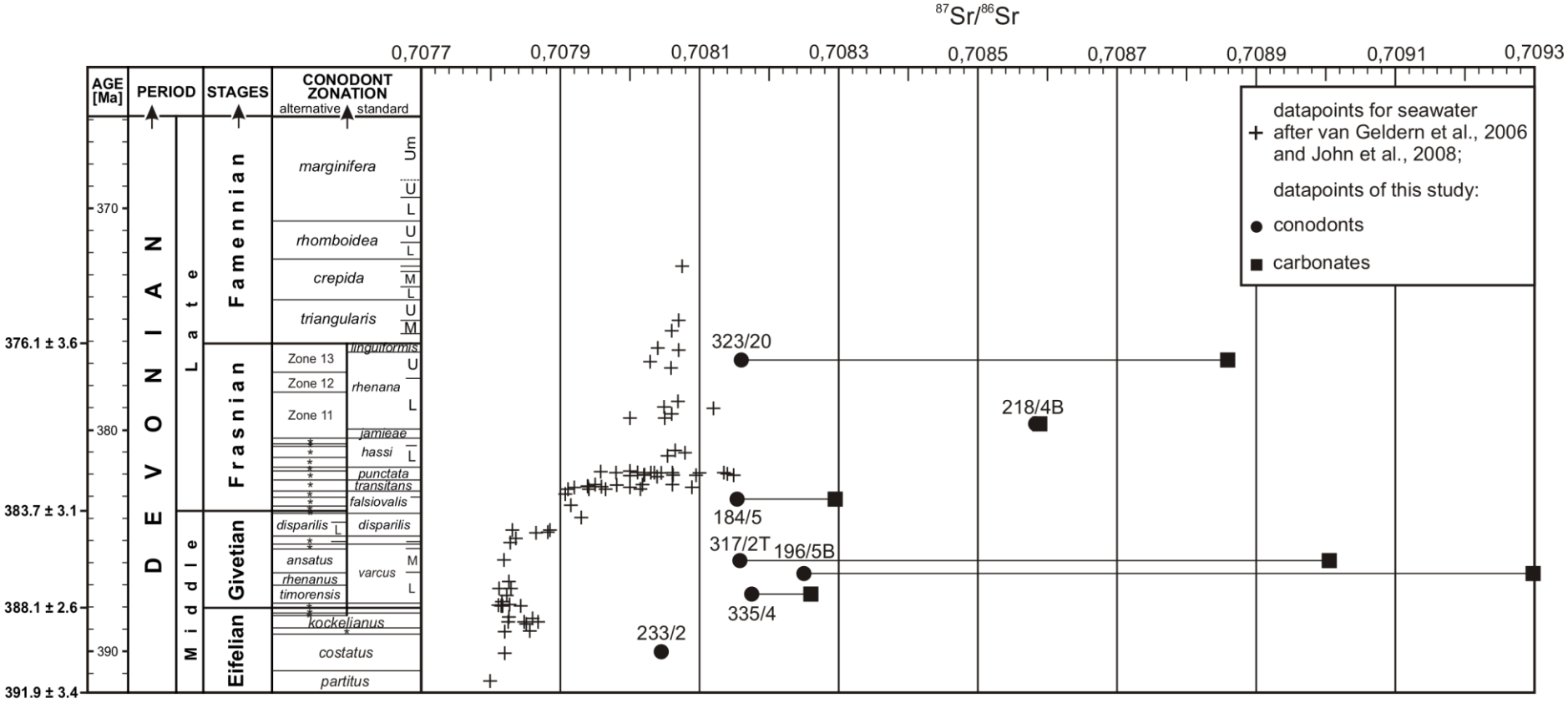

Figure 27. $^{87}Sr/^{86}Sr$ values of the Middle and Late Devonian conodonts and carbonates in the Ahnet and Mouydir basins. Note their deviation from the composition of seawater (conodont zonation and absolute age after Kaufmann, 2006).

Within the above mentioned sources the Silurian shales seem to be the most probable source of radiogenic strontium. They are extensively distributed in the whole investigated area, and underly directly the Devonian succession. In contrast, there is no documented presence of acid magmatic rocks in the Ahnet-Mouydir area. More radiogenic ratios observed in host-rock in comparison to those of conodonts are certainly related to different resistance of carbonates and phosphates on chemical exchange. The isotopic system of carbonates opens in lower temperatures than that of phosphates and, thus Sr from external source could influence longer and, as consequence carbonates could assimilate larger amount of radiogenic strontium. On the other hand, a significant increase of $^{87}Sr/^{86}Sr$ ratio can also be observed in carbonates exposed to influence of meteoric waters, which in most cases are enriched in ^{87}Sr relative to seawater (Veizer, 1992). This causes shift of isotopic ratio towards higher values. Meteoric waters frequently are charged with CO_2, thus became aggressive to carbonates which relatively easy undergo dissolving and transformation into more stable phase recording new isotopic signal. It is highly possible that Sr from both, Silurian shales and meteoric waters affected carbonates in the Ahnet-Mouydir area. Isotopic ratios in three carbonates samples (184/5, 218/4B and 335/4) are only slightly more radiogenic than conodonts and in three remaining ones (196/5B, 317/2T and 323/20) differences in the Sr isotopic composition are significantly larger. It is suggested that in the latter their isotopic signal has been overprinted by the activity of meteoric waters. A strong support for meteoric alteration provide carbon and oxygen isotopic data obtained for calcite cements of stromatactis cavities in mud mounds from Ahnet (Wendt et al., 1997).

10. BURIAL AND THERMAL HISTORY

Based on general geology data, analysis of conodont CAI, electron spin resonance data, mineralization and textural alteration phenomena the following thermal history of the Ahnet and Mouydir basins during the Middle Devonian up to the end of the Carboniferous is proposed. Due to slight differences in development of the basins separated scenarios are postulated for each of them. They have, however, some common elements. The framework of the models is summarized in subsidence curves for compacted Middle Devonian to Carboniferous successions presented in Figure 28. The curve of the Ahnet Basin has been constructed for the Bled el Mass area, that of the Mouydir Basin for the Adrar Idjerane area.

Ahnet Basin

Middle Devonian. The Middle Devonian sediments (thickness of 40 m) were deposited with an average accumulation rate of about 3 m/Ma. The entire succession represents an open marine environment with depths lower than 200 m (Wendt et al., 1997, 2006). And, there is no indication that the subsidence rate have changed considerably during this time. In early Givetian time hydrothermal fluids operated along the major lineaments, what resulted in corrosion of conodonts and formation of the CAI anomalies. Although the temperature of hydrothermal fluids could reach locally up to 300°C (see chapter 8, section 8.7.), their thermal influence on the conodont colour remained unsignificant. This was because of short duration of the hydrothermal event.

Late Devonian. During this time sedimentation rate increased considerably. About 1200 m of deposits accumulated, with an average rate of c. 46 m/Ma. The sedimentation rate must have exceeded the subsidence since the sequence yields a clear shallowing-up trend (see Wendt et al., 2006). During the late Frasnian this sequence was locally influenced by hydrothermal fluids. Their activity has caused corrosion of conodont elements but their impact on the conodont colour was unnoticeable. At the end of Late Devonian time the buried Middle Devonian succession still remained immature.

Early Carboniferous. In the early Tournaisian sedimentation have been temporarily disrupted by a regional uplift (see Wendt et al., 2009). This was a time of an extensive hydrothermal activity across the entire basin. Its record is a widespread apatite, haematite and piryte mineralization. This is only noticeably effect of action of these hot solutions.

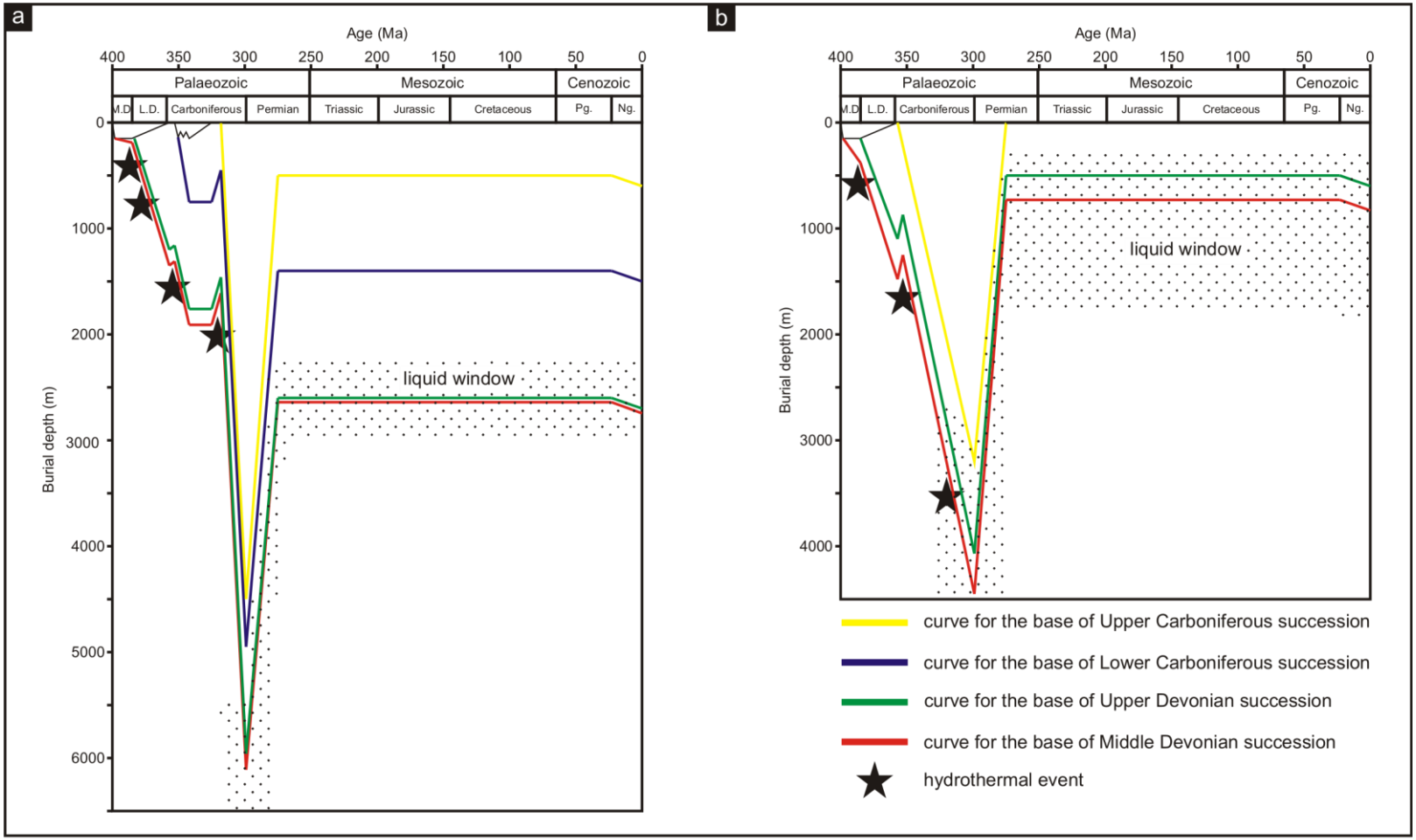

Figure 28. (a) Burial and thermal history curve for the western Ahnet Basin (Bled el Mass area). (b) Burial and thermal history curve for the western Mouydir Basin (Adrar Idjerane area).

The uplift was followed by deposition of 600 m of the middle Tournaisian to lower Visean deposits which represent three transgression-regression cycles (see chapter 2). Accumulation rate remains similar to those during the Late Devonian (about 54 m/Ma). Since middle Visean time a regressive trend is visible. It culminated in the uplift during the latest Early Carboniferous (see Wendt et al., 2009) and as a consequence, sedimentation was terminated again. During this time Carboniferous deposits were penetrated by hot mineralized brines along the major lineaments. Conodonts were overgrown by scheelite and baryte crystals. There is no, however, evidence for an increase of thermal maturity due to action of the fluids. At the end of Early Carboniferous time the base of Middle Devonian succession reached depths with temperature of only 20°C.

Late Carboniferous. This time was the most critical for the burial and thermal development of the basin. As thick as 4500 m deposits accumulated. The thickness of Late Carboniferous infill suggests a significant acceleration of accumulation rate which could exceed 200 m/Ma. In consequence, the Middle Devonian and a part of the Upper Devonian sequence entered into the liquid window zone. In contrast, the Lower Carboniferous succession remained immature although it reached its maximum burial depth. At the Carboniferous/Permian transition an uplift began starting cooling from maximum burial temperatures. During Mesozoic time deformations and erosion of Palaeozoic strata occurred. In a result of erosion most of the Upper Carboniferous rocks (up to c. 4000 m) have been removed.

The obtained data do not support assumption of Cawley et al. (1995) and Takherist et al. (1995) that the Cretaceous continental deposits are responsible for re-burial of exposed Palaeozoic succession and increase of their thermal maturity level. This scenario is moreover unlikely due to lack of Mesozoic rocks in the Ahnet-Mouydir area, which were probably never deposited there (see chapter 2). Additionally, obtained ESR data excluding re-heating during the Cretaceous (see chapter 7). The 100 m of Cenozoic deposits did not have any influence on the maturity of the Palaeozoic. The new data do not support also a thermal activation triggered by Late Triassic-Early Jurassic magmatic activity postulated by as a mechanism of re-heating of Palaeozoic deposits by Logan & Duddy (1998) and Makhous & Galushkin (2003). Magmatic rocks are first of all known only from the NW margin of the Ahnet Basin and form up 20 m thick doleritic sills (Smith et al., 2006). The study presented by Galushkin (1997) shows that influence of heat produced by magmatic

intrusions on surrounding rocks is limited, e.g., approximately 120 m thick sill would increase of thermal maturity of surrounding rocks on the distance up to 200 m. Taking into account this study a significant impact on thermal maturity of rocks in the Ahnet Basin (geothermal gradient up to 100°C/km) as proposed by Logan & Duddy (1998) would require magmatic body(ies) with dimension comparable to the surface area of the basin. In contrast, the mineral overgrowth and the textural alteration of conodont elements provide clear evidence for the occurrence of hydrothermal activity in the investigated area as previously suggested by Makhous & Galushkin (2003). On the other hand, the data obtained during present study suggest a different source of hot solutions and a different timing of their activity. Moreover, they do not confirm the significance of hydrothermal impact on the maturity level of Palaeozoic rocks proposed by these authors.

Mouydir Basin

Middle Devonian. During the Middle Devonian 200 m of sediments were accumulated with a rate of c. 17 m/Ma. The succession have been deposited in an open-marine environment (Wendt et al., 2006). The subsidence rate seems to be quite stable during this time. In the early Givetian hydrothermal fluids circulated through the sequence and caused alteration of conodonts, i.e. their corrosion and anomalous changes of colouration.

Late Devonian. Like in the Ahnet Basin, Late Devonian time was characterized also in the Mouydir Basin by an acceleration of subsidence. About 1100 m of sediments were accumulated with a rate of c. 42 m/Ma). The Late Devonian overburden pushed down the Middle Devonian succession to depths with temperatures of about 40°C.

Carboniferous. The deposition of the Carboniferous sediments was preceded by a regional emergence in the early Tournaisian (see Wendt et al., 2009). During this time hot solutions from the Cambro-Ordovician clastics were released. They are responsible for apatite and co-occuring mineral overgrowths on Devonian conodonts. Lack of any noticeable changes in colour of these conodonts occurring along the faults attest a weak thermal impact of fluids on the maturity of rocks. The maturity data indicate the presence of about 3200 m of the carboniferous cover which accumulated with rates higher than 50 m/Ma. During this phase an another hydrothermal event must have occurred. It is recorded by scheelite and baryte mineralization on conodonts. Similar to the previous hydrothermal events, this hydrothermal activity had also a local influence. It did not contribute to the growth of the

thermal maturity of rocks in the whole basin. In the late Early Carboniferous the Middle and Upper Devonian sequences must have reached the top of the liquid window zone. But it was most probably in latest Carboniferous time that both successions achieved their maximium burial depth. Consequently, it is postulated that the uplift and cooling begun in the Carboniferous/Permian transition interval as a result of final collision of Gondwana and Euramerica. The Mesozoic was time of intensive erosion and folding of the Palaeozoic succession. Erosion removed majority of the Carboniferous deposits in the basin (c. 2700 m).

REFERENCES:

Abdallah, N., Liégeois, J.-P., De Waele, B., Fezaa, N. & Ouabadi, A., 2007. The Temaguessine Fe-cordierite orbicular granite (Central Hoggar, Algeria): U-Pb SHRIMP age, petrology, origin and geodynamical consequences for the late Pan-African magmatism of the Tuareg shield. *Journal of African Earth Sciences*, **49**, 153-178.

Acef, K., Liégeois, J.-P., Ouabadi, A. & Latouche, L., 2003. The Anfeg post-collisional Pan-African high-K calc-alkaline batholith (Central Hoggar, Algeria), result of the LATEA microcontinent metacratonization. *Journal of African Earth Sciences*, **37**, 295-311.

Aït-Hamou, F., Dautria, J.M., Cantagrel, J.M., Dostal, J. & Briqueu, L., 2000. Nouvelles données géochronologiques et isotopiques sur le volcanisme cénozoïque de l'Ahaggar (Sahara algérien): des arguments en faveur de l'existence d'un panache. *Comptes Rendus de l`Académie des Sciences de Paris, Sciences de la Terre et des planètes*, **330**, 829-836.

Aldridge, R.J., 1984. Thermal metamorphism of the Silurian strata of the Oslo region, assessed by conodont colour. *Geological Magazine*, **121**, 347-349.

Aldridge, R.J., Briggs, D.E.G., Clarkson, E.N.K. & Smith, M.P., 1986. The affinities of conodonts-new evidence from the Carboniferous of Edinburgh, Scotland. *Lethaia*, **19**, 279-291.

Armstrong, H.A., Smith, M.P., Aldridge, R.J. & Tull, S.J., 1994. Thermal maturation of the Lower Palaeozoic strata of northern Greenland from conodont colour alteration index (CAI) data: implications for burial history and hydrocarbon exploration. *Geological Magazine*, **131**, 219-230.

Askri, H., Belmecheri, A., Benrabach, B., Boudjema, A., Boumendjel, K., Daoudi, M., Drid, M., Ghalem, T., Docca, A.M., Ghandriche, H., Ghomari, A., Guellati, N., Khennous, M., Lounici, R., Naili, H., Takherist, D. & Terkmani, M., 1995. Geology of Algeria. *In: Schlumberger/Sonatrach Algeria Well Evaluation Conference*, 1-93. Available at www.mem-algeria.org/fr/hydrocarbures/w1_0.pdf

Ayadi, A., Dorbath, C., Lesquer, A. & Bezzeghoud, M., 2000. Crustal and upper mantle velocity structure of the Hoggar swell (Central Sahara, Algeria). *Physics of the Earth and Planetary Interiors*, **118**, 111-123.

Bandara, T.S., Kannangara, G.S.K., Wilson, M.A., Boreham, C.J. & Fisher, K., 2005. The study of Australian coal maturity: relationship between solid-state NMR aromaticities and organic free-radical count. *Energy & Fuels*, **19**, 954-959.

Barnes, C.R., Sass, D.B. & Monroe, E.A., 1973. Ultrastructure of some Ordovician conodonts. *Geological Society of America Special Paper*, **141**, 1-30.

Barrick, J.E., Over, D.J. & Landis, C.R., 1990. Conodont fluorescence emission spectra: potential for high resolution evaluation of organic maturation in hydrocarbon-bearing basins. *Meeting of the south-central section of the Geological Society of America and associated societies, Stillwater, Oklahoma*, abstract with Programs, **22**.

Barwise, A.J.G., Clarke, P.N., Bishop, C.D. & Malek, B., 2003. Charge modelling in the Ahnet-Timmimoun Basin, Algeria-timing of gas generation and migration. *The American Association of Petroleum Geologists Hedberg Conference, Algiers, Algeria* (abstract). Available at http://www.searchanddiscovery.com/abstracts/pdf/2003/hedberg_algeria/#B

Bastida, F., Brime, C., García-López, S. & Sarmiento, G.N., 1999. Tectono-thermal evolution in a region with thin-skinned tectonics: the western nappes in the Cantabrian Zone (Variscan belt of NW Spain). *International Journal of Earth Sciences*, **88**, 38-48.

Bau, M., Romer, R.L., Lüders, V. & Dulski, P., 2003. Tracing element sources of hydrothermal mineral deposits: REE and Y distribution and Sr-Nd-Pb isotopes in fluorite from MVT deposits in the Pennine Orefield, England. *Mineralium Deposita*, **38**, 992-1008.

Belka, Z., 1990. Thermal maturation and burial history from conodont colour alteration data, Holly Cross Mountains, Poland. *Courier Forschung-Institut Senckenberg*, **118**, 241-251.

Belka, Z., 1991. Conodont colour alteration patterns in Devonian rocks of the eastern Anti-Atlas, Morocco. *Journal of African Earth Sciences*, **12**, 417-428.

Belka, Z., 1993. Thermal and burial history of the Cracow-Silesia region (southern Poland) assessed by conodont CAI analysis. *Tectonophysics*, **227**, 161-190.

Belka, Z., 1994. Dewońskie budowle węglanowe (carbonate buildups) Sahary środkowej i ich związek z podmorskimi źródłami termalnymi. *Przegląd Geologiczny*, **42**, 341-346.

Belka, Z., Miaskiewicz, K. & Zydorowicz, T., 1987. The electron spin resonance technique in conodont studies. *In: Austin, R.L. (ed.), Conodonts: investigative techniques and applications,* Ellis Horwood Limited, Chichester, 230-240.

Benmoussa, L., Amossé, J., Giraud, P. & Oliver, R., 1987. A geochemical study of the concentration process of tungsten and tin in the „Taourirts" granites of central Ahaggar, Algeria. *Chemical Geology*, **63**, 121-132.

Bennacef, A., Beuf, S., Biju-Duval, B., de Charpal, O., Gariel, O. & Rognon, P., 1971. Example of cratonic sedimentation: Lower Paleozoic of Algerian Sahara. *The American Association of Petroleum Geologists Bulletin*, **55**, 2225-2245.

Beuf, S., Biju-Duval, B., de Charpal, O., Rognon, P., Gariel, O. & Bennacef, A., 1971. Les grès du Paléozoique inférieur au Sahara. Sédimentation et discontinuités, évolution structurale d`un craton. *Publications de l`Institut Français du Pétrole, Collection Science et Technique du Pétrole*, **18**. Éditions Technip, Paris, 464 pp.

Black, R., Latouche, L., Liégeois, J.-P., Caby, R. & Bertrand, J.M., 1994. Pan-African displaced terranes in the Tuareg shield (central Sahara). *Geology*, **22**, 641-644.

Boissonnas, J., 1974. Les granites à structure concentrique et quelques autres granites tardifs de la chaîne pan-africaine en Ahaggar (Sahara Central, Algérie). *Thesis, University of Paris VI, Paris, edition BRGM (Bureau de Recherches Géologiques et Minières), Paris*, 662 pp.

Boote, D.R.D., Clark-Lowes, D.D. & Traut, M.W., 1998. Palaeozoic petroleum systems of North Africa. *In: Macgregor, D.S., Moody, R.T.J. & Clark-Lowes, D.D. (eds.), Petroleum geology of North Africa. Geological Society, London, Special Publications*, **132**, 7-68.

Bruckschen, P., Bruhn, N., Veizer, J. & Buhl, D., 1995. $^{87}Sr/^{86}Sr$ isotopic evolution of Lower Carboniferous seawater: Dinantian of western Europe. *Sedimentary Geology*, **100**, 63-81.

Burnett, R.D., 1987. Regional maturation patterns for Late Visean (Carboniferous, Dinantian) rocks on northern England based on mapping of conodont colour. *Irish Journal of Earth Sciences*, **8**, 165-185.

Caby, R., 2003. Terrane assembly and geodynamic evolution of central-western Hoggar: a synthesis. *Journal of African Earth Sciences*, **37**, 133-159.

Cawley, S.J., Wilson, N.P., Primmer, T. & Oxtoby, N., 1995. Palaeozoic gas charging in the Ahnet-Timimoun Basin, Algeria. *The American Association of Petroleum Geologists Bulletin*, **79**, 1202 (abstract).

Chabou, M.C., Sebai, A., Féraud, G. & Bertrand, H., 2007. Datation $^{40}Ar/^{39}Ar$ de la province magmatique de l'Atlantique central dans le Sud-Ouest algérien. *Comptes Rendus Geoscience*, **339**, 970-978.

Chang, L.L.Y., Howie, R.A. & Zussman, J., 1996. Rock-forming minerals, vol. 5B: non-silicates. Sulphates, carbonates, phosphats and halides (2nd ed.). Longman, 392 pp.

Chaouche, A., 2008. Permis de prospection de Tan Chaffao ouest, Hoggar, Algérie. *Rapport de travaux géologiques 2007-2008, Mines Cancor Inc*., 69 pp. Available at http://www.cancor.ca/documents/rapport-travaux-FINAL-COMPLET-TCO-nov-08.pdf

Chorowicz, J. & Fabre, J., 1997. Organization of drainage networks from space imagery in the Tanezrouft plateau (Western Sahara): implications for recent intracratonic deformations. *Geomorphology*, **21**, 139-151.

Chowdhury, S. & Lentz, D.R., 2011. Mineralogical and geochemical characteristics of scheelite-bearing skarns, and genetic relations between skarn mineralization and petrogenesis of the associated granitoid pluton at Sargipali, Sundergarh District, Eastern India. *Journal of Geochemical Exploration*, **108**, 39-61.

Colin, C., Turpin, L., Bertaux, J., Despraires, A. & Kissel, C., 1999. Erosional history of the Himalayan ranges during the last two glacial-interglacial cycles. *Earth and Planetary Science Letters*, **171**, 647-660.

Conrad, G., 1969. L`evolution continentale post-Hercynienne du Sahara Algérien (Saoura, Erg Chech-Tanezrouft, Ahnet-Mouydir). Centre National de la Recherche Scientifique, Paris, 527 pp.

Conrad, J., 1984. Les séries carbonifères du Sahara central Algérien. Stratigraphie, sédimentation, evolution structurale, *Thèse de doctorat d`etat ès-Sciences naturelles, Universitè d`Aix-Marseille*, 370 pp.

Cottin, J.Y., Lorand, J.P., Agrinier, P., Bodinier, J.L. & Liégeois, J.-P., 1998. Isotopic (O, Sr, Nd) and trace element geochemistry of the Laouni layered intrusions (Pan-African belt, Hoggar, Algeria): evidence for post-collisional continental tholeiitic magmas variably contaminated by continental crust. *Lithos*, **45**, 197-222.

Coward, M.P. & Ries, A.C., 2003. Tectonic development of North African basins. *In: Arthur, T.J., Macgregor, D.S. & Cameron, N.R. (eds), Petroleum Geology of Africa: New Themes and Developing Technologies. Geological Society, London, Special Publications*, **207**, 61-83.

Craig, J., Rizzi, C., Said, F., Thusu, B., Lüning, S., Asbali, A.I., Keeley, M.L., Bell, J.F., Durham, M.J., Eales, M.H., Beswetherick, S. & Hamblett, C., 2006. Structural styles and prospectivity in the Precambrian and Palaeozoic hydrocarbon systems of North Africa, pre-print. *In: proceedings of Geology of East Libya Symposium, Binghazi, Libya*, 52 pp.

Deaton, B.C., Nestell, M. & Balsam, W.L., 1996. Spectral reflectance of conodonts: a step toward quantitative color alteration and thermal maturity indexes. *The American Association of Petroleum Geologists Bulletin*, **80**, 999-1007.

Denison, R.E., Koepnick, R.B., Burke, W.H., Hetherington, E.A. & Fletcher, A., 1997. Construction of the Silurian and Devonian seawater $^{87}Sr/^{86}Sr$ curve. *Chemical Geology*, **140**, 109-121.

Derder, M.E.M., Smith, B., Henry, B., Yelles, A.K., Bayou, B., Djellit, H., Ait ouali, R. & Gandriche, H., 2001. Juxtaposed and superimposed paleomagnetic primary and secondary components from the folded Middle Carboniferous sediments in the Reggane Basin (Saharan craton, Algeria). *Tectonophysics*, **332**, 403-422.

Derder, M.E.M., Henry, B., Amenna, M., Bayou, B., Djellit, H., Guemache, M.A. & Hemmi, A., 2009. New structural implications for the central Sahara (Algeria), from the revisited Upper Carboniferous "Hassi Bachir" Formation: Paleomagnetic constraints. *Tectonophysics*, **463**, 69-76.

Derry, L.A. & France-Lanord, C., 1996. Neogene Himalayan weathering history and river $^{87}Sr/^{86}Sr$: impact on the marine Sr record. *Earth and Planetary Science Letters*, **142**, 59-74.

Djellit, H., Bellon, H., Ouabadi, A., Derder, M.E.M., Henry, B., Bayou, B., Khaldi, A., Baziz, K. & Merahi, M.K., 2006. Âge $^{40}K/^{40}Ar$, Carbonifère inférieur, du magmatisme basique filonien du synclinal paléozoïque de Tin Serririne, Sud-Est du Hoggar (Algérie). *Compte Rendus Geoscience*, **338**, 624-631.

Djouka-Fonkwé, M.L., Schulz, B., Schüssler, U., Tchouankoué, J.-P. & Nzolang, C., 2008. Geochemistry of the Bafoussam Pan-African I- and S-type granitoids in western Cameroon. *Journal of African Earth Sciences*, **50**, 148-167.

Doetschman, D.C., Mehlenbacher, R.C. & Ito, O., 1994. A study of coal extraction with electron paramagnetic resonance and proton nuclear magnetic resonance relaxation techniques. *Energy & Fuels*, **8**, 907-919.

Donoghue, P.C.J., 1998. Growth and patterning in the conodont skeleton. *Philosophical Transactions of the Royal Society London B*, **353**, 633-666.

Dopieralska, J., 2003. Neodymium isotopic composition of conodonts as a palaeoceanographic proxy in the Variscan oceanic system. *Ph.D. Thesis, Justus-Liebig-University, Giessen*, 1-111. Available at http://geb.uni-giessen.de/geb/volltexte/2003/1168/.

Douglas, G.B., Gray, C.M., Hart, B.T. & Beckett, R., 1995. A strontium isotopic investigation of the origin of suspended particulate matter (SPM) in the Murray-Darling River system, Australia. *Geochimica et Cosmochimica Acta*, **59**, 3799-3815.

Durand, B., Alpern, B., Pittion, J.L. & Pradier, B., 1986. Reflectance of vitrinite as a control of thermal history of sediments. *In: Burrus, J. (ed.), Thermal modeling in sedimentary basins.* Editions Technip, Paris, 441-474.

Ebinger, C.J. & Sleep, N.H., 1998. Cenozoic magmatism throughout east Africa resulting from impact of a single plume. *Nature*, **395**, 788-791.

Ebneth, S., Diener, A., Buhl, D. & Veizer, J., 1997. Strontium isotopic systematics of conodonts: Middle Devonian, Eifel Mountains, Germany. *Palaeogeography, Palaeoclimatology, Palaeoecology*, **132**, 79-96.

Ellison, S., 1944. The composition of conodonts. *Journal of Paleontology*, **18**, 133-140.

Epstein, A.G., Epstein, J.B. & Harris, L.D., 1977. Conodont color alteration-an index to organic metamorphism. *U.S. Geological Survey Professional Paper*, **995**, 27 pp.

Evans, A.M., 1993. Ore geology and industrial minerals: an introduction (3rd ed.). Geosciences Texts, Blackwell Sciences, 389 pp.

Fabre, J., 1988. Les séries Paléozoiques d`Afrique: une approche. *Journal of African Earth Sciences*, **7**, 1-40.

Fabre, J. (ed.), Caby, R., Girod, M. & Moussine-Pouchkine, A., 1976. Introduction a la geologie du Sahara Algerien et des regions voisines. Société Nationale d`Edition et Diffusion, Alger, 422 pp.

Fabre, J. (ed.), Latouche, L., Kazi Tani, N., Moussine-Pouchkine, A., Aït-Hamou, F., Dautria, J.M. & Maza, M., 2005. Géologie du Sahara occidental et central. *Tervuren African Geoscience Collection*, **108**. Musée Royal de l`Afrique Central-Belgique, Tervuren, 610 pp. Available at http://www.africamuseum.be/research/publications/rmca/online/Sahara.pdf

Fagel, N., André, L. & Debrabant, P., 1997. Multiple seawater-derived geochemical signature in Indian oceanic pelagic clays. *Geochimica et Cosmochimica Acta*, **61**, 989-1008.

Fekirine, B. & Abdallah, H., 1998. Palaeozoic lithofacies correlatives and sequence stratigraphy of the Saharan Platform, Algeria. *In: Macgregor, D.S., Moody, R.T.J. & Clark-Lowes, D.D. (eds.), Petroleum geology of North Africa. Geological Society, London, Special Publications*, **132**, 97-108.

Follot, J., 1952. Ahnet et Mouydir. *XIX^{ème} Congrès Géologique International. Monographies Régionales, 1re série: Algérie 1*, Alger, 79 pp.

Galushkin, Yu.I., 1997. Thermal effects of igneous intrusions on maturity of organic matter: a possible mechanis of intrusion. *Organic Geochemistry*, **26**, 645-658.

García-López, S., Brime, C., Bastida, F. & Sarmiento, G.N., 1997. Simultaneous use of thermal indicators to analyse the transition from diagenesis to metamorphism: an example from the Variscan Belt of northwest Spain. *Geological Magazine*, **134**, 323-334.

García-López, S., Bastida, F., Aller, J. & Sanz-López, J., 2001. Geothermal gradients and metamorphic zonation from the conodont colour alteration index (CAI). *Terra Nova*, **13**, 79-83.

Gawlick, H.J., Krystyn, L. & Lein, R., 1994. Conodont colour alteration indices: Palaeotemperatures and metamorphism in the Northern Calcareous Alps-a general view. *Geologische Rundschau*, **83**, 660-664.

van Geldern, R., Joachimski, M.M., Day, J., Jansen, U., Alvarez, F., Yolkin, E.A. & Ma, X.-P., 2006. Carbon, oxygen and strontium isotope records of Devonian brachiopod shell calcite. *Palaeogeography, Palaeoclimatology, Palaeoecology*, **240**, 47-67.

Geology map of Africa with major ore deposits, 2004. Bureau de Recherches Géologiques et Minières (BRGM-Centre scientifique et technique), Map prepared in occasion of 20th Colloquium of African Geology, Orléans, France. Available at http://cag20.brgm.fr/circulaires/Afrique_map_10M.pdf

Gilinskaya, L.G., 1990. A new type of PO_3^{2-} center in apatite. *Journal of Structural Chemistry*, **31**, 892-898.

Gilinskaya, L.G., 2005. Electron paramagnetic resonance spectra of carbonate centers in natural apatites. *Inorganic Materials*, **41**, 503-508.

Gilinskaya, L.G., Zanin, Yu.N., Knubovets, R.G., Korneva, T.A. & Fadeeva, V.P., 1992. Organophosphorus radicals in natural apatites $Ca_2(PO_4)_3(F, OH)$. *Journal of Structural Chemistry*, **33**, 859-870.

Graham, U.M. & Ohmoto, H., 1994. Experimental study of formation mechanisms of hydrothermal pyrite. *Geochimica et Cosmochimica Acta*, **58**, 2187-2202.

Grün, R., 1989. Die ESR Alterbestimmungs methode. Springer-Verlag, 132 pp.

Guiraud, R., 1998. Mesozoic rifting and basin inversion along the northern African Tethyan margin: an overview. *In: Macgregor, D.S., Moody, R.T.J. & Clark-Lowes, D.D. (eds.), Petroleum geology of North Africa*. *Geological Society, London, Special Publications*, **132**, 217-229.

Guiraud, R., Doumnang Mbaigane, J.-C., Carretier, S. & Dominguez, S., 2000. Evidence for a 6000 km length NW-SE striking lineament in northern Africa: the Tibesti lineament. *Journal of the Geological Society, London*, **157**, 897-900.

Guiraud, R., Bosworth, W., Thierry, J. & Delplanque, L., 2005. Phanerozoic geological evolution of Northern and Central Africa: An overview. *Journal of African Earth Sciences*, **43**, 83-143.

Haddoum, H., Guiraud, R. & Moussine-Pouchkine, A., 2001. Hercynian compressional deformations of the Ahnet-Mouydir Basin, Algerian Saharan Platform: far-field stress effects of the Late Palaeozoic orogeny. *Terra Nova*, **13**, 220-226.

Harris, A.G., Rexroad, C.B., Lierman, R.T. & Askin, R.A., 1990. Evaluation of a CAI anomaly, Putnam County, central Indiana, U.S.A.: possibility of a Mississippi Valley-Type hydrothermal system. *Courier Forschung-Institut Senckenberg*, **118**, 253-266.

Hass, W.H., 1962. Conodonts. *In: Hass, W.H., Häntzschel, W., Fisher, D.W., Howell, B.F., Rhodes, F.H.T., Müller, K.J. & Moore, R.C., Treatise on Invertebrate Paleontology, part W*, Geological Society of America and University of Kansas Press, 3-98.

Helsen, S. & Königshof, P., 1994. Conodont thermal alteration patterns in Palaeozoic rocks from Belgium, northern France and western Germany. *Geological Magazine*, **131**, 369-386.

Helsen, S., David, P. & Fermont, W.J.J., 1995. Calibration of conodont color alteration index using color image analysis. *Journal of Geology*, **103**, 257-267.

Héroux, Y., Chagnon, A., & Bertrand, R., 1979. Compilation and correlation of major thermal maturation indicators. *The American Association of Petroleum Geologists Bulletin*, **63**, 2128-2144.

Houzar, S., Litochleb, J., Sejkora, J., Cempírek, J. & Cícha, J., 2008. Unusual mineralization with niobian titanite and Bi-tellurides in scheelite skarn from Kamenné doly quarry near Písek, Moldanubian Zone, Bohemian Massif. *Journal of Geosciences*, **53**, 1-16.

International Stratigraphic Chart, 2009. International Commission on Stratigraphy.

John, E.H., Cliff, R. & Wignall, P.B., 2008. A positive trend in seawater $^{87}Sr/^{86}Sr$ values over the Early Middle Frasnian boundary (Late Devonian) recorded in well-preserved conodont elements from the Holy Cross Mountains, Poland. *Palaeogeography, Palaeoclimatology, Palaeoecology*, **269**, 166-175.

Jones, G.L., 1992. Irish Carboniferous conodonts record maturation levels and the influence of tectonism, igneous activity and mineralization. *Terra Nova*, **4**, 238-244.

Kaufmann, B., 2006. Calibrating the Devonian Time Scale: A synthesis of U-Pb ID-TIMS ages and conodont stratigraphy. *Earth-Science Reviews*, **76**, 175-190.

Kesler, S.E., Jones, L.M. & Ruiz, J., 1988. Strontium isotope geochemistry of Mississippi Valley-type deposits, East Tennessee: Implications for age and source of mineralizing brines. *Geological Society of America Bulletin*, **100**, 1300-1307.

Klein, C. & Hulburt jr, C.S., 1985. Manual of mineralogy (20th ed.). Wiley & Sons, 596 pp.

Klett, T.R., 2000. Total petroleum systems of the Grand Erg/Ahnet province, Algeria and Morocco-the Tanezzuft-Timimoun, Tanezzuft-Ahnet, Tanezzuft-Sbaa, Tanezzuft-Mouydir, Tanezzuft-Benoud, and Tanezzuft-Béchar/Abadla. *U.S. Geological Survey Bulletin*, **2202-B**, 144 pp. Available at http://pubs.usgs.gov/bul/b2202-b/b2202-bpo.pdf

Königshof, P., 2003. Conodont deformation patterns and textural alteration in Paleozoic conodonts: examples from Germany and France. *Senckenbergiana Lethaea*, **83**, 149-156.

Königshof, P. & Boncheva, I., 2005. Maturation patterns in Palaeozoic rocks of north-eastern Bulgaria based on conodont colour alteration index (CAI) data. *Bulletin of Geosciences*, **80**, 223-237.

Kovács, S. & Árkai, P., 1987. Conodont alteration in metamorphosed limestones from northern Hungary, and its relationship to carbonate texture, illite crystalinity and vitrinite reflectance. *In: Austin, R.L. (ed.), Conodonts: investigative techniques and applications*, Ellis Horwood Limited, Chichester, 209-229.

Kovács, S., Rálisch-Felgenhauer, E. & Bóna, J., 2006. Conodont colour alteration related to a half-graben structure: an example from the Mesozoic of the Mecsek and Villány Hills area (Tisza Megaunit, Southern Hungary). *Geologica Carpathica*, **57**, 257-268.

Leach, D.L., Apodaca, L.E., Repetski, J.E., Powell, J.W. & Rowan, E.L., 1997. Evidence for hot Mississippi Valley-Type brines in the Reelfoot rift complex, south-central United States, in Late Pennsylvanian-Early Permian. *U.S. Geological Survey Professional Paper*, **1577**, 44 pp.

Lee, G.S.H., Mar, G.L., Rose, H.R., Marshall, C.P., Young, B.R., Skilbeck, C.G. & Wilson, M.A., 1998. X-ray photoelectron spectroscopy of conodonts. *Organic Geochemistry*, **28**, 759-765.

Lefranc, J.Ph. & Guiraud, R., 1990. The Continental Intercalaire of northwestern Sahara and its equivalents in the neighbouring regions. *Journal of African Earth Sciences*, **10**, 27-77.

Legall, F.D., Barnes, C.R. & Macqueen, R.W., 1981. Thermal maturation, burial history and hotspot development, Paleozoic strata of southern Ontario-Quebec, from conodont and acritarch colour alteration studies. *Bulletin of Canadian Petroleum Geology*, **29**, 492-539.

Le Heron, D.P. & Craig, J., 2008. First-order reconstructions of a Late Ordovician ice sheet. *Journal of the Geological Society, London*, **165**, 19-29.

Lesquer, A., Bourmatte, A. & Dautria, J.M., 1988. Deep structure of the Hoggar domal uplift (Central Sahara, south Algeria) from gravity, thermal and petrological data. *Tectonophysics*, **152**, 71-87.

Lesquer, A., Bourmatte, A., Ly, S. & Dautria, J.M., 1989. First heat flow determination from the central Sahara: relationship with the Pan-African belt and Hoggar domal uplift. *Journal of African Earth Sciences*, **9**, 41-48.

Lesquer, A., Takherist, D., Dautria, J.M. & Hadiouche, O., 1990. Geophysical and petrological evidence for presence of an "anomalous" upper mantle beneath the Saharan basins (Algeria). *Earth and Planetary Science Letters*, **96**, 407-418.

Liégeois, J.-P., Latouche, L., Boughrara, M., Navez, J. & Guiraud, M., 2003. The LATEA metacraton (Central Hoggar, Tuareg shield, Algeria): behaviour of an old passive margin during the Pan-African orogeny. *Journal of African Earth Sciences*, **37**, 161-190.

Liégeois, J.-P., Benhallou, A., Azzouni-Sekkal, A., Yahiaoui, R. & Bonin, B., 2005. The Hoggar swell and volcanism: Reactivation of the Precambrian Tuareg shield during Alpine convergence and West

African Cenozoic volcanism. *In: Foulger, G.R., Natland, J.H., Presnall, D.C. & Anderson, D.L., (eds.), Plates, plumes, and paradigms. Geological Society of America Special Paper*, **388**, 379-400.

Lindström, M., 1964. Conodonts. Elsevier, 196 pp.

Logan, P. & Duddy, I., 1998. An investigation of the thermal history of the Ahnet and Reggane Basins, Central Algeria, and the consequences for hydrocarbon generation and accumulation. *In: Macgregor, D.S., Moody, R.T.J., Clarck-Lowes, D.D. (eds), Petroleum Geology of North Africa. Geological Society, London, Special Publications*, **132**, 131-155.

Lounissi, R. (co-ordinator), Daoudi, N.E., Remidi, H., Lassouani, L., Derguini, K., Dib, N., Daoudi, N.E., Radja, T., Chenna, K., Tadjin, E.T., Abdous, L., Benkhannouche, M.S., Zattouta, B., Belhameche, F., Ghoul, H., Badsi, M., Tenkhi, T., Khanfar, Y., Rahmani, F.A., Malek, B., Goucem, A., Sadallah, N., 2007. Petroleum Geology of Algeria. *In: Sonatrach/Schlumberger Algeria Well Evaluation Conference*, 94 pp.

Lüning, S., Craig, J., Loydell, D.K., Štorch, P. & Fitches, B., 2000. Lower Silurian 'hot shales' in North Africa and Arabia: regional distribution and depositional model. *Earth-Science Reviews*, **49**, 121-200.

Lüning, S., Wendt, J., Belka, Z. & Kaufmann, B., 2004. Temporal-spatial reconstruction of the early Frasnian (Late Devonian) anoxia in NW Africa: new field data from the Ahnet Basin (Algeria). *Sedimentary Geology*, **163**, 237-264.

Macgregor, D.S., 1996. The hydrocarbon systems of North Africa. *Marine and Petroleum Geology*, **13**, 329-340.

Makhous, M., 2001. The formation of hydrocarbon deposits in the North African basins: geological and geochemical conditions. *Lecture Notes in Earth Sciences*, **89**, 310 pp.

Makhous, M. & Galushkin, Yu.I., 2003. Burial history and thermal evolution of the southern and western Saharan basins: synthesis and comparison with the eastern and northern Saharan basins. *The American Association of Petroleum Geologists Bulletin*, **87**, 1799-1822.

Makhous, M., Galushkin, Yu.I. & Lopatin, N., 1997. Burial history and kinetic modeling for hydrocarbon generation, part I: the GALO model. *The American Association of Petroleum Geologists Bulletin*, **81**, 1660-1678.

Marshall, C.P., Rose, H.R., Lee, G.S.H., Mar, L.G. & Wilson, M.A., 1999. Structure of organic matter in conodonts with different colour alteration indexes. *Organic Geochemistry*, **30**, 1339-1352.

Marshall, C.P., Mar, L.G., Nicoll, R.S. & Wilson, M.A., 2001. Organic geochemistry of artificially matured conodonts. *Organic Geochemistry*, **32**, 1055-1071.

Mastalerz, M., Bustin, R.M., Orchard, M. & Forster, P.J.L., 1992. Fluorescence of conodonts: implications for organic maturation analysis. *Organic Geochemistry*, **18**, 93-101.

McArthur, J.M., Howarth, R.J. & Bailey, T.R., 2001. Strontium isotope stratigraphy: LOWESS version 3: best fit to the marine Sr-isotope curve for 0-509 Ma and accompanying look-up table for deriving numerical age. *The Journal of Geology*, **109**, 155-170.

Michard, A., Saddiqi, O., Chalouan, A & Frizon de Lamotte, D. (eds.), 2008. Continental evolution: the geology of Morocco. Structure, stratigraphy, and tectonics of the Africa-Atlantic-Mediterranean triple junction. *Lecture Notes in Earth Sciences*, **116**, 424 pp.

Mining potentialities map of Algeria, 2001. Office National de Recherche Géologique et Minière (ORGM). Available at http://www.mem-algeria.org/mining/map_pot.htm

Mining potentialities map of Hoggar Massif, undated. Available at http://www.mem-algeria.org/english/index.php?page=potentialites

Morency, M., Emond, P.L. & von Bitter, P.H., 1970. Dating conodonts using electron spin resonance: a possible technique. *Kansas Geological Survey Bulletin*, **199**, 17-19.

Morse, J.W. & Wang, Q., 1997. Pyrite formation under conditions approximating those in anoxic sediments: II. Influence of precursor iron minerals and organic matter. *Marine Chemistry*, **57**, 187-193.

Munoz, M., Premo, W.R. & Courjault-Radé, P., 2005. Sm-Nd dating of fluorite from the worldclass Montroc fluorite deposit, southern Massif Central, France. *Mineralium Deposita*, **39**, 970-975.

Narkiewicz, K., Grotek I. & Matyja, H., 1998. Dojrzałość termiczna materii organicznej w utworach górnodewońskich obszaru Radomsko-Lubelskiego i Pomorskiego. *In: Narkiewicz, M. (ed.), Analiza basenów sedymentacyjnych Niżu Polskiego. Prace Państwowego Instytutu Geologicznego*, **165**, 235-244.

Nathan, Y. & Sass, E., 1981. Stability relations of apatites and calcium carbonates. *Chemical Geology*, **34**, 103-111.

Nowlan, G.S. & Barnes, C.R., 1987. Application of conodont colour alteration indices to regional and economic geology. *In: Austin, R.L. (ed.), Conodonts: investigative techniques and applications*, Ellis Horwood Limited, Chichester, 188-202.

Nöth, S., 1998. Conodont color (CAI) versus microcrystalline and textural changes in Upper Triassic conodonts from Northwest Germany. *Facies*, **38**, 165-174.

Nöth, S. & Richter, D.K., 1992. Infrared spectroscopy of Triassic conodonts: a new tool for assessing conodont diagenesis. *Terra Research*, **4**, 668-675.

Ohfuji, H. & Rickard, D., 2005. Experimental syntheses of framboids-a review. *Earth-Science Reviews*, **71**, 147-170.

Ouzegane, K., Kienast, J.R., Bendaoud, A. & Drareni, A., 2003. A review of Archaean and Paleoproterozoic evolution of the In Ouzzal granulitic terrane (Western Hoggar, Algeria). *Journal of African Earth Sciences*, **37**, 207-227.

Peterman, Z.E., Hedge, C.E. & Tourtelot, H.A., 1970. Isotopic composition of strontium in seawater throughout Phanerozoic time. *Geochimica et Cosmochimica Acta*, **34**, 105-120.

Pietzner, H., Vahl, J., Werner, H. & Ziegler, W., 1969. Zur chemischen Zusammensetzung und Mikromorphologie der Conodonten. *Palaeontographica Abteilung A: Paläozoologie-Stratigraphie*, **128**, 115-152.

Pin, Ch., Briot, D., Bassin, Ch. & Poitrasson, F., 1994. Concomitant separation of strontium and samarium-neodymium for isotopic analysis in silicate samples, based on specific extraction chromatography. *Analytica Chimica Acta*, **298**, 209-222.

Pirajno. F., 2009. Hydrothermal processes and mineral systems. Springer Science+Business Media, 1273 pp.

Rasmussen, J.A. & Smith, M.P., 2001. Conodont geothermometry and tectonic overburden in the northernmost East Greenland Caledonides. *Geological Magazine*, **138**, 687-698.

Rejebian, V.A., Harris, A.G. & Huebner, J.S., 1987. Conodont color and textural alteration: An index to regional metamorphism, contact metamorphism, and hydrothermal alteration. *Geological Society of America Bulletin*, **99**, 471-479.

Relvas, J.M.R.S., Munhá, C.C.G.T.J. & Barriga, F.J.A.S., 2001. Multiple sources for ore-forming fluids in the Neves Corvo VHMS Deposit of the Iberian Pyrite Belt (Portugal): strontium, neodymium and lead isotope evidence. *Mineralium Deposita*, **36**, 416-427.

Repetski, J.E. & Narkiewicz, M., 1996. Conodont color and surface textural alteration in the Muschelkalk (Triassic) of the Silesian-Cracow Zn-Pb district, Poland. *In: Górecka, E., Leach, D.L. & Kozłowski, A. (eds.), Złoża cynku i ołowiu w skałach węglanowych na obszarze śląsko-krakowskim. Prace Państwowego Instytutu Geologicznego*, **154**, 113-122.

Repetski, J.E., Ryder, R.T., Avary, K.L. & Trippi, M.H., 2005. Thermal maturity patterns (CAI and %Ro) in the Ordovician and Devonian rocks of the Appalachian basin in West Virginia. *U.S. Geological Survey, Open-File Report*, **2005-1078**, 72 pp. Available at http://pubs.usgs.gov/of/2005/1078/2005-1078.pdf

Repetski, J.E., Ryder, R.T., Weary, D.J., Harris, A.G. & Trippi, M.H., 2008. Thermal maturity patterns (CAI and $\%R_o$) in Upper Ordovician and Devonian rocks of the Appalachian Basin: a major revision of USGS Map I–917–E using new subsurface collections. Available at http://pubs.usgs.gov/sim/3006/SIM3006.pdf

Robb, L., 2005. Introduction to ore-forming processes. Blackwel Publishing, 373 pp.

Rognon, P., 1967. Climatic influences on the African Hoggar during the Quaternary, based on geomorphologic observations. *Annals of the Association of American Geographers*, **57**, 115-127.

Sarmiento, G.N., García-López, S. & Bastida, F., 1999. Conodont colour alteration indices (CAI) of Upper Ordovician limestones from the Iberian Peninsula. *Geologie en Mijnbouw*, **77**, 77-91.

Sassano, G.P. & Schrijver, K., 1989. Framboidal pyrite:early diagenetic, late-diagenetic, and hydrothermal occurences from the Acton Vale quarry, Cambro-Ordovician, Quebec. *American Journal of Science*, **289**, 167-179.

Schönlaub, H.P., 1979. Das Paläozoikum in Österreich Verbreitung, Stratigraphie, Korrelation, Entwicklung und Paläogeographie nicht-metamorpher und metamorpher Abfolgen. *Abhandlungen der Geologischen Bundesanstalt*, **33**, 142 pp.

Schönlaub, H.P., Flajs, G. & Thalmann, F., 1980. Conodontenstratigraphie am Steirischen Erzberg (Nördliche Grauwackenzone). *Jahrbuch der Geologischen Bundesanstalt*, **123**, 169-229.

Selley, R.C. (ed.), 1997. African basins. Sedimentary basins of the world, **3**, Elsevier, 372 pp.

Singoyi, B. & Zaw, K., 2001., A petrological and fluid inclusion study of magnetite-scheelite skarn mineralization at Kara, Northwestern Tasmania: implications for ore genesis. *Chemical Geology*, **173**, 239-253.

Smith, B., Derder, M.E.M., Henry, B., Bayou, B., Yelles, A.K., Djellit, M., Amenna, M., Garces, M., Beamud, E., Callot, J.P., Eschard, R., Chambers, A., Aifa, T., Ait ouali, R. & Gandriche, H., 2006. Relative importance of the Hercynian and post-Jurassic tectonic phases in the Saharan platform: a palaeomagnetic study of Jurassic sills in the Reggane Basin (Algeria). *Geophysical Journal International*, **167**, 380-396.

Souza Neto, J.A., Legrand, J.M., Volfinger, M., Pascal, M.-L. & Sonnet, P., 2008. W-Au skarns in the Neo Proterozoic Seridó Mobile Belt, Borborema Province in northeastern Brazil: an overview with emphasis on the Bonfim deposit. *Mineralium Deposita*, **43**, 185-205.

Stancin, A.M., Gleason, J.D., Rea, D.K., Owen, R.M., Moore jr, T.C., Blum, J.D. & Hovan, S.A., 2006. Radiogenic isotopic mapping of late Cenozoic eolian and hemipelagic sediment distribution in the east-central Pacific. *Earth and Planetary Science Letters*, **248**, 840-850.

Sunagawa, I., 2005. Crystals: growth, morphology, and perfection. Cambridge University Press, 295 pp.

Sweet, W.C., 1988. The Conodonta: morphology, taxonomy, paleoecology, and evolutionary history of a long-extinct animal phylum. *Oxford Monographs on Geology and Geophysics*, **10**, 212 pp.

Takanohashi, T. & Iino, M., 1990. Extraction of argonne premium coal samples with CS_2-N-Methyl-2-pyrrolidinone mixed solvent at room temperature and ESR parameters of their extracts and residues. *Energy & Fuels*, **4**, 452-455.

Takherist, D. & Lesquer, A., 1989. Mise en évidence d`importantes variations régionales du flux de chaleur en Algérie. *Canadian Journal of Earth Sciences*, **26**, 615-626.

Takherist, D., Arezki, A. & Mouaici, R., 1995. Characterization and evolution of Paleozoic rock organic matter in Algerian Central Sahara. *The American Association of Petroleum Geologists Bulletin*, **79**, 1251 (abstract).

Tissot, B.P., Pelet, R. & Ungerer, P., 1987. Thermal history of sedimentary basins, maturation indices, and kinetics of oil and gas generation. *The American Association of Petroleum Geologists Bulletin*, **71**, 1445-1466.

Traut, M.W., Boote, D.R.D. & Clark-Lowes, D.D., 1998. Exploration history of the Palaeozoic petroleum systems of North Africa. *In: Macgregor, D.S., Moody, R.T.J. & Clark-Lowes, D.D. (eds.), Petroleum geology of North Africa. Geological Society, London, Special Publications*, **132**, 69-78.

Trotter, J.A. & Eggins, S.M., 2006. Chemical systematics of conodont apatite determined by laser ablation ICPMS. *Chemical Geology*, **233**, 196-216.

Trotter, J.A., Fitz Gerald, J.D., Kokkonen, H. & Barnes, C.R., 2007. New insights into the ultrastructure, permeability, and integrity of conodont apatite determined by transmission electron microscopy. *Lethaia*, **40**, 97-110.

Vecoli, M., Videt, B. & Paris, F., 2008. First biostratigraphic (palynological) dating of Middle and Late Cambrian strata in the subsurface of northwestern Algeria, North Africa: Implications for regional stratigraphy. *Review of Palaeobotany and Palynology*, **149**, 57-62.

Veizer, J., 1992. Depositional and diagenetic history of limestones: stable and radiogenic isotopes. *In: Clauer, N. & Chaudhuri, S. (eds.), Isotopic signatures and sedimentary record. Lecture Notes in Earth Sciences*, **43**, 13-48.

Veizer, J., Buhl, D., Diener, A., Ebneth, S., Podlaha, O.G., Bruckschen, P., Jasper, T., Korte, C., Schaaf, M., Ala, D. & Azmy, K., 1997. Strontium isotope stratigraphy: potential resolution and event correlation. *Palaeogeography, Palaeoclimatology, Palaeoecology*, **132**, 65-77.

Voldman, G.G., Albanesi, G.L. & do Campo, M., 2008. Conodont palaeothermometry of contact metamorphism in Middle Ordovician rocks from the Precordillera of western Argentina. *Geological Magazine*, **145**, 449-462.

Wang, Q. & Morse, J.W., 1996. Pyrite formation under conditions approximating those in anoxic sediments: I. Pathway and morphology. *Marine Chemistry*, **52**, 99-121.

Wardlaw, B.R. & Harris, A.G., 1984. Conodont-based thermal maturation of Paleozoic rocks in Arizona. *The American Association of Petroleum Geologists Bulletin*, **68**, 1101-1106.

Wendt, J. & Kaufmann, B., 1998. Mud buildups on a Middle Devonian carbonate ramp (Algerian Sahara). *In: Wright, V.P. & Burchette, T.P. (eds), Carbonate ramps. Geological Society, London, Special Publications*, **149**, 397-415.

Wendt, J., Belka, Z. & Moussine-Pouchkine, A., 1993. New architectures of deep-water carbonate buildups: Evolution of mud mounds into mud ridges (Middle Devonian, Algerian Sahara). *Geology*, **21**, 723-726.

Wendt, J., Belka, Z., Kaufmann, B., Kostrewa, R. & Hayer, J., 1997. The world`s most spectacular carbonate mud mounds (Middle Devonian, Algerian Sahara). *Journal of Sedimentary Research*, **67**, 424-436.

Wendt, J., Kaufmann, B., Belka, Z., Klug, C. & Lubeseder, S., 2006. Sedimentary evolution of a Palaeozoic basin and ridge system: the Middle and Upper Devonian of the Ahnet and Mouydir (Algerian Sahara). *Geological Magazine*, **143**, 269-299.

Wendt, J., Neumann, U. & Schulz, H., 2008. Pleistocene neotectonics and Fe-mineralizations in the Ahnet-Mouydir area (northern margin of the Hoggar Massif, Algerian Sahara). *Acta Geologica Polonica*, **58**, 13-26.

Wendt, J., Kaufmann, B., Belka, Z. & Korn, D., 2009. Carboniferous stratigraphy and depositional environments in the Ahnet Mouydir area (Algerian Sahara). *Facies*, **55**, 443-472.

Wenk, H.R. & Bulakh, A., 2004. Minerals: their constitution and origin. Cambridge University Press, 646 pp.

White, W.M., 2007. Geochemistry, chapter 8: radiogenic isotope geochemistry. 313-358. Available at http://www.imwa.info/white-geochemistry.html

Wilkin, R.T. & Barnes, H.L., 1996. Pyrite formation by reactions of iron monosulfides with dissolved inorganic and organic sulphur species. *Geochimica et Cosmochimica Acta*, **60**, 4167-4179.

Wilkin, R.T., Barnes, H.L. & Brantley, S.L., 1996. The size distribution of framboidal pyrite in modern sediments: an indicator of redox conditions. *Geochimica et Cosmochimica Acta*, **60**, 3897-3912.

Williams, F.M. & Kennan, P.S., 1983. Stable isotope studies of sulphide mineralisation on the Leinster Granite margin and some observations on its relationship to coticule and tourmalinite rocks in the aureole. *Mineralium Deposita*, **18**, 399-410.

Wilson, M. & Guiraud, R., 1998. Late Permian to recent magmatic activity on the African-Arabian margin of Tethys. *In: Macgregor, D.S., Moody, R.T.J. & Clark-Lowes, D.D. (eds.), Petroleum geology of North Africa. Geological Society, London, Special Publications*, **132**, 231-263.

Winter, B.L., Johnson, C.M. & Clark, D.L., 1997. Strontium, neodymium, and lead isotope variations of authigenic and silicate sediment components from the Late Cenozoic Arctic Ocean: implications for sediment provenance and the source of trace metals in seawater. *Geochimica et Cosmochimica Acta*, **61**, 4181-4200.

Zazoun, R.S., 2001. La tectogenèse hercynienne dans la partie occidentale du bassin de l`Ahnet et la region de Bled El-Mass, Sahara Algérien: un continuum de déformation. *Journal of African Earth Sciences*, **32**, 869-887

PLATE 1

A - conodont elements showing a variety of CAI values within a single sample (sample 106/2).

B - decolourized conodont elements (sample 184/3T).

C - carminate conodont elements with corroded edges of platforms and corroded along keels; corroded areas are covered by grey patina (sample 317/2T).

D - corroded surface of pectiniform conodont element. Note grey patina covering corroded area (sample 183/3T).

E - corroded ramiform conodont element (sample 227/6T).

F - angulate conodont element with corroded surface (sample 227/6T).

G - carminate conodont elements covered by grey patina. The corrosion is limited to the edges of platform, carina and keels (sample 331/46).

All photos were taken under binocular; scale bar in each photo = 1 mm

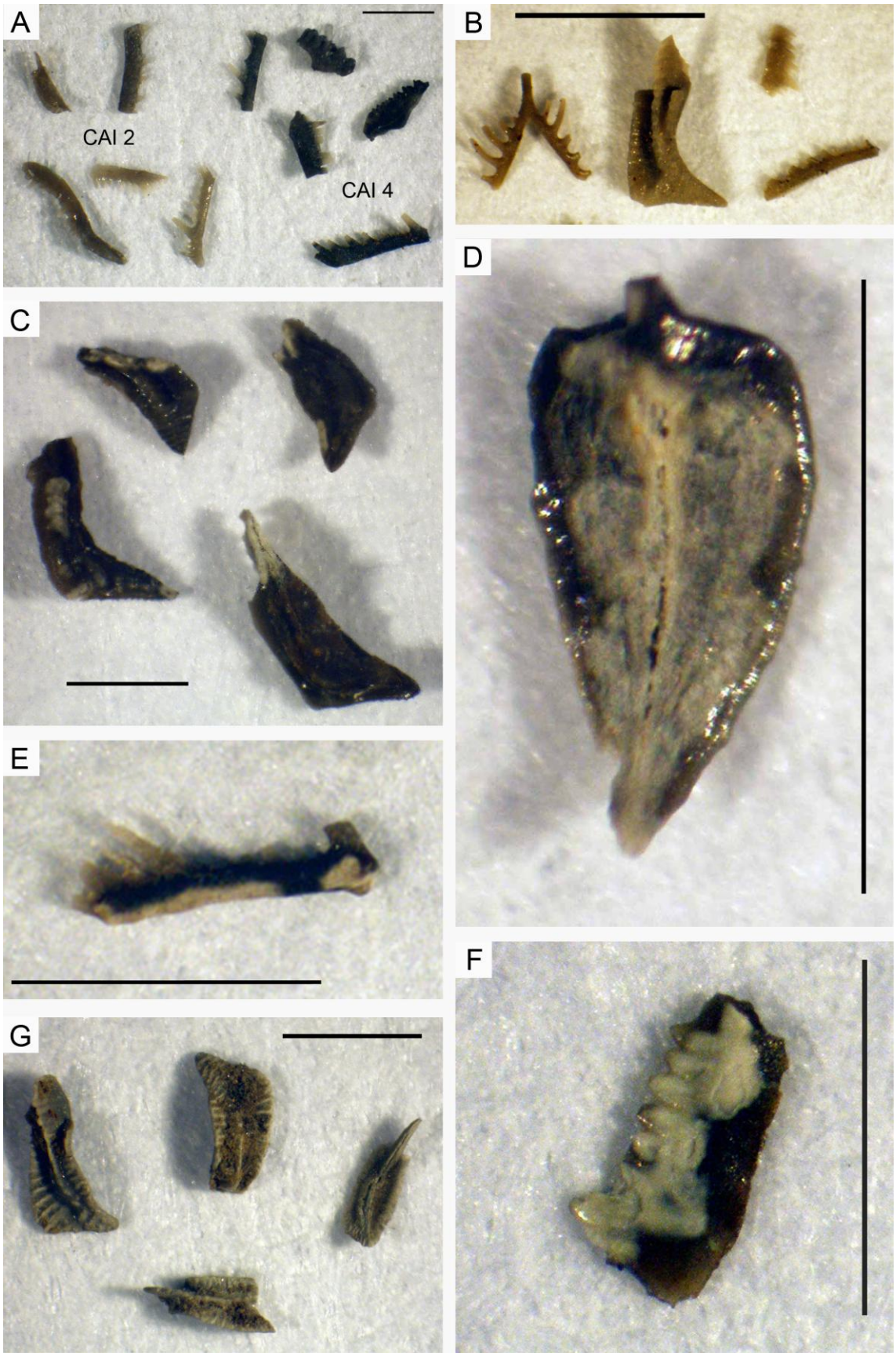
A
CAI 2
CAI 4
B
C
D
E
F
G

PLATE 2

A - thin section of bioclastic limestone with shells of brachiopods and bivalves (sample 267/20; cross-polarized light).

B - thin section of iron-stained bioclastic limestone (sample 233/2, plane-polarized light).

C - thin section of bioclastic limestone with stiliolinids; stiliolinids shells are overgrown by “rosete” cement crystals (sample 202/9, plane-polarized light).

D - thin section of bioclastic limestone, with stiliolinids and mollusc shells; in the centre shell of juvenile cephalopod (sample 317/2T, cross-polarized light).

E, F - thin sections of calcareous sandstone (samples 214/8B and 421/3 respectively, cross-polarized light).

All microphotographs were taken under transmitted light.

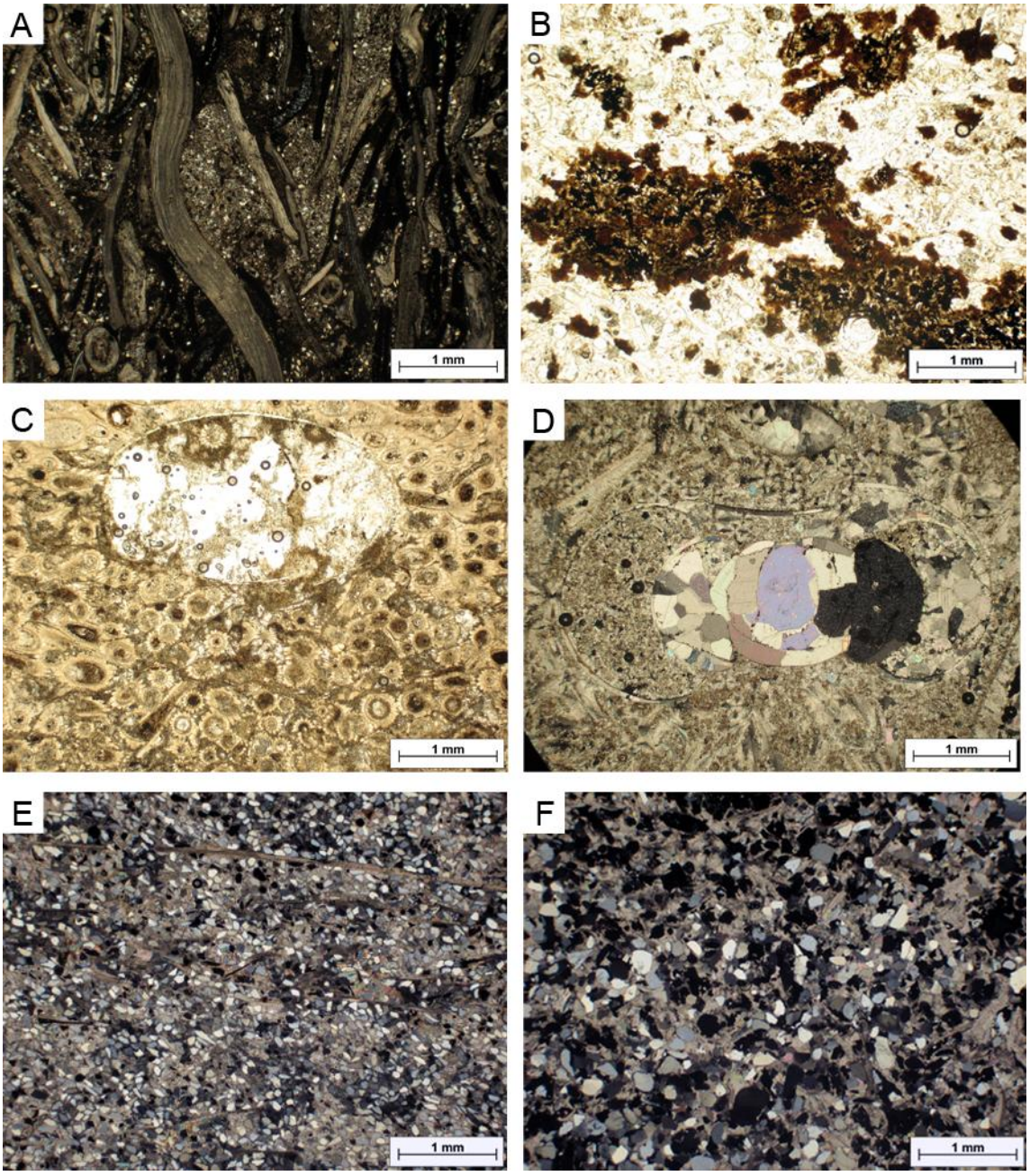
A
1 mm
B
1 mm
C
1 mm
D
1 mm
E
1 mm
F
1 mm

PLATE 3

A - pectiniform and pastinate conodont elements overgrown by reddish coloured apatite crystals. Hexagonal prismatic crystals surround the denticles (sample 184/5).

B - pectiniform and pastinate conodont elements overgrown by colourless apatite crystals. Crystals on pectiniform and pastinate elements differs in size and habit (sample 332/1).

C, D - pectiniform conodont elements overgrown by whitish thin tabular crystals of scheelite (sample 196/5T).

E - bright-blue fluorescence of scheelite crystals (sample 196/5B, ultraviolet light, optical microscope; presented photograph has been compilled by overlaping of two images. Photograph taken by Jacek Michniewicz).

All photographs, except of E, were taken under binocular. Scale bar on all photos, except of E, = 1 mm.

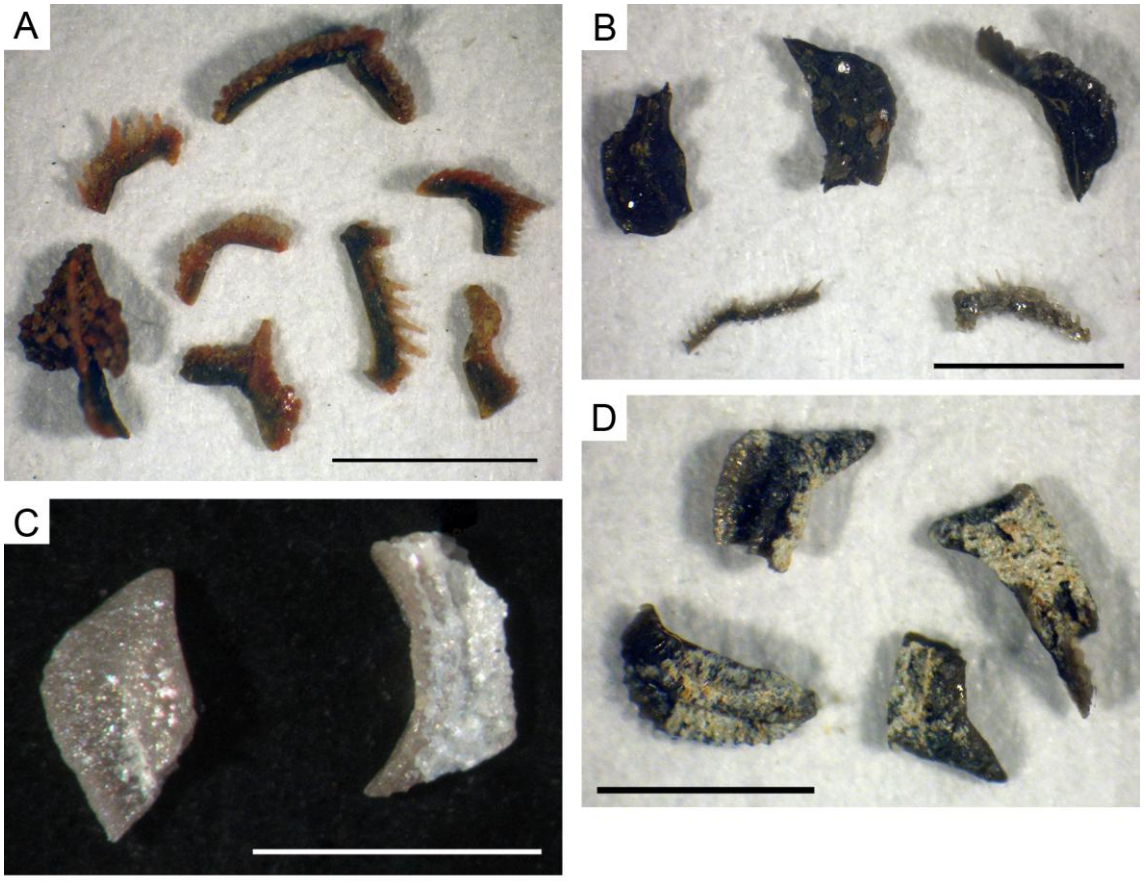
A
B
C
D
E
0,2 mm

PLATE 4

A, B - carminate conodont element with apatite mineralization. Note occurrence of crystals along kells and around basal pit.

C - orientation of the c-axis of apatite crystals in relation to orientation of c-axis of crystallites of hyaline tissue of conodonts.

D - crystals of apatite growing along the keel. Arrows marks places of crystal attachment to crystallites of hyaline tissue of conodonts.

E - general view on apatite crystals occuring on the platform of conodont element

F - orientation of tabular apatite crystals in relation to orientation of crystallites of hyaline tissue.

G - apatite crystals growing along the keel.

H - framboidal pyrite between apatite crystals.

All photographs were taken under scanning electron microscope for the same conodont element from sample 317/2T.

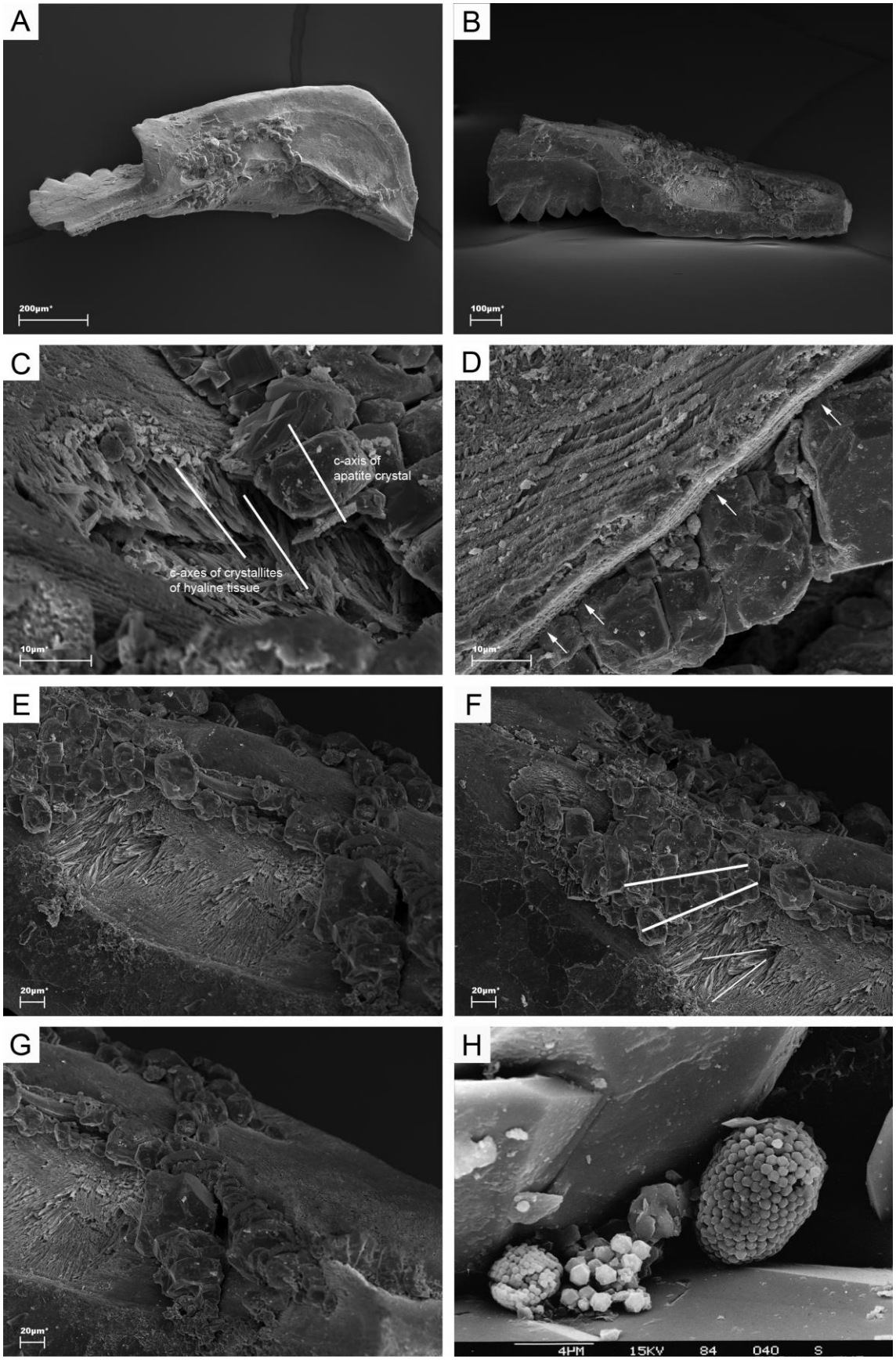
A
200µm*
B
100µm*
C
c-axis of
apatite crystal
c-axes of crystallites
of hyaline tissue
10µm*
D
10µm*
E
20µm*
F
20µm*
G
20µm*
H
4PM 15KV 84 040 S

PLATE 5

A - angulate conodont element overgrown by hexagonal prismatic crystals. Note homoaxial orientation of apatite crystals and denticles (sample 298/12).

B - ramiform conodont element overgrown by apatite. Note hexagonal prismatic habit of crystals that occurs on denticles and thin tabular habit of crystals below denticles (sample 298/12).

C - angulate conodont element overgrown by apatite crystals. Crystals around the denticles are prismatic, whereas those on the blade are tabular in habit. In addition, framboidal pyrite (arrowed) occurs on apatite (sample 367/11).

D - conodont element covered entirely by apatite crystals (sample 298/10).

E, F - carminate conodont elements overgrown by thin tabular crystals of scheelite (sample 196/5T).

G - angulate conodont element overgrown by apatite and baryte (black asteriks; sample 214/8).

H - conodont element overgrown by rombohedric crystals of haematite (sample 327/44).

All photographs were taken under scanning electron microscope.

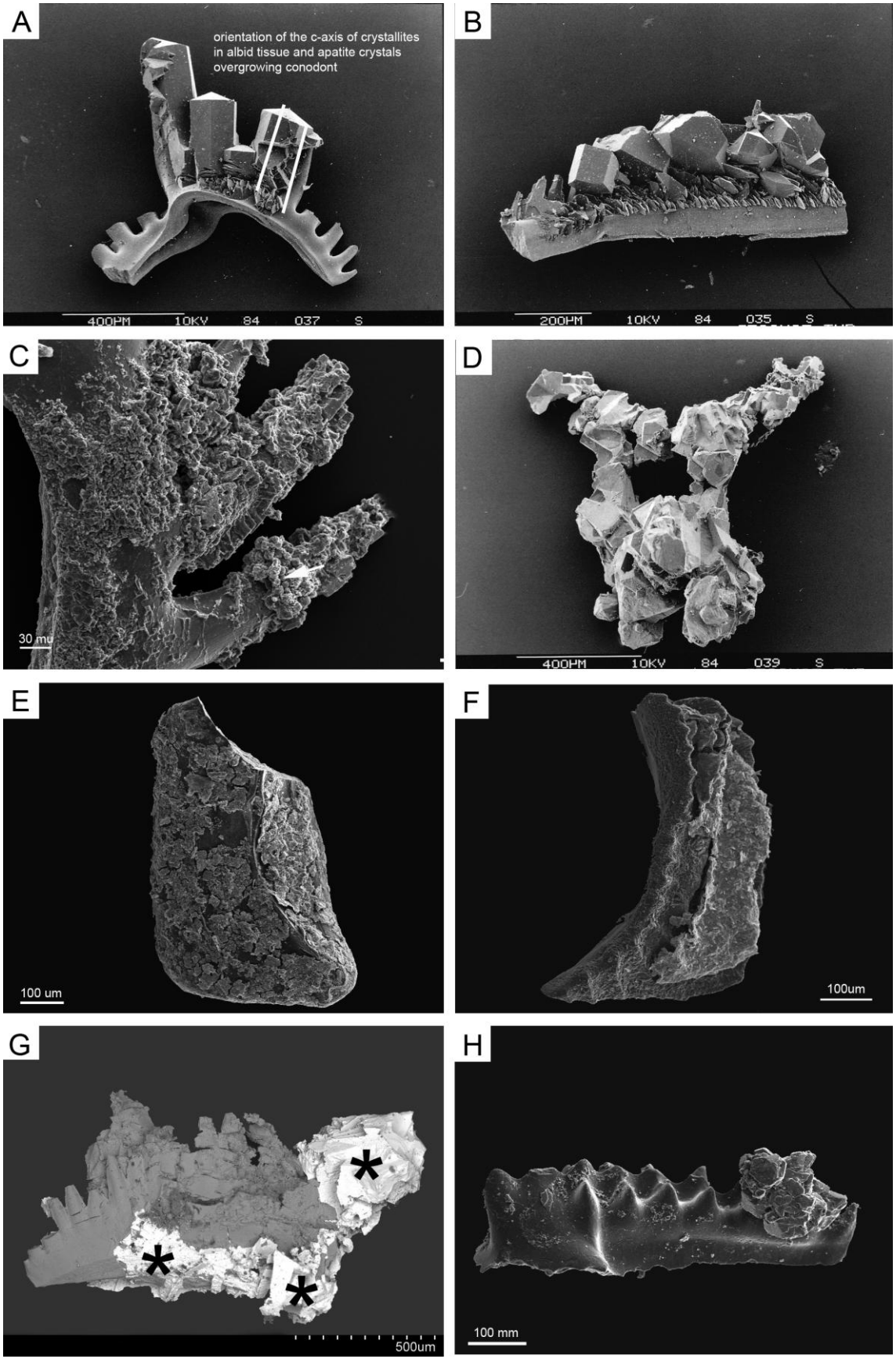
A
orientation of the c-axis of crystallites
in albid tissue and apatite crystals
overgrowing conodont
400PM 10KV 84 037 S
B
200PM 10KV 84 035 S
C
30 mu
D
400PM 10KV 84 039 S
E
100 um
F
100um
G
500um
H
100 mm

PLATE 6

A - corroded surface on aboral side of carminate conodont element (sample 233/2).

B - corroded aboral side of carminate conodont element. The textural alteration occurs mainly along keels, around basal pit and on the edges of platform (sample 354/7).

C - same sample as picture B.

D - corroded surface of ramiform conodont element. Note circular holes at the base of denticles and textural alteration along the bar (sample 268/4).

E - same sample as picture D.

F - carminate conodont element covered entirely by superficial grey patina. The corrosion occurs only along the margin of platform and along carina (sample 331/46).

All photographs were taken under scanning electron microscope.

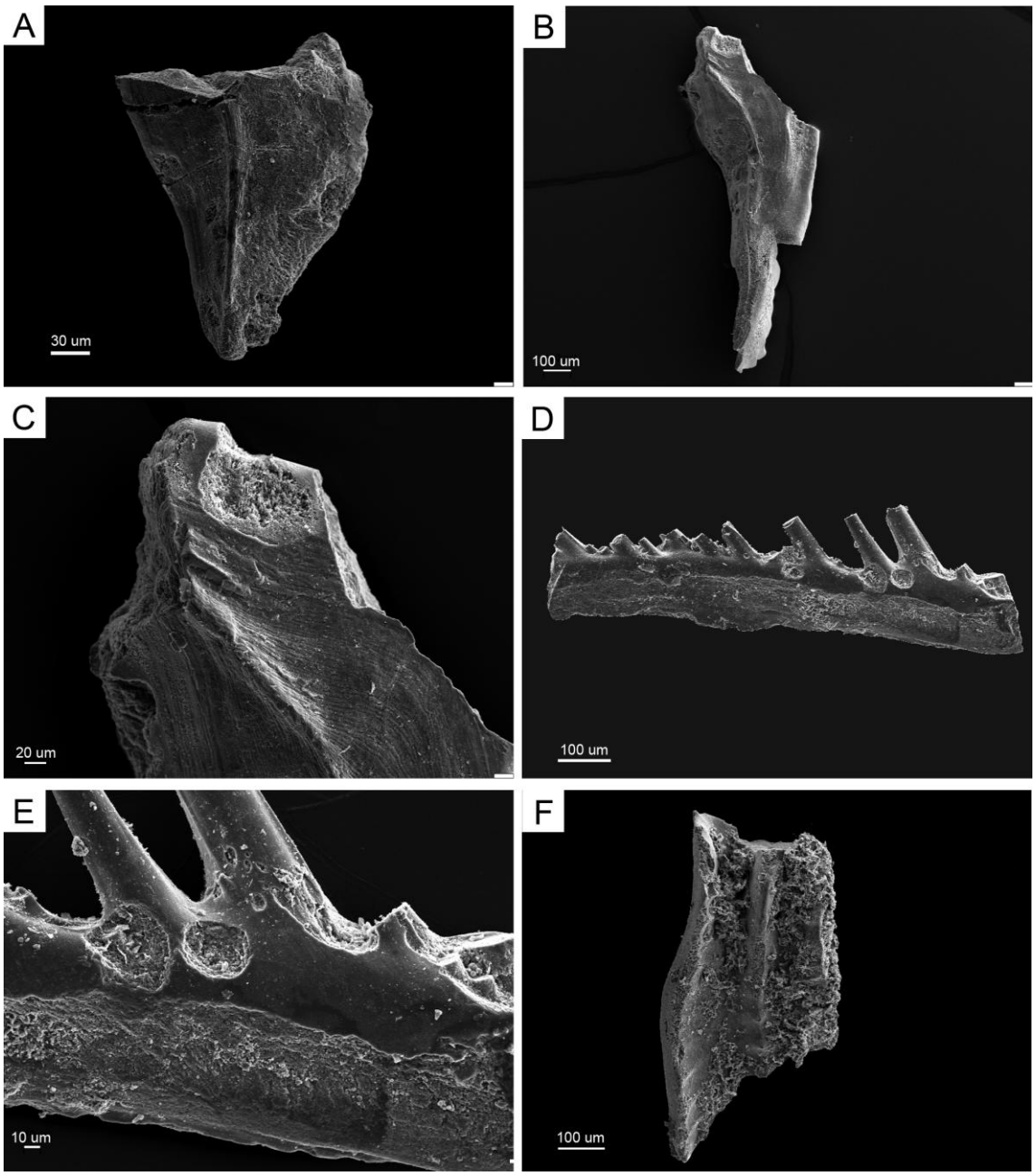
A
30 um
B
100 um
C
20 um
D
100 um
E
10 um
F
100 um

APPENDIX

Table 1. Register of analysed samples, their age, CAI values and selected phenomena.

A 96 Inahas				
no.	**sample number**	**age**	**CAI**	**phenomena**
1	96/8T	Eifelian-Givetian	2 ?	
2	96/7B	Eifelian-Givetian	2 ?	
3	96/5T	Eifelian-Givetian	2-2.5	apatite mineralization
4	96/4B	Eifelian-Givetian	1.5 ?	
A 99 Tiguelguemine				
Equivalent of A 371 Tiguelguemine				
A 184, 242 Ouzdaf Atoll SW				
5-6	184/6, 119/7T	Frasnian	1.5-2; 2	apatite mineralization
7	184/5T	Frasnian	2	apatite mineralization
8	184/5	Frasnian	2	apatite mineralization, haematite
9	184/3T	Givetian	false 6	fade
10	184/3a	Givetian	false 6	fade
11	119/5B	Givetian	1.5-2	
12	119/2a	Givetian	1.5-2	apatite mineralization
13	119/2B	Givetian	1.5-2	
14	184/1T	Givetian	2	
A 212 Adrar Morat SW				
barren				
A 227 Hassi Bel Rezaim				
15	227/11T	Frasnian	2	apatite mineralization
16	227/10	Givetian	2	
17	227/8	Givetian	2	
18	227/6T	Givetian	2	corrosion
19	227/6B	Givetian	2 ?	
20	227/4-5	Givetian	2	
21	227/2	Givetian	2	
A 231 Ain Redjem				
22	231/11	Eifelian-Givetian	3 ?	apatite mineralization
23	231/9B	Eifelian	3 ?	
A 258 Tes Ereghet				
barren				

A 260 SW of Erg Teguentour				
24	259/1	Tournaisian	1.5-2	
25	259/4	Tournaisian	1.5-2	
A 262 SW of Erg Teguentour				
26	261/11	Frasnian	2	apatite mineralization
27	261/9B	Givetian	2	
28	261/4	Givetian	2	apatite mineralization
A 268 Ain Behaga				
29	268/12	Famennian	2	
30	268/10	Famennian	2	
31	268/6	Famennian	2	
32	268/4	Famennian	2	baryte mineralization
A 292 WSW Gara Azzel Matti				
33-34	292/24a-c	Visean	1.5-2	scheelite mineralization
35	292/21	Tournaisian	1.5-2	baryte mineralization
A 295 Oued Ouzdaf N				
36	295/5T	Givetian	2	
37	295/4T	Givetian	2	haematite
38	295/4B	Eifelian-Givetian	2	
A 297 Aoulef el Arab				
39	297/4	Eifelian	1.5-2	
40	297/3	Eifelian ?	1.5-2	
A 299 Illirhene				
41	298/22	Frasnian	2	corrosion
42	298/16	Frasnian	2	
43	298/12	Frasnian	2	apatite mineralization
44	298/10	Frasnian	2	apatite mineralization
45	298/8	Eifelian-Frasnian	2-2.5 ?	
46	298/4	Eifelian-Frasnian	2	
47	298/2	Eifelian-Frasnian	2	
A 300 Oued Ouzdaf Intermound				
48	300/5	Frasnian	2	
49	183/1	Givetian	2	
A 307 Bled el Mas				
50-51	326/1, 194/9	Famennian	2; 2	
52	194/6	Frasnian	2	
52	194/5	Frasnian	2-2.5	haematite
54	194/3	Frasnian	2	
55	306/118	Frasnian	2	

56	305/5a	Frasnian	2	apatite mineralization, haematite
57	305/3a	Frasnian	2	
58	305/2B	Emsian	1.5-2	
A 319 Oued In Somar				
59	319/8	Frasnian	2 ?	apatite mineralization
60	319/6	Frasnian	2	apatite mineralization
61	319/5	Givetian	2	
62-63	317/2T, 319/1	Givetian	3?; 2?	apatite mineralization, corrosion
64	317/2B	Givetian	3?	anomaly in CAI
A 320 Oued Temertasset				
65	266	Tournaisian	2	
66	320/8B	Tournaisian	3?	
67	320/6	Tournaisian	2	
A 325 Jebel Berga				
68	325/7T	Bashkirian	1	
A 326 Bled el Mas				
69	326/3	undeterminable	1.5-2	apatite mineralization
70	326/1	Frasnian	2	
A 327 Djebel Tamamat				
71	327/44	Frasnian	2	apatite mineralization
72	202/9	Frasnian	2	haematite
73	327/31	Frasnian	2	haematite
74	202/8	Frasnian	2?	apatite mineralization, haematite
75	327/24	Frasnian	2?	
76	202/7	Frasnian	2	apatite mineralization
77	202/6	Frasnian	2?	
78	202/3	Frasnian	2	apatite mineralization, corrosion
79	202/1	Givetian	2	
80	327/3	Givetian	2	apatite mineralization
81	201/3B	Givetian	2	haematite
A 328 Adrar Morat N				
82	214/8	Frasnian	2	apatite, scheelite and baryte mineralization
83	214/6	Frasnian	2?	
84	214/5	Givetian	2	haematite
85	214/3	Givetian	2	haematite
86	214/2	Givetian	2	
87	213/18	Givetian	2	
88	213/14	Givetian	2	

89	213/12	Givetian	2	haematite
90	213/9	Eifelian	2?	
91	213/5	Eifelian	2	scheelite mineralization, corrosion
A 329 Ain Behaga				
92	267/20T	Frasnian	2	
93	329/2	Frasnian	2	scheelite mineralization
94	267/13	Givetian	2	apatite mineralization
95	329/1	Givetian	2?	
96	267/11	Givetian	2.5-3	
97	267/11B	Givetian	2-3	
98	267/9T	Eifelian	2-3	apatite mineralization
99	267/8	Eifelian	2	
100	267/6	Eifelian	2	
101	267/4	Eifelian	2?	
A 330 N of Ain Tiouendjiguine				
102	330/14	Famennian	2	apatite and scheelite mineralization
103	330/10T	Famennian	2	baryte mineralization
104	330/8	Famennian	2	
105	330/6	undeterminable	2	
106	330/4T	Famennian?	2	
107	330/2	Famennian?	2	
A 332 Ain Inahas				
108	269/21T	Frasnian	3	apatite mineralization
109	331/72	Frasnian	2?	
110	331/60	Frasnian?	2?	apatite mineralization
111	331/46	Givetian	2?	anomaly in CAI, corrosion
112	269/21B	Givetian	3	anomaly in CAI
113	331/19	Givetian	3?	
114	269/14	Givetian	2	apatite mineralization
115-16	331/8, 269/2	Givetian	2.5-3; 3	
117	331/3	Givetian	3?	apatite mineralization
118	332/1	Eifelian	3	apatite mineralization, haematite
A 333 Ain Bagline				
119	312/16	Frasnian	2?	apatite mineralization
120	312/11B	Givetian	2	
121	312/10T	Givetian	3	apatite mineralization, corrosion
122	312/6	Emsian-Eifelian	3?	
123	312/5	Emsian-Eifelian	2	

A 335 Rhedir				
124	334	Givetian-Frasnian	2	apatite mineralization, anomaly in CAI
125	238/5	Givetian	3?	apatite mineralization
126	335/4	Eifelian	2	apatite mineralization, corrosion
A 340 Azzel Matti				
127-28	340/13, 13a	Frasnian	2; 2?	
129	340/9	Frasnian	2	apatite and scheelite mineralization
130	134/6	Frasnian	2	apatite mineralization
131	134/5	Frasnian	2	apatite mineralization
132	134/3	Givetian	2	corrosion
133-35	134/2a-c	Givetian	2	anomaly in CAI
136-39	133/2,4,5,7,9,10	Givetian	2	apatite mineralization, corrosion
A 344 Adrar In Allarene W				
140	344/7	Frasnian	2	
141	344/3T	Frasnian	2	apatite mineralization
142	343-2-3	Givetian	2?	
143	343-1-1	Eifelian	2?	haematite
A 346 Ain Tikkidne				
144	218/4B, 4T	Frasnian	2	
145-46	218/2T, 346/5	Givetian?	2; 3?	
147	346/4a	undeterminable	2	
148	346/3	Eifelian-Frasnian	2?	
149	346/2	Eifelian-Frasnian	2?	
A 349 Erg Tagsist				
150	217/2	Givetian	2	
151	217/1	Givetian	2?	
152	347a	Givetian	2?	
153	216/13	Givetian	2	
154	216/9M	Givetian	2	
155	347/5B	Givetian	2	
156	347/4	Givetian	2	
A 354 Adrar Tiressoiune S				
157	354/11	Givetian	2	
158	354/10	Givetian	2	corrosion, anomaly in CAI
159	354/7	Givetian	2?	scheelite mineralization, corrosion
160	354/5	Eifelian-Frasnian	2	
161	354/2	Eifelian?	2?	
A 356 Tiressouine S				

162	220/11	Frasnian	2	apatite mineralization
163	355/8	Frasnian	2	
164	220/6	Givetian	2	
165	355/4T	Givetian	2	
166-67	220/2, 221/3B	Givetian	2; 2	
A 357 Adrar Tiressouine N				
168	357/9	Frasnian	2	apatite mineralization, haematite
169	357/8	Frasnian	2?	
170-71	221/7, 357/7	Givetian	2; 2	apatite mineralization
172	357/6	Givetian	2	haematite
173	357/5	Givetian		
174	221/3T	Givetian	2	
175	221/3B	Givetian	2	
A 358 Adrar Tadioune W				
176	358/7	Givetian	2?	apatite mineralization
177	223/5	Givetian	2	
178	223/2	Eifelian	2	apatite mineralization
179	223/1	Eifelian	3?	apatite mineralization
A 361 Bel Khenafis				
180-81	224/13; 361/7	Givetian	2; 2	
182	361a	Givetian	2?	
183	224/1	Eifelian	2	
A 362 Imeddene-n-Azarif S				
184	226/3T	Frasnian	2	apatite mineralization
185	226/3B	Givetian	2	
186	362/5	Givetian	2	
187-88	362/3; 226/1	Givetian	2; 2	
A 363 Imeddene-n-Azarif N				
189	363/8	Frasnian	2	apatite mineralization
190	225B	Frasnian	2	apatite mineralization
191-92	225T; 363/4	Givetian-Frasnian	2; 2	
193	363/2	Givetian	2	
A 366 Tin Khelifa N				
194	366/8	Frasnian	2	apatite mineralization
195-96	170/9T; 366/6T	Frasnian	2; 2	apatite mineralization
197	170/4T	Eifelian-Givetian	2	
198	170/4B	Givetian	2	
199-	171/7; 366/2	Givetian	2; 2	apatite mineralization, haematite

200				
A 367 Ain Kahla				
201	323/21	Frasnian	2?	apatite mineralization
202	323/20	Frasnian	3?	apatite mineralization
203	323/18T	Frasnian	2?	
204	323/17	Frasnian	2	apatite mineralization
205	323/13T	Givetian-Frasnian	2	apatite mineralization
206	323/12T	Frasnian	2	
207	367/11	Givetian	2	apatite and scheelite mineralization
208	323/10T	Givetian	2	
209	367/2	Givetian	2?	
210	323/9T	Givetian	2	apatite mineralization
211	323/6	Eifelian	2	
212	323/4	Eifelian	2	
A 369 Jebel Assaz Syncline				
213	91/5	Givetian	2	apatite mineralization
214	91/6B	Givetian	2	apatite mineralization
215	368/4	Givetian	2?	apatite mineralization, haematite
216	91/4T	Givetian	2	apatite mineralization, haematite
217	91/4B	Givetian	2	apatite mineralization
218	91/7	Givetian	2	apatite mineralization
219	91/8B	Eifelian	2	
A 370 Jebel Assaz				
220	272/2B	Famennian	2	
221	370/8	Frasnian	2	apatite mineralization
222	271/8	Frasnian	2	apatite mineralization
223	271/7B	Givetian	2	
224	271/4B	Eifelian	2	
A 371 Tiguelgumine				
225-26	229/3; 371/5T	Givetian	2; 2	apatite mineralization, anomaly in CAI
227	229/2	Givetian	2	
228	229/1	Givetian	2	
229	228/13T	Givetian	2	apatite mineralization, haematite
230	99/6	Eifelian	2	apatite mineralization
231	228/10	Eifelian	2-2.5?	apatite mineralization
232	99/5B	Eifelian	2	apatite mineralization
233	99/4	Eifelian	2	
A 372 Ain Tidjoubar				

234	230/8T	Eifelian-Givetian	2?	apatite mineralization
235-36	230/6T; 372/3T	Eifelian-Givetian	2; 2	
237	230/5	Eifelian	2	apatite mineralization
A 376 Erg Teganet				
238	375/3	Givetian	3.5?	apatite mineralization
239	376/3T	Givetian	3.5?	
240	233/4T	Eifelian	3	apatite mineralization
241	233/2	Eifelian	3	apatite mineralization, corrosion
A 385 Hassi Taibine				
242	385/1	Bashkirian	2	
243	303/26	Bashkirian	1	
244	303/24M	Bashkirian	1	
245	303/20	Visean	1,5	
246	303/18	Visean	1.5	
247	303/4	Tournaisian	3.5	
A 387 Jebel Aberraz				
248	386/7	Givetian	2	
249-50	386/5T; 387B	Givetian	2; 2?	
251	386/5B	Givetian	2	
A 390 Jebel Tamamate S				
252	390/3	Eifelian-Frasnian	2	
253	196/7T	Givetian	2	
254	196/5T	Givetian	2	scheelite mineralization
255	196/5B	Givetian	2	scheelite mineralization
256	196/3	Givetian	2	
A 393 Jebel Tamamat S				
257	393/7	Frasnian	2	
258	392/3	Devonian	2?	
A 396 Gouiret ed Diab				
259	396/10	Frasnian	2	haematite
260	396/8	Frasnian	2	scheelite mineralization
261	396/6	Frasnian	2	
262	396/4	Frasnian	2	
A 397 Oued Ouzdaf				
263	182/30	Frasnian	2	haematite
264	182/27b	Givetian	2	haematite
265	182/27a	Givetian	2	haematite
266	182/26	Givetian	2	
267	182/24	Givetian	2	

268	182/20	Givetian	2	
269	182/18B	Givetian	2	
270	182/14	Givetian	2	
271	182/13	Givetian	2	
271	182/5B	Givetian	2	
273	183/3T	Givetian	2	corrosion
274	182/1	Givetian	2	
A 398 Sebkha Mekerhane N				
275-76	106/4; 180/1	Eifelian-Frasnian	2; 2	
277	180/3	Eifelian-Frasnian	2	scheelite mineralization
278	180/2	Eifelian-Frasnian	2?	
279	107/4	Eifelian-Givetian	2	
280	107/3T	Givetian	2	haematite
281	106/2	Givetian	2	anomaly in CAI
A 399 Akabli				
282	178/11	Frasnian	2	
283-84	178/9T; 399/9T	Frasnian	2?; 2	
285-86	178/8B; 399/8B	Givetian	2-2.5; 2	
287	399/6	Givetian	2	scheelite mineralization
288	178/4	Givetian	2	
289	178/3	Givetian	2	
290	178/2B	Givetian	2	scheelite mineralization, corrosion
291	178/0	Givetian	2	
A 400 SW of Oued In Tarhlift				
292	42/10b	Givetian	1.5-2	
293	42/4	Givetian	2	
294	42/2	Givetian	2	
A 401 Bahar El Hammar W				
295	401/10	Givetian	2	
296	401/7b	Givetian	2?	
A 403 Tirechchoumine				
297	252/58	Bashkirian	1.5	
298	251/30	Visean	1.5-2	
299	251/29	Visean	1.5-2	
300	251/26-27	Visean	1.5-2	
301	251/24	Visean	2	
302	251/20	Visean	1.5-2	baryte mineralization
303	403/18	Visean	1.5-2	

304	403/16	Visean	2	
305	251/15	Visean	1.5-2	
A 404 Bahar El Hammar E				
306	404/9T	Givetian	2.5?	
307	248/2	Givetian	2	
A 405 Gouiret Bou el Mout S				
308	164/16T	Frasnian	2	
309	164/15	Givetian-Frasnian	2	
310	164/9T	Givetian	2	apatite mineralization
311	164/3	Givetian	2	
312	164/2T	Eifelian-Givetian	2	apatite mineralization
313	164/1	Eifelian-Givetian	2	scheelite mineralization
A 406 Gouiret Bou el Mout N				
314	279/12	Eifelian	2	scheelite mineralization
315	279/8	Eifelian	2	scheelite mineralization
316	279/4	Emsian-Eifelian	2?	
317	406/7	Eifelian	2?	
318	406/5	Eifelian	2?	
319	406/4	Eifelian	2	scheelite mineralization
320	280/3	Eifelian-Frasnian	2	scheelite mineralization
A 410 Gouiret es Sud				
321	70/5c	Frasnian	2	
322	72/8	Givetian	2	
323	148/17	Givetian	2	apatite mineralization
324	148/16	Givetian	2	corrosion
325	148/13	Givetian	2	
326	148/12	Givetian	2	haematite
327	148/11	Givetian	2	
328	148/8	Givetian	2	
329	72/3	Eifelian	2	haematite
330	148/1	Eifelian	2	
331	409	Eifelian	2	
A 411 Les Haouds W				
332	285/14	Frasnian	1.5-2	
333-34	285/12; 411/12	Frasnian	1.5-2; 2	apatite mineralization
335	285/8	Givetian	2?	
336	285/6	Givetian	1.5-2	

337	285/4	Givetian	2	apatite mineralization
338	285/2B	Givetian	1.5	
A 412 Les Haouds E				
339	287/30	Frasnian	2	
340	287/28	Frasnian	2	
341	287/26	Frasnian	2	
342	287/20	Givetian	2	
343	287/18	Givetian	2	
344	287/12	Givetian	2	apatite mineralization
345	287/10	Givetian	2	
346	412/2	Givetian	2	
347-48	287/2; 412/1	Givetian	2; 2	haematite
A 414 Kermaz Syncline				
349	414/6	Eifelian-Frasnian	2	
350	414/5	Frasnian ?	2	apatite mineralization
351	414/3	Frasnian	2	
352	413/13	undeterminable	2.5?	
353	413/11	Eifelian-Frasnian	2	
354	413/9	Givetian	2	
A 416 In Heguis N				
355	416/4	Givetian	2	
A 418 In Heguis S				
356	418/8	Givetian	2	
357	418/7	Givetian	2	corrosion
358	417/6	Givetian	2	
359	417/4	Givetian	2	
A 419 Adrar Tadioune N				
360	360/T	Givetian	2	
361	222/15+16	Givetian	2	
362	222/4	Givetian	2	apatite mineralization
363	222/3	Givetian	2	apatite mineralization
A 420 Tin Khelifa S				
364	365/11T	Frasnian	2	
365	169/7B	Frasnian	2	apatite mineralization
366	169/2-5	Givetian	2	
A 422 Gour Bou Kreis				
367	421/15	Frasnian	2?	
368	421/13	Frasnian	2	apatite mineralization
369	421/11	Givetian	2	

370	421/8	Givetian	2	apatite mineralization, corrosion
371	421/3	Eifelian	2	apatite mineralization
A 426 Ain Redjem N				
372	426	undeterminable	2	apatite mineralization
373	425/6	Frasnian	2	apatite mineralization
374	425/4	Frasnian	2?	
375	425/2T	Eifelian-Givetian	2	apatite mineralization
A 427 Ain Tilekchot				
376	101/5	Frasnian	2	apatite mineralization
377-78	373/7B; 101/4B	Givetian	2; 2	corrosion
379	373/5T	Eifelian-Frasnian	2?	haematite
380	373/4B	Eifelian-Frasnian	2	
A 435 SSE Jebel Mouima				
381	435/24	Visean	2	
382	435/14T	Visean	2	scheelite mineralization
383	435/14B	Tournaisian	2	corrosion
384	435/8	Tournaisian	2	haematite

Table 2. Coordinates of sections

section	coordinates	section	coordinates
A 96 Inahas	27°06'05.35"N 3°41'15.04"E	A 361 Bel Khenafis	25°12'46.26"N 3°03'53.33"E
A 99 Tiguelguemine	26°15'36.23"N 3°30'59.19"E	A 362 Imeddene-n-Azarif S	25°07'23.96"N 3°17'57.05"E
A 184 Ouzdaf Atol SW	26°35'16.75"N 1°05'37.52"E	A 363 Imeddene-n-Azarif N	25°09'57.59"N 3°17'49.17"E
A 212 Adrar Morrat SW	25°31'30.84"N 1°22'46.02"E	A 366 Tin Khelifa N	25°35'34.43"N 3°18'13.81"E
A 227 Hassi Bel Rezaim	25°48'51.15"N 3°19'21.58"E	A 367 Ain Kahla	27°22'06.77"N 3°25'53.69"E
A 231 Ain Redjem	26°26'51.48"N 3°47'05.97"E	A 369 Jebel Assaz syncline	27°21'26.92"N 3°19'38.36"E
A 242 Ouzdaf Atoll SW	26°32'24.11"N 1°05'46.06"E	A 370 Jebel Assaz	27°11'23.19"N 3°25'38.32"E
A 258 Tes Ereghet	25°04'33.61"N 3°18'06.08"E	A 371 Tiguelguemine	26°07'17.22"N 3°30'46.10"E
A 260 SW of Erg Teguentour	26°07'38.98"N 2°51'41.16.22"E	A 372 Ain Tidjoubar	26°28'54.07"N 3°29'10.28"E
A 262 SW of Erg Teguentour	26°13'35.35"N 2°53'08.67"E	A 376 Erg Teganet	25°53'21.55"N 4°22'48.07"E
A 268 Ain Behaga	26°47'21.33"N 3°40'55.70"E	A 385 Hassi Taibine	26°34'70.12"N 0°26'45.11"E
A 292 WSW Gara Azzel Matti	25°36'33.49"N 0°53'43.34"E	A 387 Jebel Aberraz	26°37'56.34"N 0°31'56.81"E
A 295 Oued Ouzdaf N	26°37'47.73"N 1°04'55.44"E	A 390 Jebel Tamamate S	26°13'32.01"N 0°42'52.82"E
A 297 Aoulef el Arab	26°50'32.91"N 1°03'23.08"E	A 393 Jebel Tamamat S	26°06'37.60"N 0°44'28.20"E
A 299 Illirhene	26°44'16.52"N 1°11'11.37"E	A 396 Gouiret ed Diab	26°26'32.09"N 0°52'10.18"E
A 300 Oued Ouzdaf intermound	26°34'15.11"N 1°05'10.63"E	A 397 Oued Ouzdaf	26°31'06.58"N 1°05'48.33"E
A 307 Bled el Mas	26°26'14.08"N 0°37'16.87"E	A 398 Sebkha Mekerhane N	26°29'04.51"N 1°11'17.44"E
A 319 Oued in Somar	26°06'29.18"N 3°52'20.02"E	A 399 Akabli	26°32'53.03"N 1°17'30.30"E
A 320 Oued Temertasset	26°36'11.73" N 3°50'10.14"E	A 400 SW Oued in Tarhlift	26°32'57.23"N 1°19'29.77"E
A 325 Jebel Berga	26°44'40.66"N 1°51'90.05"E	A 401 Bahar el Hammar W	26°17'49.15"N 1°48'59.92"E
A 326 Bled el Mas	26°24'39.33"N 0°37'51.87"E	A 403 Tirechchoumine	26°12'55.04"N 1°55'20.12"E
A 327 Djebel Tamamat	26°11'02.92"N 0°45'55.03"E	A 404 Bahar el Hammar E	26°16'42.30"N 1°49'53.21"E
A 328 Adrar Morat N	25°45'52.25"N 1°29'24.71"E	A 405 Gouiret Bou el Mout S	26°07'47.10"N 1°12'12.51"E
A 329 Ain Behaga	26°47'21.22"N 3°40'55.84"E	A 406 Gouiret Bou el Mout N	26°09'35.85"N 1°11'19.51"E
A 330 N of Ain Tiouendjiguine	26°57'03.77"N 3°35'37.59"E	A 410 Gouiret es Sud	25°51'09.73"N 1°14'41.20"E
A 332 Ain Inahas	27°07'20.07"N 3°42'23.66"E	A 411 Les Haouds W	24°57'20.60"N 0°42'40.64"E
A 333 Ain Bagline	26°09'55'.29'N 3°47'57.38"E	A 412 Les Haouds E	24°56'30.69"N 0°55'41.92"E

A 335 Rhedir	26°31'06.88"N 4°51'34.79"E	A 414 Kermaz syncline	24°59'48.50"N 1°29'55.05"E
A 340 Azzel Matti	25°44'21.07"N 1°09'13.99"E	A 416 In Heguis N	25°30'52.99"N 2°40'52.23"E
A 344 Adrar in Allarene W	25°17'56.57"N 1°23'42.07"E	A 418 In Heguis S	25°28'04.40"N 2°41"29.76"E
A 346 Ain Tikkidine	25°30'44.02"N 1°24'38.86"E	A 419 Adrar Tadioune N	25°17'28.58"N 2°55'03.33"E
A 349 Erg Tagsist	25°11'00.41"N 1°33'18.80"E	A 420 Tin Khelifa S	25°33'26.37"N 3°19'07.21"E
A 354 Adrar Tiressouine S	25°01'20.63"N 2°31'22.77"E	A 422 Gour Bou Kreis	26°23'04.49"N 3°11'30.22"E
A 356 Tiressouine S	25°08'23.30"N 2°32'53.21"E	A 426 Ain Redjem N	26°29'24.24"N 3°46'42.04"E
A 357 Adrar Tiressouine N	25°27'53.96"N 2°34'39.03"E	A 427 Ain Tilekchot	26°34'58.11"N 3°46'07.90"
A 358 Adrar Tadioune W	25°12'11.11"N 2°52'42.70"E	A 435 SSE Jebel Mouima	25°46'50.68"N 2°48'42.22"E

Table 3. Chemical analysis

Sample 72/8									
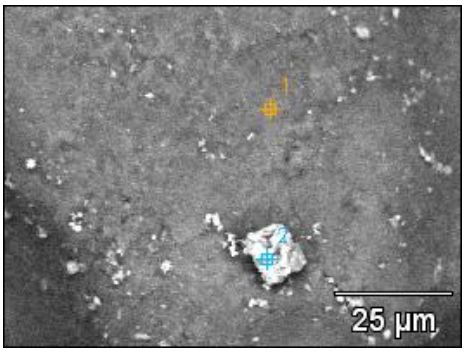									
Compound % (concern to all presented analysis)									
	CO_2	**MgO**	**Al_2O_3**	**SiO_2**	**P_2O_5**	**Cl**	**K_2O**	**CaO**	**Fe_2O_3**
1	22.72	1.60	2.64	70.91			0.28	0.40	1.47
2	8.45		1.07	2.22	2.76	0.29		7.59	77.62

Sample 72/8											
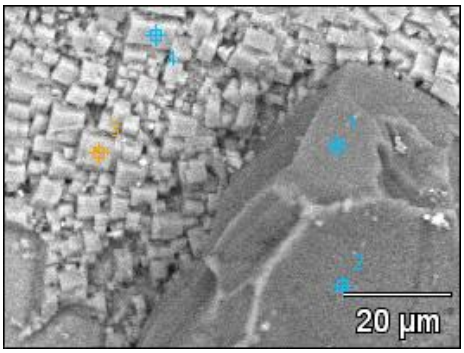											
	CO_2	**MgO**	**Al_2O_3**	**SiO_2**	**P_2O_5**	**K_2O**	**CaO**	**Sc_2O_3**	**TiO_2**	**MnO**	**Fe_2O_3**
1	43.77	11.22		0.73			30.48	0.31		2.01	11.48
2	35.80			0.67	4.12		36.90			5.32	17.18
3	20.35				33.46		45.09				1.10
4	17.81		1.78	3.99	28.02	0.44	44.57		1.33		2.05

Sample 91/4T

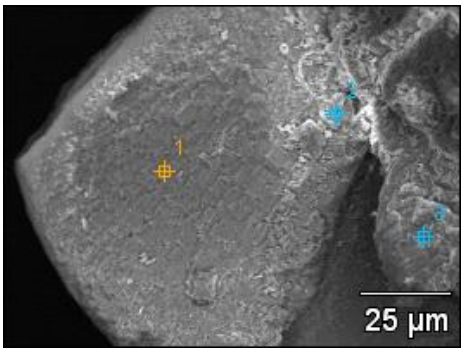

	CO_2	F	Na_2O	Al_2O_3	SiO_2	P_2O_5	CaO	Fe_2O_3
1	18.48	5.88	0.60			34.89	40.16	
2	30.33			4.92			64.76	
3	7.69			0.92	1.10		85.63	4.66

Sample 91/4T

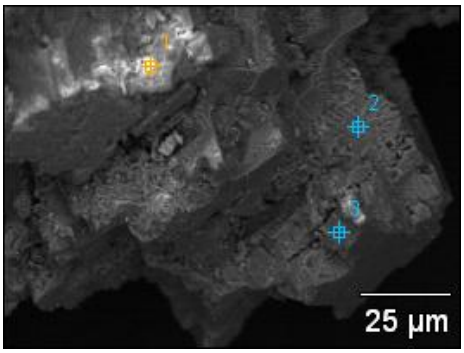

	CO_2	MgO	Al_2O_3	SiO_2	P_2O_5	SO_3	K_2O	CaO	Fe_2O_3
1	21.63	10.00	7.42	21.44	4.74	1.02	0.94	24.23	8.58
2	85.22							14.78	
3	25.75	14.66						53.79	5.79

Sample 91/4T
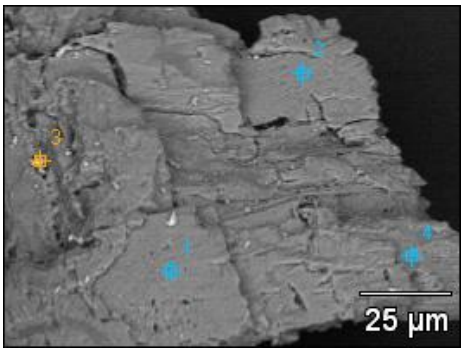

	CO_2	MgO	Al_2O_3	SiO_2	CaO	Sc_2O_3	Fe_2O_3
1	38.78	23.00			36.88		1.34
2	35.56	23.64			38.98	0.26	1.56
3	27.01	18.84	0.56	2.26	42.60		8.73
4	35.00	23.85			40.00		1.15

Sample 91/4T
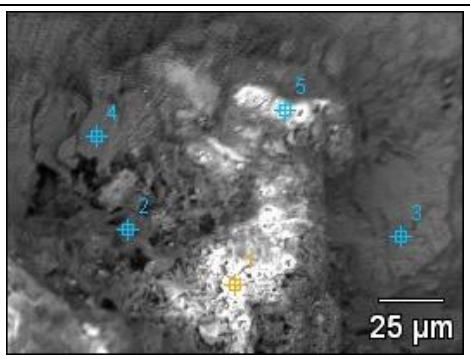

	CO_2	Na_2O	MgO	Al_2O_3	SiO_2	P_2O_5	CaO	Sc_2O_3	Fe_2O_3	MoO_3
1	19.54		3.29	2.24	9.41		2.35		63.16	
2	34.26		9.12	2.64	37.66		2.28		14.04	
3	7.35	0.35	0.56		0.40	32.15	54.74	0.36	2.64	1.46
4	40.04		23.47	0.57	0.59		35.33			
5	22.53		9.85	2.44	51.99		0.97		12.22	

Sample 96/8T										
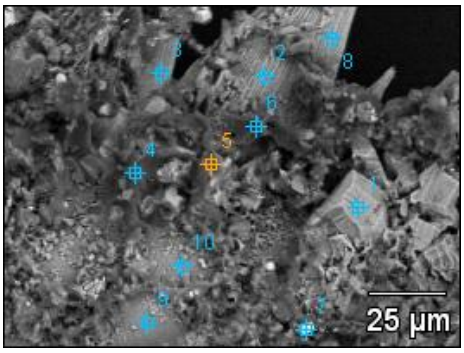										
	CO_2	**F**	**Na_2O**	**Al_2O_3**	**SiO_2**	**P_2O_5**	**SO_3**	**K_2O**	**CaO**	**Fe_2O_3**
1	30.46	4.72				29.36			35.45	
2	5.32			0.58	0.56	7.63			85.92	
3	56.91								43.09	
4	88.62	0.73			1.51	3.27	1.68	0.27	3.93	
5	79.49			1.87	3.30	6.29	1.02	0.45	7.57	
6	93.12		0.54	1.27	2.67		1.99		0.42	
7	29.79				0.34		48.38			21.49
8	24.02			0.83		3.93			71.22	
9	7.48				1.60	22.20			68.72	
10	7.39				2.21	23.43			66.98	

Sample 96/8T							
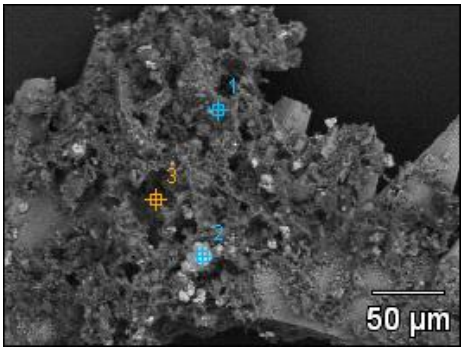							
	CO_2	**Al_2O_3**	**SiO_2**	**SO_3**	**K_2O**	**CaO**	**Fe_2O_3**
1	21.80	13.28	59.08		5.83		
2	30.23	0.09		46.50			23.18
3	14.96	3.26	9.69			72.10	

Sample 106/2

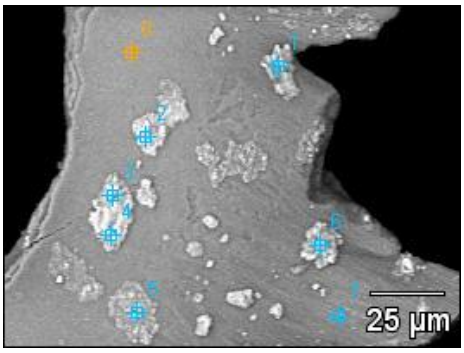

	CO_2	F	Na_2O	MgO	Al_2O_3	SiO_2	P_2O_5	SO_3	Cl	K_2O	CaO	Fe_2O_3	Cu_2O	MoO_3
1	18.92			0.76	0.60	1.33	12.03		0.34		21.79	44.24		
2	17.76			1.51	1.01	2.35	2.85		0.50		5.21	68.80		
3	19.93			0.33	0.92	1.53	12.54		0.26		25.56	38.93		
4	11.37			1.47	3.46	5.22	10.14		0.29	0.47	16.96	50.62		
5	20.00			0.49	0.60	0.98	21.33		0.21		34.45	20.22	1.01	0.71
6	13.38			1.49	0.96	2.13	7.25		0.38		13.01	61.40		
7	26.61		0.52		1.84	1.64	25.49				36.66	7.24		
8	25.95	4.12	0.76		0.63		30.79	0.44			37.05		0.26	0.00

Sample 134/3

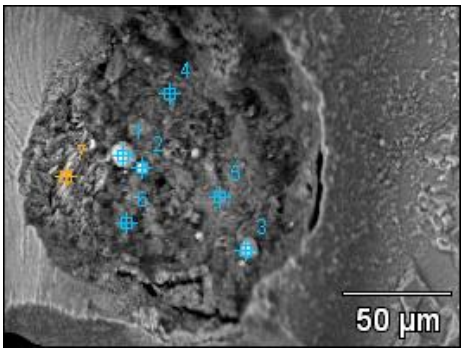

	CO_2	MgO	Al_2O_3	SiO_2	P_2O_5	K_2O	CaO	Fe_2O_3	Cu_2O	Ta_2O_5
1	76.51		2.10	2.06	7.29		12.05			
2	68.53		2.71	3.47	8.27		13.26	3.76		
3	13.39	1.08	2.67	5.76	2.99	0.33	3.79	70.00		
4	76.82		1.52		8.53		13.14			
5	72.39		1.73	1.34	9.05		12.52		2.97	
6	74.05			2.57	8.49		12.50	2.39		
7	74.54		2.70	2.46	7.54		11.96			0.79

Sample 134/3

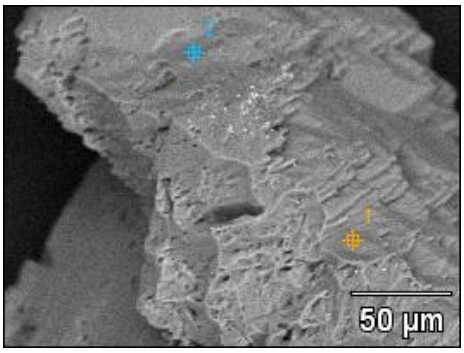

	CO_2	MgO	CaO	MoO_3
1	49.85	1.38	48.77	
2	59.83	0.94	38.54	0.69

Sample 164/1B

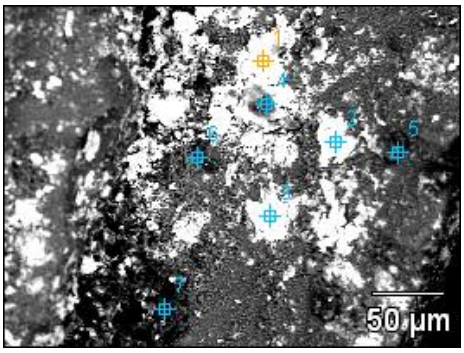

	CO_2	Na_2O	MgO	Al_2O_3	SiO_2	P_2O_5	SO_3	CaO	Fe_2O_3	WO_3
1	8.27		0.60	1.13				11.61		78.38
2	9.26		0.39				1.09	11.83		77.43
3	11.45	0.75	0.69	0.72		7.93		14.93		63.53
4	8.90		0.27	0.99		23.75		30.69	1.56	33.84
5	15.33		0.08	0.71	2.14	20.16	13.37	46.55	1.67	
6	10.64		0.41	0.89	0.68	27.03		58.59	1.75	
7	26.69		18.19	2.62	3.87	3.38		35.39	9.86	

Sample 164/1B

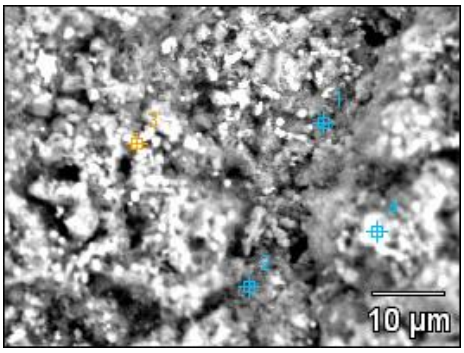

	CO_2	Na_2O	MgO	Al_2O_3	SiO_2	P_2O_5	K_2O	CaO	V_2O_5	Fe_2O_3	MoO_3
1	11.46	0.13	3.20	17.49	23.37	10.44	1.30	13.99		18.64	
2	10.22	0.45	2.91	21.96	30.22	3.84	1.78	5.65		22.23	0.73
3	6.93		1.35	4.90	5.91	2.68		4.80		73.44	
4	18.15	0.18	2.30	13.51	17.41	5.67	1.66	7.93	0.71	32.49	

Sample 164/1B											
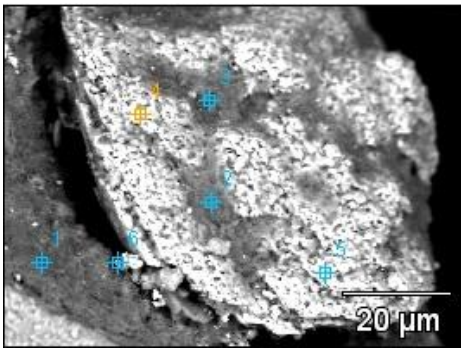											
	CO_2	**Na_2O**	**MgO**	**Al_2O_3**	**SiO_2**	**P_2O_5**	**SO_3**	**K_2O**	**CaO**	**Fe_2O_3**	**As_2O_3**
1	19.93			31.71	37.42	1.48			2.15	5.50	1.82
2	23.90		0.92	24.20	29.23	1.01			1.59	19.15	
3	21.95	0.17	1.73	27.79	33.76	0.82		0.32	0.93	12.52	
4	19.47		0.97	3.94	3.96	1.03	0.66		1.87	68.11	
5	11.62		0.39	3.85	4.39	1.15			1.97	76.63	
6	12.92		0.59	10.43	11.13	1.11			2.10	61.73	

Sample 164/1B									
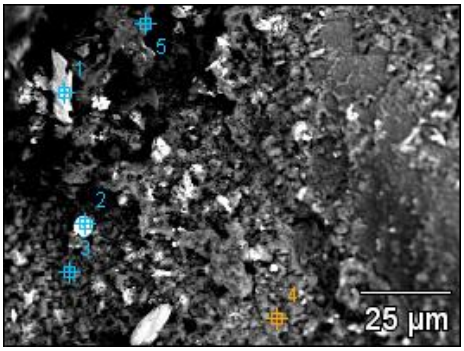									
	CO_2	**Na_2O**	**MgO**	**Al_2O_3**	**SiO_2**	**P_2O_5**	**CaO**	**Fe_2O_3**	**WO_3**
1	74.14		0.80	3.62	2.15	4.37	11.80	3.11	
2	52.21		0.74	3.56		5.92	7.96	2.88	26.74
3	77.43	0.93	0.73	3.39	1.91	3.26	8.29	4.07	
4	12.70		0.79	2.51	2.67	32.13	44.74	4.46	
5	45.81		1.58	5.37	6.40	12.64	19.26	8.94	

Sample 164/1B

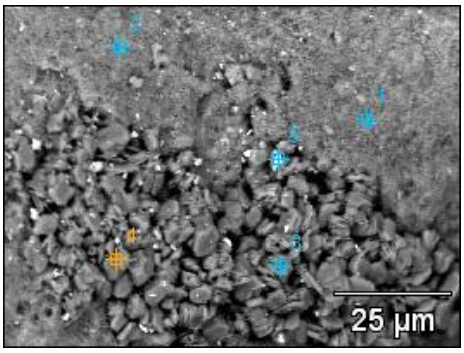

	CO_2	MgO	Al_2O_3	SiO_2	P_2O_5	K_2O	CaO	Fe_2O_3
1		0.89	42.10	53.25		0.31	1.00	2.46
2	3.11	1.18	39.06	49.02	1.11	0.84	1.13	4.55
3	12.78		38.05	46.31	0.88		0.58	1.40
4			43.91	54.42	0.98		0.70	
5	9.11	0.57	15.94	15.22	0.77		1.31	57.10

Sample 178/0

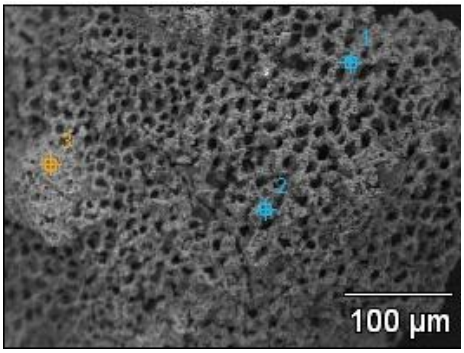

	CO_2	MgO	Al_2O_3	SiO_2	K_2O	Fe_2O_3
1	40.13	3.32	14.22	19.41	0.66	22.25
2	7.51	1.44	11.88	17.75	2.36	59.06
3	30.43	2.55	19.24	26.60	2.73	18.45

Sample 178/2B

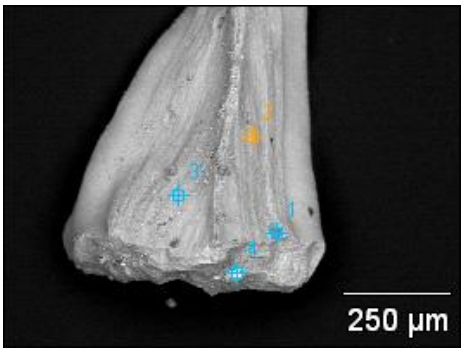

	CO_2	F	Na_2O	MgO	Al_2O_3	SiO_2	P_2O_5	CaO	Fe_2O_3	MoO_3
1	32.37		0.27		0.39	62.22	2.42	2.33		
2	19.93		0.36	0.19	0.64	0.53	32.27	44.84	1.08	0.16
3	17.08	5.89			0.40		33.73	42.91		
4	28.35				1.09		2.44	3.94	64.18	

Sample 178/2B

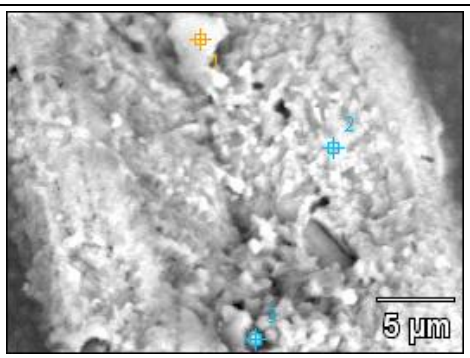

	CO_2	F	Na_2O	MgO	Al_2O_3	SiO_2	P_2O_5	K_2O	CaO	Fe_2O_3
1	19.42			5.00	10.68	13.71	14.44		15.42	21.32
2	20.53	6.02	0.37		0.49		32.29		40.31	
3	21.58		0.21	0.71	3.78	4.41	27.41	0.49	37.03	4.38

Sample 178/2B

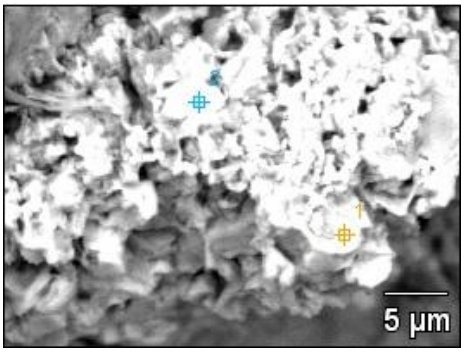

	CO_2	F	Al_2O_3	SiO_2	P_2O_5	CaO	Fe_2O_3
1	21.99		0.60	0.34	1.74	2.07	73.26
2	47.44	0.99	1.41		4.64	6.25	39.28

Sample 178/2B

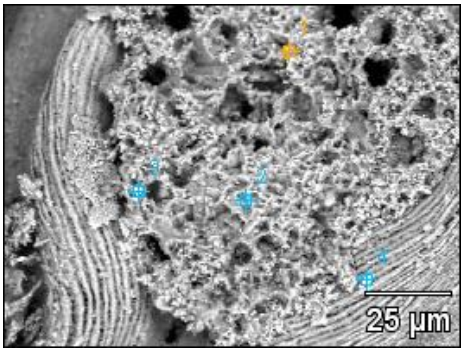

	CO_2	MgO	Al_2O_3	SiO_2	P_2O_5	K_2O	CaO	Fe_2O_3	WO_3
1		5.21	23.60	30.29	1.95	0.73	4.24	33.98	
2	9.84	3.30	18.81	23.02	2.09	0.58	3.98	38.37	
3	10.38	1.00	6.98		6.48	0.52	10.32	8.18	56.14
4	11.87		0.63		17.55		20.14		49.82

Sample 178/2B

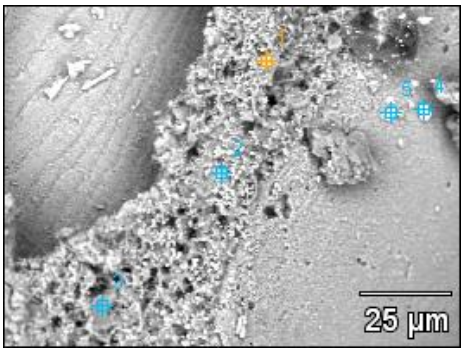

	CO_2	Na_2O	MgO	Al_2O_3	SiO_2	P_2O_5	K_2O	CaO	Fe_2O_3	MoO_3	WO_3
1	17.51	0.28	0.95	5.38	6.53	25.98	0.28	36.59	6.27	0.24	
2	16.71		0.46	3.68	6.08	13.99	1.05	32.39	22.93	2.71	
3	10.26	0.25	1.33	22.86	33.94	8.38	5.69	12.59	4.70		
4	16.69			0.86		11.61		16.16	2.11		52.58
5	16.30			0.82		16.68		22.87	1.40		41.94

Sample 178/11

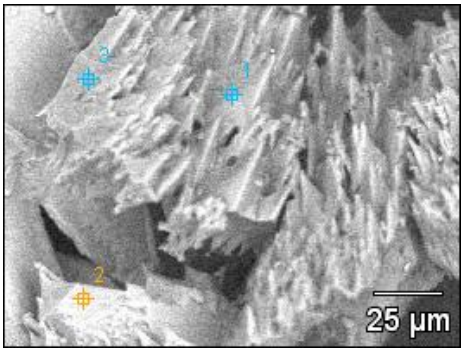

	CO_2	MgO	P_2O_5	CaO	Sc_2O_3
1	42.69			57.27	0.04
2	32.62	1.23		66.15	
3	50.55		3.44	46.01	

Sample 178/11

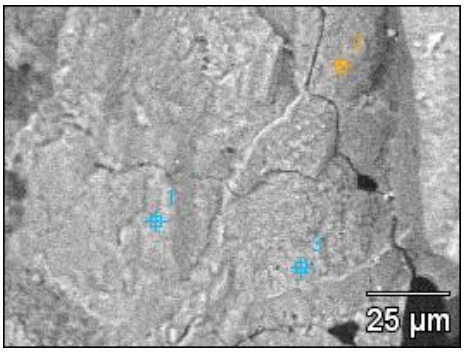

	CO_2	Na_2O	MgO	CaO	Fe_2O_3
1	42.61	0.51	22.97	33.05	0.86
2	31.84		21.87	46.29	
3	36.66		19.37	36.74	7.23

Sample 178/11

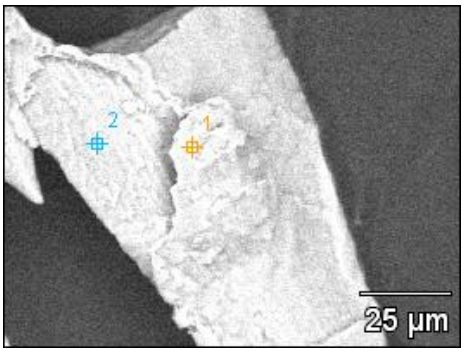

	CO_2	F	P_2O_5	CaO
1	11.35	3.00	25.31	60.34
2	42.22			57.78

Sample 178/11						
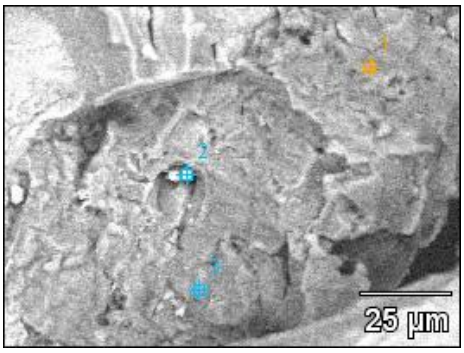						
	CO_2	**MgO**	**P_2O_5**	**SO_3**	**CaO**	**Fe_2O_3**
1	61.42	17.45		0.32	20.81	
2	24.83	5.19	2.46		15.61	51.92
3	35.10	21.28			36.90	6.72

Sample 180/3				
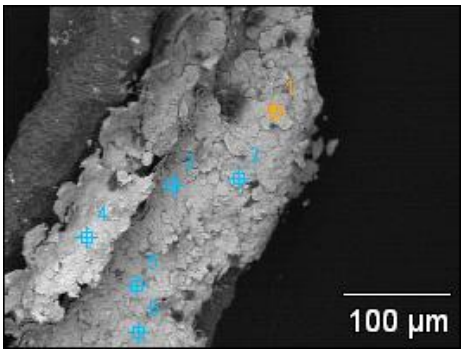				
	CO_2	**Na_2O**	**CaO**	**WO_3**
1	27.46	3.90	2.63	66.00
2	20.37	4.12	2.38	73.13
3	32.60	4.57	2.93	59.90
4	28.91	4.66	3.46	62.98
5	27.45	4.75	2.57	65.24
6	32.31	5.16	2.70	59.83

Sample 180/3

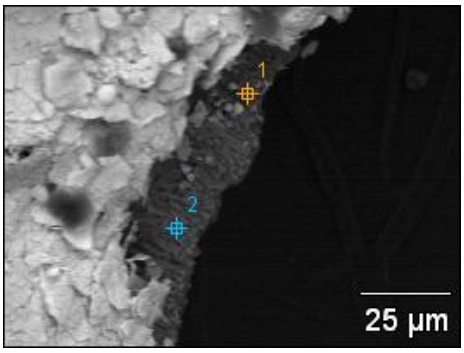

	CO_2	F	SiO_2	P_2O_5	CaO	BaO
1	20.75	1.98		31.66	45.60	
2	34.63	3.55	0.50	26.11	34.48	0.73

Sample 184/3T

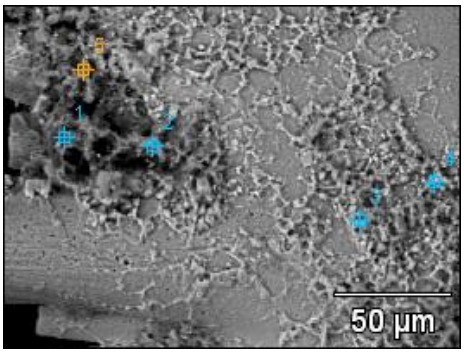

	CO_2	Na_2O	MgO	Al_2O_3	SiO_2	P_2O_5	K_2O	CaO	TiO_2	Fe_2O_3
1	40.28		1.81	16.40	26.31	3.54	2.02	5.86		3.78
2	26.99	0.41	2.13	19.47	30.53	5.13	2.64	6.99	0.80	4.91
3	20.19		0.92	5.43	7.65	28.42	0.38	37.00		
4	23.43		0.60	4.25	7.54	26.25	0.70	36.16		1.07
5	25.66		1.77	11.97	18.44	16.43	1.32	21.35		3.07

Sample 184/5

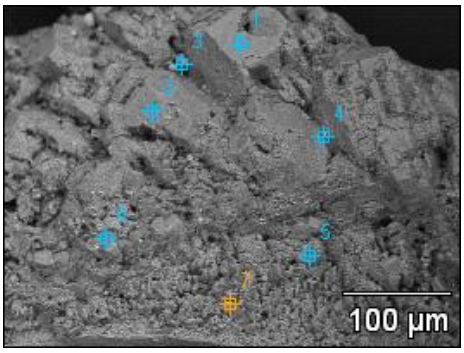

	CO_2	F	Na_2O	MgO	Al_2O_3	SiO_2	P_2O_5	K_2O	CaO	Fe_2O_3
1	47.05			0.52	1.58	3.69	18.92		28.24	
2	16.63				0.60	1.04	10.23		71.51	
3	46.52								5.47	48.01
4	19.20								5.89	74.91
5	26.17						26.70		47.13	
6	39.08			3.56	15.44	29.40		4.28	1.58	6.67
7	33.83	1.05	0.33				25.82		38.97	

Sample 194/5

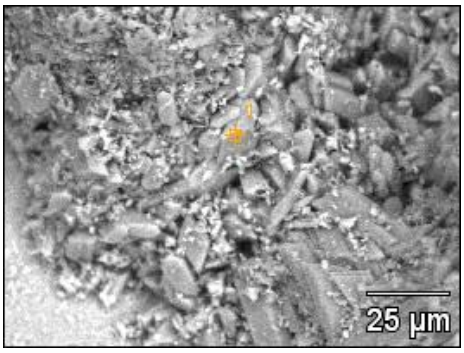

	CO_2	SO_3	CaO
1	14.60	49.27	36.14

Sample 194/5

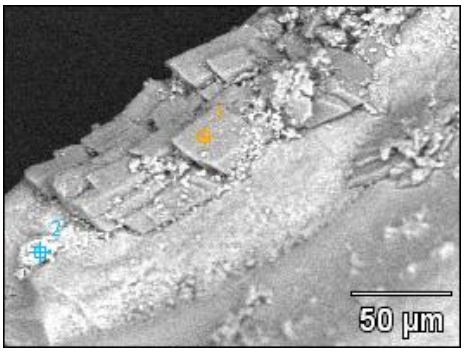

	CO_2	MgO	Al_2O_3	SiO_2	P_2O_5	SO_3	Cl	CaO	Sc_2O_3	Fe_2O_3
1	18.73					49.80		31.45	0.02	
2	14.87	2.66	1.46	4.48	1.61		0.48	2.98		71.45

Sample 194/5

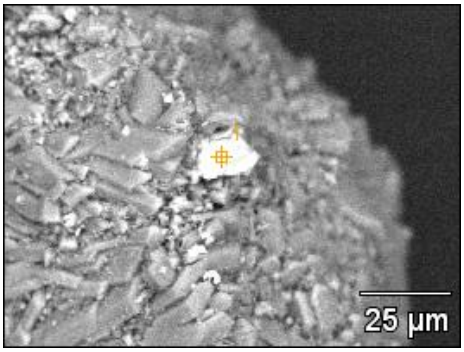

	CO_2	MgO	Al_2O_3	SiO_2	CaO	Fe_2O_3
1	16.57	0.92	0.38	1.91	1.38	78.84

Sample 194/5

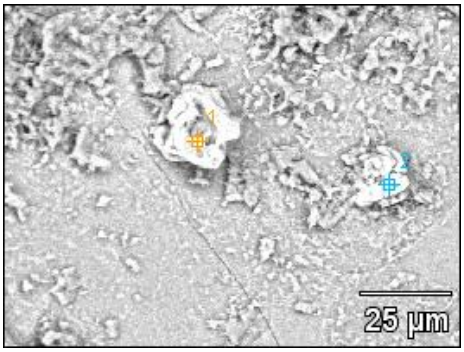

	CO_2	MgO	Al_2O_3	SiO_2	P_2O_5	SO_3	CaO	Fe_2O_3
1	13.23		0.92	4.28	1.18	3.29	3.01	74.09
2	20.64	2.35	0.96	3.13	1.33	2.04	3.08	66.48

Sample 196/5B

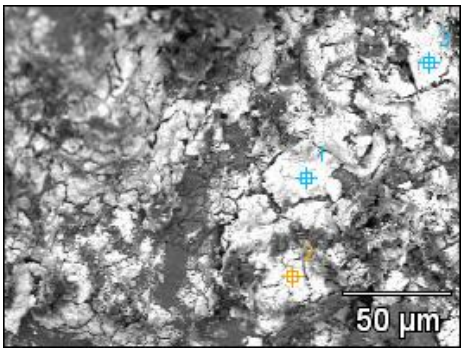

	CO_2	Al_2O_3	P_2O_5	K_2O	CaO	WO_3
1	10.21	1.51		0.11	1.39	86.77
2	6.21	0.77	0.47		3.62	88.93
3	10.90	0.71			6.30	82.09

Sample 196/5T

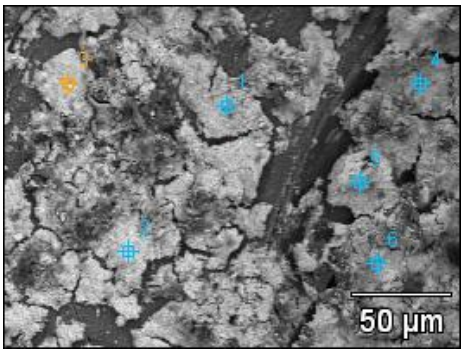

	CO_2	Al_2O_3	CaO	WO_3
1	29.12		6.94	63.94
2	29.45		5.70	64.85
3	31.36		6.64	62.00
4	41.65	0.99	6.08	51.28
5	39.05		5.66	55.29
6	45.32	3.00	5.57	46.10

Sample 202/19

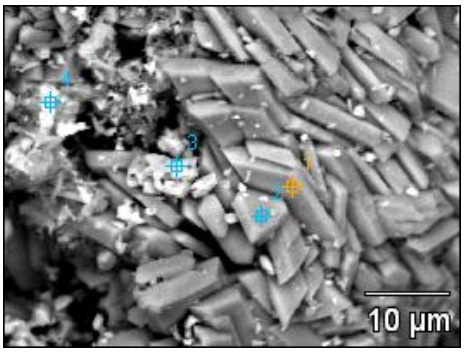

	CO_2	Na_2O	Al_2O_3	SiO_2	P_2O_5	SO_3	CaO	Fe_2O_3
1	16.56		0.22	0.20		48.64	34.38	
2	11.45			0.31		53.36	34.88	
3	9.66	0.26	0.44			53.84	35.80	
4	14.81		0.75	1.23	0.58	6.71	6.59	69.32

Sample 202/19

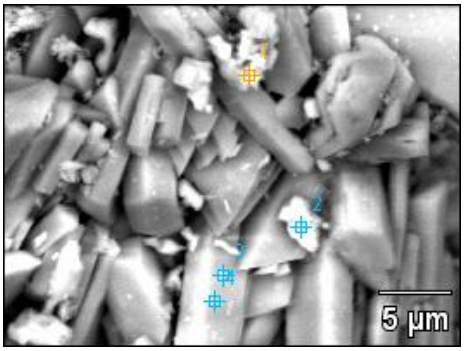

	CO_2	Na_2O	Al_2O_3	SiO_2	SO_3	CaO	Fe_2O_3	Pt
1	32.83	0.57	0.33	0.45	32.42	21.34	10.58	1.48
2	26.61		0.34	0.21	36.34	35.35	1.14	
3	26.83		0.34	0.24	31.58	31.37	9.64	
4	18.51		0.20		45.85	35.44		

Sample 213/5

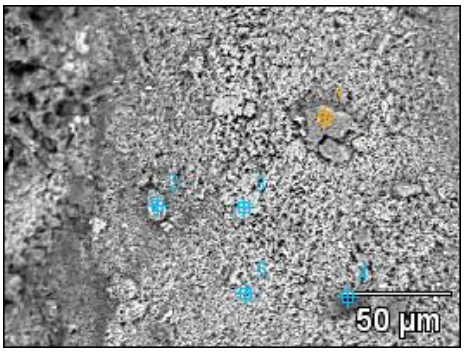

	CO_2	F	Na_2O	MgO	Al_2O_3	SiO_2	P_2O_5	Cl	K_2O	CaO	TiO_2	Fe_2O_3	As_2O_3	MoO_3
1	18.44			0.79	22.48	36.38	3.08		3.67	5.82	6.50	2.84		
2	20.24	5.09	1.12	0.23	0.90	1.58	29.41			40.52		0.91		
3	18.19	4.52	0.71		0.31		33.89			42.38				
4	83.70	0.00	1.41		0.78	1.08	4.39	0.67	0.64	5.81			0.32	1.20
5	16.06	4.95	0.79				33.96			44.24				

Sample 213/5

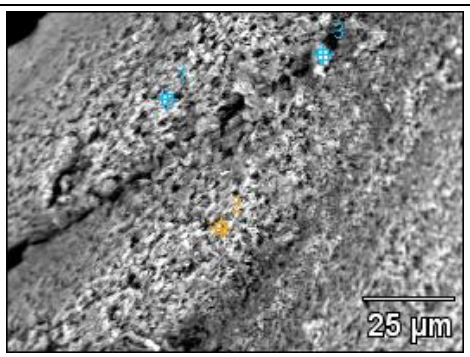

	CO_2	Na_2O	MgO	Al_2O_3	SiO_2	P_2O_5	Cl	K_2O	CaO	TiO_2	Fe_2O_3	MoO_3
1	18.19	0.33		1.20	2.17	27.98			47.94	0.47		1.71
2	17.97			0.72	0.89	30.27			50.15			
3	11.96	0.47	1.23	5.33	8.85	5.37	0.29	0.52	9.00		57.00	

Sample 213/5						
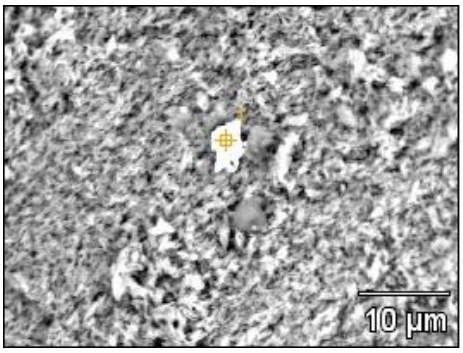						
	CO_2	**Na_2O**	**MgO**	**P_2O_5**	**CaO**	**WO_3**
1	20.98	0.32	0.44	6.11	12.91	59.25

Sample 214/8															
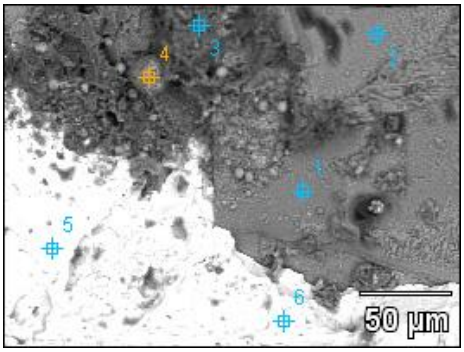															
	CO_2	**F**	**Na_2O**	**MgO**	**Al_2O_3**	**SiO_2**	**P_2O_5**	**SO_3**	**Cl**	**K_2O**	**CaO**	**Fe_2O_3**	**SrO**	**ZrO_2**	**BaO**
1	12.94				1.17	2.78	6.99	1.89			69.48				4.76
2	10.59	3.43	0.62		1.01	1.02	35.48				47.85				
3	9.76			0.29	2.77	17.92		40.55			27.49			1.21	
4	1.45		1.66	2.25	12.99	24.05	1.90	1.66	0.28	2.10	3.17	47.18			1.31
5	1.65				0.89			34.88			0.91		2.14	0.27	59.26
6	2.96				1.06	2.07		32.29			1.52	1.64		0.69	57.79

Sample 214/8											
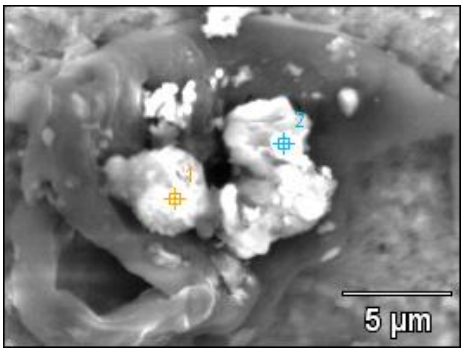											
	CO_2	**Na_2O**	**Al_2O_3**	**SiO_2**	**P_2O_5**	**SO_3**	**CaO**	**Fe_2O_3**	**ZrO_2**	**BaO**	**WO_3**
1	7.60	0.38	0.62	0.94		59.77	1.71	27.15	0.80	1.02	
2	18.13	0.34	0.72		3.57	23.40	18.24	1.05		1.23	33.30

Sample 214/8														
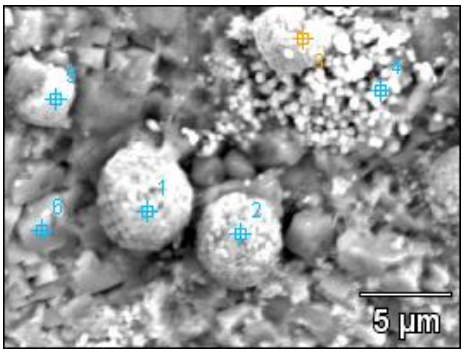														
	CO_2	**Na_2O**	**MgO**	**Al_2O_3**	**SiO_2**	**P_2O_5**	**SO_3**	**Cl**	**K_2O**	**CaO**	**TiO_2**	**Fe_2O_3**	**MoO_3**	**BaO**
1	4.21		1.37	1.26	2.89	1.85	12.22			4.23		69.08		2.89
2	9.19	0.76	1.81	5.70	11.39	1.76	2.00		0.54	4.35	0.54	60.42		1.54
3	7.75	1.05	2.06	5.16	10.83	2.34	2.06	0.25	0.56	5.38		60.96		1.60
4	7.82	0.86	1.79	4.30	8.97	2.14	6.16		0.52	4.79		61.07		1.58
5	4.96	0.98	1.53	8.61	14.60	5.00	1.91		1.01	7.97		50.93		2.50
6	7.64			1.26	1.97	28.53				54.42		1.35	2.06	2.77

Sample 214/8

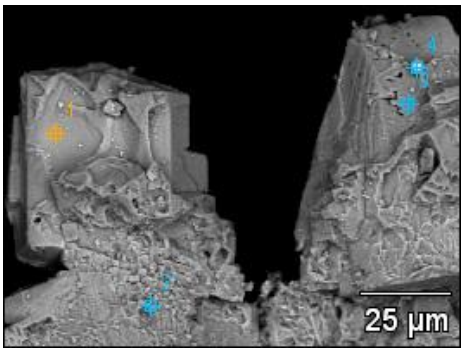

	CO_2	F	Na_2O	Al_2O_3	SiO_2	P_2O_5	CaO	GeO_2	Tl_2O_3
1	22.53	6.28	0.66	0.30		31.33	38.91		
2	18.89	7.49	0.47	0.85	0.92	30.98	40.41		
3	21.20	7.89	1.14			30.98	35.89	2.89	
4	34.71	4.82	0.70	0.47	0.50	24.43	32.98		1.39

Sample 218/4B

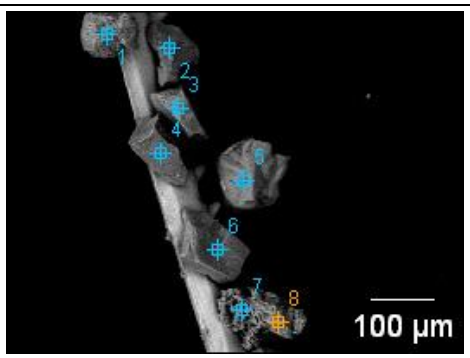

	CO_2	Al_2O_3	SiO_2	P_2O_5	Cl	K_2O	CaO
1	16.67		82.88				0.45
2	15.06		83.18	1.22			0.54
3	14.97		84.69				0.33
4	82.72	1.16	13.56	1.13			1.43
5	50.75	0.66	43.54	2.42			2.63
6	17.05	0.00	82.59			0.36	
7	19.14	35.26	42.37	1.38	0.16	0.55	1.14
8	57.19	0.78	39.22	1.38			1.44

Sample 218/4B

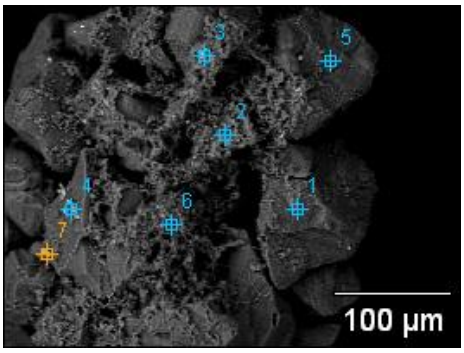

	CO_2	Na_2O	MgO	Al_2O_3	SiO_2	P_2O_5	Cl	K_2O	CaO	TiO_2	Fe_2O_3	MoO_3
1	21.69			0.40	77.91							
2	15.47		0.80	31.93	41.77			1.07	0.37	3.10	5.50	
3	21.30		0.94	13.42	19.71		1.07	2.16	1.12		40.30	
4	21.79		1.67	3.41	14.72	1.47			0.69		56.25	
5	23.50			0.20	76.30							
6	19.72	0.20	1.30	25.99	37.86			2.08	0.90	0.59	10.59	0.77
7	32.24		2.04	3.02	12.94	0.97			0.48		48.31	

Sample 218/4B (host rock)

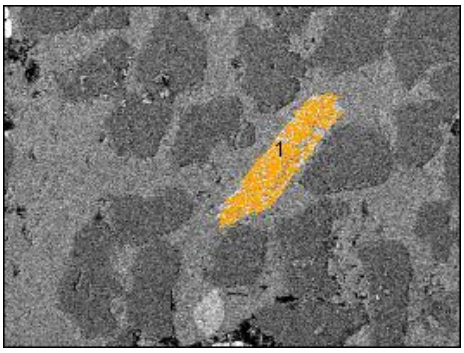

	Na_2O	MgO	P_2O_5	CaO	Sc_2O_3
1	1.13	0.73	38.50	59.22	0.43

Sample 218/4B (host rock)

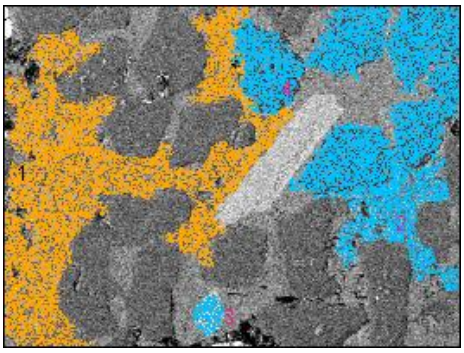

	MgO	SiO_2	P_2O_5	CaO	Sc_2O_3
1	4.42	1.60		93.97	
2	3.19	13.50		83.20	0.10
3			41.02	58.51	0.48
4		100.00			

Sample 218/4B (host rock)

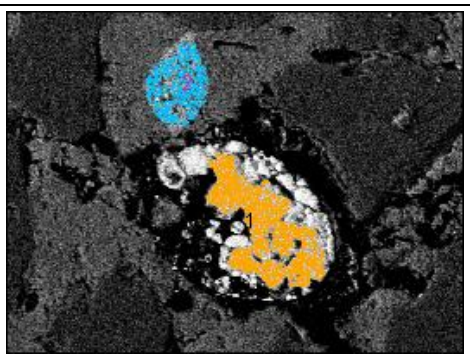

	MgO	SiO_2	P_2O_5	CaO	Sc_2O_3	Fe_2O_3
1	1.68	4.91		1.01		92.40
2			41.98	57.42	0.60	

Sample 218/4B (host rock)						
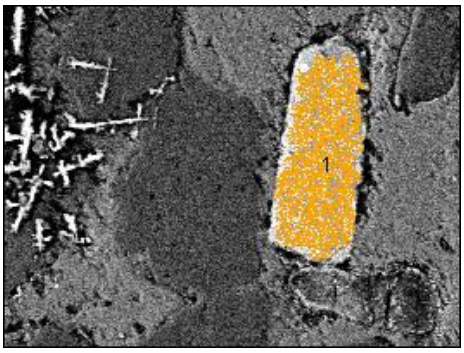						
	Na_2O	**MgO**	**SiO_2**	**P_2O_5**	**CaO**	**Fe_2O_3**
1	0.83	0.58	1.44	36.14	53.63	7.38

Sample 218/4B (host rock, mapping)

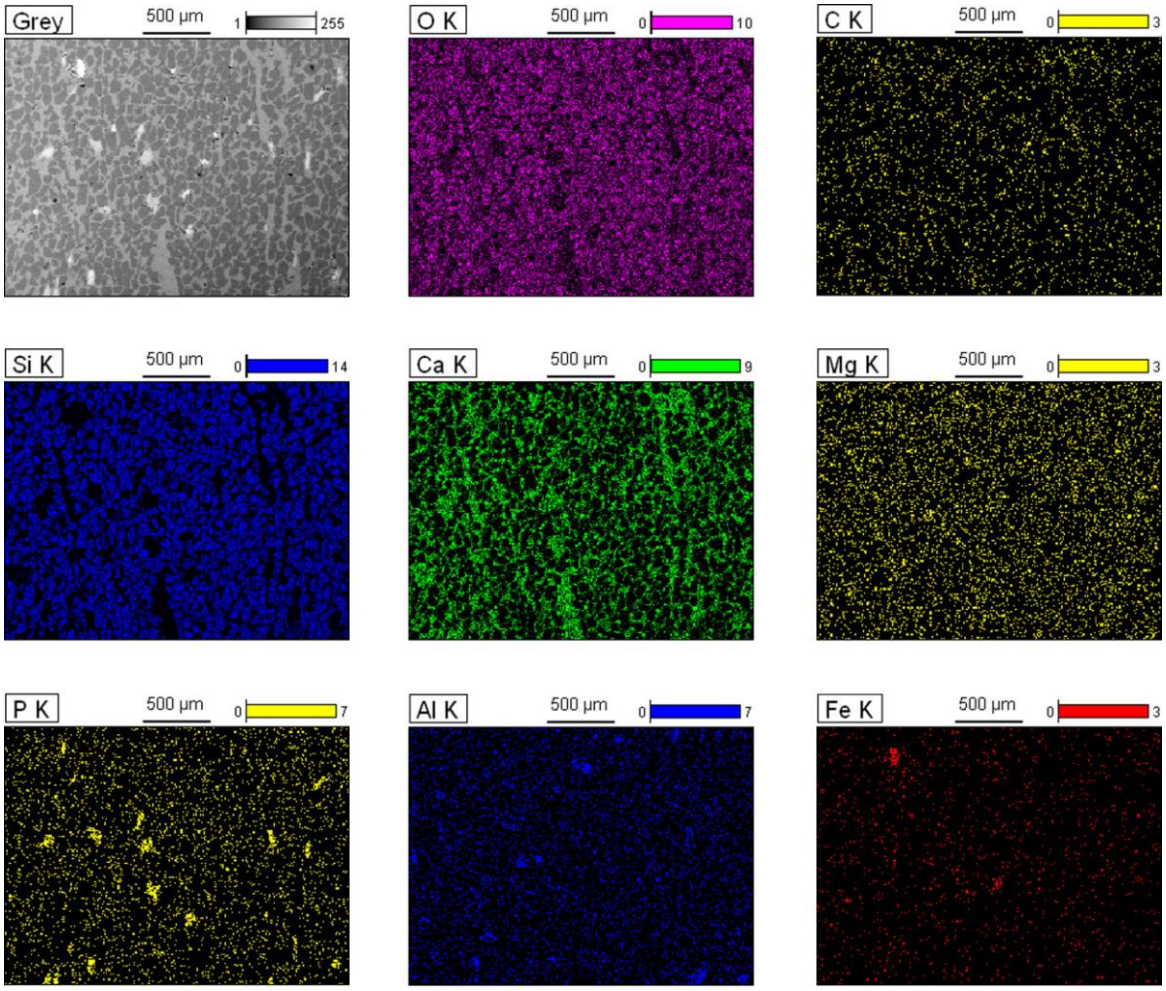

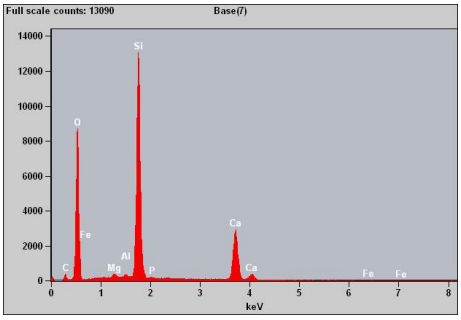

Sample 233/2b

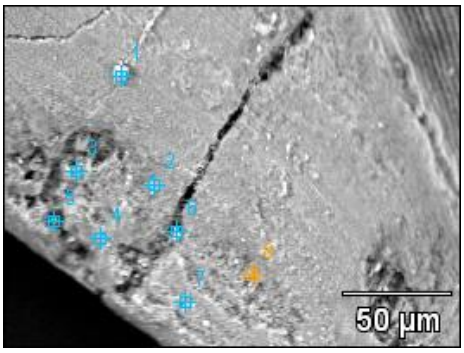

	CO_2	Na_2O	Al_2O_3	P_2O_5	CaO	MnO	Fe_2O_3
1	19.43			30.51	50.05		
2	90.52		1.42	2.72	5.34		
3	89.54	0.45	1.33	3.14	5.54		
4	90.19		1.26	3.45	5.10		
5	91.25			4.04	4.55	0.16	
6	84.71		1.73	5.79	7.76		
7	82.14		2.21	5.24	8.28		2.12
8	91.81			3.36	4.83		

Sample 233/2c

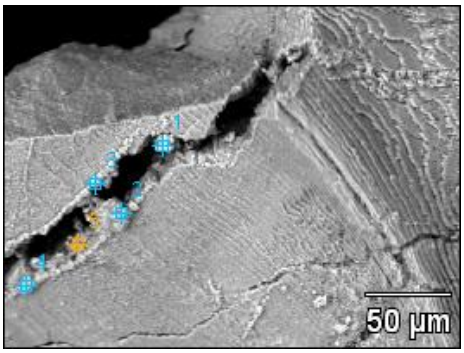

	CO_2	F	MgO	Al_2O_3	SiO_2	P_2O_5	K_2O	CaO	TiO_2	MnO	Fe_2O_3
1	29.15		1.48	2.92	5.10	4.27	0.35	6.19		2.30	48.24
2	21.53	4.11		0.79	0.66	31.81		41.11			
3	19.95			0.58	0.33	33.60		45.54			
4	27.13	2.38		2.18	3.51	24.69	0.86	39.25			
5	46.97			0.93	2.07	6.78	2.22	31.20	1.75		8.07

Sample 251/20																
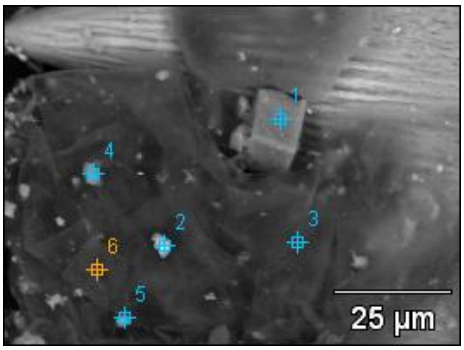																
	CO_2	**Na_2O**	**MgO**	**Al_2O_3**	**SiO_2**	**P_2O_5**	**SO_3**	**Cl**	**K_2O**	**CaO**	**TiO_2**	**MnO**	**Fe_2O_3**	**Cu_2O**	**MoO_3**	**Ta_2O_5**
1	50.46		20.10	1.14	1.10					26.30			0.89			
2	66.91	0.77	0.65	1.20	2.32	1.54	0.63	0.27	0.13	2.14		0.50	22.55	0.38		
3	61.13	0.62	0.16	0.40	0.80	15.19		0.36	0.25	19.99					1.09	
4	62.62	0.31	0.46	3.22	30.39	0.41	0.46	0.11	0.60	0.33	0.14		0.95			
5	66.22	0.43	0.66	5.64	18.83	1.33	0.75	0.21	1.47	2.22	0.33		1.88			0.05
6	89.45	1.23	0.30	0.32	0.54	1.89	2.16	0.80	0.32	2.47				0.53		

Sample 251/20

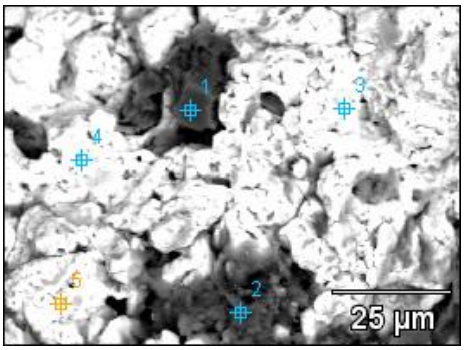

	CO_2	Na_2O	MgO	Al_2O_3	SiO_2	P_2O_5	SO_3	K_2O	CaO	Fe_2O_3	SrO	BaO
1	45.33	5.83		10.68	36.98		0.43					0.75
2	40.25	5.45	1.42	10.62	30.52	0.31	3.40	0.61	0.22	2.35		4.85
3	21.76		0.19	1.18			29.02		0.11			47.74
4	25.77			0.58			25.29		0.11		1.77	46.46
5	20.26			0.71	1.50		28.80		0.36	0.39		47.96

Sample 251/20

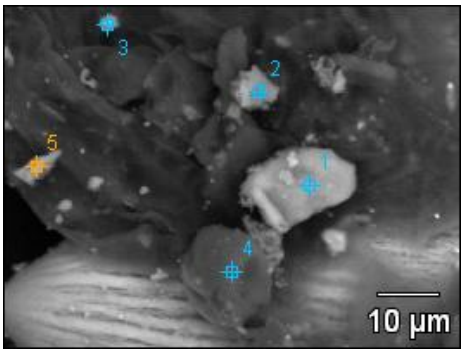

	CO_2	N_2O_5	F	Na_2O	MgO	Al_2O_3	SiO_2	P_2O_5	SO_3	Cl	K_2O	CaO	TiO_2	Fe_2O_3	Cu_2O	ZnO	MoO_3
1	30.83		2.26	0.66		0.31	0.66	27.13				36.80		0.32	0.43		0.60
2	47.15			0.23	0.60	0.46	0.72			0.10		50.00					0.74
3	64.39	0.00		0.30	0.43	2.77	26.27	0.96	0.53	0.15	0.64	1.03	0.90	1.40	0.24		
4	90.27					0.19	0.29	0.25	0.40		0.06	0.27			3.77	4.52	
5	59.07	7.90		0.44	0.58	0.78	0.99	1.03	0.56	0.14		28.25		0.28			

Sample 251/20

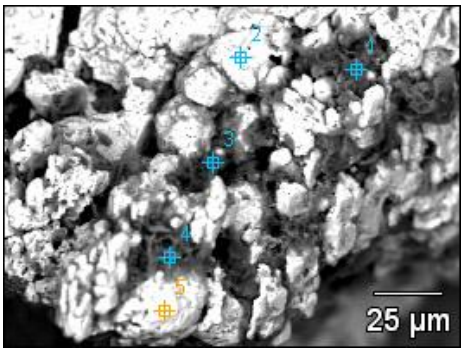

	CO_2	Na_2O	MgO	Al_2O_3	SiO_2	P_2O_5	SO_3	K_2O	CaO	TiO_2	Fe_2O_3	SeO_2	SrO	BaO	Tl_2O_3
1	34.70	11.08		12.60	40.24	0.37			0.11		0.22			0.37	0.30
2	19.73			0.72	1.19		23.69		0.35					54.32	
3	47.12	0.53	2.05	11.67	23.91	0.35	2.60	1.89	0.41		4.03	0.78		4.65	
4	37.82	0.10	1.50	12.88	32.10	0.85	1.34	3.08	1.24	0.61	5.96			2.52	
5	35.88			0.47			22.41						2.57	38.66	

Sample 251/20

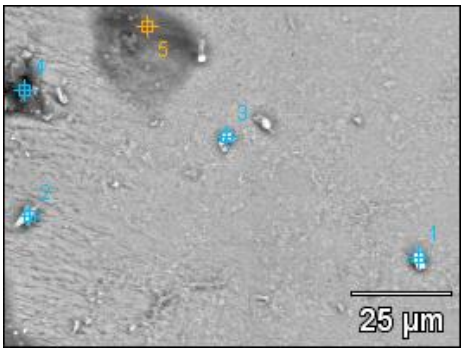

	CO_2	N_2O_5	F	Na_2O	MgO	Al_2O_3	SiO_2	P_2O_5	Cl	K_2O	CaO	V_2O_5	Cr_2O_3	MnO	Fe_2O_3	NiO	Cu_2O	ZnO	MoO_3
1	26.06					0.33	0.82	1.23			1.91		12.60	1.24	49.53	5.03	0.91		0.34
2	54.25			0.58	0.51	0.36	0.27	12.13			31.91								
3	49.88		3.82	0.50	0.14	0.92	1.16	19.31			23.86	0.01			0.40				
4	74.09				0.23	0.61	0.85	8.79	1.04	0.27	10.64				0.40		0.75	0.81	1.52
5	43.42	16.52	1.79	0.56		0.14	0.05	17.37	0.19		19.96								

Sample 251/24

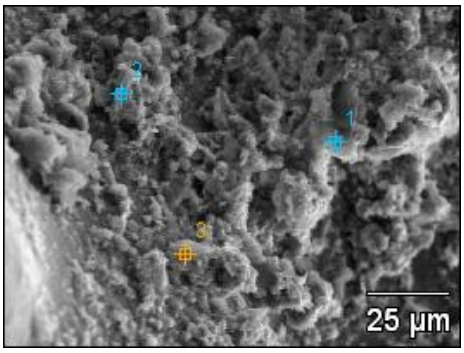

	CO_2	Na_2O	MgO	Al_2O_3	SiO_2	P_2O_5	Cl	K_2O	CaO	TiO_2	Fe_2O_3
1	42.60	0.38	0.98	7.47	43.32	0.72		1.19	1.43	0.15	1.75
2	44.11	0.32	1.82	9.29	35.56	0.68	0.03	1.35	4.10	0.15	2.59
3	29.70	0.40	2.49	14.57	33.78	3.27	0.09	2.49	8.03	0.33	4.86

Sample 251/24

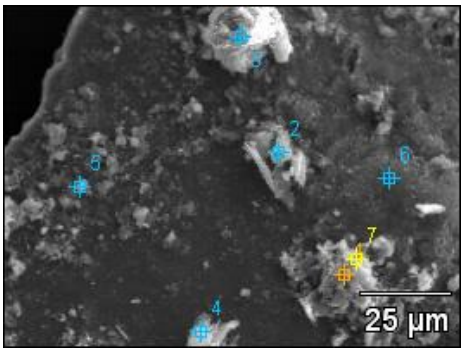

	CO_2	Na_2O	MgO	Al_2O_3	SiO_2	P_2O_5	Cl	K_2O	CaO	TiO_2	Cr_2O_3	MnO	Fe_2O_3	Ta_2O_5
1	46.07	0.75	2.80	12.53	27.87	0.99		1.82	2.27	0.24			4.68	
2	95.74		0.06	0.29	0.56	0.50	0.02	0.04	0.68		0.31		1.81	
3	35.09	0.27	0.58	3.19	8.09	1.31		0.49	49.41	0.09			1.39	0.08
4	88.28	0.22		0.37	0.70	5.01		0.07	5.24				0.07	0.03
5	47.92	0.35	0.57	3.12	5.70	17.43		0.33	23.49	0.13			0.95	
6	29.47	0.42	0.72	1.42	5.04	16.81	0.18		24.18			0.87	20.89	

Sample 251/26

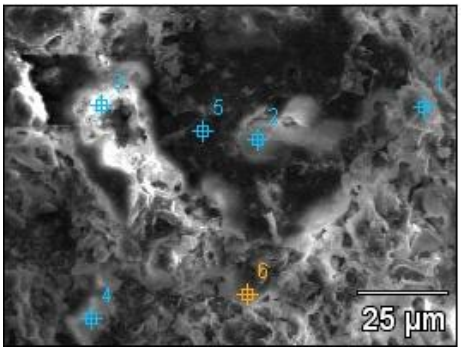

	CO_2	Na_2O	MgO	Al_2O_3	SiO_2	P_2O_5	K_2O	CaO	TiO_2	Fe_2O_3	Cu_2O
1	97.17	0.13	0.11	0.66	1.25	0.14	0.13	0.11		0.22	0.08
2	23.17	0.33	2.34	21.46	39.85	0.43	5.68		0.44	5.98	0.32
3	10.91	0.21	1.55	17.28	36.71		7.04	2.72	1.58	21.21	0.77
4	25.56	0.20	1.52	13.48	23.64	7.52	2.55	21.63	0.39	3.50	
5	18.54	0.29	2.16	21.14	46.21		4.13	0.76	0.64	6.13	
6	28.07		1.72	18.66	34.24	0.37	4.60	0.64	6.62	4.83	0.25

Sample 251/26

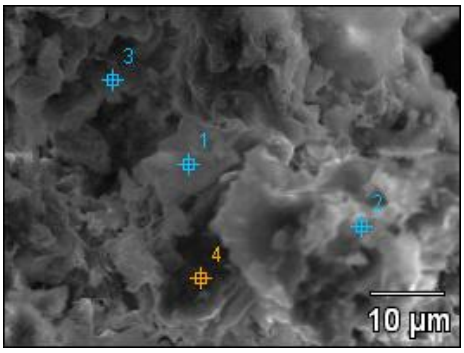

	CO_2	Na_2O	MgO	Al_2O_3	SiO_2	P_2O_5	K_2O	CaO	TiO_2	Fe_2O_3	Cu_2O	In_2O_3	Tl_2O_3
1	42.88	0.35	1.89	13.22	33.00	0.34	1.66	0.56	0.49	5.02			0.60
2	30.84	0.37	2.05	15.27	41.97	0.34	3.18	0.50	0.49	4.62	0.38		
3	23.73	0.69	0.83	8.66	22.66		4.23	1.94	2.29	34.96			
4	23.62	0.15	0.23	1.60	72.98					0.37		0.71	0.33

Sample 251/29

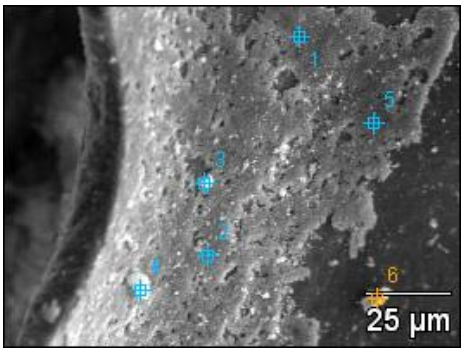

	CO_2	F	Na_2O	MgO	Al_2O_3	SiO_2	P_2O_5	SO_3	Cl	K_2O	CaO	TiO_2	V_2O_5	MnO	Fe_2O_3	Cu_2O	Ta_2O_5
1	34.01	0.94	0.11		0.27	0.23	22.41				41.57				0.44		0.01
2	38.14	1.08	0.13		0.21	0.14	18.90				41.34						0.06
3	58.01		0.41	0.68	4.94	7.90	6.66	0.98		0.72	9.93	0.09		0.61	9.06		
4	71.33		0.24	0.20	0.90	1.74	6.96				14.94			0.20	3.26	0.22	
5	37.15	1.38	0.13		0.34	0.37	23.22				36.96				0.45		
6	48.03		0.00	17.64	0.64	0.89	3.98		0.13		27.43		0.18		1.08		

Sample 251/29

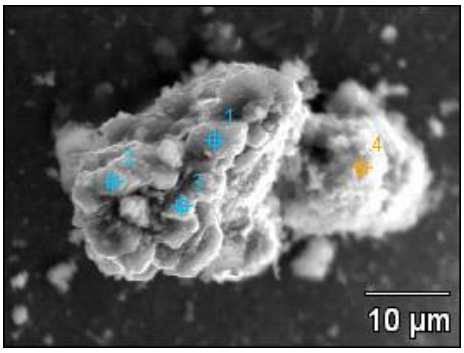

	CO_2	Na_2O	MgO	Al_2O_3	SiO_2	P_2O_5	SO_3	K_2O	CaO	MnO	Fe_2O_3	MoO_3	In_2O_3
1	41.59	0.09		0.38	0.50	0.76	33.08		22.99		0.60		
2	38.12			0.41	0.70	0.97	34.68		24.50		0.62		
3	52.62		0.05	0.68	1.14		26.10		18.24		0.65		0.52
4	35.21		0.28	2.08	5.91	18.10		0.42	29.39	0.13	7.33	1.15	

Sample 251/29

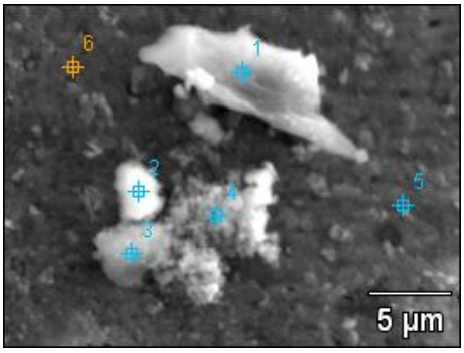

	CO_2	F	Na_2O	MgO	Al_2O_3	SiO_2	P_2O_5	K_2O	CaO	MnO	Fe_2O_3	As_2O_3
1	35.47		0.44	0.65	1.25	1.35	12.08		47.14		1.63	
2	56.11		0.23		0.76	30.87	5.81		5.10		1.05	0.07
3	40.26		0.25		10.65	14.44	12.71	0.59	17.02		4.05	0.03
4	33.40		0.80	1.13	1.51	2.52	8.99		11.19	0.79	39.66	
5	29.53	5.28	0.29		0.59	0.49	28.13		34.75		0.94	
6	30.91		0.47	0.60	2.49	2.49	26.08		33.73		3.23	

Sample 251/29

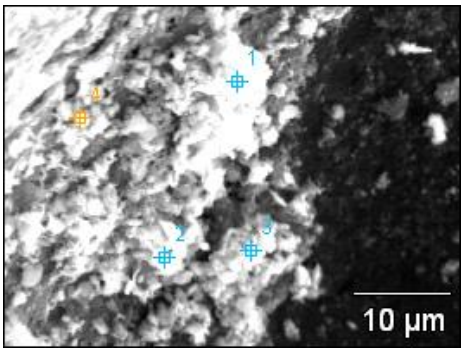

	CO_2	Na_2O	Al_2O_3	SiO_2	P_2O_5	SO_3	CaO	Fe_2O_3	Cu_2O	MoO_3	Ta_2O_5
1	90.12	0.40	0.56	0.58	2.16	0.63	3.68	0.63	1.24		
2	92.44	0.38	0.47	0.44	1.13	0.62	2.44	0.48	1.61		
3	85.29	0.43	0.80	0.60	1.87		3.74	1.16		0.88	5.23
4	92.49	0.35	0.47	0.42	1.44	0.66	2.74	1.10			0.34

Sample 252/58

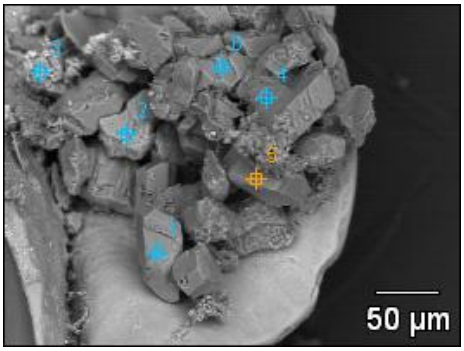

	CO_2	Na_2O	Al_2O_3	SiO_2	P_2O_5	K_2O	CaO	TiO_2	Fe_2O_3	As_2O_3	BaO	Tl_2O_3
1	29.89	9.16	15.57	43.15			2.22					
2	26.28	0.66	14.34	46.80	0.39	10.74		0.17			0.62	
3	32.73	0.53	13.00	41.40	0.48	9.24		0.65	1.76	0.21		
4	35.63	11.18	12.95	38.12	0.74		1.28					0.10
5-No Data.												
6	27.25	12.37	13.97	45.90	0.39		0.11					0.00

Sample 252/58																	
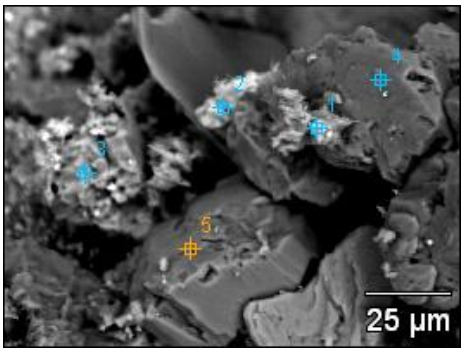																	
	CO_2	**Na_2O**	**MgO**	**Al_2O_3**	**SiO_2**	**P_2O_5**	**K_2O**	**CaO**	**TiO_2**	**V_2O_5**	**MnO**	**Fe_2O_3**	**Cu_2O**	**MoO_3**	**BaO**	**Ta_2O_5**	**Tl_2O_3**
1	18.14	0.15		0.75	1.55	0.30	0.19	0.80	77.25	0.24		0.53	0.11				
2	21.51	1.10	0.54	4.52	10.33	2.63	0.53	3.06	0.77		0.27	54.74					0.00
3	29.76	0.45		14.89	41.82		11.44					0.50			0.61	0.41	0.13
4	34.91	8.85		12.62	42.28	0.57	0.12	0.31	0.07			0.26					
5		15.73		18.78	63.69	0.75		0.29						0.77			

Sample 252/58

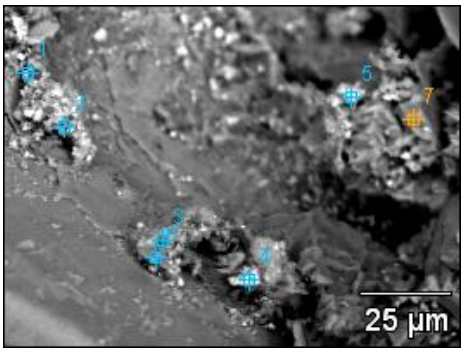

	CO_2	Na_2O	MgO	Al_2O_3	SiO_2	P_2O_5	SO_3	Cl	K_2O	CaO	Sc_2O_3	TiO_2	Fe_2O_3	MoO_3	BaO	Ta_2O_5
1	28.45	2.98		8.99	28.71	3.90	2.78		0.86	6.53		0.47	16.32			
2	17.77	0.45		10.43	35.63	1.31	7.33		8.86	3.30		0.35	13.90		0.66	
3	33.88	0.55	0.99	4.31	11.94	2.13	4.61		0.51	3.75		0.40	36.94			
4	20.42	0.55	0.86	1.05	4.53	3.24			0.18	3.39			65.79			
5	14.11	0.90	0.84	3.01	11.06	0.65	0.66	0.13	0.67	1.11			66.84			
6	29.45	0.35	0.18	0.85	62.70	2.79				1.70			0.99	0.89		0.10
7	19.33	0.43		13.60	48.59	0.53			16.92		0.05		0.54			

Sample 252/58

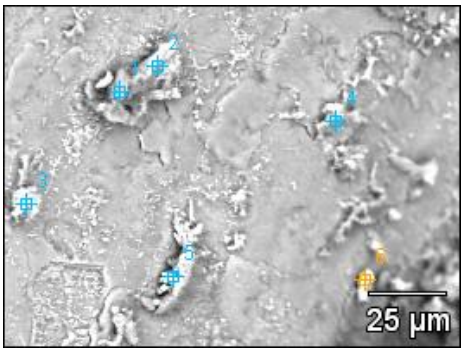

	CO_2	Na_2O	MgO	Al_2O_3	SiO_2	P_2O_5	SO_3	Cl	K_2O	CaO	TiO_2	Fe_2O_3
1	39.28	0.44	1.31	14.03	31.53	1.14			4.00	1.30	1.30	5.69
2	21.93	0.60	0.80	6.37	15.82	2.10	6.82		1.98	3.40	0.59	39.58
3	32.37	0.64	0.90	2.81	7.75	6.97		0.05	0.43	9.02	0.24	38.83
4	22.18	0.52	0.79	7.55	19.65	8.96	4.72		2.35	15.72	0.79	16.75
5	39.21	0.53	0.29	1.57	4.24	2.28	21.40		0.29	8.86	0.16	21.16
6	17.02	0.52	0.10	0.72	2.59	1.42	45.84		0.19	3.65		27.95

Sample 259/1

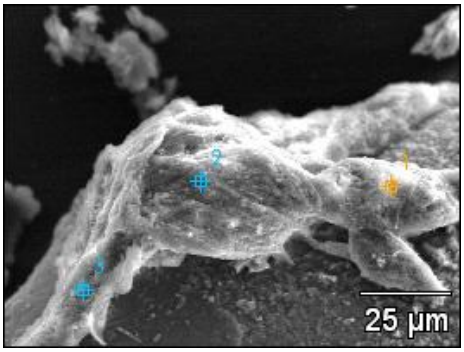

	CO_2	MgO	Al_2O_3	SiO_2	Cl	CaO
1	49.66	0.32	0.43			49.59
2	32.49	0.72	0.63	0.43	0.21	65.51
3	38.78	0.61	0.42	0.30	0.28	59.6

Sample 259/1

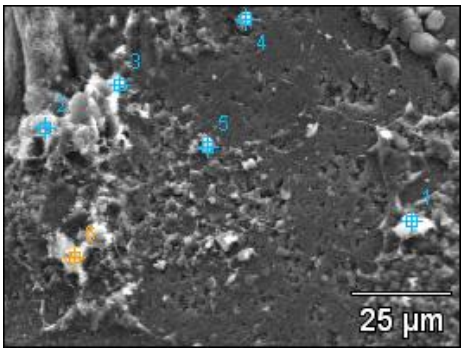

	CO_2	F	Na_2O	MgO	Al_2O_3	SiO_2	P_2O_5	Cl	K_2O	CaO	TiO_2	Fe_2O_3
1	46.63		0.26	2.48	11.70	13.20	4.19	0.12	0.16	5.03		16.22
2	27.11		0.10	1.00	5.37	7.40	12.93	0.29	0.46	37.73		7.62
3	37.99		0.16	1.77	8.70	9.71	11.56	0.14	0.26	17.54		12.16
4	41.07	4.01	0.26	0.05	0.45	0.34	23.70			29.69		0.42
5	39.09		0.22		0.62	39.97	9.66			10.18		0.25
6	37.46		0.05	2.54	12.73	14.99	5.10	0.08	0.28	6.70	0.14	19.92

Sample 259/1

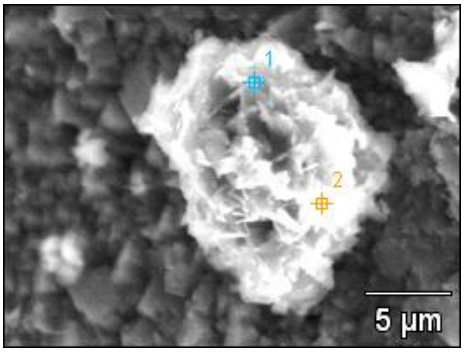

	CO_2	Na_2O	MgO	Al_2O_3	SiO_2	P_2O_5	Cl	K_2O	CaO	TiO_2	Fe_2O_3
1	32.91	0.24	2.39	17.22	26.17	1.35	0.08	1.46	2.88	0.88	14.42
2	39.59		1.90	11.43	13.83	4.11	0.08	0.39	6.64	0.21	21.81

Sample 266

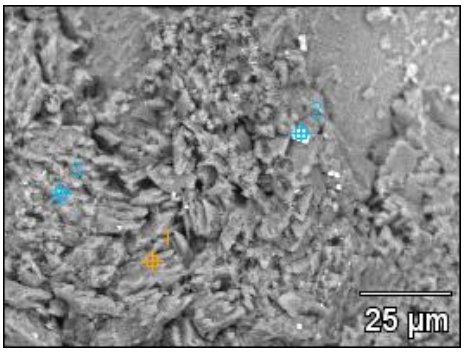

	CO_2	MgO	Al_2O_3	SiO_2	K_2O	CaO	Sc_2O_3	Fe_2O_3	NiO	WO_3
1	40.92	2.08	1.21			55.71	0.08			
2	28.88					30.10	0.38			40.64
3	26.30	1.86	5.42	7.13	0.74	54.65	0.77	2.18	0.93	

Sample 266

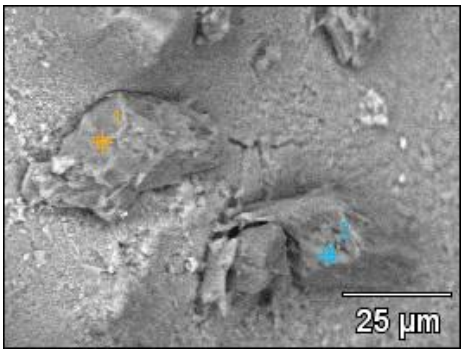

	CO_2	MgO	Al_2O_3	SiO_2	P_2O_5	CaO	Sc_2O_3
1	47.76	1.14	1.02	1.68	2.39	46.01	
2	28.46	1.23		1.32		68.53	0.46

Sample 266

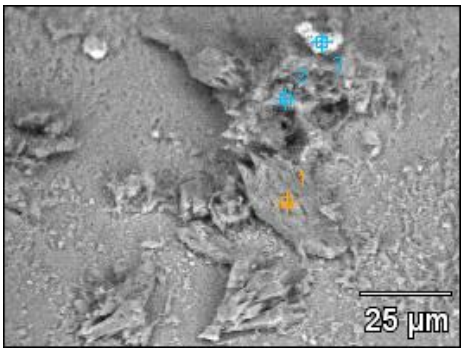

	CO_2	Na_2O	MgO	Al_2O_3	SiO_2	P_2O_5	K_2O	CaO	Sc_2O_3	TiO_2	Fe_2O_3
1	38.08		1.39	0.94	1.51			57.04	1.04		
2	34.10		1.38	13.63	33.53	1.76	3.03	5.08		0.59	6.89
3	26.42	1.13		1.87	3.22	29.77		37.59			

Sample 267/13

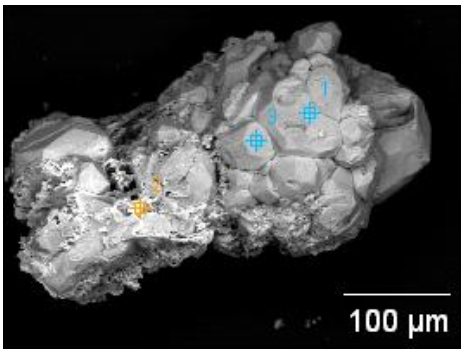

	CO_2	Na_2O	MgO	Al_2O_3	SiO_2	P_2O_5	SO_3	Cl	K_2O	CaO	Fe_2O_3
1	9.08	0.51	1.51	1.01	6.98	0.38		0.23		0.76	79.53
2	33.01	0.36	0.47	2.03	9.15	0.47	0.49		0.20	0.92	52.89
3	10.39	0.30	0.72	0.66	7.42	0.62		0.15		1.07	78.65

Sample 267/13			
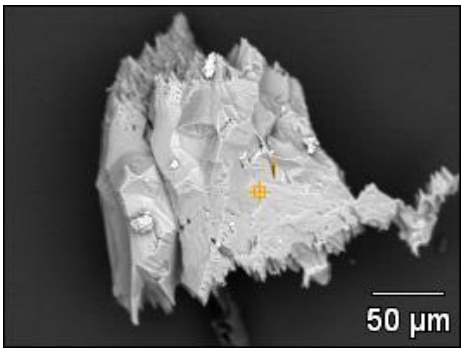			
	CO_2	**MgO**	**CaO**
1	27.66	0.64	71.69

Sample 267/13					
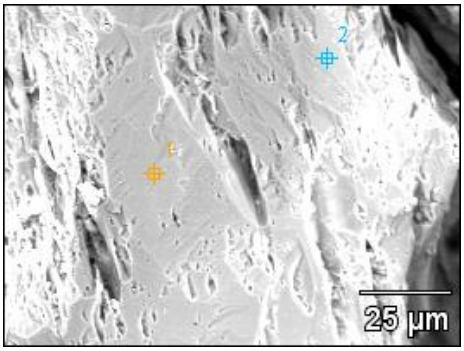					
	CO_2	**MgO**	**Al_2O_3**	**SiO_2**	**CaO**
1	32.44	0.72	0.60	0.58	65.66
2	29.20	0.59	0.33		69.88

Sample 267/13					
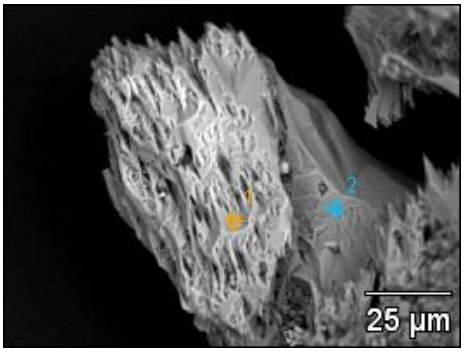					
	CO_2	**MgO**	**Al_2O_3**	**SiO_2**	**CaO**
1	42.68	0.95	0.50		55.86
2	28.95			3.21	67.84

Sample 267/13

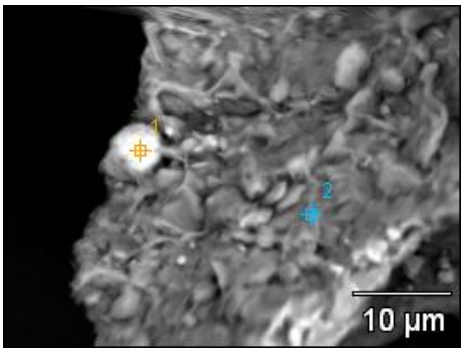

	CO_2	Na_2O	MgO	Al_2O_3	SiO_2	P_2O_5	SO_3	K_2O	CaO	TiO_2	Fe_2O_3	MoO_3
1	19.86		0.94	7.05	13.73		1.48	0.60	1.96		54.37	
2	32.58	0.39	1.08	20.00	38.14	0.52		2.94	1.39	0.90	1.32	0.74

Sample 267/20T

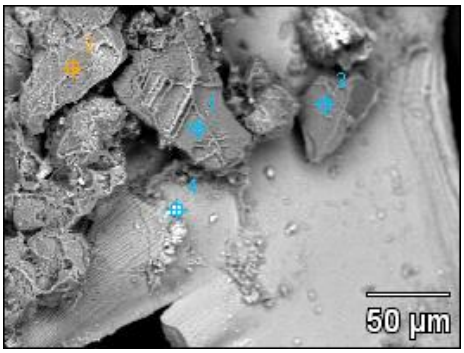

	CO_2	Na_2O	Al_2O_3	SiO_2	P_2O_5	CaO	Fe_2O_3	MoO_3
1	6.73	0.30	0.52	89.65			1.68	1.12
2	8.64	0.38	0.00	89.70				1.28
3	0.00	0.43	0.04	97.52	0.64			1.37
4	7.70		0.35	1.59	0.25	3.02	87.10	

Sample 268/4								
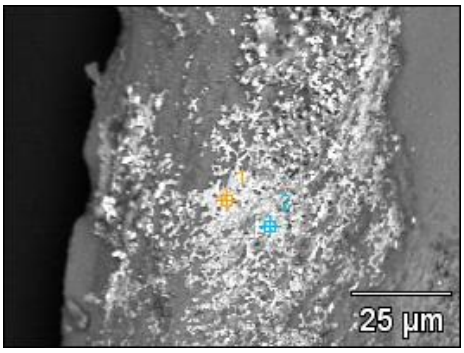								
	CO_2	**Na_2O**	**Al_2O_3**	**P_2O_5**	**SO_3**	**CaO**	**SrO**	**BaO**
1	20.77	0.88	0.39	13.22	16.44	17.79	0.92	29.59
2	16.99		0.29	15.80	15.92	20.21	1.46	29.33

Sample 268/4															
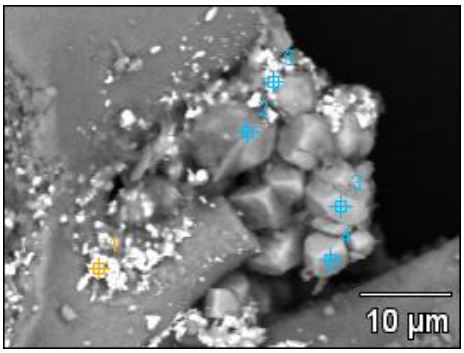															
	CO_2	**MgO**	**Al_2O_3**	**SiO_2**	**P_2O_5**	**SO_3**	**K2O**	**CaO**	**TiO_2**	**MnO**	**Fe_2O_3**	**CoO**	**As_2O_3**	**ZrO_2**	**BaO**
1	11.05		1.28	1.86		29.84		2.83			0.68			1.48	50.98
2	19.77	1.04	6.20	10.79	0.70	0.54		1.29	2.74		56.92				
3	4.23	1.51	0.74	4.86				1.18			87.49				
4	0.00	0.66	0.59	3.71	3.40			4.24		0.49	86.90				
5	18.77		3.39	5.00		22.36	0.19	1.44			7.87	0.18	0.88	0.42	39.49

Sample 268/4
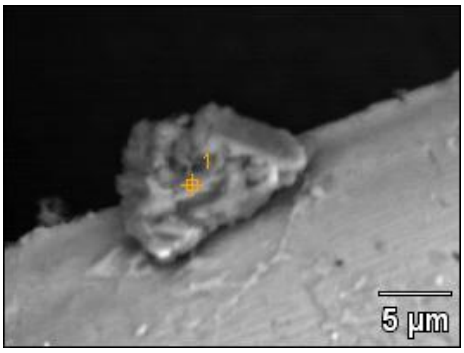

	CO_2	Na_2O	MgO	Al_2O_3	SiO_2	P_2O_5	Cl	CaO	Fe_2O_3	MoO_3
1	17.27	0.32	0.20	30.90	45.15	1.99	0.06	2.88	0.57	0.67

Sample 268/4
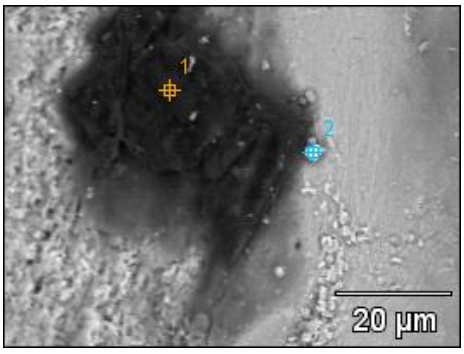

	CO_2	Na_2O	MgO	Al_2O_3	SiO_2	P_2O_5	SO_3	Cl	K_2O	CaO	Fe_2O_3	MoO_3
1	75.58	1.12		0.25	0.31	8.25	3.90	0.48	0.16	9.94		
2	17.78	0.72	0.45	1.90	4.83	9.67			0.26	12.85	51.26	0.28

Sample 268/4

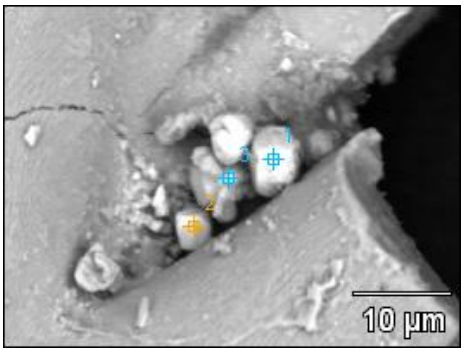

	CO_2	Na_2O	MgO	Al_2O_3	SiO_2	P_2O_5	Cl	CaO	Fe_2O_3
1	7.20	0.31	1.21	1.16	6.08	2.41		2.64	78.98
2	2.12	0.29	1.04	0.68	3.11	2.83	0.16	4.37	85.39
3	3.43		0.17	0.51	2.71	1.40		3.18	88.61

Sample 279/4

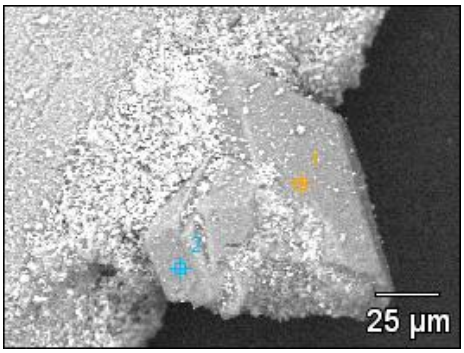

	CO_2	MgO	Al_2O_3	SiO_2	P_2O_5	SO_3	CaO	Fe_2O_3
1	19.29	0.28				49.29	31.15	
2	36.94		0.80	0.99	1.42	24.26	17.46	18.13

Sample 279/4

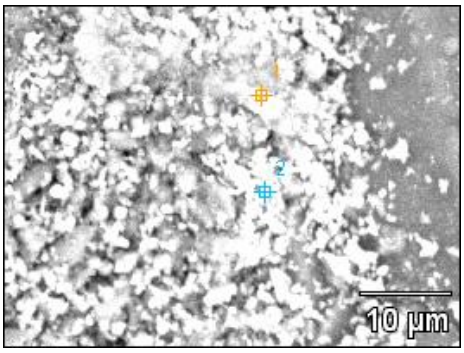

	CO_2	Al_2O_3	SiO_2	P_2O_5	CaO	Sc_2O_3	Fe_2O_3	MoO_3
1	19.38	1.86	1.63	33.27	41.23		2.63	
2	8.04	3.28	5.86	14.89	38.01	0.69	27.03	2.20

Sample 279/8

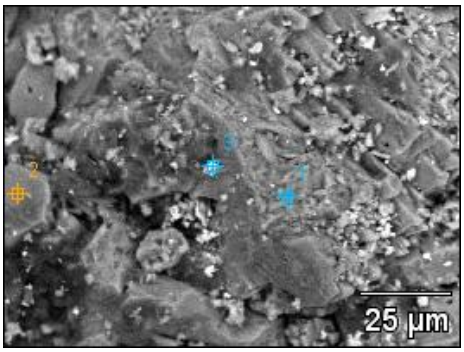

	CO_2	Al_2O_3	SiO_2	CaO	MnO	Fe_2O_3
1	44.39			55.61		
2	38.14			61.86		
3	25.63	1.60	2.65	6.18	0.60	63.34

Sample 279/8

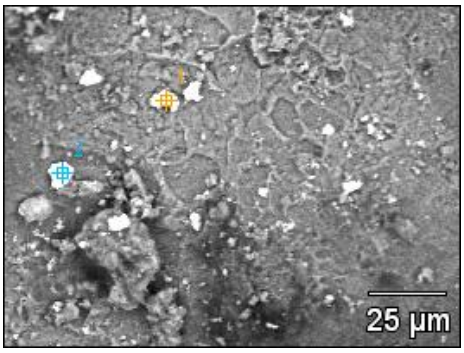

	CO_2	P_2O_5	CaO	Fe_2O_3	WO_3
1	11.46	11.68	11.68		65.19
2	25.91		9.09	1.72	63.28

Sample 279/12

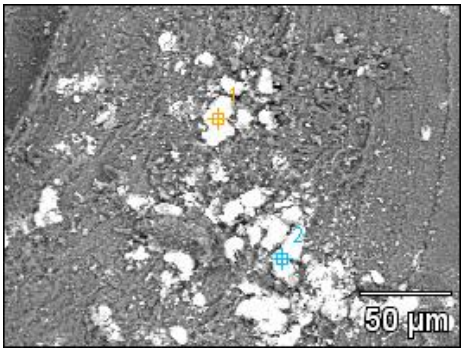

	CO_2	MgO	Al_2O_3	SO_3	CaO	Fe_2O_3	WO_3	PbO
1	16.17	1.07	2.13	0.65	8.10	5.75	66.14	0.00
2	11.06	0.74	4.21	4.54	12.75	5.29	55.81	5.59

Sample 280/3

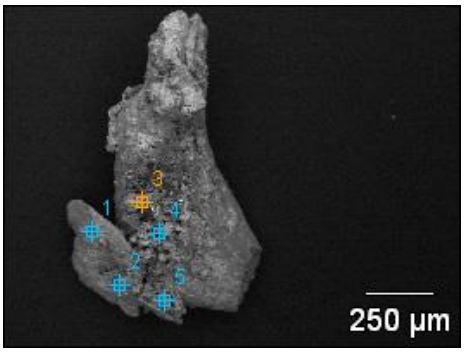

	CO_2	Na_2O	MgO	Al_2O_3	SiO_2	CaO	Fe_2O_3	WO_3
1	38.97						61.03	
2	43.10	1.57	2.50	9.12		0.78	23.32	19.61
3	9.80		1.96	8.50	19.03		60.71	
4							100.00	
5	5.09					1.44	28.99	64.47

Sample 292/21

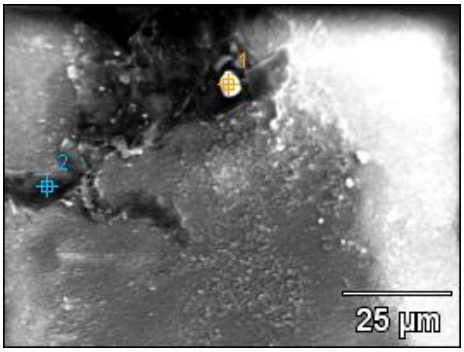

	CO_2	N_2O_5	F	Na_2O	Al_2O_3	SiO_2	P_2O_5	SO_3	K_2O	CaO	BaO
1	13.55				0.64	0.68	1.01	28.91		3.92	51.29
2	50.56	20.57	1.53	1.05	0.47	1.12	12.20		0.14	12.35	

Sample 292/21

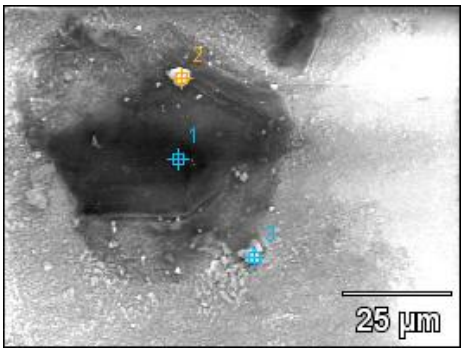

	CO_2	N_2O_5	F	Na_2O	MgO	Al_2O_3	SiO_2	P_2O_5	Cl	K_2O	CaO	Fe_2O_3	MoO_3
1	51.24	17.82	0.67	0.52	0.12	0.61	1.18	11.74	0.37	0.14	13.79		1.80
2	16.48			0.56	1.14	1.51	4.91	3.57			5.37	66.46	
3	21.64		7.08	0.43	0.17	0.94	1.02	29.88			38.84		

Sample 292/21

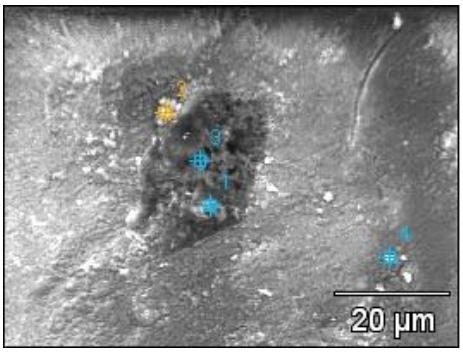

	CO_2	N_2O_5	Na_2O	MgO	Al_2O_3	SiO_2	P_2O_5	Cl	CaO	Fe_2O_3	MoO_3
1	20.46	5.06	0.62	0.37	1.24	2.87	5.58	0.12	6.02	57.65	
2	17.72	6.24	0.86	0.32	1.32	2.45	28.28	0.18	39.53	3.08	
3	22.06		0.71	0.34	0.74	1.95	28.96		39.26	5.54	0.43
4	15.83		1.42	1.33	3.06	5.62	20.24		27.06	23.66	1.77

Sample 292/24b

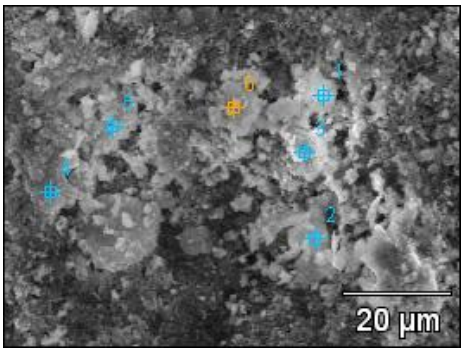

	CO_2	Na_2O	MgO	Al_2O_3	SiO_2	P_2O_5	K_2O	CaO	V_2O_5	Fe_2O_3	MoO_3	In_2O_3	WO_3
1	35.73	0.26	1.89	10.69	13.35	7.30	0.17	10.08	0.20	20.34			
2	18.96	0.28	0.52	2.47		9.82		15.57		3.16	0.19		49.03
3	39.94	0.29	1.54	8.61	10.86	10.70		13.75		14.33			
4	35.89	0.07	0.76	4.92	7.09	13.03		23.91		14.33			
5	20.11	0.06	0.66	4.67	7.07	18.17		35.07		13.19		1.01	
6	16.80	0.80	0.76	1.99		4.69		8.29		2.97			63.70

Sample 292/24b														
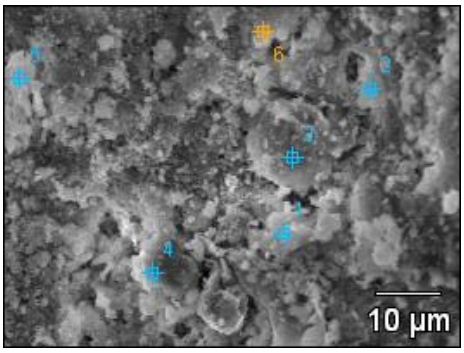														
	CO_2	**Na_2O**	**MgO**	**Al_2O_3**	**SiO_2**	**P_2O_5**	**SO_3**	**K_2O**	**CaO**	**Cr_2O_3**	**Fe_2O_3**	**MoO_3**	**In_2O_3**	**WO_3**
1	30.97	0.76	1.93	11.92		4.48		0.95	7.78		12.36			28.86
2	35.76	2.36	0.43	3.34		8.90		0.27	12.27		4.78			31.88
3	15.84	0.30	0.87	0.92			0.78		7.90		1.97			71.42
4	34.77	0.34	2.75	14.89	20.26	1.68		0.61	2.72	0.15	21.83			
5	30.55	0.61	0.52	2.80		8.19			11.34		4.61	0.33		41.05
6	41.67	0.37	0.57	3.50	5.94	15.80			24.01		7.33		0.81	

Sample 292/24c

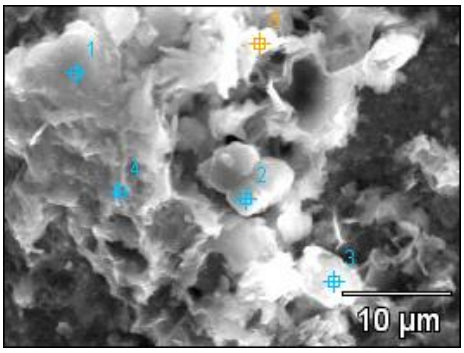

	CO_2	Na_2O	MgO	Al_2O_3	SiO_2	P_2O_5	Cl	K_2O	CaO	TiO_2	Fe_2O_3	As_2O_3	WO_3	Au
1	39.14	0.49	2.49	13.60	18.92	0.57		1.42	1.04	0.53	17.72		4.08	
2	26.37	3.87		26.13	29.42	0.69	0.10	0.79	9.01		3.31	0.32		
3	38.38	0.47	2.31	15.79	20.41	2.12		1.64	2.87		13.57		2.44	
4	31.13	0.17	1.00	7.48	10.28	0.84		1.05	2.62		38.49		6.94	
5	41.42	0.66	2.26	12.17	15.33	1.21		0.80	1.36	0.30	21.29		2.91	0.29

Sample 292/24c

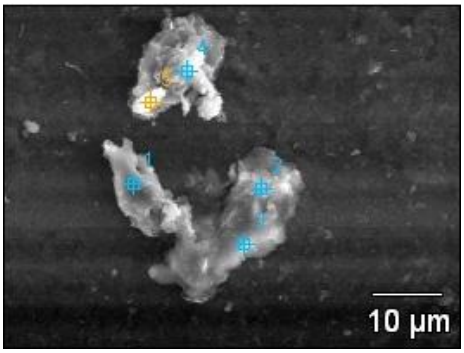

	CO_2	Na_2O	MgO	Al_2O_3	SiO_2	P_2O_5	SO_3	K_2O	CaO	TiO_2	Fe_2O_3	WO_3
1	37.79		0.71	0.57	0.33	1.77			58.16		0.67	
2	37.87	0.55	2.21	13.38	24.44	3.65	0.20	2.09	4.32	3.48	7.82	
3	33.75	0.27	2.24	12.78	20.53	4.50		1.84	9.49	0.42	11.71	2.49
4	96.40			0.11	0.31	1.47			1.65		0.05	
5	89.52	0.13	0.03	0.21	0.54	3.95			5.46		0.15	

Sample 292/24c

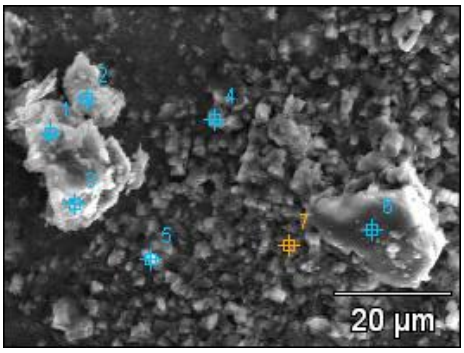

	CO_2	F	Na_2O	MgO	Al_2O_3	SiO_2	P_2O_5	Cl	K_2O	CaO	TiO_2	Cr_2O_3	Fe_2O_3	In_2O_3
1	98.21		0.11		0.16	0.25	0.51	0.02	0.08	0.55			0.11	
2	94.93		0.14		0.21	0.39	1.88	0.06	0.10	1.89		0.06	0.33	
3	80.44		0.16		0.80	1.56	4.75	0.15	0.67	5.41		0.79	5.26	
4	34.50		0.47	0.43	2.16	2.31	23.19			28.31			7.68	0.95
5	48.38		0.35	0.13	1.26	1.46	20.76		0.16	26.02	0.39		1.10	
6	40.99			0.61	8.86	15.22	8.17		5.18	16.41	0.32		4.25	
7	21.02	1.99	0.23	0.09	0.80	0.88	28.94			45.64			0.41	

Sample 307/2T (host rock)

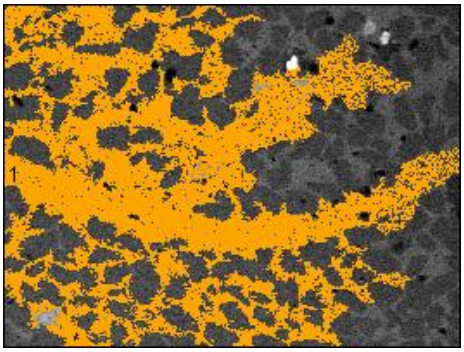

	MgO	SiO_2	CaO	Sc_2O_3
1	2.39	7.27	89.92	0.42

Sample 307/2T (host rock, mapping)

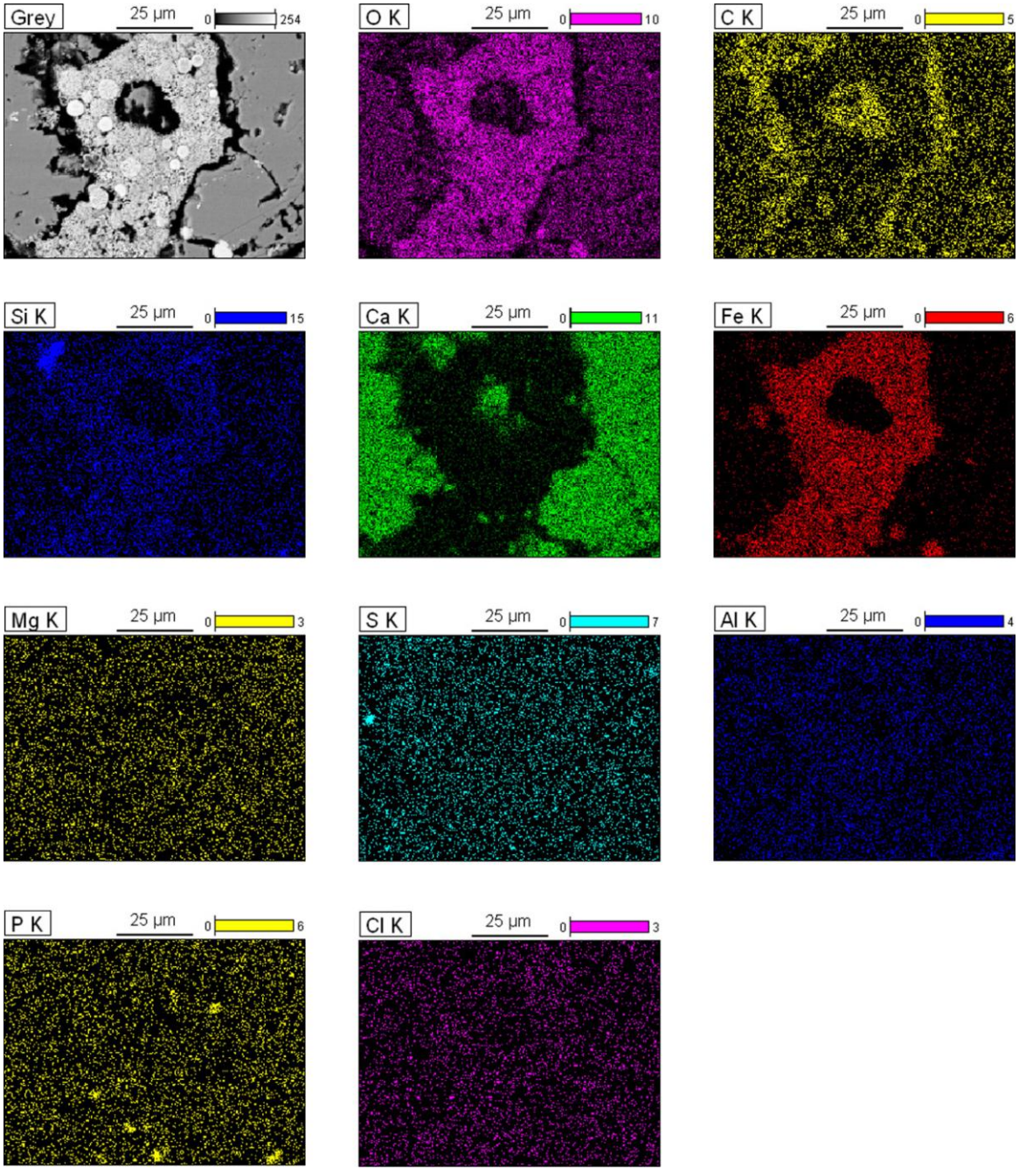

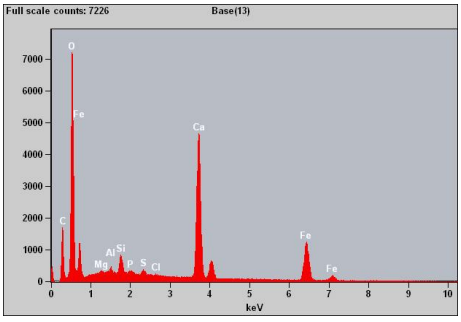

Sample 312/16

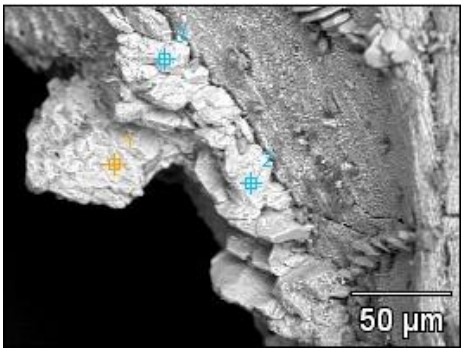

	CO_2	F	Al_2O_3	P_2O_5	CaO	Cu_2O
1	3.91		0.39	20.79	74.20	0.71
2	12.08	5.85	0.23	35.74	46.10	
3	12.14	5.79		35.86	46.21	

Sample 312/16

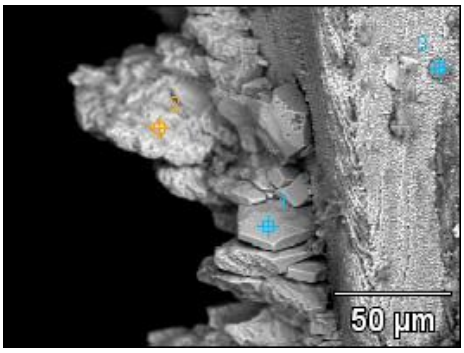

	CO_2	F	Na_2O	MgO	Al_2O_3	SiO_2	P_2O_5	SO_3	Cl	CaO	Fe_2O_3
1	14.61	8.20			0.27	0.13	34.81			41.98	
2	15.90	7.64			0.24		34.25			41.98	
3	50.00		0.25	0.85	0.32	0.19	2.21	3.53	0.43	41.35	0.86

Sample 312/16								
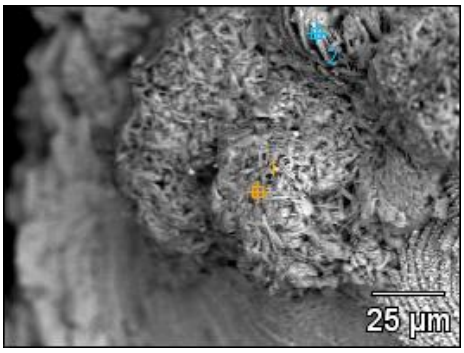								
	CO_2	**Na_2O**	**MgO**	**Al_2O_3**	**P_2O_5**	**SO_3**	**CaO**	**Fe_2O_3**
1	30.87	0.20	0.79	0.22		28.50	39.42	
2	25.76	0.18	0.21	0.15	0.55	42.80	29.91	0.43

Sample 312/16				
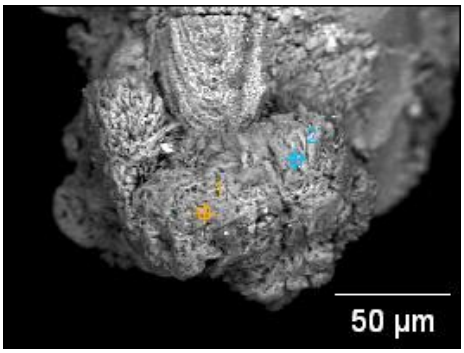				
	CO_2	**MgO**	**SO_3**	**CaO**
1	25.39	0.20	32.56	41.85
2	21.36		42.10	36.54

Sample 317/2T

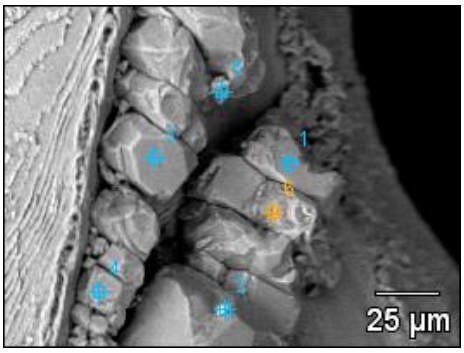

	CO_2	F	MgO	Al_2O_3	SiO_2	P_2O_5	CaO	Fe_2O_3
1	20.71	5.00				33.67	40.62	
2	35.05		0.29	1.35	2.47	13.30	15.44	32.11
3	19.39	4.25				31.40	44.95	
4	16.47	4.52				34.63	44.38	
5	56.79					11.18	32.03	
6	18.99	4.65				33.34	42.02	1.00

Sample 317/2T

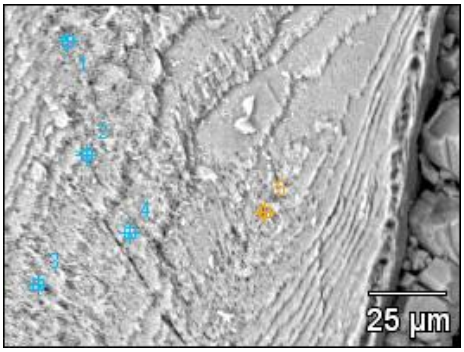

	CO_2	F	Na_2O	Al_2O_3	P_2O_5	CaO
1	17.49	4.24	0.73	0.40	34.10	43.03
2	18.82	4.78	0.72	0.37	33.07	42.23
3	17.11	3.76			34.22	44.91
4	17.91	5.15		0.35	34.28	42.32
5	16.50	4.19	0.86	0.29	34.55	43.61

Sample 317/2T

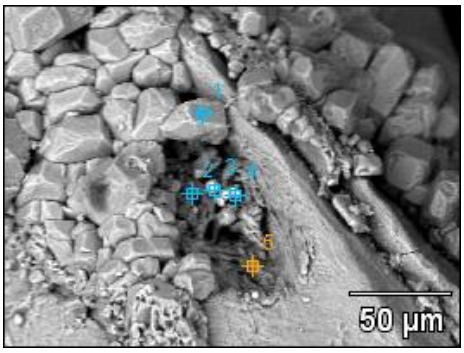

	CO_2	F	Na_2O	MgO	Al_2O_3	SiO_2	P_2O_5	CaO	Fe_2O_3
1	22.17	8.37			0.30	0.06	32.24	36.85	
2	22.22				1.10	1.32	12.46	58.85	4.06
3	15.19			0.51	2.32	4.31	5.85	8.44	63.38
4	21.92				1.26	3.16	6.54	9.48	57.64
5	20.22	6.47	0.80		0.86	0.65	31.86	39.14	

Sample 327/44

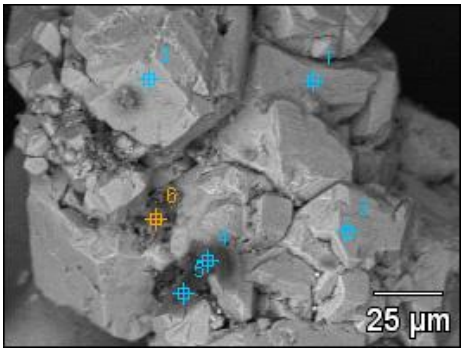

	CO_2	MgO	SiO_2	Cl	CaO	Fe_2O_3
1	31.85	1.01	2.55			64.59
2	35.01	1.22	2.57			61.19
3	23.64		1.90			74.46
4	93.76	0.80	1.16	0.19	0.85	3.24
5	92.78	1.67	2.33	0.47		2.74
6	5.90				4.76	89.34

Sample 327/44

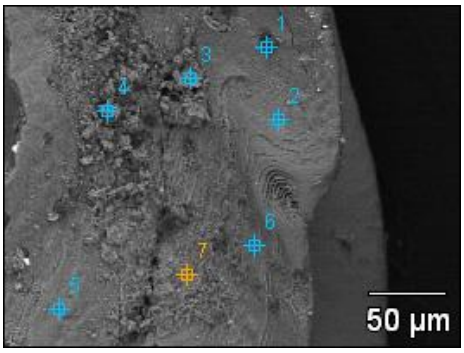

	CO_2	F	Na_2O	MgO	Al_2O_3	SiO_2	P_2O_5	SO_3	Cl	CaO	Fe_2O_3	As_2O_3	SrO	MoO_3
1	85.35		1.08	0.58			1.08	2.98	0.37	8.57				
2	33.51	2.53	0.47		0.21		26.69			36.58				
3	34.01				19.95		25.68			6.94			9.67	3.75
4	59.76				17.34	5.02	13.85			2.75		0.28		0.99
5	38.54	5.11	0.72				23.96			31.68				
6	27.57						9.11			63.32				
7	19.81						22.05			55.60	2.54			

Sample 329/2

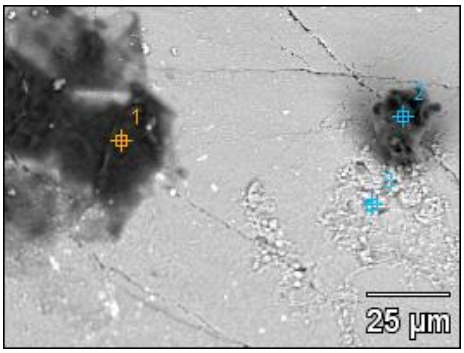

	CO_2	N_2O_5	F	Na_2O	Al_2O_3	SiO_2	P_2O_5	SO_3	Cl	K_2O	CaO
1	67.66	18.74		0.49	0.89		4.16	2.59	0.88	0.14	4.45
2	95.96				0.14		1.84				2.06
3	19.11		7.31	0.29	0.25	0.12	32.46				40.46

Sample 329/2

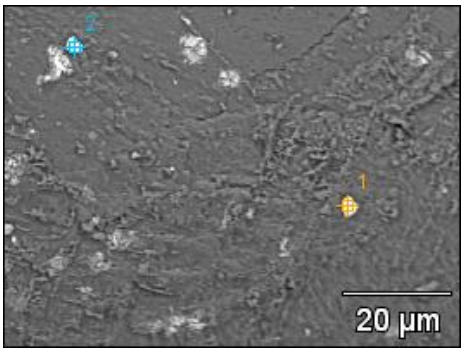

	CO_2	Na_2O	MgO	Al_2O_3	P_2O_5	CaO	Fe_2O_3	MoO_3	WO_3
1	13.23	0.19		0.39	13.22	16.44	0.75	0.07	55.70
2	13.74		0.16	0.49	11.08	13.88	2.38	0.30	57.97

Sample 330/10T

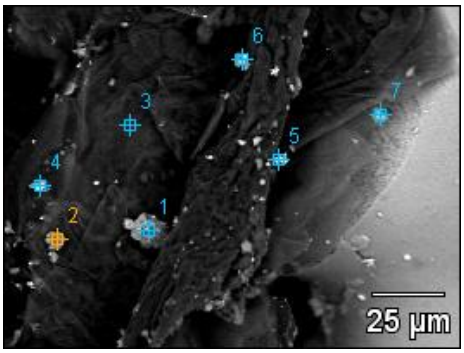

	CO_2	N_2O_5	Na_2O	MgO	Al_2O_3	SiO_2	P_2O_5	SO_3	Cl	K_2O	CaO	TiO_2	Fe_2O_3	Tl_2O_3
1	28.43		0.41	1.44	19.81	30.18	0.81	3.98		1.80	0.95	1.02	11.17	
2	27.96				33.38	38.67								
3	77.12	18.56	0.64	0.14				1.66	0.94	0.12	0.83			
4	42.28	11.87	1.01	0.28	0.70	1.01	17.01		0.36		23.35		1.38	0.75
5	25.84			1.31	0.91	2.39	0.68				0.96		67.91	
6	18.04			0.51	0.63	2.30	0.66		0.19		1.12		76.55	
7	33.61		0.44	0.71	11.28	15.91	14.60		0.34	2.65	18.62	0.20	1.65	

Sample 330/10T
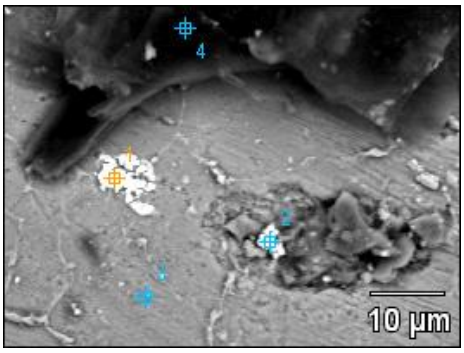

	CO_2	N_2O_5	Na_2O	MgO	Al_2O_3	SiO_2	P_2O_5	Cl	K_2O	CaO	Fe_2O_3	MoO_3	WO_3
1	8.94		0.71		0.48		24.32	0.14	0.83	34.96			29.61
2	6.69		0.30	1.75	4.23	7.43	4.83	0.23		6.25	68.28		
3	17.95		0.53		1.05	1.73	32.15			42.50	4.09		
4	66.88	16.46	0.73	0.21	0.30	0.39	4.96	0.93	0.13	6.93	0.47	1.62	

Sample 330/10T
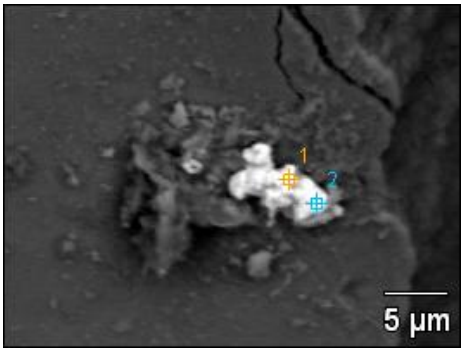

	CO_2	Al_2O_3	SiO_2	SO_3	CaO	Fe_2O_3	SrO	ZrO_2	BaO
1	7.78	0.79		26.45	2.33		2.42		60.23
2	12.16	1.50	2.13	28.27	1.83	0.47		0.35	53.28

Sample 330/14
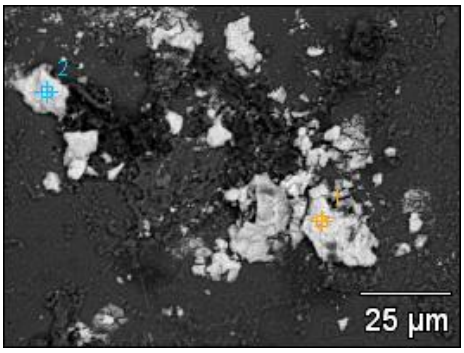

	CO_2	MgO	SO_3	CaO	Fe_2O_3	MoO_3	WO_3
1	11.47	0.49	0.39	7.33			80.32
2	11.88	0.59		7.34	0.93	0.69	78.58

Sample 330/14
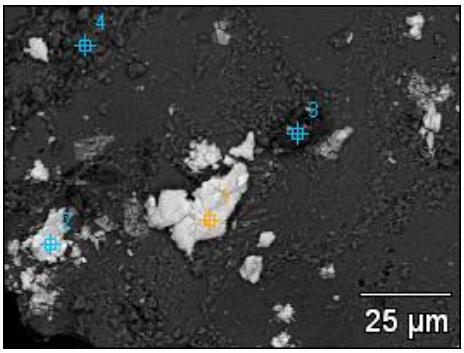

	CO_2	Na_2O	MgO	Al_2O_3	SiO_2	P_2O_5	SO_3	Cl	K_2O	CaO	Fe_2O_3	As_2O_3	Nb_2O_5	WO_3
1	13.67		0.41				0.31	0.15		7.11				78.36
2	7.06		0.53							8.56				83.85
3	19.92	0.30	0.20	4.40	66.19	3.47			0.61	4.02	0.69		0.21	
4	9.73			8.58	10.94	22.83			0.68	44.37	2.32	0.54		

Sample 331/46

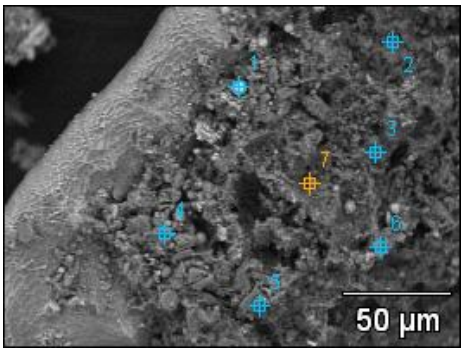

	CO_2	MgO	Al_2O_3	SiO_2	SO_3	K_2O	CaO	Fe_2O_3
1	31.95	0.74	1.11	4.95			1.72	59.52
2	26.16	1.30	21.94	46.63		3.96		
3	42.82	1.29	17.68	33.61		4.60		
4	36.18	1.33	18.33	35.19		2.96	1.58	4.44
5	58.37	1.06	13.05	24.16		2.77	0.60	
6	48.39	0.95	15.35	27.00		1.89	1.32	5.10
7	37.42		1.93	54.80	4.23	0.23		1.38

Sample 332/1

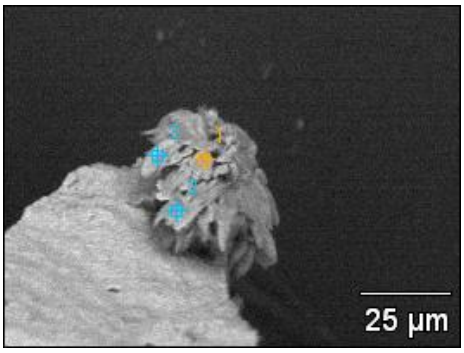

	CO_2	SO_3	CaO
1	32.58	39.04	28.39
2	56.22	24.79	18.98
3	29.39	38.29	32.32

Sample 332/1				
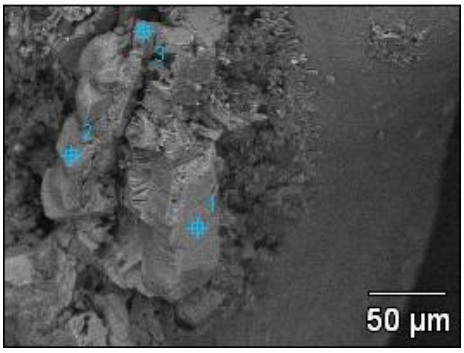				
	CO_2	**F**	**P_2O_5**	**CaO**
1	33.97	7.70	26.56	31.77
2	19.30		18.86	61.84
3				100.00

Sample 354/7														
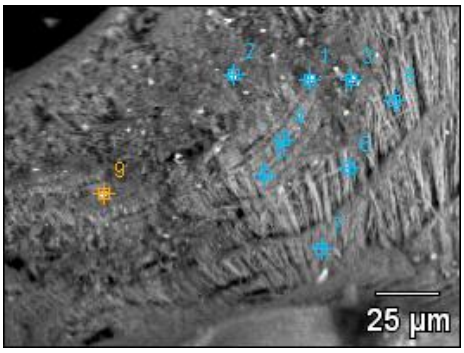														
	CO_2	**F**	**Na_2O**	**MgO**	**Al_2O_3**	**SiO_2**	**P_2O_5**	**SO_3**	**K_2O**	**CaO**	**Fe_2O_3**	**Cu_2O**	**As_2O_3**	**WO_3**
1	36.59			0.88	5.36		12.10	3.46	0.73	15.92	2.12			22.84
2	24.38				2.73	4.46	3.14	39.68	0.37	5.37	18.90		0.95	
3	22.14		1.33	0.67	5.58	10.08	7.11		0.64	8.77	43.66			
4	28.03	5.34	0.99		1.07	2.33	27.94			33.75		0.55		
5	16.22	6.34	0.80				33.99			42.64				
6	15.55	4.07	0.81		0.78	0.86	32.82			45.12				
7	26.23	5.86	0.90		0.69	0.64	29.63			36.05				
8	27.37	6.43	1.34		0.56		28.96		0.25	34.73	0.36			
9	37.84		0.92		2.06	4.22	24.38		0.41	30.17				

Sample 354/7

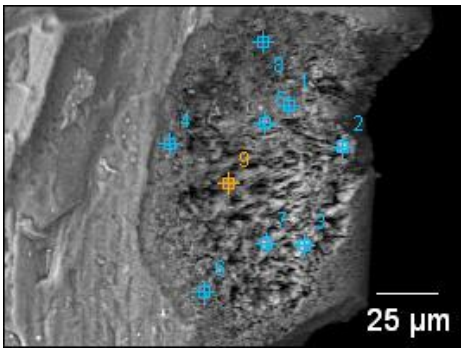

	CO_2	F	Na_2O	MgO	Al_2O_3	SiO_2	P_2O_5	K_2O	CaO	Fe_2O_3	Cu_2O
1	31.35			0.50	4.51	7.31	18.02	0.66	30.99	5.87	0.79
2	33.97	4.23	0.69				26.71		34.40		
3	26.59	4.06	0.66		0.46		29.50		38.74		
4	24.02						28.83		47.15		
5	26.86				1.09	1.52	28.60		41.08	0.85	
6	20.64				1.56	2.29	29.76		45.74		
7	23.66	5.15	0.90				31.04		39.24		
8	63.15				0.89		5.29	0.50	21.79	8.38	
9	26.05	2.08	0.35		0.44		28.65		41.87		0.56

Sample 354/7

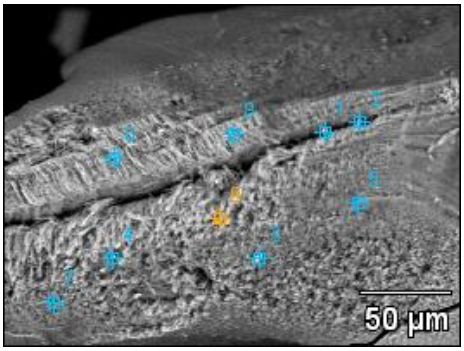

	CO_2	F	Na_2O	Al_2O_3	SiO_2	P_2O_5	K_2O	CaO	TiO_2	Fe_2O_3	Cu_2O	As_2O_3
1	10.54			1.13	2.63	12.47		14.02		56.17	0.67	2.38
2	23.69	7.60	1.88	1.24	1.50	26.71		36.56	0.83			
3	33.99			3.51	6.24	5.25	0.92	11.43		37.85		0.81
4	21.38		0.45	0.91	6.01	18.75		34.08		18.42		
5	14.68			3.09	5.77	27.52	0.72	45.10		3.12		
6	17.82	4.61	0.74			33.58		43.25				
7	16.36	1.03				28.13		54.48				
8	17.70	5.30	0.77			30.91		45.32				
9	15.92	3.67	0.48	0.38		33.35		46.20				

Sample 367/11

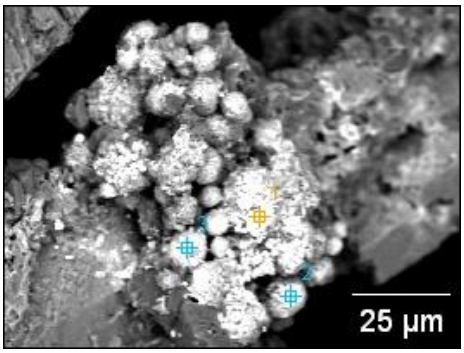

	CO_2	Na_2O	Al_2O_3	P_2O_5	SO_3	CaO	Fe_2O_3	WO_3
1	10.65	2.55	1.42		0.69	2.83	24.89	56.97
2	11.83	0.21	0.50			1.52	43.15	42.79
3	2.32		0.41	0.48		2.18	67.79	26.81

Sample 367/11

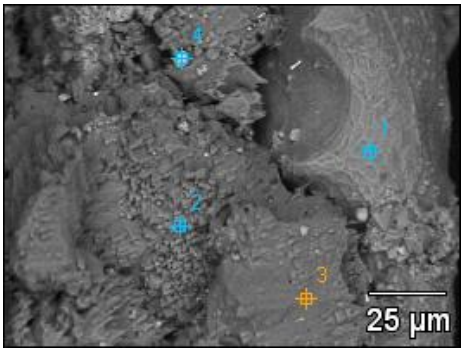

	CO_2	F	Na_2O	MgO	Al_2O_3	SiO_2	P_2O_5	CaO	Fe_2O_3
1	14.60	4.95	0.69				34.46	45.31	
2	7.74				0.56	0.72		90.98	
3	31.95			0.75				67.29	
4	11.76				1.06	7.29	0.93	5.35	73.60

Sample 367/11

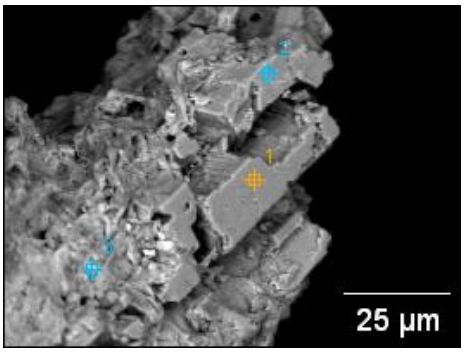

	CO_2	F	Na_2O	MgO	Al_2O_3	SiO_2	P_2O_5	K_2O	CaO	TiO_2	Fe_2O_3	WO_3
1	20.03	6.82					29.83		43.31			
2	20.33	7.07			0.41		29.24		42.95			
3	12.45		0.82	1.22	19.62	37.32		5.20	1.40	0.69	5.40	15.90

Sample 367/11

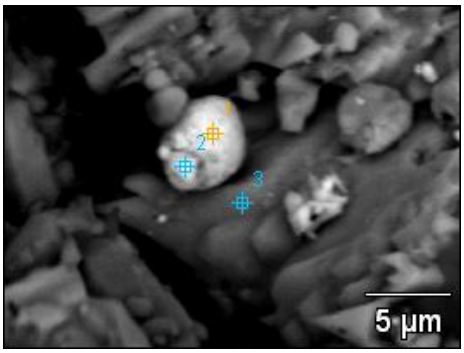

	CO_2	MgO	Al_2O_3	SiO_2	P_2O_5	CaO	Fe_2O_3
1	12.30	0.37	1.82	7.61	1.03	5.27	71.60
2	18.53	0.24	1.24	10.95	1.20	5.57	62.27
3	26.02	0.59	0.38	1.50		71.52	

Sample 367/11
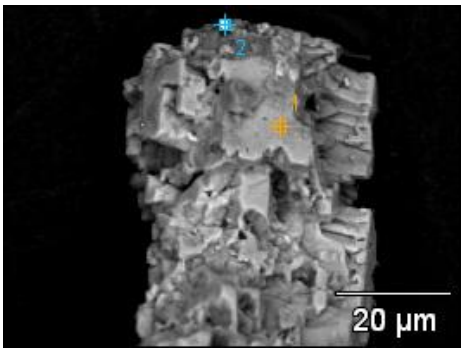

	CO_2	F	Na_2O	MgO	Al_2O_3	SiO_2	P_2O_5	K_2O	CaO	Fe_2O_3	WO_3
1	18.40	6.16	0.53	0.46	3.62	6.09	27.18	0.49	37.07		
2	39.61			0.56	2.45		2.30		5.64	3.00	46.44

Sample 367/11
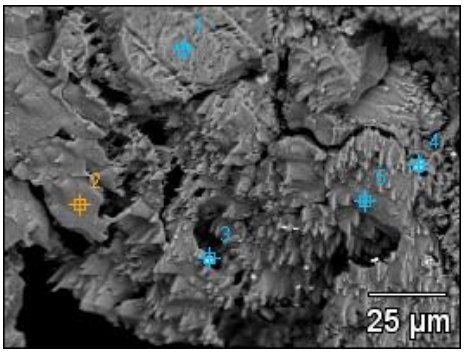

	CO_2	Na_2O	MgO	Al_2O_3	SiO_2	SO_3	Cl	K_2O	CaO	Fe_2O_3
1	14.48		0.59						84.94	
2	9.54			0.19					90.27	
3	4.47			0.53	1.79				3.50	89.70
4	18.59	0.50	0.57	3.47	11.18	0.69	0.18	0.45	6.76	57.59
5	7.67			0.32					92.01	

Sample 367/11									
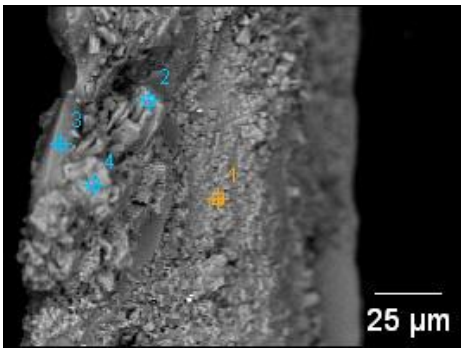									
	CO_2	**F**	**Na_2O**	**MgO**	**Al_2O_3**	**SiO_2**	**P_2O_5**	**K_2O**	**CaO**
1	11.47	2.63			0.32	0.25	34.21		51.12
2	19.14	5.06					33.07		42.73
3	24.69	6.12	0.75		0.26	0.26	29.86		38.06
4	14.94			0.42	5.26	10.05	25.37	1.29	42.67

Sample 367/11		
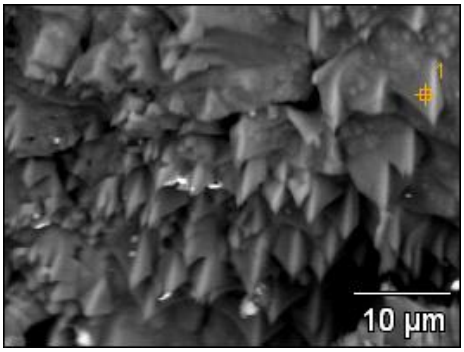		
	CO_2	**CaO**
1	7.87	92.13

Sample 367/20T			
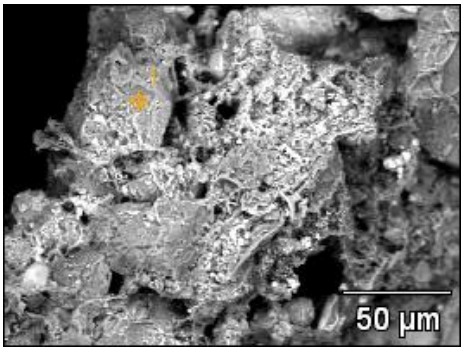			
	Al_2O_3	**SiO_2**	**MoO_3**
1	0.09	98.89	1.02

Sample 396/4		
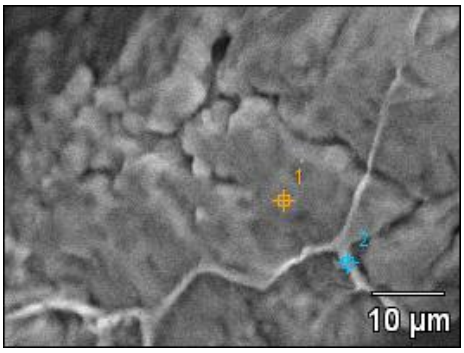		
	CO_2	**SiO_2**
1	20.11	79.89
2	22.60	77.40

Sample 396/4		
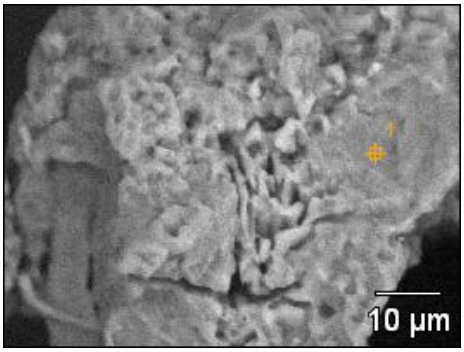		
	CO_2	**SiO_2**
1	18.18	81.82

Sample 396/8				
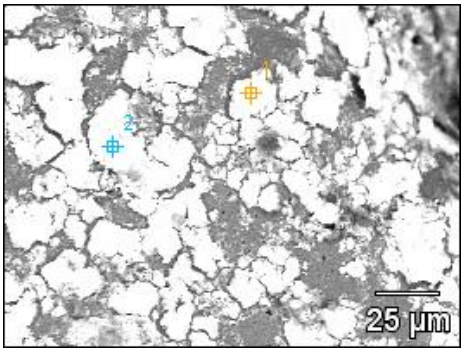				
	CO_2	**CaO**	**Fe_2O_3**	**WO_3**
1	25.72	9.66		64.62
2	23.94	10.70	0.73	64.63

Sample 396/8					
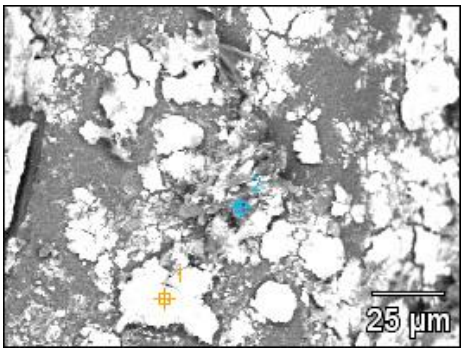					
	CO_2	**Al_2O_3**	**P_2O_5**	**CaO**	**WO_3**
1	18.41		11.11	18.10	52.38
2	15.14	2.35		13.70	68.82

Sample 399/6					
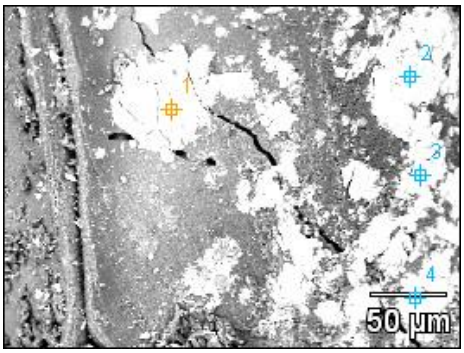					
	CO_2	**SO_3**	**CaO**	**MoO_3**	**WO_3**
1	9.24	1.04	10.52		79.20
2	19.70	0.53	8.50		71.27
3	15.33		7.92	0.60	76.14
4	11.77		10.78		77.44

Sample 399/6							
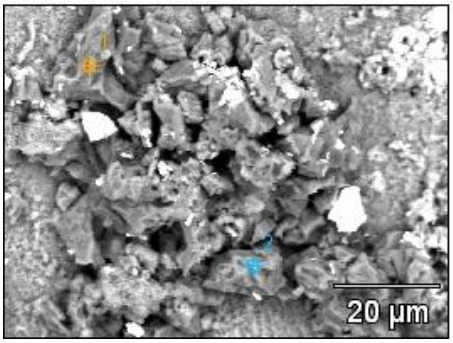							
	CO_2	**Al_2O_3**	**SiO_2**	**P_2O_5**	**SO_3**	**CaO**	**ZrO_2**
1	11.77	0.35	0.76	1.40	46.28	39.43	
2	9.58	0.44			52.20	36.32	1.46

Sample 406/4														
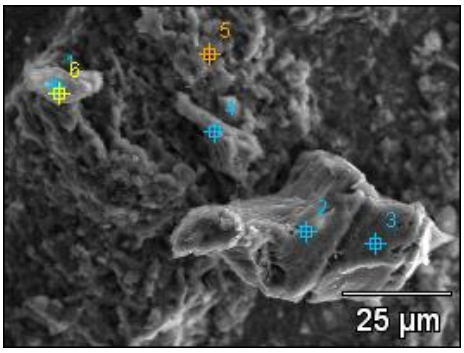														
	CO_2	**N_2O_5**	**F**	**Na_2O**	**MgO**	**Al_2O_3**	**SiO_2**	**P_2O_5**	**Cl**	**K_2O**	**CaO**	**MnO**	**Fe_2O_3**	**Tl_2O_3**
1	48.97	24.52		0.52	0.35	1.42	2.88	7.75		0.12	9.56		3.42	0.48
2	27.76				0.37	0.53	0.25				69.69	0.46	0.95	
3	30.09				0.29	0.43					67.98		1.21	
4	37.69				0.45	0.79	0.75	3.56			54.07		2.69	
5	17.03		1.44			0.27		34.38	0.10		46.78			

Sample 406/4

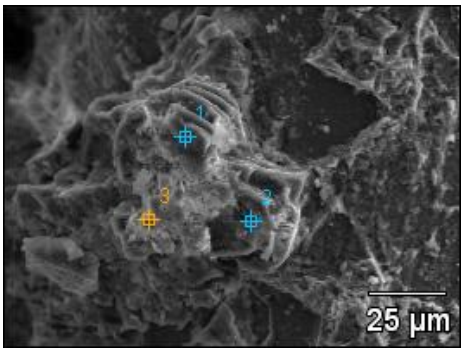

	CO_2	MgO	Al_2O_3	SiO_2	SO_3	Cl	CaO	MnO	Fe_2O_3	NiO	ZnO	As_2O_3
1	24.47		2.36	4.76		0.13	46.72	0.47	9.41	0.31	11.23	0.16
2	17.26	0.40	1.08	1.26			78.28		1.72			
3	28.82	0.29	0.53		0.67	0.08	66.49	0.46	0.72	1.95		

Sample 416/4

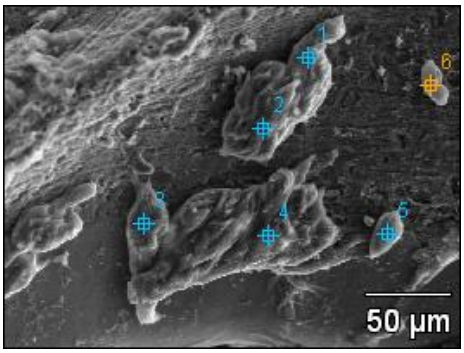

	CO_2	Na_2O	MgO	Al_2O_3	SiO_2	P_2O_5	Cl	CaO	V_2O_5	Fe_2O_3	Rb_2O	MoO_3
1	50.82		1.23	0.43	0.27		0.47	46.48		0.29		
2	31.38		0.74	0.47			0.35	67.06				
3	31.30		1.04	0.44			0.40	66.81				
4	16.94		1.50	0.44			0.98	80.01			0.12	
5	35.23		1.11	0.35	0.37	1.75	0.70	60.31	0.18			
6	50.62	0.34	1.47	0.38	0.33	3.43	0.75	41.44		0.34		0.90

Sample 416/4														
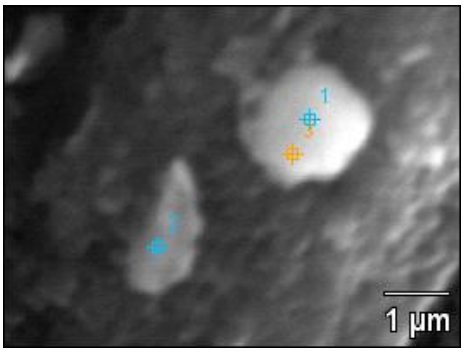														
	CO_2	**MgO**	**Al_2O_3**	**SiO_2**	**P_2O_5**	**SO_3**	**Cl**	**K_2O**	**CaO**	**Cr_2O_3**	**MnO**	**Fe_2O_3**	**Cu_2O**	**ZnO**
1	45.12	1.08	1.02	1.41		0.92	0.15		8.70	0.28	0.46	38.66	2.20	
2	45.22	0.95	3.26	4.74			0.37	0.39	44.29			0.78		
3	56.52	0.43	0.62	1.15	0.31	0.56	0.15		9.38	0.29		28.46	1.67	0.46

Sample 416/4										
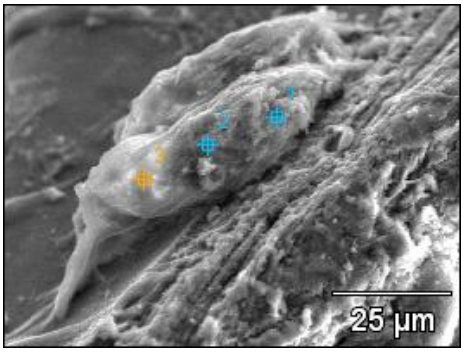										
	CO_2	**Na_2O**	**MgO**	**Al_2O_3**	**SiO_2**	**P_2O_5**	**SO_3**	**Cl**	**CaO**	**Cu_2O**
1	50.94	0.39	1.30	0.60		1.40		0.35	45.04	
2	50.11		1.12	0.60	0.27			0.42	47.49	
3	50.04		0.70	0.95	0.80		6.78	0.33	40.15	0.26

Sample 416/4

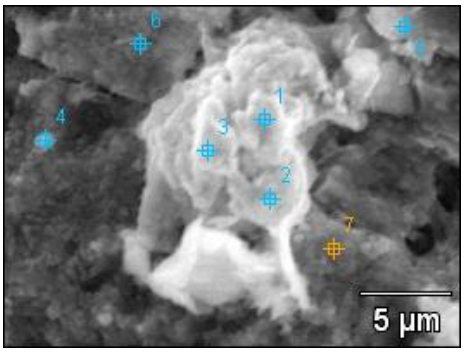

	CO_2	F	Na_2O	MgO	Al_2O_3	SiO_2	P_2O_5	Cl	CaO	Fe_2O_3	Cu_2O	MoO_3
1	54.52		0.38	0.67	0.64	1.18	12.25	0.36	28.30	0.66		1.05
2	46.83		0.33	0.76	0.93	1.25	15.57	0.36	33.11	0.86		
3	60.65		0.30	0.73	0.80	1.32	9.29	0.35	24.37	1.07		1.13
4	39.30		0.32	0.32	1.27	0.91	21.23	0.19	27.03	8.95	0.47	
5	50.63		0.36	1.95	1.17	1.20	8.40	0.98	19.57	14.40	0.52	0.84
6	33.22	2.48	0.24	0.19	0.28	0.34	26.38		36.88			
7	26.86	4.17	0.47	0.07	0.33	0.26	29.40		37.64	0.52	0.27	

Sample 435/8

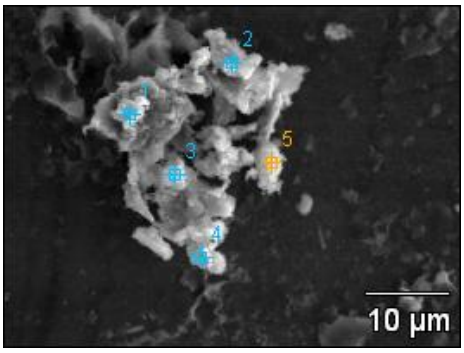

	CO_2	MgO	Al_2O_3	SiO_2	P_2O_5	K_2O	CaO	Cr_2O_3	MnO	Fe_2O_3	NiO	Cu_2O	MoO_3	Ta_2O_5
1	31.14		0.51	0.87	1.89	0.11	2.41	12.58	1.60	39.61	8.62	0.65		
2	6.88	0.26	1.62	3.19	2.43	0.16	3.14	19.22	1.76	47.07	12.47	1.17	0.63	
3	74.14	0.13	0.66	1.04	2.09	0.07	3.14	4.12	0.49	13.16	0.84			0.13
4	15.28		0.53	1.07	1.31		2.26	13.17	1.34	57.53	7.51			
5	20.83		0.71	1.67	4.92	0.14	5.62	15.66	2.61	43.72	3.05	1.07		

Sample 435/8

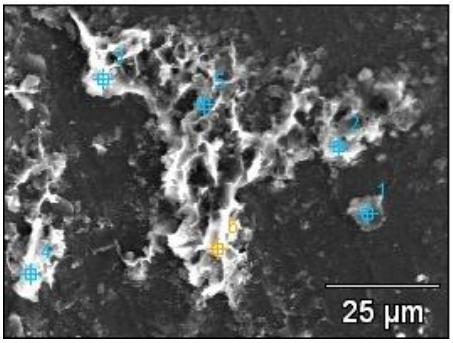

	CO_2	Na_2O	MgO	Al_2O_3	SiO_2	P_2O_5	K_2O	CaO	TiO_2	Fe_2O_3	Cu_2O	MoO_3	WO_3
1	27.88	0.30	0.21	1.72	4.03	25.27	0.22	39.29		1.07			
2	22.90	0.26	0.60	1.78		6.90	0.29	14.13				0.25	52.89
3	50.02	0.14	0.80	13.98	23.36	1.81	2.53	2.91	0.84	3.43	0.17		
4	37.31	0.04	1.19	14.78	23.18	5.09	3.82	12.17	0.27	2.14			
5	32.97	0.14	0.72	11.18	22.87	5.77	1.76	15.40	0.17	9.03			
6	45.59	0.14	0.87	15.73	26.45	1.27	3.82	1.88	0.21	4.04			

Sample 435/8

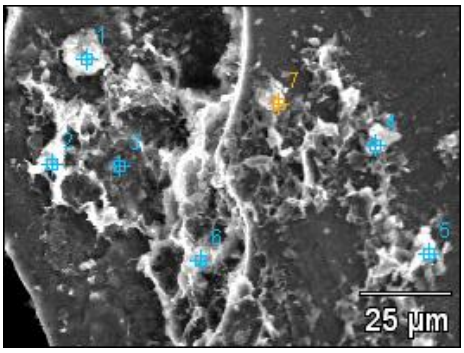

	CO_2	Na_2O	MgO	Al_2O_3	SiO_2	P_2O_5	SO_3	Cl	K_2O	CaO	TiO_2	MnO	Fe_2O_3	Cu_2O	MoO_3	WO_3
1	28.95	0.69	0.51	1.96		2.88	0.36		0.34	7.15			1.02			56.14
2	41.89	0.34	1.08	17.49	29.77	0.81			2.95	0.99	0.46		4.01	0.22		
3	23.43	0.34	0.65	5.87	8.47	18.67			0.63	32.20			9.73			
4	36.27	0.40	1.37	13.99	24.72	4.78		0.06	1.27	7.08	0.66		9.41			
5	35.36	0.24	0.44	12.76	17.43	6.31			0.51	8.47	11.72		6.76			
6	12.15	0.49	2.01	24.18	45.00	0.70			4.70	1.05	0.37	0.05	8.96		0.34	
7	36.90	0.50	0.51	5.98		15.84			0.41	26.01			2.49			11.36

Sample 435/14T							
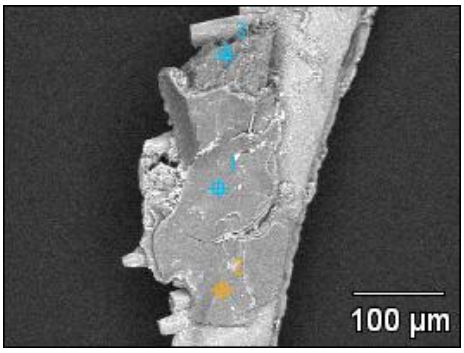							
	CO_2	**Na_2O**	**Al_2O_3**	**SiO_2**	**K_2O**	**TiO_2**	**Fe_2O_3**
1	27.99		25.27	31.16	13.99	1.59	
2	20.04	0.91	29.26	38.81	8.70	0.88	1.40
3	19.86		0.34	79.19			0.61

Sample 435/14T								
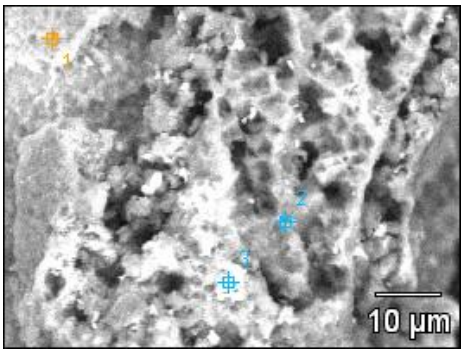								
	CO_2	**MgO**	**Al_2O_3**	**SiO_2**	**K_2O**	**CaO**	**Fe_2O_3**	**WO_3**
1	20.02					30.70	49.29	
2	13.05	1.81	10.64	21.79	2.48	1.87	48.35	
3	10.16	0.79	4.99	6.93		1.93	63.78	11.42

Sample 435/14T

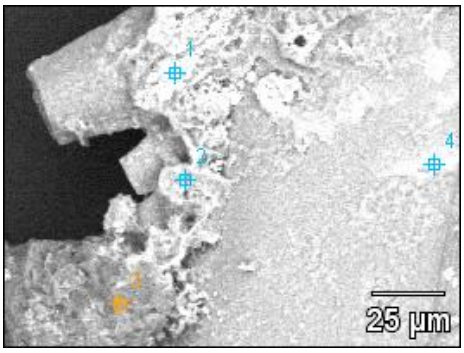

	CO_2	MgO	Al_2O_3	SiO_2	P_2O_5	K_2O	CaO	TiO_2	Fe_2O_3	WO_3
1	4.61		1.00				4.24		57.91	32.24
2	23.53	1.57	16.06	29.90		3.25	1.72		23.95	
3	17.22		0.66	80.79			0.33	0.98		
4	21.87	1.45	4.16		16.04		30.29		10.67	15.53